



**HAL**  
open science

# Study of the effects of nanoparticles on the immune system

Arindam Dey

► **To cite this version:**

Arindam Dey. Study of the effects of nanoparticles on the immune system. Human health and pathology. Université Grenoble Alpes [2020-..], 2020. English. NNT : 2020GRALV057 . tel-03789717

**HAL Id: tel-03789717**

**<https://theses.hal.science/tel-03789717v1>**

Submitted on 27 Sep 2022

**HAL** is a multi-disciplinary open access archive for the deposit and dissemination of scientific research documents, whether they are published or not. The documents may come from teaching and research institutions in France or abroad, or from public or private research centers.

L'archive ouverte pluridisciplinaire **HAL**, est destinée au dépôt et à la diffusion de documents scientifiques de niveau recherche, publiés ou non, émanant des établissements d'enseignement et de recherche français ou étrangers, des laboratoires publics ou privés.

THÈSE

Pour obtenir le grade de

**DOCTEUR DE L'UNIVERSITÉ GRENOBLE ALPES**

École doctorale : CSV- Chimie et Sciences du Vivant

Spécialité : Virologie - Microbiologie - Immunologie

Unité de recherche : IAB : Epigenetics, Environment, Cell Plasticity, Cancer (UGA / Inserm U1209 / CNRS UMR 5309)

**Etude des effets des nanoparticules sur le système immunitaire**

**Study of the effects of nanoparticles on the immune system**

Présentée par :

**Arindam DEY**

Direction de thèse :

**Patrice MARCHE**

Directeur de Recherche, Université Grenoble Alpes

Directeur de thèse

Rapporteurs :

**EMILIE ROGER**

MAITRE DE CONFERENCES HDR, UNIVERSITE D'ANGERS

**BERNARD VERRIER**

DIRECTEUR DE RECHERCHE, CNRS DELEGATION RHONE AUVERGNE

Thèse soutenue publiquement le **2 décembre 2020**, devant le jury composé de :

**PATRICE MARCHE**

DIRECTEUR DE RECHERCHE, INSERM DELEGATION ALPES

Directeur de thèse

**EMILIE ROGER**

MAITRE DE CONFERENCES HDR, UNIVERSITE D'ANGERS

Rapporteuse

**BERNARD VERRIER**

DIRECTEUR DE RECHERCHE, CNRS DELEGATION RHONE AUVERGNE

Rapporteur

**XAVIER LE GUEVEL**

CHARGE DE RECHERCHE HDR, CNRS DELEGATION ALPES

Examineur

**VALERIE FOREST**

PROFESSEUR, ECOLE DES MINES DE SAINT-ETIENNE

Examineur

**WALID RACHIDI**

PROFESSEUR DES UNIVERSITES, UNIVERSITE GRENOBLE ALPES

Président

Invités :



*Dedicated to my beloved parents*

# Study of the effects of nanoparticles on the immune system

## Acknowledgement

I would like to take this opportunity to extend my heartfelt gratitude towards the following people whose contributions have made this endeavor possible.

Firstly, I would like to express my sincere gratitude to the members of the jury Dr. Bernard Verrier, Dr. Emilie Roger, Prof. Valérie Forest, Prof. Walid Rachidi, and Dr. Xavier Le Guevel, for taking the time and effort to evaluate this work.

I am thankful to my supervisor Dr. Patrice N Marche, for giving me the freedom to organize my research work and explore the subject. We had started working together five years back when I came to France as an Erasmus Master's student. His wisdom, enthusiasm, and support over the last few years has helped me understand and focus on the project and the subject. His stories about different discoveries in science, especially immunology, influenced me to build a stronger interest in the subject. Outside science, we spent many hours discussing French history, current politics, and different wines. We also travelled together many countries to attend different project meetings and gathered lifetime memories during those trips. In the end, I will say, thank you for believing in me and help me to grow both personally and professionally. I will always be indebted to you.

I am profoundly grateful to every member of Institute for Advanced Biosciences (IAB), Grenoble, who have helped me in making beautiful memories. Especially, I would like to thank present and former members of Team Marche (Alexis Gonon, Alexis Leroy, Benoît Manfroi, Bertrand Huard, Christian Villiers, Christine Charrat, Carole Fournier, Flora Clement, Herve Lerat, Laurie Baert, Lydie Carreres, Mashal Ahmed, Marion Ressejac, Mariam Mroweh, Mylene Pezet, Keerthi Kurma and Zuzana Macek Jílková), whose company I have enjoyed, and whose laugh and discussions I have digested. I would like to thank various platforms and facilities at IAB (Mylene Pezet, Alexei Grichine, and Jacques Mazzega: Microscopy platform) (Animal facility: Anthony Lucas) for great support.

This Ph.D. work would not have been possible without financial support. I would like to thank the European Union's Horizon 2020 project "NEWDEAL" to support my Ph. D. project. I would like to acknowledge EURONANOMED European Research project "NANOGLIO" and institutional grants from Institut National de la Santé et de la Recherche Médicale (INSERM) for providing financial support to conduct experiments. I would also like to extend my thanks to University Grenoble Alpes for the IDEX Mobility fellowship to conduct a part of my Ph.D. research at Institut d'Investigacions Biomèdiques August Pi I Sunyer (IDIBAPS), Barcelona.

I would like to express my utmost appreciation to Adrien Nougarede, Dorothée Jary, Fabrice P. Navarro from CEA-Leti, Grenoble, for providing lipid nanoparticles and Jiaxuan Chen, Ling Peng from Aix-Marseille Université, Marseille for providing the dendrimers. My deepest gratitude to Team NEWDEAL and Team NANOGGIO for productive discussion to conduct my experiments.

I would like to express my special thanks of gratitude to my school teacher Somnath Kundu. Your teaching style influenced me to opt for a career in biology.

I am delighted to have met so many amazing people during my time in Grenoble. Thank you, Pushpendra, Shashank, and Ritesh, to accompany me on our "TGVMax journey" to explore every corner of France and make wonderful memories which I will cherish for the rest of my life. A big part of my personal and professional growth belongs to the influence brought in my life by you all. I would like to mention how much you all mean to me by presenting a summary of the trip to my memory lane.

Finally, I am blessed to have my family and friends for always being there and supporting me no matter what. Warmest thanks to Keerthi for being a supportive colleague, a caring sister, and a fantastic roommate. My journey of life would remain incomplete if I have not met you in Grenoble. I am overwhelmed by the presence of my closest friends, Shailesh, Sayantan, Sumanta, Nikita, Aparajita, and Shreyasi, for standing beside me throughout my Ph.D. journey. Special thanks to Kaberi for her support and encouragement during the challenges of graduate school. Even being miles apart, you helped me to vent out the stress; you people are amazing. Thank you, Shailesh, for being an amazing travel buddy in several euro trips, which was a major energy source to withstand Ph.D. stress. I would like to express my most heartfelt thanks to my parents, Sujit Kumar Dey and late Rikta Dey, for their unconditional love and mental support throughout my life.

## Summary

The unique characteristics of nanomaterials (NMs) are valuable in many industrial and biomedical applications. However, NMs might also give rise to unforeseen toxicity that could adversely affect the biological system specially the immune system. In the immune system as phagocytes can engulf foreign materials therefore they are appropriate for immunotoxicity screening because these cells participate in unspecific and specific immune responses.

In this study, we investigated the impact of different NMs, such as gold nanoparticles (AuNPs), neutral lipid nanoparticles (NLCs), cationic lipid nanoparticles (CLCs), and amphiphilic dendrimers (ADs) on primary macrophages (BMDMs) and dendritic cells (BMDCs) by two approaches. In the first approach, we investigated the direct effect of exposure to NMs. In the second approach, we studied the indirect effect by activating the NMs exposed cells with different activators (LPS and IL-4).

The study of direct effect of NMs shows that none of the tested NMs altered the phagocytosis capacity. All of the NMs had none or little direct effect on BMDCs activation. In case of BMDMs, AuNPs, CLCs, and ADs significantly decreased cell activation while NLCs did not. The study of cytokine production based on IL-6 and TNF- $\alpha$  production, NO production, and cellular metabolism based on the investigation of glycolysis and mitochondrial metabolism also indicated no or little direct effect on BMDCs and BMDMs. However, we have noticed a significant increase in MCP-1 production by CLCs and ADs exposed cells while AuNPs and NLCs did not modulate MCP-1 production. Also, we noted that CLCs and NLCs at high concentrations could slightly increase ROS production while AuNPs and ADs did not modulate ROS production by BMDMs and BMDCs.

Investigation of indirect effect of NMs revealed, when NMs exposed cells were challenged with LPS, we have recorded NMs specific modulation in the response of BMDCs based on cell activation, cytokine and chemokine secretion, NO, and ROS production. All NMs showed none or little modification of cellular metabolism of BMDCs. On the other hand, we have recorded a significant alteration in NMs exposed BMDMs upon LPS challenge in response to cell activation, cytokine and chemokine secretion, NO production, and cellular metabolism. However, ROS production remains unaltered in the case of all the NMs exposed BMDMs.

The study of in vitro antigen presentation, revealed that exposure to different NMs altered T cell-specific cytokines reflecting alteration in CD4 + T lymphocytes polarization.

Overall, these results demonstrate that NMs directly do not modify phagocytic activity, cytokine and chemokine production, NO and ROS production, cellular metabolism, but when instigated with an activation signal like LPS or IL-4, NMs exposed cells respond differently.

The outcome of this study enriches the knowledge regarding NMs specific immunotoxicity, which may facilitate the design of nanomaterials that retain their useful properties, but display reduced toxicity (i.e., safety-by-design). This research will also improve our understanding of how different NMs can modulate the immune system, which might help suggest new therapy acting on the immune system such as anti-inflammatory drugs or vaccines.

## Résumé

Les caractéristiques uniques des nanomatériaux (NM) sont précieuses dans de nombreuses applications industrielles et biomédicales. Toutefois, les MR pourraient également donner lieu à une toxicité imprévue qui pourrait nuire au système biologique en particulier au système immunitaire. Les phagocytes du système immunitaire ont la capacité d'ingérer des matériaux étrangers ; ils sont donc appropriés pour l'étude de l'immunotoxicité car ils sont impliqués dans les réponses immunitaires non spécifiques et spécifiques.

Dans cette étude, nous avons étudié l'impact de différents nano matériaux (NM), telles que des nanoparticules d'or (AuNPs), des nanoparticules lipidiques neutres (NLCs) ou cationiques (CLCs), et des dendrimères amphiphiliques (ADs) sur les macrophages primaires (BMDMs) et des cellules dendritiques (BMDCs) par deux approches. Dans la première, nous avons recherché les effets directs de l'exposition. Dans la seconde, nous avons étudié les effets indirects sur l'activation du LPS ou de l'IL-4 des cellules exposées aux NMs.

Nos résultats concluent que tous les NMs testés n'ont pas modifié la capacité de phagocytose. Une analyse plus approfondie montre que tous les NMs ne montrent aucun, ou peu, effet direct sur l'activation des BMDC. Pour le BMDMs, les AuNPs, les CLCs et les ADs ont considérablement diminué l'activation cellulaire tandis que les NLCs n'ont d'effet. L'étude de la production de cytokine basée sur la production d'IL-6 et de TNF- $\alpha$ , de la production de NO et du métabolisme cellulaire basée sur l'étude de la glycolyse et du métabolisme mitochondrial n'a également pas ou peu d'effet direct sur les BMDCs et les BMDMs. Cependant, nous avons remarqué une augmentation significative de la production de MCP-1 par les CLCs et les cellules exposées aux ADs, tandis que les AuNPs et les NLCs n'ont pas d'effet sur la production de MCP-1. De plus, nous avons noté que les CLCs et les NLCs à forte concentration pourraient légèrement augmenter la production de ROS, tandis que les AuNPs et les ADs ne modulaient pas la production de ROS par les BMDM et les BMDC.

L'étude des effets indirects de NMs a montré que quand les cellules exposées aux NMs sont stimulées par du LPS, nous avons observé une modulation de la réponse des BMDCs au niveau de l'activation cellulaire, la sécrétion de cytokine et de chimiokine, NO, et la production de ROS. Toutes les NMs n'affectent pas, ou peu, le métabolisme des BMDCs. D'autre part, nous avons enregistré une altération significative chez les BMDMs exposés aux NMs dans leur réponse à l'activation par le LPS au niveau de l'activation cellulaire, la sécrétion de cytokine et de chimiokine, la production de NO et le métabolisme cellulaire. Cependant, la production de ROS reste inchangée dans le cas des BMDMs exposés aux NMs.

L'étude in vitro de la présentation d'antigène, a indiqué que l'exposition à différents NMs modifie les cytokines produites par les cellules T, reflétant l'altération de la polarisation des lymphocytes T CD4 +.

Dans l'ensemble, ces résultats démontrent que les NMs ne modifient pas directement l'activité phagocytaire, la production de cytokine et de chimiokine, la production de NO et de ROS, le métabolisme cellulaire des cellules phagocytaires, mais lorsqu'elles sont confrontées à un signal d'activation comme le LPS ou l'IL-4, les cellules exposées aux NMs réagissent différemment.



## Contents

1.	List of abbreviation.....	8
2.	List of Figures.....	14
3.	List of tables.....	16
4.	General Introduction .....	17
5.	Immune System: Art of War .....	20
5.1	Introduction.....	20
5.2	Innate Immune response .....	21
5.2.1	Anatomic and Physiologic barriers .....	22
5.2.2	Phagocytic and endocytic barriers .....	22
5.3	Adaptive Immune response .....	32
5.3.1	T lymphocytes.....	34
5.3.2	B lymphocytes .....	38
5.4	Linking Innate and Adaptive immunity .....	39
5.4.1	Major histocompatibility complex: .....	39
5.4.2	T cell receptors (TCRs) .....	41
5.4.3	B cell receptors (BCRs).....	43
5.5	Immunometabolism .....	44
5.5.1	Glycolysis in immunity.....	47
5.5.2	The TCA cycle in immunity .....	49
6.	Nanoparticles, between promise and challenges .....	51
6.1	Introduction.....	51
6.2	Classification.....	52
6.2.1	Inorganic NMs .....	52
6.2.2	Carbon-based NMs.....	53
6.2.3	Organic NMs.....	54
6.3	Biomedical usage of nanoparticles.....	54
6.3.1	Gold nanoparticles (AuNPs).....	55
6.3.2	Lipid nanoparticles (LNs) .....	57
6.3.3	Dendrimer .....	61
6.4	Immunotoxicity of nanoparticles .....	65
7	Aim of the thesis.....	66
8	Objectives of the thesis .....	66

9	Results .....	67
9.1	Impact of Gold nanoparticles on the functions of macrophages and dendritic cells .....	67
9.2	Impact of Lipid nanoparticles on the functions of macrophages and dendritic Cells.....	96
9.3	Impact of Amphiphilic dendrimers on the functions of macrophages and dendritic cells .....	138
9.3.1	Synthesis and use of an amphiphilic dendrimer for siRNA delivery into primary immune cells	140
9.3.2	Immunotoxicity of Amphiphilic dendrimers.....	188
10	Discussion .....	223
11	References.....	237

## 1. List of abbreviation

APCs	Antigen-Presenting Cells
AuNPs	Gold Nanoparticles
ADs	Amphiphilic Dendrimers
ALRs	non-melanoma 2 (AIM2)-like receptors
AIS	Adaptive Immune System
Akt	Protein kinase B
ATP	Adenosine triphosphate
AOCS	N-Arginine-N-octyl chitosan
ANLC	N-Arginine-N-octyl chitosan modified lysosomolytic nanocarriers
AFSSAPS	Agence Française de Sécurité Sanitaire des Produits de Santé
$\alpha$ -KG	alpha-ketoglutarate
BCR	B cell receptor
BMDMs	Bone Marrow-Derived Macrophages
BMDCs	Bone Marrow-Derived Dendritic cells
bis-MPA	poly(2,2-bis(hydroxymethyl)propionic acid
CD	Cluster of Differentiation
CVD	chemical vapor deposition
CAGR	Compound Annual Growth Rate
CLCs	Cationic Lipid nanocarriers
CLRs	C-type lectins

CTLs	cytotoxic T lymphocytes
CDPs	common DC progenitors
cDCs	conventional DCs
DAMPs	Danger-associated molecular patterns
DCs	Dendritic cells
ERK	Extracellular signal-regulated kinases
FoxP3	Forkhead box P3
FAO	Fatty acid oxidation
GMDPs	granulocyte, monocyte and DC progenitors
HIF1 $\alpha$	Hypoxia-inducible factor 1-alpha
HIV	Human Immunodeficiency Viruses
IL-1	Interleukin 1
IL-4	Interleukin 4
IL-6	Interleukin 6
IL-10	Interleukin 10
IL-12	Interleukin 12
IL-13	Interleukin 13
IL-17	Interleukin 17
IFN- $\gamma$	Interferon gamma
ICAM	intercellular adhesion molecule
IKK $\epsilon$	I $\kappa$ B kinase- $\epsilon$
ldh	isocitrate dehydrogenase

Ig	immunoglobulin
iNOS	Inducible nitric oxide synthase
JAK1	Janus kinase 1
LT	T lymphocytes
LPS	Lipopolysaccharides
LCs	Lipid Carriers
LN <sub>s</sub>	lipid nanoparticles
LDH	Lactate dehydrogenase
MHC-I	Major Histocompatibility Class I Proteins
MHC-II	Major Histocompatibility Class II Proteins
MDPs	monocyte and DC progenitors
MAPK	Mitogen-activated protein kinase
mTOR	mammalian target of rapamycin
MCP-1	Monocyte Chemoattractant Protein-1
MRC	Maximal respiration capacity
mDC <sub>s</sub>	Conventional myeloid dendritic cells
NPs	Nanoparticles
NMs	Nanomaterials
NF-κB	nuclear factor-κB
NSLC	Nano structured Lipid Carriers
NLC <sub>s</sub>	Neutral Lipid nanocarriers
NLR <sub>s</sub>	Nucleotide Oligomerization (nod)-like receptors

NO	Nitric oxide
NLRP3	NOD-, LRR- and pyrin domain-containing 3 regulator
NKT cells	Natural Killer T cells
nDDSs	Targeted drug delivery Nanosystem
OVA	Ovalbumin
OXPHOS	oxidative phosphorylation
PAMPs	Pathogen-associated molecular patterns
PRR	Pattern recognition receptor
PPP	Pentose Phosphate Pathway
PKM2	Pyruvate kinase isoenzyme M2
PDT	Photodynamic therapy
PPTT	plasma photothermal therapy
PEG	Poly-Ethylene-Glycol
PAMAM	poly(amidoamine)
PLL	poly(L-lysine)
PPI	polypropylenimine
PGLSA-OH	poly (glycerol succinic acid)
PPH	Poly-(phosphohydrazone)
PLC $\gamma$ 2	Phosphoinositide-specific phospholipase C gamma 2
PI3K	Phosphoinositide 3-kinase
pDNAs	plasmid DNAs
pDCs	Plasmacytoid dendritic cells

RIG-I	retinoic acid-inducible gene I
RLRs	retinoic acid-inducible gene I (RIG-I)-like receptors
ROS	Reactive oxygen species
Rag1	Recombination Activating Genes 1
Rag2	Recombination Activating Genes 2
SLNs	Solid lipid nanoparticles
SRC	Spare respiratory capacity
SDH	Succinate dehydrogenase
siRNA	Small interfering RNA
TLRs	Toll-like receptors
Th1	T helper type 1
Th2	T helper type 2
Th9	T helper type 9
Th17	T helper type 17
Treg	Regulatory T cells
TCR	T cell receptor
TNF- $\alpha$	Tumor necrosis factor alpha
TGF- $\beta$	transforming growth factor $\beta$
TCA cycle	Tricarboxylic Acid Cycle
TBK1	TANK Binding Kinase 1
UDP-GlcNAc	Uridine diphosphate N-acetylglucosamine
uPFK2	ubiquitous isoform of phosphofructokinase-2

VDJ	variable–diversity–joining
WPs	Work packages



## 2. List of Figures

Figure	Title	Page
1	Immunotoxicity assessment.	19
2	The components of the innate and adaptive immune system.	21
3	The polarization of macrophages.	27
4	Classification of DCs in humans and mice.	29
5	Differentiation of mDCs.	30
6	Story of Adaptive immune system.	34
7	Overview of the development of thymocytes.	36
8	B-cells become plasma cells to attack the invader.	39
9	Antigen processing and presentation by MHC Class I and MHC Class II.	41
10	Schematic representation of the T-cell receptor-CD3 complex.	43
11	B cell antigen receptor signal transduction cascade.	44
12	Six major metabolic pathways.	46
13	Glycolysis is the predominant source of energy in M1 macrophages.	49
14	In LPS activated M1-like macrophages, TCA cycle is broken in two places — after citrate and after succinate.	50
15	The role of nanoscience and nanotechnology in science and engineering.	51
16	Carbon-based nanomaterials.	53
17	Organic nanoparticles: a – Dendrimers, b – Liposomes, and c – micelles.	54
18	Biomedical applications of AuNPs.	56
19	Lipid structure.	60

20	Three-dimensional projection of dendrimer.	61
21	Chemical structures of several commonly used dendrimer.	62
22	Representation of interaction between amphiphilic dendrimer and siRNA for siRNA deliver.	64
23	Objectives of the thesis.	66
24.	NEW DEAL global methodology	97
25	Identification of nDDSs without cytotoxicity.	139
26	Panel of ex vivo tests assesses the impact of different NMs.	224
27	Evaluation of the direct effect of different NMs on APCs.	228
28	Evaluation of indirect effect of different NMs on APCs.	232

### 3. List of tables

Table	Title	Page
1	Defensive barriers of the innate immune system.	22
2.	Common Innate Immune Recognition Strategies.	24
3	Surface marker expression of cDCs subsets in human and mouse.	31
4	Surface marker expression of pDCs subsets in human and mouse.	32
5	Biomedical application of solid lipid nanoparticles (SLN).	58
6	Biomedical application of nanostructured lipid carriers (NSLC).	59
7	Changes in different secretory molecule production by NMs exposed BMDCs.	233
8	Changes in different secretory molecule production by NMs exposed BMDMs.	233
9	Effect of positive charge on different cellular function.	235

## 4. General Introduction

In the field of nanotechnology, nanoparticles (NPs) are defined as a small object which behaves as a unit with respect to its delivery and other properties. NPs (or Nanopowder or nanocluster or nanocrystal) are microscopic particles with three dimensions less than 100 nm (Khan *et al*, 2019). It is observed that they have quite distinct properties because of their surface structure and small volume-to-surface area ratio, which can impact the solubility, shape, surface reactivity, and aggregation. The smaller the diameter of a spherical particle, the more the surface-to-volume ratio increases, leading to increased chemical reactivity. This greatly affects the interactions with biological structures and living species. Engineered nanomaterials, particularly NPs, have been rapidly developed for the production of a wide variety of objects for a large range of applications, including industrial products, food, agriculture, and health.

Since long time extensive libraries of NPs, composed of an assortment of different sizes, shapes, and materials, and with various chemical and surface properties, have been used in different biomedical applications (McNamara & Tofail, 2017; Mudshinge *et al*, 2011)

As the field of nanotechnology is under constant and rapid growth and new additions continue to supplement these libraries. Owing to the fast-paced growth of nanomaterials, Nanotoxicology has emerged to evaluate safety during in the industrial processes and for the use of products. A functional understanding of the acute and chronic toxicological effects of engineered nanomaterials is not well understood and may represent a significant limitation to the nanomaterial development and application.

The immune system acts as a guardian of the body integrity either directly against exogenous intruders, which can be microbes during infections or indirectly against host cell modifications resulting from external stresses (UV, heat, chemicals, tissue destruction). Along with this task, the immune system ensures tolerance to the host components preventing auto-destruction. Defects in these missions are associated with a wide range of diseases: chronic inflammations, cancers, autoimmunity, and many more.

The immune system includes an innate and an adaptive contribution. The innate immune system is considered as the first line of defense against a foreign pathogen (Chaplin, 2010a). It includes several kinds of phagocytic cells whose main role is to engulf and digest cellular debris, pathogens, particles taken up from their environment. Neutrophils are the most abundant white blood cell in humans and mice, and they are the first immune cells recruited at the site of inflammation in response to chemotactic cues such as CXCL8 (interleukin-8) produced by stressed tissue cells and tissue-resident immune cells like macrophages. Macrophages are a subset of such phagocytes of the innate immune system. They

contribute to a rapid and non-specific defense, efficient against most pathogens (Klopffleisch, 2016). Dendritic cells (DCs) are defined as professional antigen-presenting cells (APCs). These cells act at the interface between innate and adaptive immune systems. After phagocytosis, the main function of these cells is to process and present antigens, associated with class II Major Histocompatibility Complex (MHC-II), to naïve T lymphocytes (LT), a process that may initiate the adaptive immune response. Upon activation by a foreign pathogen, DCs also secrete a wide variety of cytokines, which are implicated in the activation of several lymphocytes, including B, T, and NK cells (Blanco *et al*, 2008). The integrity of innate and adaptive immune cell population is necessary to ensure proper responses to an infection; these cells are thus likely the most relevant experimental models for system for toxicology studies.

Immune cells display a wide range of diversity in response to the microenvironment and adopt different phenotypes. Metabolic profile of these cells plays a very important role in their functions. While lipopolysaccharides (LPS) induced, classically activated cells are pro-inflammatory in nature and display enhanced glycolytic metabolism and take part in direct host-defense against pathogens, such as phagocytosis and secretion of pro-inflammatory cytokines and microbicidal molecules. On the other hand, IL-4 induces alternatively activated cells are anti-inflammatory in nature and show high mitochondrial oxidative phosphorylation (OXPHOS) and play an important role in the regulation of the immune response to parasites as well as allergic reactions (Ley, 2017; O'Neill *et al*, 2016). Growing evidence support the metabolic status of immune cells determines their functions, and perturbations of distinct metabolic networks are implicated in immune cell-associated diseases. In short, alteration of the metabolic profile of a particular cell type could lead to different disease conditions but can also be used to treat a particular kind of disease.

The presented works were designed to provide an accurate evaluation of the impact of some NPs on the immune system. We have selected macrophages and DCs as targets because of the roles in the regulations of the immune responses and the inflammation. The studied NMs are issued from collaborative works in the frame of National or European projects, including **gold nanoparticles (AuNPs)**, **neutral lipid nanoparticles (NLCs)**, **cationic lipid nanoparticles (CLCs)**, and **Amphiphilic dendrimers (ADs)**. We analyzed the toxicity, the functions, and the metabolic pathways of the exposed cells. Effects on macrophage and dendritic cell metabolism could lead to modifications in their respective functions that may propose cell reprogramming using NPs in the frame of novel therapeutic approaches for the treatment of inflammatory diseases. For this reason, we analyzed whether exposure to subtoxic doses of these nanoparticles leads to the alteration of the functions of the cells. We evaluated the effect of NPs on (1) Macrophages and DCs

metabolism, (2) Macrophages and DCs activation, (3) cytokine production, (3) Redox profile, (4) the phagocytic capacity of macrophages, and (5) T cell activation by DCs (Figure 1).

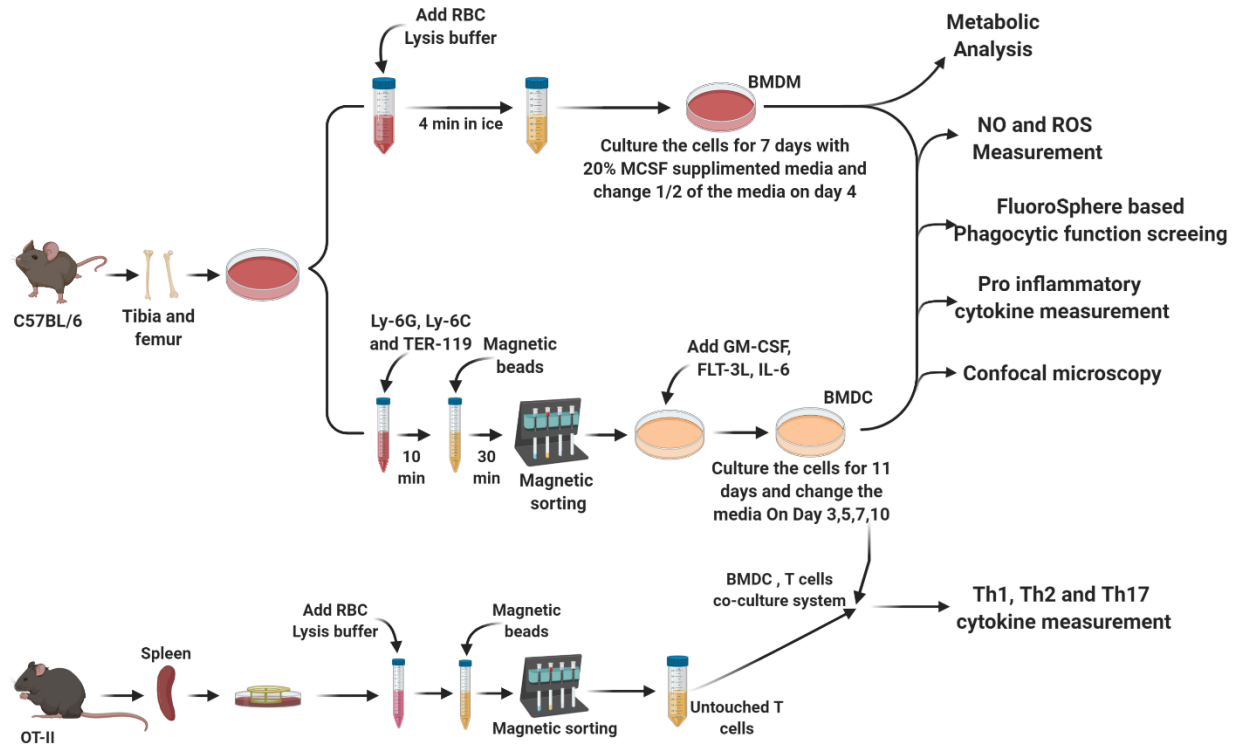


Figure 1: Immunotoxicity assessment (Created with BioRender.com) BMDMs and BMDMs were cultured from mouse BM for 11 and 7 days, respectively. After harvesting, the cells were seeded either in 12, 24, or 96 wells plates from Falcon® or Seahorse XFe96 cell culture with AuNPs at 10 and or 50 µg/mL final concentrations. After 24 h of cell culture, cells were washed and stimulated with LPS or IL-4 for 24 h, and several downstream experiments were conducted according to the protocol.

In this manuscript, in the first part, I describe 1) The immune system and some of its components, 2) The importance of the metabolism governing different immune cell functions, and 3) A summary of different nanoparticles used in the study, including their usage for the treatment and the diagnosis of different diseases as well as their known impact on the immune system. In the second part, I present the results in the format of journal publications. Finally, a common discussion is presented at the end of the manuscript.

## 5. Immune System: Art of War

### 5.1 Introduction

Study of strategic warfare has shown that a detailed understanding of the enemy and one's own temperament is key to victory – by preparation, strategy, and carefully guided execution. Interestingly, all living organisms are connected with each other through a chain of interactions. Although many of them are harmless, some are not. Therefore, every living organism has developed a mechanism for identifying and neutralize threats from other species, commonly known as the “immune system.” Likewise, in constant battle between metazoans and pathogenic invaders, evolution developed a strong “immune system” based on discrimination between self and infectious/pathogenic non-self (Buchmann, 2014).

To fight the intruders of the immune system developed a highly effective arsenal of weapons through integrated systems broadly categorized as ‘innate’ or ‘adaptive’ immunity. Innate immunity, a primitive immunological mechanism for fighting against an intruding pathogen, recognizes the pathogenic non-self through a fixed number of germ-line-encoded receptors, which recognize structural components of microorganisms and viruses (Chaplin, 2010b). This achieves the “immediate immune response,” which is triggered within minutes or hours of an attack. Adaptive immunity has been acquired during evolution by vertebrates and cartilaginous fishes, allowing specific immune responses towards molecular targets called antigens. The specificity relies on the clonal expansion of antigen-specific effector cells (B or T cells) selected for the expression of an antigen receptor (immunoglobulin and T cell receptor (TCR), respectively), which is generated by an original mechanism of gene rearrangements (Smith et al, 2019). This enables the host to mount a specific immune response towards a large panel of targets. Furthermore, the immune system keeps memory of the specific immune allowing quick response in the case of secondary exposure to the antigens.

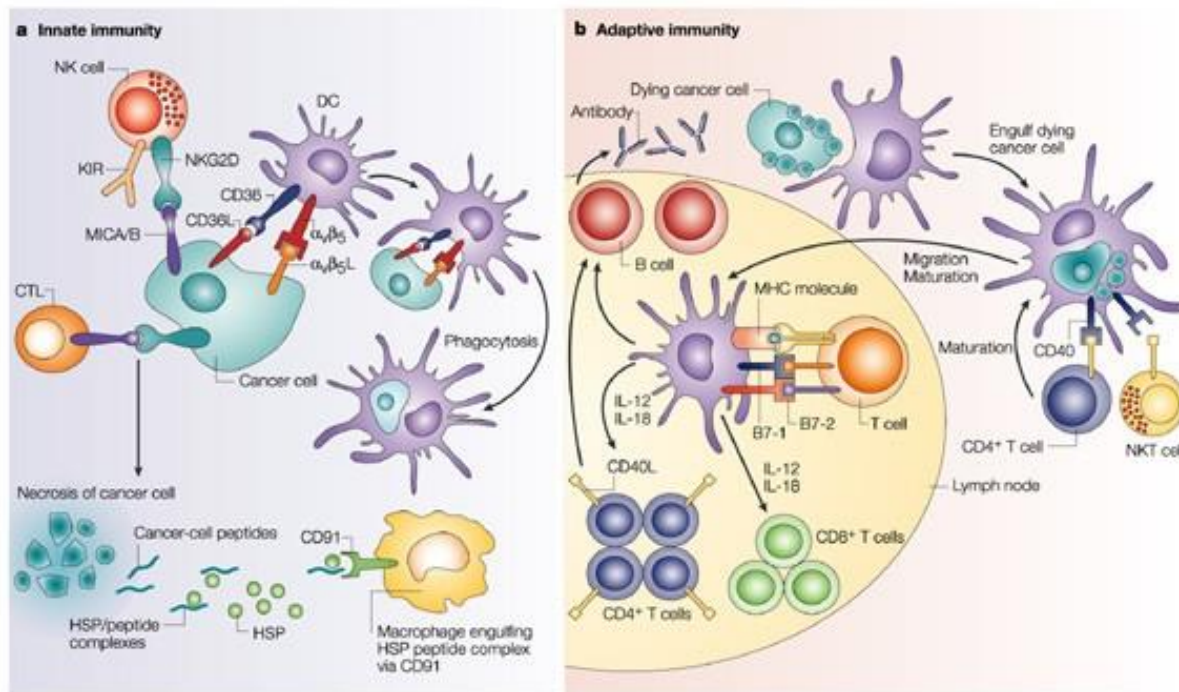


Figure 2: The components of the innate and adaptive immune system. The innate immune system act as the first line of defense against infections. It consists of soluble factors such as complement system and various cellular components, including granulocytes (basophils, eosinophils, and neutrophils), mast cells, macrophages, dendritic cells, and natural killer cells. The adaptive immune system takes time to respond but manifests as increased antigen specificity and memory. It consists of antibodies, B cells, and CD4<sup>+</sup> and CD8<sup>+</sup> T lymphocytes. Natural killer T cells and  $\gamma\delta$  T cells are cytotoxic lymphocytes that come at the interface of innate and adaptive immunity. (Adapted from (Dranoff, 2004))

## 5.2 Innate Immune response

The innate immune system is the first line of defense against the intruders. The system responds in the same way to all germs and non-self-agents. That is why the innate system is also known as a “non-specific immune system.” Pathogens often enter through epithelial barriers such as the skin, gut, or respiratory tracks. The innate immune system could stop the intruders either by providing physical protection to the host by the skin and mucous membrane or by its specialized cellular system (defense system) and proteins. Based on the type of defense barrier, the innate immune system can be classified into two categories (1) anatomic (epithelium and mucous membrane) and physiologic (temperature, low pH, and chemical mediators) barrier (2) endocytic and phagocytic barriers.

Table 1 summarizes the non-specific host-defense mechanisms for each of these barriers (Marshall et al, 2018).



Defensive barriers	Mechanism of action
Anatomic and Physiologic barrier	
Epithelium	<ul style="list-style-type: none"> <li>• Mechanical barrier retards entry of microbes</li> <li>• Acidic environment (pH 3–5) retards growth of microbes</li> </ul>
Mucous membrane	<ul style="list-style-type: none"> <li>• Normal flora competes with microbes for attachment sites</li> <li>• Mucous entraps foreign microbes</li> <li>• Cilia propel microbes out of body</li> </ul>
Temperature	<ul style="list-style-type: none"> <li>• Body temperature/fever response inhibits growth of some pathogens</li> </ul>
Low pH	<ul style="list-style-type: none"> <li>• Acidic pH of stomach kills most undigested microbes</li> </ul>
Chemical mediators	<ul style="list-style-type: none"> <li>• Lysozyme cleaves bacterial cell wall</li> <li>• Interferon induces antiviral defences in uninfected cells</li> <li>• Complement lyses microbes or facilitates phagocytosis</li> </ul>
Phagocytic and endocytic barriers	
	<ul style="list-style-type: none"> <li>• Tissue damage and infection induce leakage of vascular fluid containing serum protein with antibacterial activity, leading to influx of phagocytic cells into the affected area</li> <li>• Various cells internalize (endocytosis) and break down foreign macromolecules</li> <li>• Specialized cells (blood monocytes, neutrophils, tissue macrophages) internalize (phagocytose), kill and digest whole organisms</li> </ul>

Table 1: Defensive barriers of the innate immune system (Adapted from (Marshall et al., 2018))

### 5.2.1 Anatomic and Physiologic barriers

All the outer and inner surfaces of the organism act as a mechanical barrier and physically block the pathogens to invade. Skin is the single most crucial mechanical barrier of our body. The outer surface of the skin, known as the epidermis, prevents the pathogens from penetrating into the body. Other than skin, another crucial mechanical barrier of the innate system is the mucous membrane. These membranes line the gastrointestinal, urinary, respiratory, and reproductive tracts and prevent intruders' entry by a slimy mucous layer.

While the anatomical barrier physically blocks pathogens from entering the body. On the other hand, physiological barriers protect the body by maintaining body temperature, pH, and various soluble secretory products against a foreign pathogen.

### 5.2.2 Phagocytic and endocytic barriers

If a pathogen passes through physical barriers, the innate immune system activates specialized immune cells and proteins to take care of the intruder.

For healthy survivability, multicellular organisms must identify dead or alive cells and the entry of microorganisms. To do that, they have developed several surveillances, defense / and repair mechanisms. In 1989, Charles Janeway Jr. suggested that the presence of a set of receptors expressed by innate immune cells is responsible for identifying the conserved products of microbial origin (Janeway, 1989). After 25 years of extensive studies, intensive debates, and a Nobel Prize on this topic, it is unquestionable that Janeway's brilliant idea has changed the entire understanding of the immune system. Later on, his idea has led to the identification of so-called Pattern Recognition Receptors (PRRs), proteins responsible for recognizing molecules that are associated with pathogens (such as Pathogen-Associated Molecular Patterns—PAMPs). In mammals, PRRs can be grouped into at least five major categories: toll-like receptors (TLRs), retinoic acid-inducible gene I (RIG-I)-like receptors (RLRs), C-type lectins (CLRs), nucleotide oligomerization (nod)-like receptors (NLRs), and non-melanoma 2 (AIM2)-like receptors (ALRs)(Jang *et al*, 2015).

Another fantastic idea came from Polly Matzinger (Matzinger, 1994), who suggested that the immune system is less concerned with the origin of antigens (self vs. non-self) than with their interaction with our body (tissue damage vs. tissue homeostasis). In her "Danger Theory," Matzinger proposed that endogenous molecules are released or activated during tissue stress or damage and trigger or propagate the inflammatory response, which signals antigen-presenting cells to initiate the adaptive immune response. Today, the molecules described in her danger theory is known as DAMPs (Damage-Associated Molecular Patterns).

At least three broad-spectrum strategies are used by the innate immune system to identify the dead or alive cells and the entry of foreign intruders (

Table 2) (Jang *et al.*, 2015; Turvey & Broide, 2010).

1. The innate immune system depends on a series of germline-encoded receptors to recognize 'microbial non-self.' These include components of microbial membranes, cell walls, proteins, and DNA and are termed pathogen-associated molecular patterns (PAMPs).
2. The innate immune system detects immunological 'danger' in the form of DAMPs. DAMPs represent typical metabolic by-products produced in the process of infection and inflammation (Bianchi, 2007).
3. Innate immune receptors detect "missing self" – molecules expressed by healthy cells but not expressed by infected cells or microorganisms. This inhibitory system is dependent on NK cells. Inhibitory receptors specific for self-MHC class I molecules play a crucial role in missing-self

recognition by NK cells, ensuring NK cells preferentially attack infected cells that downregulate their Major Histocompatibility Class I Proteins (MHC-I) (Joncker & Raulet, 2008)

Innate Immune Recognition Strategy	Receptor Families	Specific examples	
		Receptor	Ligand
Detecting 'microbial non-self' (i.e. PAMPs)	Toll-like receptors	TLR 1	Triacyl lipopeptides
		TLR 2	Di-/triacyl lipopeptides, Multiple lipoproteins, Lipoteichoic acid, Zymosan (fungi)
		TLR 3	dsRNA (virus)
		TLR 4	LPS
		TLR 5	Flagellin
		TLR 6	Triacyl lipopeptides
		TLR 7	ssRNA (virus)
		TLR 8	
		TLR 9	Unmethylated CpG DNA
	NOD-like receptors	NOD2	Muramyl dipeptide
		IPAF	Flagellin (intracellular)
	Collectin family	MBP	Microbial terminal mannose residues
Detecting common metabolic consequences of cell infection or injury (i.e. DAMPs)	NOD-like receptors	NOD1, NOD2, NLRP3 (or NALP3)	Peptidoglycan (Gram- positive and negative bacteria) Uric acid, K <sup>+</sup> efflux, ATP
	RAGE (receptor of advanced glycation end product) family		
Detecting 'missing self'	MHC-class-I-specific inhibitory receptors	KIR	Self MHC class I (inhibitory signal)
		CD94-NKG2A heterodimers	Self MHC class I (inhibitory signal)

Table 2: Common Innate Immune Recognition Strategies. (Adapted from (Jang et al., 2015; Turvey & Broide, 2010))

Intruders can be recognized and stopped by specialized cells. The most important cells that take part in recognizing and stopping foreign intruders are known as phagocytes. Phagocytes are special kinds of scavenger cells that use phagocytosis to engulf bacteria, foreign particles, and dying cells to protect the

body. They engulf pathogens and internalize them in a phagosome, which acidifies and fuses with lysosomes to destroy the contents. This mechanism is used by the immune system to remove potentially pathogenic material. The three most important phagocytic cells are neutrophils, monocytes/macrophages, and dendritic cells in the immune system.

#### *5.2.2.1 Neutrophils*

Neutrophils are the most abundant group of granulocytes in the blood and essential for acute inflammation. Notably, they are the first immune cells to arrive at the site of infection. Neutrophils are short-lived cells, and they usually undergo self-destruction followed by phagocytosis and the use of their granules. That is why they are the main component of pus seen with infection. Neutrophils produce significant amounts of antimicrobial peptides, enzymes, and reactive oxygen species to kill bacteria.

Additionally, they also produce enzymes involving tissue remodeling and repair after injury. Substantial quantity of neutrophil accumulation at the site of bacterial infection and tissue injury ensure the destruction and degradation of microbes and other antigenic materials. Therefore, it is clear that neutrophil plays an essential role in the clearance of microbial pathogens and repair of tissue injury. Neutrophils are also crucial for initiating inflammation and recruiting other inflammatory cells by producing a large quantity of cytokines, Tumor Necrosis Factor (TNF) and interleukin-12 (IL-12), as well as specific chemokines (Chaplin, 2010b). This indicates an immunoregulatory role of neutrophils. Compared to neutrophils, eosinophils and basophils have lower phagocytic capacity and act mainly by releasing enzymes, toxic compounds, and pro-inflammatory, to eliminate the pathogens.

The other group of granulocytes are eosinophils and basophils. Eosinophils have prominent cytoplasmic granules that contain toxic molecules and enzymes that are especially active against helminths and other parasites. IL-5 stimulates the development of bone marrow-derived eosinophils and supports their survival in peripheral tissues, making them productive in most allergic responses (Chaplin, 2010b).

Basophils and mast cells are morphologically similar, but they represent distinct lineages. Based on the cell surface receptors for IgE (FcεRI), they are the main initiators of immediate hypersensitivity responses and host response to helminthic parasites, releasing histamine and other preformed mediators from their granules and generating large quantities of lipid mediators that induce tissue inflammation, edema, and smooth muscle contraction. Interestingly, Mast cells and basophils can release IL-4, indicating that they can play important roles in allergic immune responses (van Panhuys et al, 2011).

### 5.2.2.2 Monocytes and macrophages

Monocytes are phagocytes found in the bloodstream. They circulate throughout the body, exit the circulation, and enter into infected or inflamed tissue. In the tissue, they differentiate into macrophages, which form the major resident population of phagocytes in healthy tissues. Both monocytes and macrophages are highly phagocytic for microbes and particles that have been marked for clearance by binding Ig and/or complement. More precisely, complement C3b and the IgG Fc fragment allow better uptake of opsonized particles. They arrive at the site of infection immediately after neutrophil mobilization, and in case of chronic inflammation and infection, they remain at the site for an extended period.

Based on the activating signal that initiates the differentiation of immature precursor cells to active macrophages, macrophages can adopt one of several phenotypes (Benoit *et al*, 2008). For example, classically activated M1 macrophages produce large amounts of pro-inflammatory cytokines such as IL-1, IFN- $\gamma$ , IL-6, IL-12, TNF to fight against infection or tissue stress by activating several antimicrobial mechanisms. M1 macrophages also produce reactive oxygen species (ROS) and nitric oxide (NO) to kill microbial pathogens. These ROS and NO are highly toxic to microorganisms but also nearby cells. Therefore, the synthesis of these compounds must be highly regulated (Nathan & Ding, 2010). Alternatively, activated M2 macrophages carry out this regulation. Alternatively activated macrophages are induced by IL-4, IL-10, or IL-13, especially in the presence of glucocorticoid hormones, and express anti-inflammatory functions through their production of IL-10, the IL-1 receptor antagonist, and transforming growth factor  $\beta$  (TGF- $\beta$ ) (Gordon, 2003). TGF- $\beta$ 1 stimulates the differentiation of fibroblasts into myofibroblasts, increases the synthesis of collagen by these myofibroblasts, and induces the Tissue Inhibitor of Metalloproteinase (TIMP, which inhibits the degradation of the extracellular matrix by metalloproteinase). Finally, M2 produces Platelet-Derived Growth Factor (PDGF), promoting the proliferation of myofibroblasts (Wynn, 2008). It is important to consider that the macrophage acts in cooperation with many other cells of the immune system (Nish & Medzhitov, 2011).

Thus, primary activation by a PAMPs is to induce the synthesis of interleukin 12 (IL-12) as well as expression of distinct adhesion molecules such as LFA-3 (CD58), lymphocyte function-associated antigen (LFA)-1 (CD11a), intercellular adhesion molecule (ICAM)-1 (CD54), ICAM-2 (CD102) and costimulatory molecules B7.1 (CD80), B7.2 (CD86), or CD40 (Fröhlich, 2015b) (Figure 2). Altogether, the activation signal initiates the processing of cytosolic proteins to be presented by MHC I or MHC II to activate T cells.

PAMPs dependent, macrophage-mediated activation of T cells initiate CD4 + Helper 1 (Th1) response. These T cells secrete IFN- $\gamma$ , which stimulates the antibacterial activity of M1 macrophages, making a positive feedback loop. In contrast, IL-4 production during a response mediated by CD4 + Helper 2 (Th2) cells induces a macrophage polarization towards the M2 phenotype and local proliferation of macrophages, allowing a self-renewal of macrophages without recruiting the bone marrow monocytes (Jenkins *et al*, 2011). Similarly, the production IL-4 by granulocytes (mainly by polymorphonuclear eosinophil) seems to be necessary for M2 polarization in adipose tissues (Figure 3) (Wu *et al*, 2011).

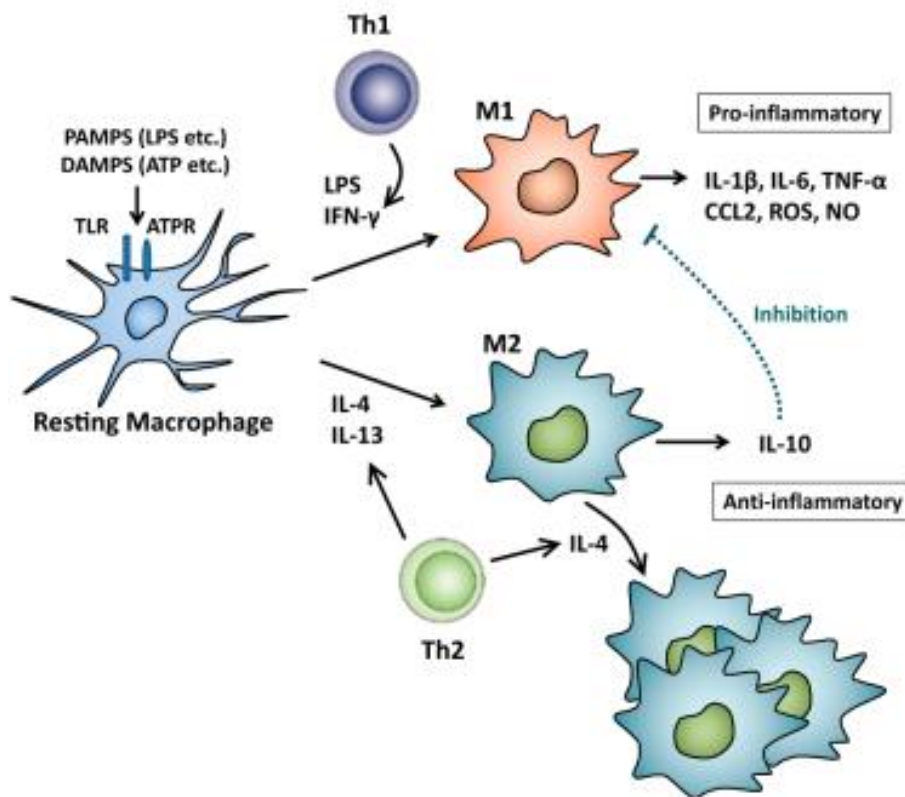


Figure 3: The polarization of macrophages depends on the factors present in their environment. M1/M2 paradigm of microglia and their immunoregulatory functions. Microglia are resident macrophage cells responsible for primary active immune defense in the central nervous system (CNS). PAMPs or DAMPs stimulates resting microglial cells through TLR or ATP receptors. In the presence of LPS and/or IFN $\gamma$ , microglial cells polarize to the M1 phenotype and produce a variety of pro-inflammatory cytokines/mediators like IL-1 $\beta$ , IL-6, TNF-5-007, CCL2, ROS, and NO. Conversely, IL-4 and IL-13 induce alternatively activated microglia, known as M2 ('M2 $\alpha$ ') phenotype, play a role in the downregulation of M1 functions by anti-inflammatory cytokine, IL-10. (Adapted from (Nakagawa & Chiba, 2014))

### 5.2.2.3 Dendritic cells (DCs)

DCs are heterogeneous populations of phagocytic cells of hematopoietic origin, except the follicular DCs, which are of mesenchymal origin. They are important innate immune cells that build a bridge between the

innate and adaptive immune systems. Immature DCs circulate throughout the bloodstream and tissue and continuously sample the pathogens via micropinocytosis. The existence of numerous cytoplasmic projections from their surface gives them a wide surface area to volume ratio that allows close contact with multiple cells. These processes look similar to the dendrites of neurons, which gave dendritic cells their name.

Although DCs are well known phagocytic cells, DCs mainly specialize in the capture and presentation of antigens to T lymphocytes, to activate the adaptive response. DCs are the only cells capable of initiating the response of naive T lymphocytes. That is why they are called "professional" antigen-presenting cells.

To initiate a T cell response, DCs are equipped with major histocompatibility complex (MHC) and different co-stimulatory molecules necessary for the activation of naive T lymphocytes. They also secrete a large panel of chemokines involved in the attraction of other effector cells of the immune system at different phases of the inflammatory response (Piqueras *et al*, 2006). Among them, IL-12, IL-10, IL-23, ICOS-1, and OX-40 are involved in the T cells' polarization in Th1, Th2, Th17, or T reg.

DCs originate from the hematopoietic stem cells of bone marrow. Three DCs precursors are recognized in humans: granulocyte, monocyte, and DCs progenitors (GMDCPs), monocyte and DCs progenitors (MDCPs), and common DCs progenitors (CDCPs). When cells differentiate, they acquire various phenotypes. It is known that they originate from CDCPs in the presence of Flt3-L, cDC1, cDC2, and pDCs. It has been established that there are many precursors in the mouse: CMPs, MDCPs, and CDCPs. CDCPs divide into pre-cDCs and pre-pDCs. Pre-cDCs give rise to pre-cDC1 and pre-cDC2, which later differentiate into cDC1 and cDC2, respectively. Pre-pDCs develop into pDCs (Figure 4) (Castell-Rodríguez *et al*, 2017). To simplify, a few examples of DCs subtypes are explained below.

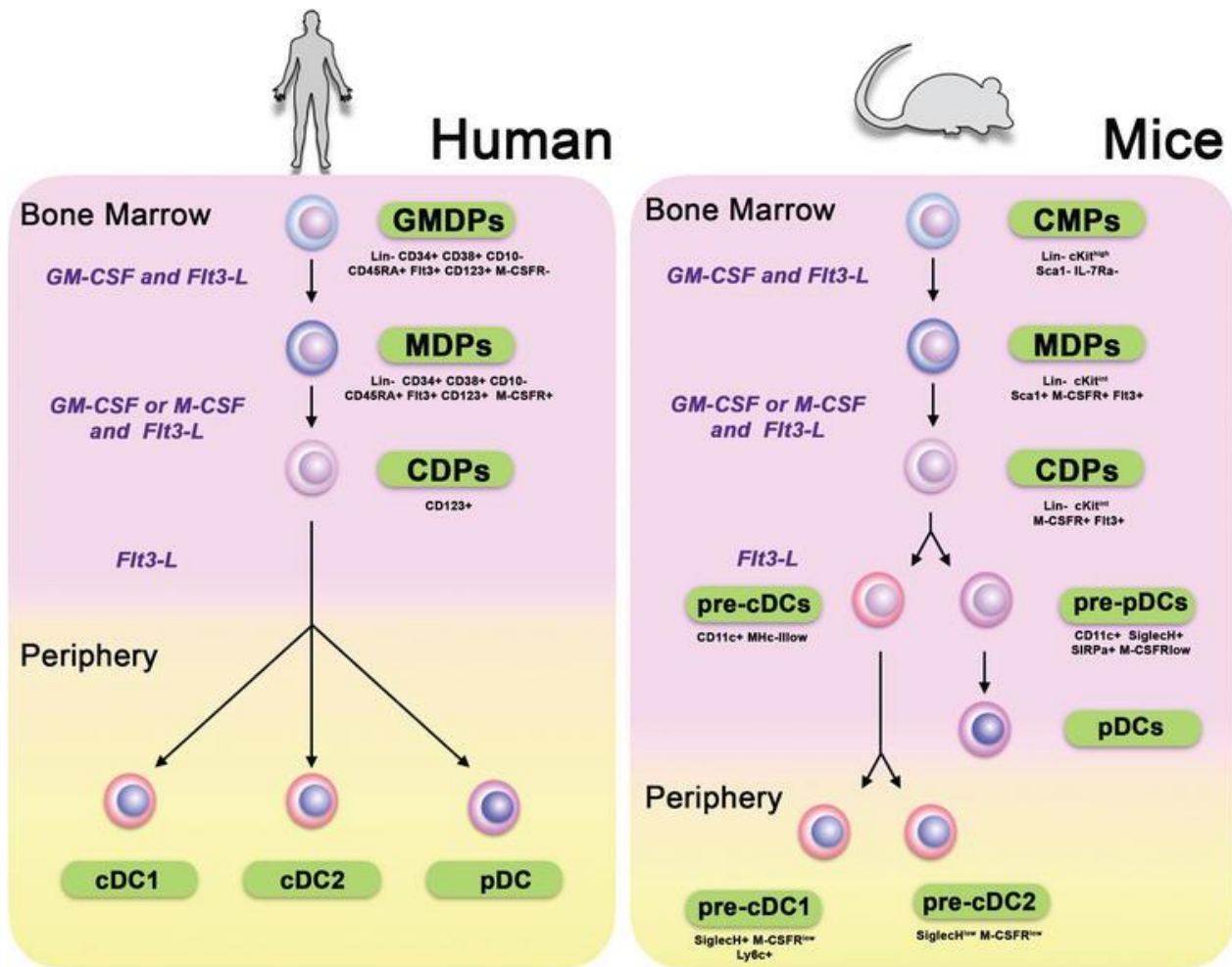


Figure 4: Classification of DCs in humans and mice. Three DCs precursors are recognized in humans: GMDPs, MDPs, and CDPs. In mice, there are many precursors, namely CMPs, MDPs, and CDPs. CDPs divide into pre-cDCs and pre-pDCs. Pre-cDCs give rise to pre-cDC1 and pre-cDC2, which later differentiate into cDC1 and cDC2, respectively. Pre-pDCs develop into pDCs. Phenotypes of each cell and cytokines involved in the development process include all myeloid progenitors (CMPs), macrophages and dendritic cells progenitors (MDPs), common myeloid progenitors (CDPs), granulocytes, macrophages and DCs progenitors (GMDPs), pre-conventional dendritic cells (pre-cDCs), pre-plasmacytoid dendritic cells (pre-pDCs), pre-conventional dendritic cells 1 (pre-cDC1), pre-conventional dendritic cells 2 (pre-cDC2), conventional dendritic cells 1 (cDC1), conventional dendritic cells 2 (cDC2), plasmacytoid dendritic cells (pDCs). (Adapted from (Castell-Rodríguez et al., 2017))

#### Conventional myeloid dendritic cells (mDCs):

To date, the development of DCs in bone marrow is well characterized in mice than in humans. Myeloid dendritic cells (mDCs) originating from CDPs are a group of professional antigen-presenting cells, responsible for identifying, processing, and presenting antigens to T cells. Morphologically, mDCs bear long dendrites. They are found in peripheral tissues, secondary lymphoid organs (spleen, lymph nodes, Peyer's patches, thymus), and blood and have a strong migratory capacity. They express TLRs 1 to 8 and TLR10 but not TLR9 (Jarrossay *et al*, 2001). These mDCs are also known as conventional DCs (cDCs). They are classified by their discrete roles and transcriptional identities and comprise two major subsets known as type 1 cDCs



(cDC1s) and type 2 cDCs (cDC2s). The difference between cDC1 and cDC2 subsets is supported by their distinct genetic signature, which is essential for defining the specific functions of the cDC subsets (Guilliams *et al*, 2014).

The pro-inflammatory function of mDCs involves the production of inflammatory molecules and to prime the pro-inflammatory subsets of effector T cells. On the other hand, tolerogenic mDCs, counter inflammation by disrupting the activity of pro-inflammatory T cells and macrophages as well as by inducing immunosuppressive regulatory T cells. Differentiation of mDCs to acquire proinflammatory or regulatory phenotype depends on the surrounding microenvironment (Figure 5).

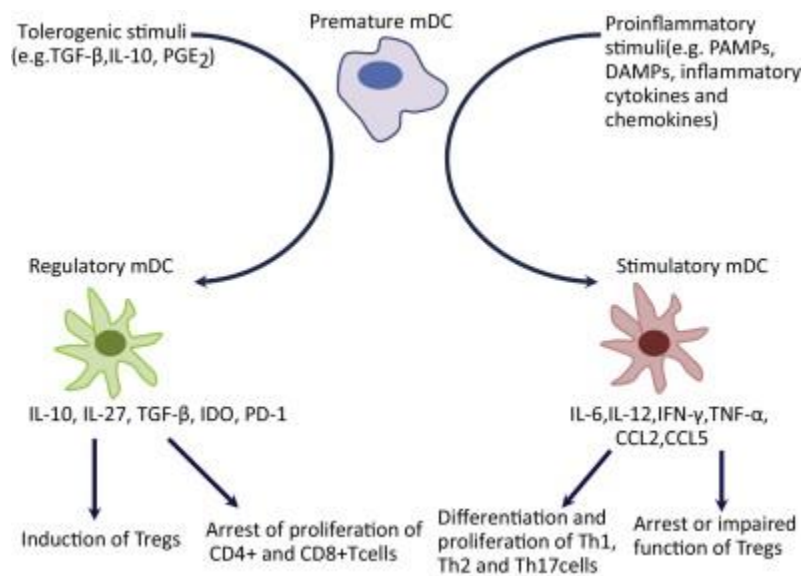


Figure 5: Differentiation of mDCs to acquire pro-inflammatory or regulatory phenotype depends on the surrounding microenvironment. The pro-inflammatory function of mDCs involves the production of inflammatory molecules and prime the pro-inflammatory subsets of effector T cells. On the other hand, tolerogenic mDCs, counterbalance inflammatory signals by regulating the activity of pro-inflammatory T cells, macrophages, and by activating immunosuppressive regulatory T cells (Adapted from (Chistiakov *et al*, 2015).

More specifically, cDC1s are mainly involved in regulating cytotoxic T lymphocytes (CTLs) as they present exogenous, cell-associated antigens to CD8 + T cells. On the other hand, the cDC2 subset takes part in immune responses involving extracellular pathogens, parasites, and allergens by presenting the soluble antigens to CD4+ T cells (Vu Manh *et al*, 2015).

Although mouse and human mDCs share many evolutionarily conserved molecular pathways, they show some distinct differences in terms of the expression of their surface markers. Murine counterparts of human cDCs are shown in

Table 3 (Robbins *et al*, 2008).

Dendritic cell subset	Surface markers	
	Human	Mouse
cDC1	CD1c/BDCA-1 <sup>+++</sup> CD11c <sup>++</sup> TLR2 <sup>+++</sup> TLR4 <sup>+++</sup>	CD11b <sup>+++</sup> CD209a <sup>+</sup> Tlr7 <sup>+</sup> Tlr9 <sup>+</sup> Tlr12 <sup>+++</sup> Tlr13 <sup>+++</sup>
cDC2	CD141/BDCA-3 <sup>+++</sup> CD11b <sup>-</sup> CD11c <sup>++</sup> CLEC9A <sup>+</sup> XCR1 <sup>+</sup> TLR3 <sup>+++</sup> TLR10 <sup>+++</sup>	CD8α <sup>+++</sup> Clec9a <sup>+++</sup> Xcr1 <sup>+</sup> Ly75 <sup>+++</sup> Tlr3 <sup>++</sup> Tlr11 <sup>+++</sup>

Table 3: Surface marker expression of cDCs subsets in human and mouse (Adapted from (Robbins *et al.*, 2008)).

#### Plasmacytoid dendritic cells (pDCs):

pDCs have an eccentric nucleus and prominent endoplasmic reticulum and Golgi (resembling a plasma cell) for the production of type I interferon. In the inactive state, these cells look like plasma cells, round with a large cytoplasm; hence they are called Plasmacytoid DCs. pDCs are the majority subtype of blood DCs (0.4% of leukocytes) and are found in secondary lymphoid organs but not in peripheral tissues, unlike mDCs. Unlike mDCs, CD11c, CD33, CD11b, or CD13 markers are not expressed by pDCs (Dzionek *et al.*, 2000; Dzionek *et al.*, 2001; MacDonald *et al.*, 2002). These cells have a very strong migratory capacity and are involved in the recognition and presentation of viruses. During stimulation by viruses (Cella *et al.*, 2000; Kadowaki *et al.*, 2000) or by interleukin-3 (IL-3) and CD40L (Grouard & Clark, 1997), these pDCs change in morphology and acquire dendrites similar to mDCs. They are characterized by the expression of α chain of IL-3 receptor (CD123), of the type C lectin BDCA-2 (CD303), and neuropilin-1 (CD304 or BDCA-4). However, they do not express the markers typical of mDCs such as CD13 or CD33. Similarly, CD11c and MHC-II are less present on the surface of pDCs than mDCs. The pDCs also express TLRs 1, 6, and 10, and more specifically, TLR7, and 9 (Jarrossay *et al.*, 2001; Kadowaki *et al.*, 2000). These cells are also capable of secreting large quantities of type I interferon (IFN-α, IFN-β, and IFN-λ) in response to viruses and TLR7 and 9 stimuli.

Although Mouse and human mDCs share many evolutionarily conserved molecular pathways, but they differ in surface marker expression. Murine counterparts of human cDCs are shown in

Table 4 (Robbins *et al.*, 2008).

Dendritic cell subset	Surface markers	
	Human	Mouse
pDC	CD11c <sup>+</sup> CD123 <sup>+</sup> BDCA-2 <sup>+++</sup> BDCA-4 <sup>+++</sup> TLR7 <sup>+++</sup> TLR9 <sup>+++</sup> CD1c <sup>low</sup> CD141c <sup>low</sup>	CD11c <sup>+</sup> B220 <sup>+</sup> mPDCA-1 <sup>+++</sup> CD11b <sup>-</sup> Clec12a <sup>+++</sup> SiglecH <sup>+++</sup> Tlr7 <sup>+++</sup> Tlr9 <sup>+++</sup>

Table 4: Surface marker expression of pDCs subsets in human and mouse (Adapted from ((Robbins et al., 2008)).

#### Monocyte-derived inflammatory DCs:

During inflammation, monocytes can develop into a particular subtype called inflammatory DCs. Inflammatory DCs express both CD1a, CD1c, and the mannose CD206 receptor. These cells produce the cytokines IL-1 $\beta$ , TNF- $\alpha$ , IL-6, and IL-23 and primarily activate the Th17 responses. In mice, inflammatory DCs were initially demonstrated in leishmaniasis and associated with other infections and inflammatory settings (Segura & Amigorena, 2013). In humans, inflammatory myeloid cells are reported in several disease conditions, including eczema, psoriasis, skin sensitization, allergic rhinitis, coeliac diseases, inflammatory bowel disease, and peritonitis (Segura *et al*, 2013). This subpopulation of DCs is still needed to be explored.

### 5.3 Adaptive Immune response

The activation of the adaptive immune system (AIS) is dependent on the actions of the innate immune system and is crucial when innate immunity is not able to destroy the foreign intruder. AIS is always fascinating to immunologists because it offers a specific yet incredibly diverse system that can fight foreign intruders and has a 'memory' — the key to vaccination — which enables a rapid response to previously encountered pathogens.

AIS in mammals, which is centered on lymphocytes bearing antigen receptors, are generated by somatic recombination and appeared approximately 500 million years ago in jawed fish (Flajnik & Kasahara, 2010b). This dynamic network of defense system consists of several molecules, mechanisms, and tissues that are not present in jawless vertebrates.

Genetic information for the immunoglobulin polypeptide chain is found in the genome of the germ-line cell in several gene segments distributed along the chromosome. During bone marrow-derived

lymphocytes development, these gene fragments are recombined, leading to the formation of a functional gene (Tonegawa, 1983).

The accuracy of adaptive immunity is accomplished by the proliferation of lymphocyte clones that bear immunoglobulin receptors for antigens of the pathogen and that are selected accordingly from an enormous pre-existing repertoire of cells with diverse receptors. Discovery of antibody answered the major questions relating to the generation of diversity lymphocyte clones in the 1970s with the detection of somatic hypermutation and variable–diversity–joining rearrangement (VDJ rearrangement) of antibody (or immunoglobulin (Ig) or B cell receptor (BCR)) genes (Maki *et al*, 1980).

T cell receptors (TCRs) were reported in the 1980s (Hedrick *et al*, 1984) , and there was universal agreement that they shared a common ancestor with BCR genes. The three components (V, D, and J) of the variable regions of the TCRs and the BCRs are each encoded in several genomic copies. However, the recombination of V(D)J segment brings them together in a single exon and, in the process, introduces numerous small insertions and deletions at the junctions, generating the vast combinatorial diversity necessary to manage the enormous diversity of antigens. Recombination Activating Genes 1 and 2 (Rag1 and Rag2) encode the key enzyme required to develop the highly diversified antigen receptor repertoire of adaptive immunity (Schatz *et al*, 2008).

The advent of the recombination-activating gene (RAG) transposon and two rounds of full genome replication are the primary reason for the appearance of AIS to support the mammalian defense system (Flajnik & Kasahara, 2010b).

The key features of AIS are:

1. The recognition of specific “non-self” antigens and distinguishing them from “self” antigens.
2. The generation of pathogen-specific immunologic response to eliminate specific pathogens or pathogen-infected cells.
3. The development of an immunological memory that can quickly eradicate a specific pathogen upon reinfection.

The adaptive immune system is made up of (Figure 6):

1. T lymphocytes
2. B lymphocytes

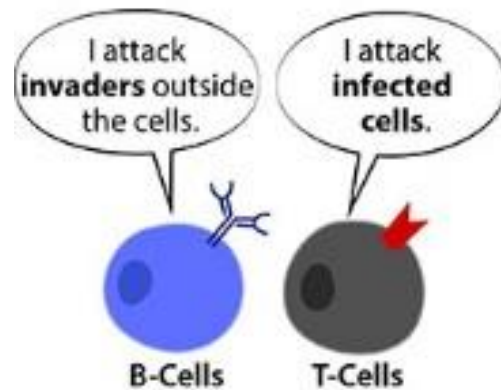


Figure 6: Story of Adaptive immune system (Adapted from "[Dr. Biology. \(2011, February 16\)](#)")

### 5.3.1 T Lymphocytes

T lymphocytes (also called T cells) are derived from hematopoietic stem cells in the bone marrow and then migrate to the thymus through the bloodstream, where they mature. As these cells mature in the thymus, that is why they are known as T cells. These cells express a set of unique antigen-binding receptors on their membrane, identified as the T-cell receptor (TCR). Each T-cell expresses a single form of TCR capable of rapid proliferation and differentiation if it receives the appropriate signals. For activation, T cells need the intervention of APCs (usually dendritic cells but also macrophages, B cells, fibroblasts, and epithelial cells) to recognize a particular antigen.

Three main functions performed by T cells are:

1. T cells use chemical messengers to trigger other immune cells to initiate the adaptive immune system (T helper cells).
2. T cells recognize and kill tumor cells and virus-infected cells (cytotoxic T cells).
3. Once the primary response is over, certain T cells become memory T cells. They can "memorize" which antigens were recognized and so that they could readily activate the adapted immune system for subsequent new exposure by the same antigens.

## T Cell subsets

While all T cells follow the fundamental aspects of thymic development and the activation mechanisms, there is a remarkable heterogeneity of effector functions that are triggered in response to stimulation.

T cells can be broadly classified on the basis of CD4 or CD8 expression on their surface. In the thymus, most developing T cells obey a pattern of development in which they first express neither CD4 nor CD8 (double negative) in the cortex and then express both CD4 and CD8 (double-positive [DP])(von Boehmer *et al*, 1989)(Figure 7). DP cells are screened in the thymic cortex through positive selection, and those that are selected on the basis of MHC-I molecules become CD4-CD8 +, and those selected on the basis of MHC-II molecules become CD4+CD8-. The fact that the CD4 molecule facilitates a stable interaction between the developing T cell and the MHC-II molecules on the selecting APCs while the CD8 molecule establishes communication between T cells and MHC-II molecules is fundamental to the association of CD4 with MHC-II restricted antigen recognition and of CD8 with MHC-I restricted antigen recognition. Cells that survive positive selection migrate to the thymic medulla for negative selection and move to the periphery. 60–70% of T cells in the blood and secondary lymphoid organs are CD4+CD8- (CD4 +) and 30–40% are CD4-CD8 + (CD8 +). The largest T cell population in the body is the CD4+  $\alpha\beta$  TCR population. During their thymic development,  $\alpha\beta$  T cells divide into distinct subpopulations, each with specified effector function repertoires. They can function as helper cells, delivering cognate (including direct cell contact) or cytokine signals to maximize both B- and T-cell responses, as well as triggering mononuclear phagocytes.

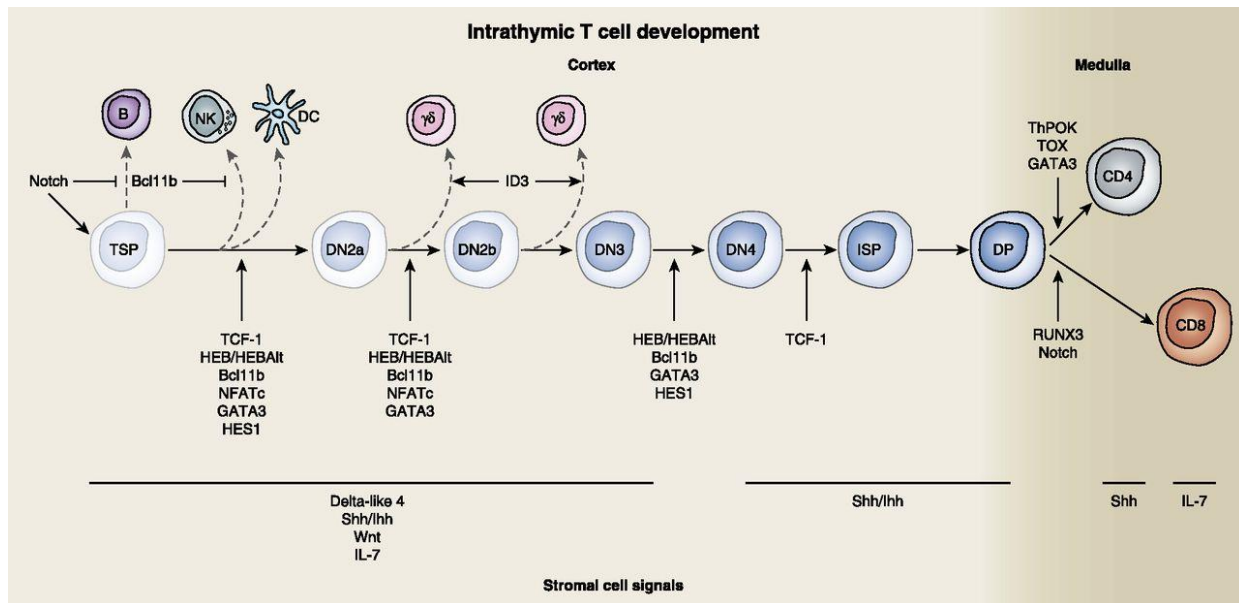


Figure 7: Overview of the development of thymocytes, emphasizing the role of key transcription factors and signaling molecules involved in the developmental process. Different thymocyte development stages are illustrated in the figure, with transcription factors and thymic stromal cells signaling. Receptor–ligand interactions are shown separately in the bottom. To determine the thymic seeding progenitor cells (TSPs) on the T cell lineage and to instruct transcription factors to adopt and commit to the T cell pathway at specific stages during differentiation, notch – Dll4 signaling is essential. Thymic epithelial signals, from Hh- (Shh and Ihh), Wnt-, and IL-7–signaling pathways, aid in the engagement with the T cell lineage and continued proliferation and survival of developing thymocytes. (Adapted from (Shah & Zúñiga-Pflücker, 2014)).

Th1 cells were characterized by their capacity to produce IL-2, IFN- $\gamma$ , and lymphotoxin and their expression of the transcription factor t-bet. While, Th2 cells secrete IL-4, IL-5, IL-10, and IL-13, and their development is influenced by IL-4 and the transcription factor GATA-3 and Th17 cells secrete IL-6 and IL-17 and express the transcription factor RORC2.

Further investigation of T helper cells revealed the existence of Th9 cells, which are generated from Th2 cells when Th2 cells are exposed to a combination of IL-4 and TGF- $\beta$ . Th9 cells can reprogramme the Th2 cells to produce IL-9, a potent growth factor for mast cells, a mediator of helminthic immunity.

Another important subset of T helper cells is Treg. Naturally occurring Treg are identified by the expression of both the CD4 T cell co-receptor and CD25, which is a component of the IL-2 receptor. Expression of the transcription factor Forkhead box P3 (FoxP3) is the defining property that determines natural Treg development and function. FoxP3 is crucial for the regulation of the immune system (Chaplin, 2010a). Naturally occurring mutations in the FOXP3 gene may give rise to a severe multisystem inflammatory disorder causing the production of self-reactive lymphocytes that cause a rare but severe disease IPEX (Immune Dysregulation, Polyendocrinopathy, Enteropathy, X-Linked syndrome) in humans and scurfy in mice (Zhou *et al*, 2008). Treg plays a crucial role in suppressing activation, proliferation, and cytokine

production of CD4+ T cells and CD8+ T cells, B cells, and dendritic cells by producing TGF-beta, IL-10, and adenosine (Sakaguchi *et al*, 2006).

Unlike CD4+ Helper T cells, CD8+ (cytotoxic) T cells are also generated in the thymus and express the T-cell receptor. However, instead of CD4 molecule, cytotoxic T cells express a dimeric co-receptor, CD8, usually composed of one CD8 $\alpha$  and one CD8 $\beta$  chain, which serves as a co-receptor for MHC class I molecule found on all nucleated cells. The CD8 heterodimer binds to a conserved region (the  $\alpha$ 3 region) of MHC-I when an antigen is presented to the T cells.

CTLs mainly opt for three different mechanisms to kill target host cells.

1. Production of cytokines, primarily TNF- $\alpha$  and IFN- $\gamma$ , which have anti-tumor and anti-viral microbial effects.
2. Production and release of cytotoxic granulates. These granules are also found in NK cells, contain mostly two families of proteins, perforin and granzymes. Perforin forms a pore within the target cell membrane, similar to the complementary membrane attack complex. This pore allows entry of granzymes into the contaminated or malignant cell. Granzymes are serine proteases that cleave the proteins inside the cell, shut down the production of viral proteins, and ultimately lead to the apoptosis of the target cell.
3. Destruction of infected cells is via Fas/FasL interactions. Activated CD8+ T cells express FasL on the cell surface, which binds to its receptor, Fas (CD95), on the surface of the target cell. This binding causes the Fas molecules to trimerise on the surface of the target cell, triggering the apoptosis of the target cell.

Gamma delta ( $\gamma\delta$ ) T cells are recognized as 'unconventional' T cells expressing a heterodimeric TCR composed of  $\gamma$  and  $\delta$  chains, and most of them are double negative (expressing neither CD4 nor CD8), with some variably CD4+ or CD8+. They are mostly found in the peripheral blood, and in human, they represent less than 5% of lymphocytes.

In contrast to  $\alpha\beta$  T cells, the majority of  $\gamma\delta$  T cells are activated in an MHC-independent manner. The antigens recognized by most  $\gamma\delta$  T cells are still unknown.

Some  $\gamma\delta$  T cells also recognize markers of cellular stress, resulting from infection or tumorigenesis. A small subpopulation of Natural Killer T (NKT) cells represents another subset of  $\gamma\delta$  T cells, which recognize nonpeptide antigens presented by nonclassical MHC molecules of the CD1 family. Activated NKT cells are



capable of rapid production of cytokines, including IL-4, and play a key role in suppressing allergic pathogenesis.

### 5.3.2 B lymphocytes

Prenatal B cell development occurs in the fetal liver later, B lymphocytes (B cells) differentiate and mature from the hematopoietic stem cells of bone marrow to establish the adaptive humoral immunity. In the bone marrow, their antigen receptors (surface Ig) are arranged to from genetic building blocks involving RAG1/RAG2 similar to that used for the production of functional TCR in the case of T lymphocytes (Thomas *et al*, 2009). During the B cell development, the amino-terminal portion of each heavy chain is created by somatic recombination encoding a variable (VH), diversity (DH), and joining (JH) region (Chaplin, 2010a). The amino-terminal portion of the light chain is created by the union of genes encoding variable and constant light chain components. The VDJ junctions formed by this recombination constitute the third hypervariable region that plays an important role in the site of antigen binding. These hypervariable sequences are combined into the Ig protein to form the antigen-binding domain of the molecule. As a result, each Ig has two identical antigen-binding sites. Carboxyl terminal portions of heavy and light chains are constant in each antibody subclass. Heavy chain constant regions combine to form the Fc domain of the molecule responsible for most of the Ig molecule's effector functions, including binding to the Fc receptors and activating the complement system (Chaplin, 2010a).

B cells are at the center of the adaptive humoral immune system and are responsible for producing antigen-specific immunoglobulin (Ig) under the direction of signals received from T cells and other cells, such as dendritic cells. Activated B cells multiply and transform themselves into plasma cells. These plasma cells quickly produce substantial amounts of antibodies and release them into the blood (Figure 8). Because only the B cells that match the attacking germs are activated, only the specific required antibodies are produced.

Some activated B cells transform into memory cells and become part of the "memory" of the adaptive immune system.

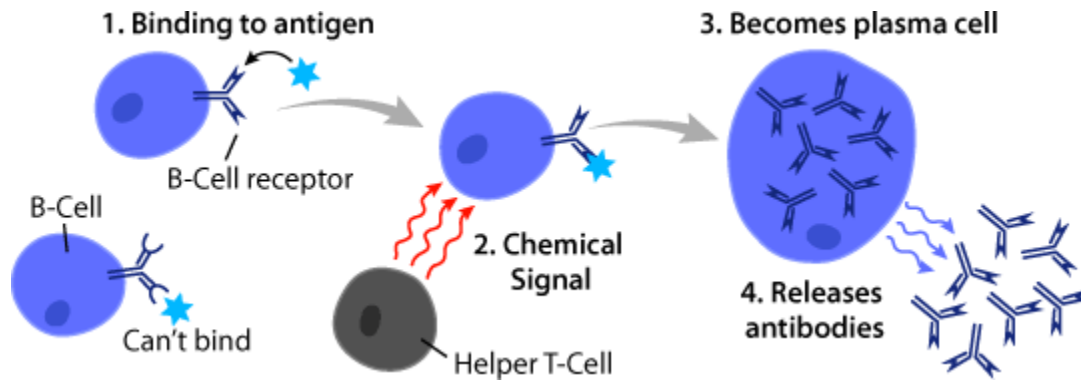


Figure 8: B-cells become plasma cells to attack the invader (Adapted from "[Dr. Biology. \(2011, February 16\)](#)")

## 5.4 Linking Innate and Adaptive immunity

Innate and adaptive immune responses together build the host defense system that ensures the safety of the host organism. Communication between innate and adaptive immunity requires correct and efficient translation of innate signals of danger to the adaptive system.

Dendritic cells play the most critical role and build a bridge between innate and adaptive immune systems. DCs are heterogeneous populations of cells found in an immature state at sites of interaction with the environment, such as the skin and mucosa. They continually sample the environment by macropinocytosis.

Interaction with a foreign particle trigger the DCs maturation. This results in the relocation of the DCs to the draining lymph node site. Here, the class II-peptide complex's stability is enhanced to facilitate the peptide loading at the site of inflammation.

Expression of Costimulatory molecule is also induced by maturation, making dendritic cells the best antigen-presenting cells (APCs) capable of activating a naive T cell. Depending on the nature of the immune response DCs activate different subset of T cells. DCs-mediated T cell activation results in the differentiation of T cells into Th1 and Th2 phenotypes. Th1 cells secrete IFN- $\gamma$  and promote cell-mediated immunity and inflammation. Th2 cells generate IL-4 and enable B cells to switch isotypes during a humoral response (see fig. 3). Three major key players of the innate and adaptive immune communications are BCR, TCR, and MHC/HLA molecules.

### 5.4.1 Major histocompatibility complex:

Antigen receptors of lymphocytes recognize a family of cell-surface molecules on APCs that are collectively known as major histocompatibility complex (MHC). MHC molecules are transmembrane glycoproteins and are subdivided into two classes according to their function (Chaplin, 2010a).

MHC-I present antigenic peptides of intracellular origin (Marshall *et al.*, 2018). These peptides can originate from intracellular pathogens (viruses or intracellular bacteria). MHC-I can also present four altered self-proteins, mutated or misfolded proteins generated during tumorigenesis. Antigenic peptides loaded on MHC-I are presented to CD8+ CTLs to destroy tumorigenic cells or virus-infected cells (Figure 9). MHC-I molecules are expressed in all somatic cells. Typically, at the start of the adaptive response to a virus, an infected DCs migrates from the site of infection to a secondary lymphoid organ (ganglion or spleen) (Alvarez *et al.*, 2008). There, the antigenic peptide loaded on MHC-I is presented to the naive CD8+ T lymphocyte. This step activates the specific CD8+ T of this antigen, which leads to clonal expansion and differentiation into mature CTLs. From then on, the CTL is responsible for the elimination of all the cells presenting the same antigen on their MHC-I.

Unlike MHC-I molecules, the expression of MHC-II is restricted to APCs (DCs, macrophages) and B lymphocytes. MHC class II presents antigenic peptides of extracellular origin coming from bacteria, viruses, or extracellular parasites (Chaplin, 2010a). These antigenic peptides are generated during the phagocytosis of a pathogen or are captured in the microenvironment by endocytosis. During the resolution of the phagolysosome, the APCs can recover these peptides and load them on MHC-II. They present the peptide to naive or mature CD4 + T cells (Figure 9), which differentiate into T helper cells, initiating a wide range of pathogen-specific responses.

Of note, in human, MHC is termed as human leukocyte antigen [HLA] and MHC-I in human can be subdivided into HLA-A/B/C, and MHC-II can be divided into HLA- DP/DQ/DR.

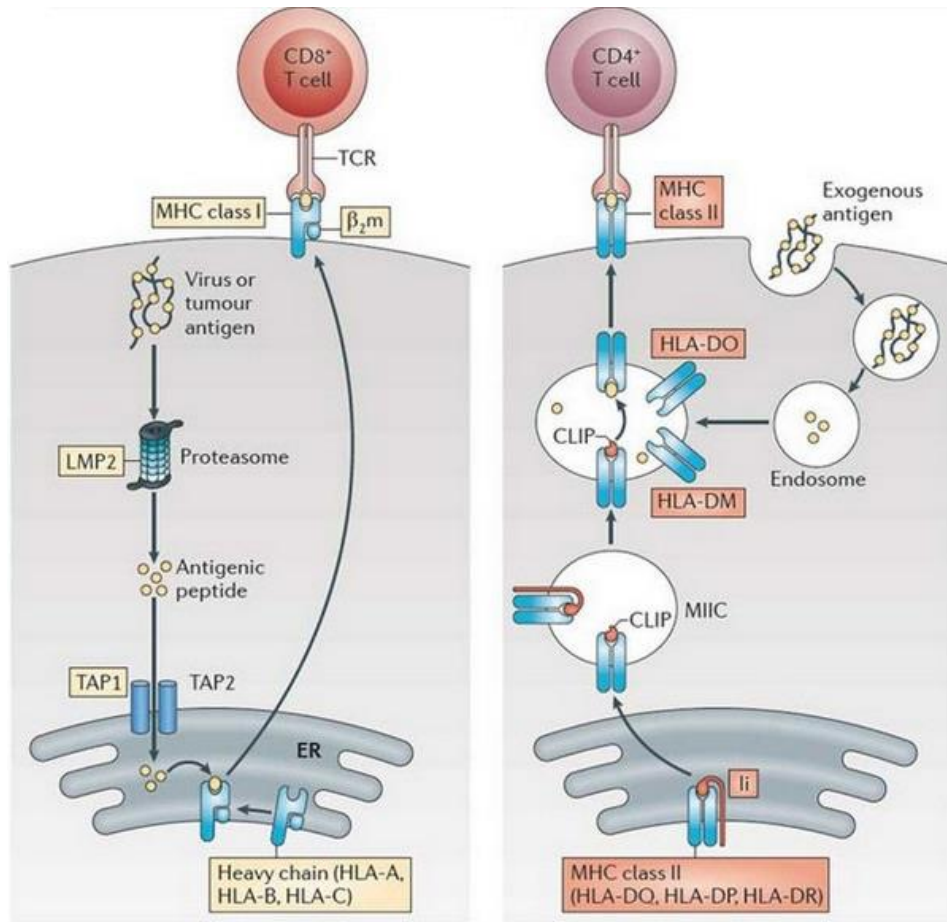


Figure 9: Antigen processing and presentation by MHC Class I and MHC Class II. The immunoproteasome, which comprises several subunits, including LMP2, processes intracellular antigens, such as virus or tumor antigens, into peptides. Transportation of peptide to the endoplasmic reticulum (ER) leads to the peptide loading into the MHC I complex groove, consisting of a heavy chain and  $\beta_2m$ . MHC class I complex present antigens on the cell surface to CD8+ T cells. Antigens derived from extracellular sources such as bacterial antigens are transformed into peptides by endolysosomal enzymes. These peptides bind to the groove of the MHC class II complex by expelling class II-related invariant chain peptide (CLIP), derived from the invariant chain (Ii) of MHC class II molecule. HLA-DO and HLA-DM control the antigen-loading process. The MHC class II complex presents antigens to CD4+ T cells. Essential proteins involved in the MHC class II pathway are Transactivator-regulated genes (CIITA), MHC class II compartment (MIIC), T cell receptor (TCR). (Adapted from (Kobayashi & van den Elsen, 2012)).

#### 5.4.2 T cell receptors (TCRs)

T-cell receptors (TCRs) are protein complexes located on T cells' surface that is responsible for the recognition of antigen fragments as peptides bound to MHC molecules.

The antigen-specific  $\alpha$  and  $\beta$  chains of the TCR associate with invariant accessory chains serve to transduce signals when the TCR binds to antigen-MHC complexes.  $\alpha\beta$  TCRs recognize both the antigen (in the form of a peptide) and the MHC class I or II molecule to which it is bound. This is known as "major

histocompatibility complex restriction" (MHC restriction) (Zinkernagel & Doherty, 1997). These  $\alpha$  and  $\beta$  chains make up the CD3 complex, consisting of the transmembrane CD3 $\gamma$ , CD3 $\delta$ , and CD3 $\epsilon$  chains plus a largely intracytoplasmic homodimer of two CD3 $\zeta$  chains (Figure 10). A translocon organization of both the  $\alpha$  and  $\beta$  TCR genes is found in all animals (Flajnik & Kasahara, 2010a). The presence of a D segment in the  $\beta$  TCR locus and the absence of D segments and the presence of a large number of J segments in the  $\alpha$  TCR locus are also evolutionarily conserved, at least from mammals to bony fish (Flajnik & Kasahara, 2010a). The many J segments in the  $\alpha$  locus allow extensive receptor editing in developing T cells, resulting in more significant opportunities for modification of the antigen receptor, followed by potential selection of self-MHC-restricted TCRs in the thymus.

$\gamma\delta$  TCRs are quite different from  $\alpha\beta$  TCRs. The basic gene organization is conserved in gnathostomes, with only J segments in the  $\gamma$  gene, usually two D segments in the  $\delta$  gene, and close linkage of the  $\delta$  and  $\alpha$  TCR genes. However, the receptor can be adapted in several ways. It was shown in mice that  $\gamma\delta$  T cells that arose early in ontogeny bear invariant receptors and home to sites, such as the skin, where they form the first line of defense and self-renew for the life of the organism.

Approximately 5–10% of T cells in the peripheral blood, lymph nodes, and spleen are CD4–CD8–. Some of these cells use  $\alpha\beta$  TCR, and others use  $\gamma\delta$  TCR.

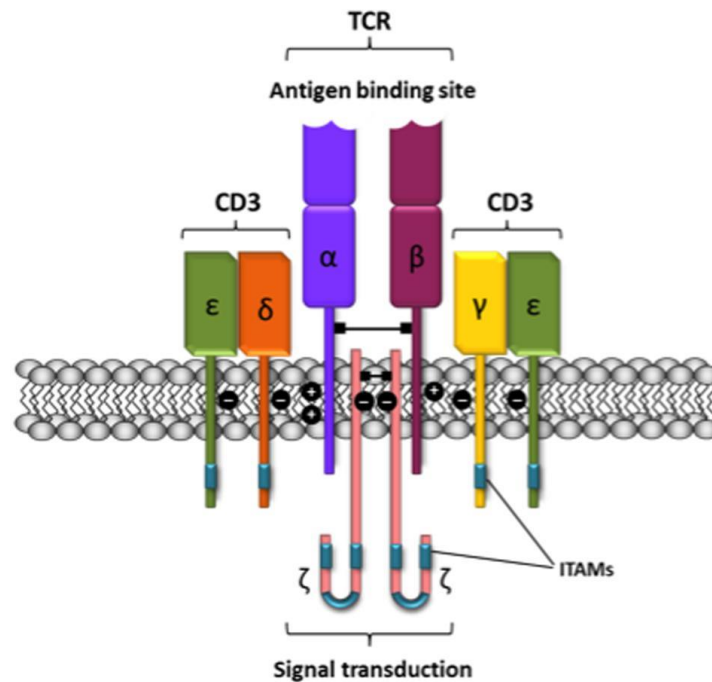


Figure 10: Schematic representation of the T-cell receptor-CD3 complex. The heterocomplex is formed by variable TCR- $\alpha$  and TCR- $\beta$  chains coupled to three dimeric signaling transduction modules CD3 $\delta/\epsilon$ , CD3 $\gamma/\epsilon$ , and CD3 $\zeta/\zeta$  or CD247. CD3, Cluster of differentiation 3; CD247, cluster of differentiation 247 or CD3 $\zeta/\zeta$ ; ITAM, immunoreceptor tyrosine-based activation motif; TCR, T-cell receptor (Adapted from (Franco et al, 2016)).

### 5.4.3 B cell receptors (BCRs)

Binding of B-cell antigen receptor (BCRs) with antigen triggers a humoral immune response. B cells identify and attack pathogens with the aid of proteins called immunoglobulins (Ig). Five immunoglobulin isotypes (IgA, IgD, IgE, IgG, and IgM) can be either secreted (sIgs) or membrane-bound (mIgs) on the cell surface (Friess et al, 2018). Membrane-bound immunoglobulins (mIgA, mIgD, mIgE, mIgG, and mIgM) are components of the so-called B-cell receptor (BCR). Just like the TCR / CD3 complex, the BCR is also a complex of oligomers (Li et al, 2019).

The mIg subunits bind the antigen, initiating the aggregation of the receptor, while  $\alpha/\beta$  subunits initiate intracellular signaling (Friess et al., 2018). Initiation of BCR signaling promptly activates the Src family kinases Lyn, Blk, and Fyn as well as the Syk and Btk tyrosine kinases. This facilitates the formation of a 'signalosome' composed of the BCR, the tyrosine kinases, adaptor proteins such as CD19 and BLNK, and signaling enzymes such as PLC $\gamma$ 2, PI3K, and Vav (Figure 11) (Dal Porto et al, 2004). Signals emanating from the signalosome activate multiple signaling cascades that involve several kinases, GTPases, and

transcription factors resulting in changes in cell metabolism, gene expression, and cytoskeletal organization. Abnormal BCR signaling is associated with the progression of lymphoma (Niemann & Wiestner, 2013) and immunological diseases, including autoimmune disorders (Rawlings *et al*, 2017).

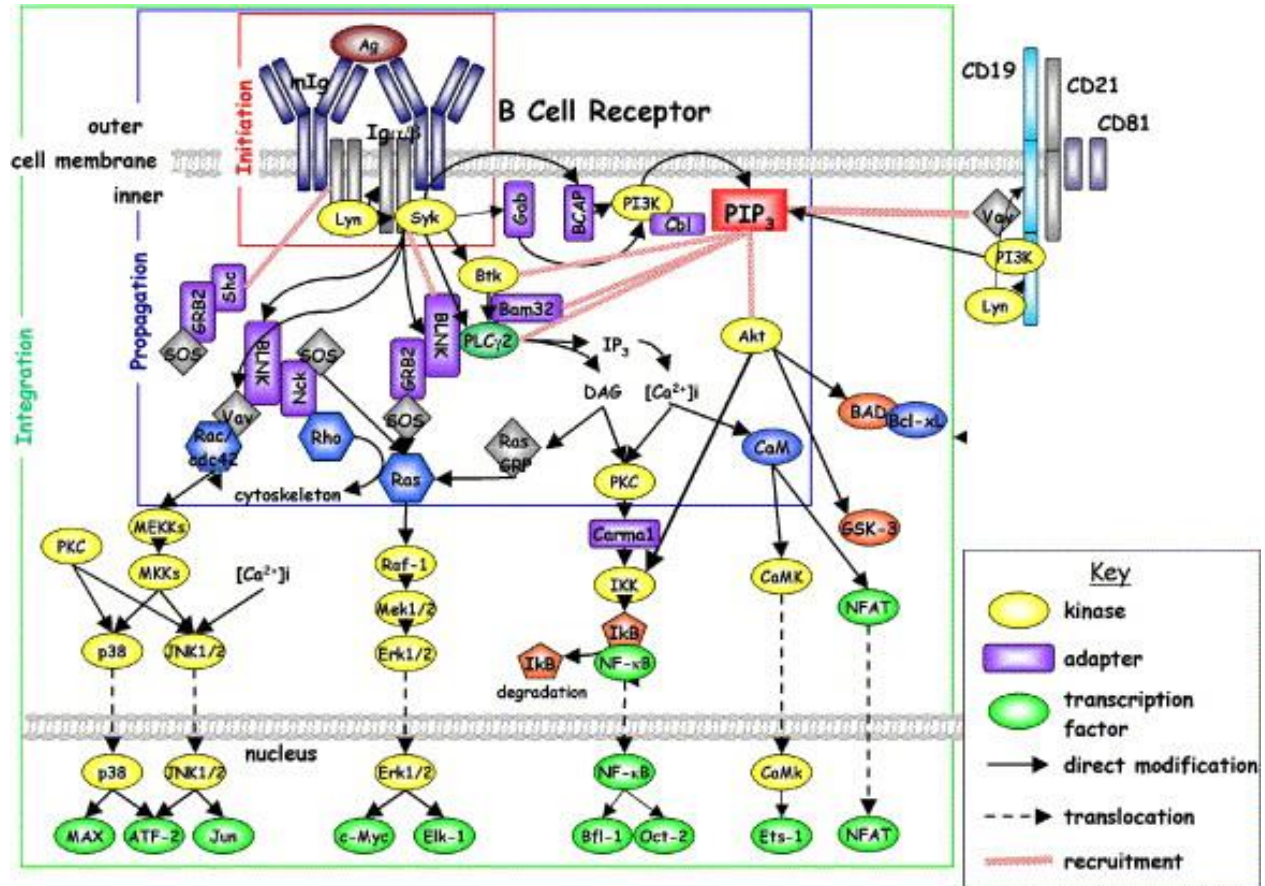


Figure 11: B cell antigen receptor signal transduction cascade. Signal transduction initiates at the cell membrane following ligand-induced aggregation of the membrane immunoglobulin (mIg) and associated signal transducing elements Igα and Igβ (Adapted from (Dal Porto *et al.*, 2004)).

### 5.5 Immunometabolism

Immunometabolism relates to the creation of a correlated interplay between the metabolic and immunological functions. The knowledge of immunometabolism ensures the accuracy of a particular immune cell function, depending on the microenvironment the cell is facing.

One of the biggest obstacles we faced in introducing a link between metabolism with immunology is that most immunologists saw these metabolic pathways as scientifically interesting but unlikely to integrate these pathways on their own growing research interests into the complexity of the immune response.

Immunology by itself as a discipline has improved tremendously in the last 40 years. Notable developments include identifying whole new immune receptor systems (most notably pattern recognition receptors (PRRs), the identification of several cytokines and immune cell types, and a better understanding of different immune cell function.

But from the last 10 years, immunologists reinvent the metabolism by discovering the importance of intracellular metabolic pathways in immune cells that regulate their functions. Immunometabolism governs the adequate response of a particular immune cell towards particular pathogens. From the knowledge about metabolism, we know that six metabolic pathways play a key role in generating key products to promote cell survival or growth. These pathways are Tricarboxylic Acid Cycle (TCA cycle), the glycolytic pathway, pentose phosphate pathway (PPP), fatty acid oxidation (FAO), fatty acid synthesis and amino acid pathways (Figure 12). Each of them has a unique purpose in the cell and is regulated by cellular signaling pathways to link their activity to cellular needs. Immune cells are also tightly governed by these six key metabolic pathways, and each metabolic pathway is essential for a particular action of an immune cell type, depending on the surrounding microenvironment.

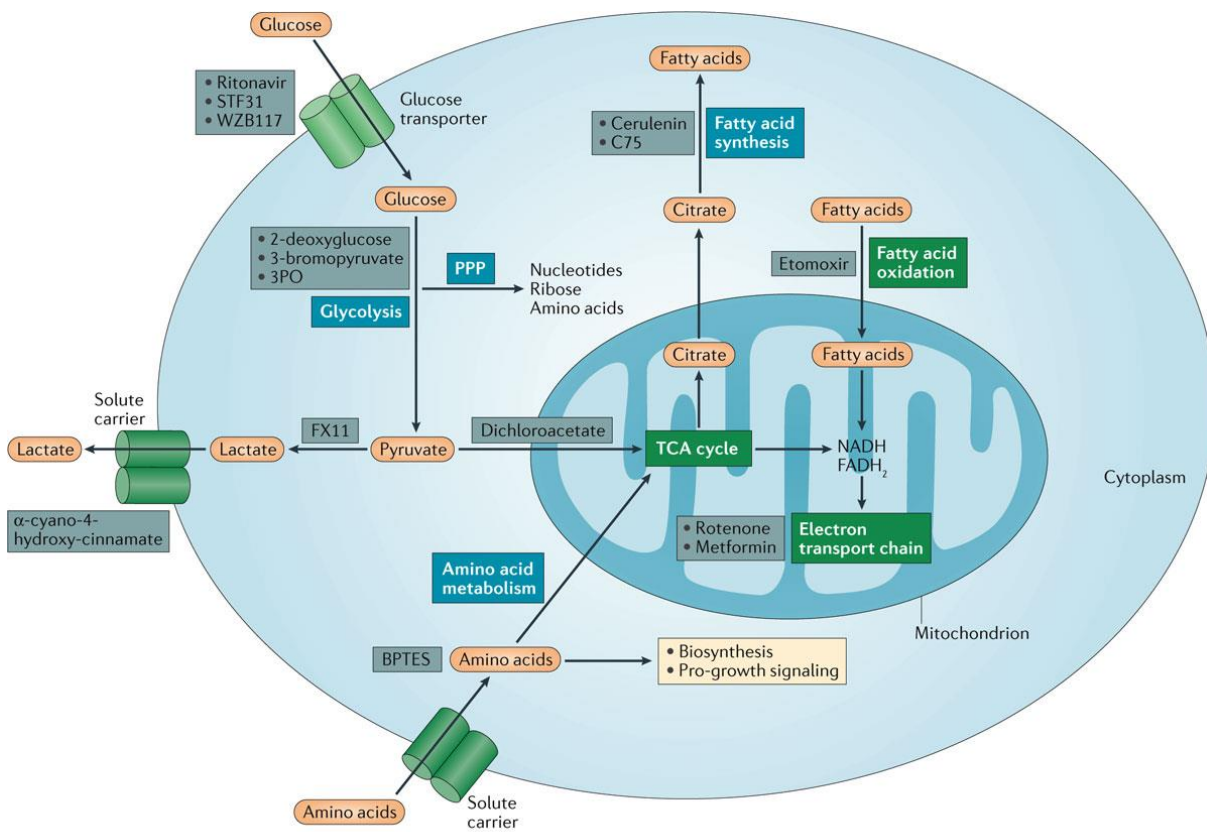
Although immunometabolism plays a role in all immune cell functions in this thesis, we only address the link of immunometabolism with DCs and macrophages. As a crucial component of the innate immune system, the DCs manage the aspect of immunity through their ability to look into the tissues and gather antigens (Lawless et al, 2017). The DCs also work detecting danger signals from tissues and the microbes within the bodies. In this instance, the provision of adequate handling for the immune responses in the body helps to bring in key management of antigens to preserve the integrity of the body (van der Windt et al, 2012). DCs have different functions to regulate the homeostatic processes within tissues and establish a system of immunity. However, handling the environment and forging reactions lead to the creation of a differentiation, which induces activation to ensure better functionality in the systems. Appropriate functionality deals with the engagement of cellular environments and the creation of typical needs for all segments to define the course of an immune response (Thwe et al, 2017). The aspect of immunometabolism, therefore, encompasses diverse aspects to increase the functionality of the DCs.

Just like DCs, macrophages play an important role as a part of the innate immune system and response against infectious organisms, with a dual role of eliminating infectious agents by phagocytosis while mediating defensive and inflammatory pathways. However, on the other side, macrophages are also involved in the late response to infections by contributing to tissue debris clearance and "wound" repair. Stimulation with TLR ligands, such as LPS and interferon- $\gamma$  (IFN $\gamma$ ) macrophages polarize into pro-



inflammatory M1 phenotype and secret several pro-inflammatory signaling factors, including cytokines and reactive nitrogen and oxygen species. Additionally, M1 macrophages show bactericidal and antitumor activity. On the other side, the Th2 cytokines, IL-4 and IL-13, polarize macrophages toward an anti-inflammatory M2 phenotype. Briefly, the energy metabolism of M1 macrophages is mainly dependent on glycolysis, PPP, fatty acid synthesis, and a truncated TCA cycle, leading to the accumulation of succinate and citrate, whereas the metabolic profile of M2 macrophages is characterized by oxidative phosphorylation (OXPHOS), Fatty acid oxidation (FAO), reduced glycolysis and PPP (Mills & O'Neill, 2016).

Notably, the immunometabolism process can lead to any of the appropriate metabolic pathways, which allow the immune cells to respond properly towards a particular immune response. The process of immunometabolism, therefore, affects the functionality of macrophages and DCs within the body.



Nature Reviews | Immunology

Figure 12: Six major metabolic pathways. The conversion of glucose in pyruvate by glycolysis is further converted into lactate or acetyl-CoA and enters into the tricarboxylic acid (TCA) cycle where it generates NADH and FADH<sub>2</sub> for the electron transport chain, leading to the production of ATP. Glycolysis also generates glucose-6-phosphate, which enters the pentose phosphate pathway (PPP) to produce ribose for nucleotides, amino acids, and NADPH. NADH is utilized for fatty acid synthesis, which uses citrate produced from the TCA cycle. Fatty acids can also be oxidized, leading to the production of NADH and FADH<sub>2</sub>, which drive the electron transport chain to produce ATP. In the end, amino acid metabolism can feed the TCA cycle, which is also crucial for cell growth and protein biosynthesis. In this diagram, the pathways requiring oxygen are shown in green boxes, and oxygen-independent pathways are shown in blue boxes. Additionally, inhibitors of different metabolic pathways are indicated in grey boxes. For example, BPTES, bis-2-(5-phenylacetamido-1,3,4-thiadiazol-2-yl) ethyl sulphide. (Adapted from (O'Neill et al., 2016))

### 5.5.1 Glycolysis in immunity

Glycolysis in macrophages and DCs requires the provision of oxygen or alternative procedures to ensure the achievement of the desired breakdowns. The use of the glycolytic procedure ensures the attaining of value for the key segments in immunometabolism and assurance of the value for each segment within the body (Shapiro et al, 2011). Mitochondria within the macrophages and DCs are instructional in the provision of a platform to engage in signaling and metabolic activations (Domínguez-Amorocho et al, 2019). The activation of these cells depends on the ability to work with mitochondrial metabolism, which initiates the ability to break down glucose within the cells (Figure 13).

Glycolytic was initially correlated as an active immune signature in various cancers and highly glycolytic tumors. A metabolic switch from OXPHOS to glycolysis in the highly metabolically active cancer cells leads to a significantly increased amount of lactate production. This phenomenon is well described in the beginning of the last century by Otto Warburg, called the 'Warburg effect' (Warburg et al, 1927). Rate of glycolysis is often elevated during immune cell activation: activated T cells show increased rates of glycolysis (Donnelly & Finlay, 2015; Wang et al, 2011), and classically activated pro-inflammatory M1 macrophages show increased glucose metabolism resulting in increased lactate production (Jha et al, 2015a).

This switch is assumed to be important for cells; otherwise, glycolysis is less efficient in generating adenosine triphosphate (ATP). OXPHOS is much more effective than glycolysis because while glycolysis generates 2 molecules of ATP from 1 molecule of glucose, OXPHOS generates 36 ATP molecules from a single molecule of glucose. Conversely, it is also known that glycolysis could be rapidly activated by activation of the enzymes involved in this pathway. By contrast, initiating OXPHOS involves mitochondrial biogenesis, which is relatively more complex and probably slower process than glycolysis. That is why cells need to make ATP urgently switch to glycolysis.

Besides, glycolysis also rapidly generates biosynthetic intermediates to support rapid cell development. Activating signals such as growth factors strongly enhanced the rate of glucose uptake and glycolysis, which supplies ATP, supports the TCA cycle and generates intermediates for PPP, glycosylation reactions, and synthesis of essential biomass constituents, including serine, glycine, alanine, and acetyl-CoA for lipid synthesis.

Enhanced glycolysis occurs in LPS activated macrophages and DCs (Rodríguez-Prados et al, 2010; Villanueva et al, 1987), in NK cells (Donnelly et al, 2014), in activated effector T cells (Anderson et al, 1988),

and in activated B cells (Doughty et al, 2006). Therefore, enhanced glycolysis can be considered a crucial metabolic change in most immune cells undergoing rapid activation, for example, in response to stimulation of PRRs, cytokine receptors, or antigen receptors. More precisely, for macrophages, this involves phagocytosis and inflammatory cytokine production; for DCs, this includes antigen presentation (Everts *et al*, 2014b).

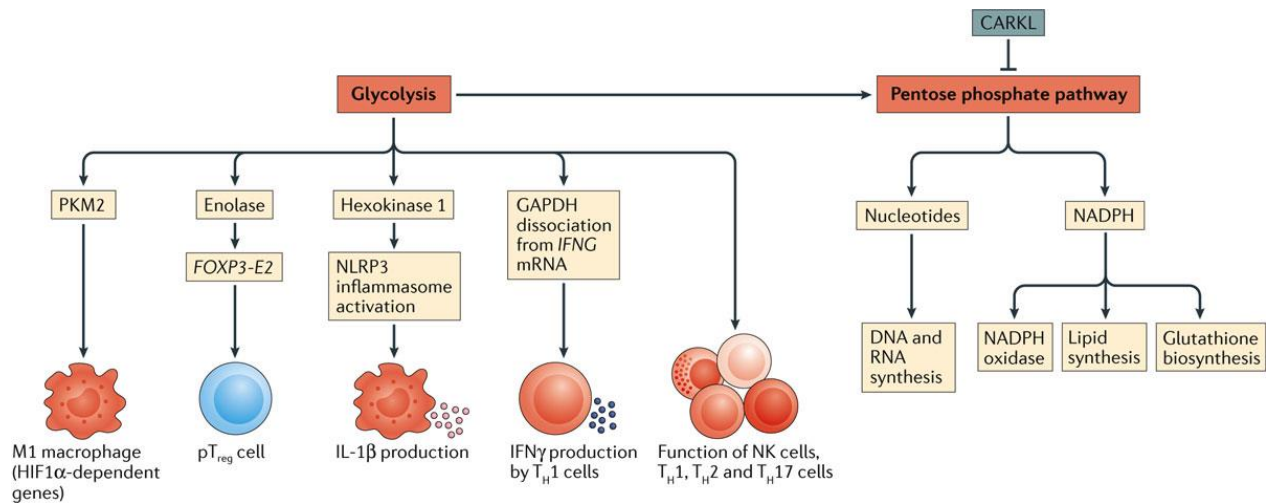
A closer look on the molecular insight associated with the signaling pathway that triggers glycolysis during immune cell activation reveals LPS induces activation of hypoxia-inducible factor 1 $\alpha$  (HIF1 $\alpha$ ), a key transcription factor that is responsible for the induction of several enzymes involved in glycolysis (Tannahill et al, 2013). Probably glycolysis also involves nuclear factor- $\kappa$ B (NF- $\kappa$ B) activation, as the ubiquitous isoform of phosphofructokinase-2 (PFK2), which is involved in the regulation of glycolysis, is still activated by LPS in HIF1 $\alpha$ -deficient cells (Rodríguez-Prados et al., 2010). LPS can also rapidly initiate glycolysis in DCs by activating TANK-binding kinase 1 (TBK1) and/or inhibitor of NF- $\kappa$ B kinase  $\epsilon$  (IKK $\epsilon$ ) and hexokinase 2, in a HIF1 $\alpha$ -independent manner (Huynh et al, 2015).

Pyruvate kinase isoenzyme M2 (PKM2) also plays an important role in the enhancement of glycolysis in LPS-activated macrophages. This form of PKM is regulated to slow glycolytic flux and allows the diversion of glycolytic intermediates into biosynthetic pathways. PKM2 also plays a role in promoting the expression of HIF1 $\alpha$ -dependent genes (Luo et al, 2011; Palsson-McDermott et al, 2015), which encode the aforementioned glycolytic enzymes and inflammatory factors, such as IL-1 $\beta$ .

It has been observed that a small molecule that forces the tetrameric state of PKM2 (in which it cannot enter into the nucleus to promote the expression of HIF1 $\alpha$ -dependent genes) leads to the reprogramming of macrophages to polarize towards M2-like in their gene-expression profiles (Palsson-McDermott et al., 2015). This clearly indicates that inhibition of HIF1 $\alpha$  alters the phenotype of the macrophage from a pro-inflammatory M1 phenotype to a pro-reparatory (or alternatively activated) M2 phenotype.

In macrophages, another important glycolytic enzyme is hexokinase 1, which acts as NLRP3 (NOD-, LRR- and pyrin domain-containing 3) regulator (Moon et al, 2015). NLRP3 is an essential caspase 1 regulator that generates mature IL-1 $\beta$  and active IL-18 and induces a sort of cell death known as pyroptosis.

As mentioned above, in addition to its function in ATP synthesis, glycolysis is also involved in generating several biosynthetic intermediates. For example, the generation of glucose-6-phosphate, which enters into PPP.



Nature Reviews | Immunology

Figure 13: Glycolysis is the predominant source of energy in M1 macrophages because of hypoxia-inducible factor 1 $\alpha$  (HIF1 $\alpha$ ) activation. HIF1 $\alpha$  is responsible for initiating glycolysis and induces several genes that encode inflammatory cytokines, especially interleukin-1 $\beta$  (IL-1 $\beta$ ). Another glycolytic enzyme, hexokinase 1, has also been involved in NLRP3 inflammasomes activation, which leads to caspase 1 activation and the processing of pro-IL-1  $\beta$ . The pentose phosphate pathway (PPP) is fed by glycolysis and generates ribose for nucleotides for DNA and RNA biosynthesis, but generates NADPH for NADPH oxidase glutathione biosynthesis, promoting an antioxidant response. (Adapted from (O'Neill et al., 2016))

### 5.5.2 The TCA cycle in immunity

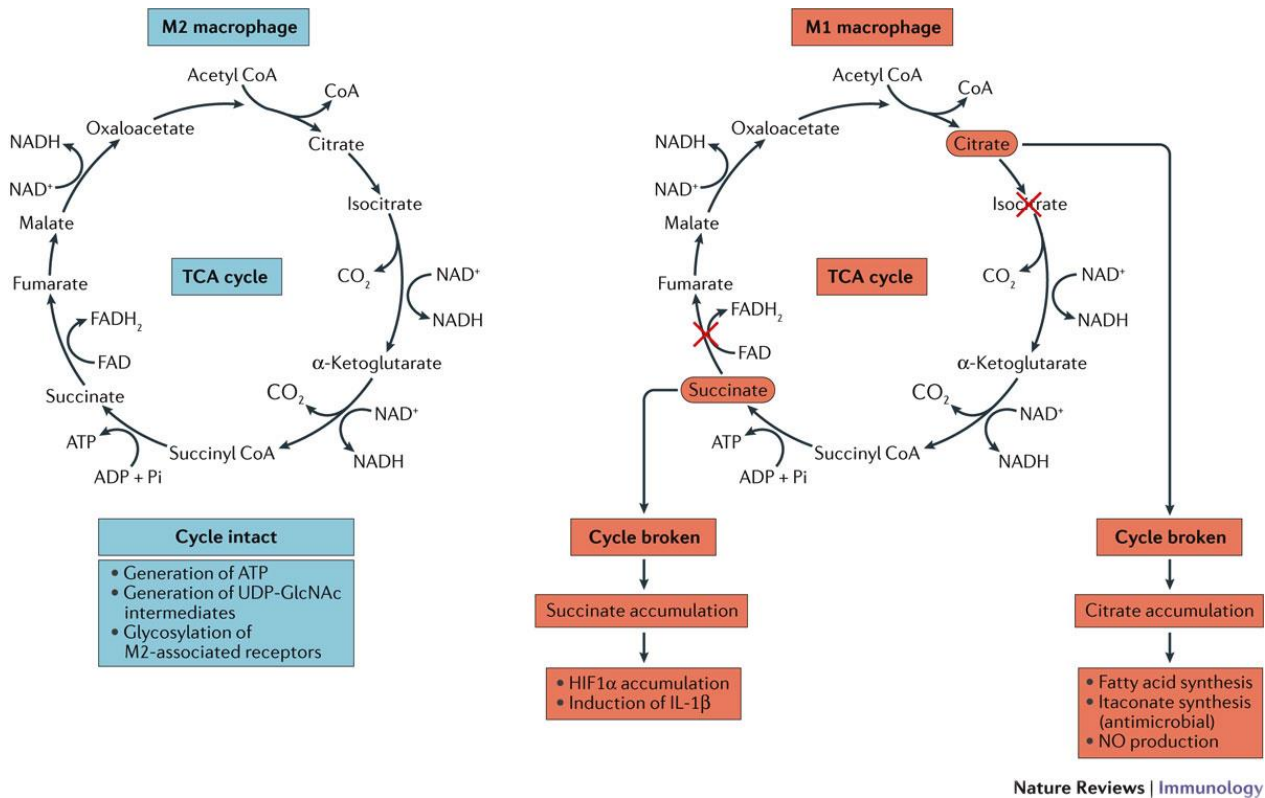
The TCA cycle and oxidative phosphorylation is extensively studied in immune cells function. It has been observed that TCA cycle is recognizably different in subtypes of macrophage (Figure 14). For example, In M2 macrophages, TCA cycle is intact and coupled to oxidative phosphorylation. This enables M2 macrophages to generate Uridine diphosphate N-acetylglucosamine (UDP-GlcNAc) intermediates, which is necessary for the glycosylation of M2-associated receptors, such as the mannose receptor. Interestingly, in M1 macrophages TCA cycle is broken in two places, (1) after citrate (owing to a decrease in expression of isocitrate lyase) and (2) after succinate (Jha et al, 2015b; Tannahill et al., 2013).

Accumulated citrate in M1 macrophages is exported from the mitochondria via the citrate transporter to produce fatty acids, which are used for membrane biogenesis. This broken TCA cycle is also observed in activated DCs and appears to be important for their function, as these cells require substantial membrane production to support antigen presentation (Everts et al., 2014b). Additionally, it has been shown that the differentiation of monocytes into DCs *in vitro* and the development of DCs in lymphoid organs and peripheral tissues *in vivo* depend on fatty acid synthesis (Rehman et al, 2013).

Excess citrate is used to produce nitric oxide and prostaglandins, which are the main effector molecules produced by macrophages (Infantino et al, 2011). A third metabolite generated from citrate is itaconic

acid, which shows a direct bactericidal role against *Salmonella enterica* subspecies *enterica* serovar *Typhimurium* and *Mycobacterium tuberculosis* (Michelucci et al, 2013). This clearly demonstrates how a metabolic rewiring event can lead to the production of several metabolites with direct antimicrobial properties.

Succinate that accumulates in M1 macrophages as a result of the broken TCA cycle plays a key role in different proinflammatory cytokine production (Tannahill et al., 2013). The molecular mechanism underlying the inhibition of prolyl hydroxylases by succinate lead to the stabilization of HIF1 $\alpha$  and the sustained production of IL-1 $\beta$ 21. Altogether, these studies show that the TCA cycle alterations that occur in M1 macrophages lead to different mitochondrial metabolite accumulation that can promote their immune function. These events are closely linked with nitric oxide production, which is responsible for disrupting the electron transport chain (Clementi et al, 1998).



Nature Reviews | Immunology

Figure 14: In LPS activated M1-like macrophages, TCA cycle is broken in two places — after citrate and after succinate. This leads to the accumulation of citrate, which is later used to generate fatty acids and prostaglandin productions. Fatty acid takes part in membrane biogenesis. The broken TCA cycle also leads to the generation of itaconic acid via the enzyme immune-responsive gene 1 (IRG1). Itaconic acid shows antimicrobial activity against *Mycobacterium tuberculosis* and *Salmonella* sp. (Adapted from (O'Neill et al., 2016))

## 6. Nanoparticles, between promise and challenges

### 6.1 Introduction

The term nanotechnology defines a variety of nanometer-scale technologies with broad application, enabling development in different industries. In past decades, Nanoparticles (NPs) and nanostructured materials (NSMs) draw the attention of researchers because of its fully-fledged techno-economic sector in the field of physical, chemical, and biological science. Nanomaterials (NMs) are, in theory, characterized as materials with a length of 1–100 nm in at least one dimension; however, according to the EU Commission, NMs are usually described as “a manufactured or natural material that possesses unbound, aggregated or agglomerated particles where external dimensions are between 1–100 nm size range”. Although, until today, a single internationally accepted definition for NMs does not exist.

Because of the nanoscale size, NMs show quite distinct properties because of their small volume-to-surface area ratio and surface structure, which affects the surface reactivity, solubility, shape, and aggregation. The smaller the diameter of a spherical particle, the more the surface-to-volume ratio increases, leading to an increase of chemical reactivity. This significantly impacts on the interactions with biological structures and living species. Engineered nanomaterials, particularly nanoparticles (NPs), have been rapidly developed to produce a wide variety of objects for different applications, including industrial products, food, agriculture, and health (Figure 15).



Figure 15: The role of nanoscience and nanotechnology in science and engineering (Adapted from (Kolahalam et al, 2019)).

## 6.2 Classification

NMs are commonly classified into different groups according to their morphology, size, and chemical properties. Based on physical and chemical characteristics, NMs can be classified into three groups.

### 6.2.1 Inorganic NMs

These NMs include metal and metal oxide NPs, Ceramics NMs, and Semiconductor NMs.

#### *Metal-based NMs*

Metal NMs are manufactured from metal precursors. These NMs can be synthesized using chemical, electrochemical or photochemical methods. Unique optical properties of Metal NMs is due to their well-known surface plasmon resonance (SPR) properties. Due to their advanced optical properties, metal NMs are used in many disciplines. Most commonly used metals for NMs synthesis are cadmium (Cd), aluminum (Al), copper (Cu), cobalt (Co), iron (Fe), gold (Au), silver (Ag), zinc (Zn), and lead (Pb).

#### *Metal oxide-based NMs*

Metal oxide-based NMs are synthesized to alter the properties of their respective metal-based nanoparticles. For example, iron nanoparticles (Fe) instantly oxidize to iron oxide ( $\text{Fe}_2\text{O}_3$ ) in the presence of oxygen at room temperature to increases its reactivity compared to iron nanoparticles. Most commonly synthesized Metal oxides, NMs are Cerium oxide ( $\text{CeO}_2$ ), Magnetite ( $\text{Fe}_3\text{O}_4$ ), Titanium oxide ( $\text{TiO}_2$ ), Aluminium oxide ( $\text{Al}_2\text{O}_3$ ), Zinc oxide (ZnO), Silicon dioxide ( $\text{SiO}_2$ ) Iron oxide ( $\text{Fe}_2\text{O}_3$ ). These NMs have shown exceptional property when compared to their metal counterparts.

#### *Ceramics NMs*

Ceramics NMs are inorganic non-metallic solids, which are synthesized by subsequent heat and cooling process. They can be found in amorphous, polycrystalline, solid, porous, or hollow forms (Sigmund et al., 2006). Therefore, due to their use in catalysis, photocatalysis, photodegradation of dyes, and imaging applications, these NMs draw special attention from the research community (Thomas et al., 2015).

#### *Semiconductor NMs*

Semiconductor materials have shown properties between metals and non-metals, making them useful in different applicative fields (Ali et al., 2017, Khan et al., 2017a). Semiconductor NPs possess wide bandgaps, which allow them to alter their properties with bandgap tuning. Therefore, they are very important materials in electronic devices, photocatalysis, and photo optics and (Sun, 2000).

## 6.2.2 Carbon-based NMs

Such NMs typically contain carbon and can be found in different morphologies such as hollow tubes, ellipsoids, or spheres. This group of carbon-based NMs mainly comprises of fullerenes (C<sub>60</sub>), carbon nanotubes (CNTs), carbon nanofibers, carbon black, graphene (Gr), carbon onions, Carbon dots, Nanodiamond and many more (Figure 16). Laser ablation, arc discharge, and chemical vapor deposition (CVD) are the commonly used production methods for these carbon-based NMs (except carbon black).

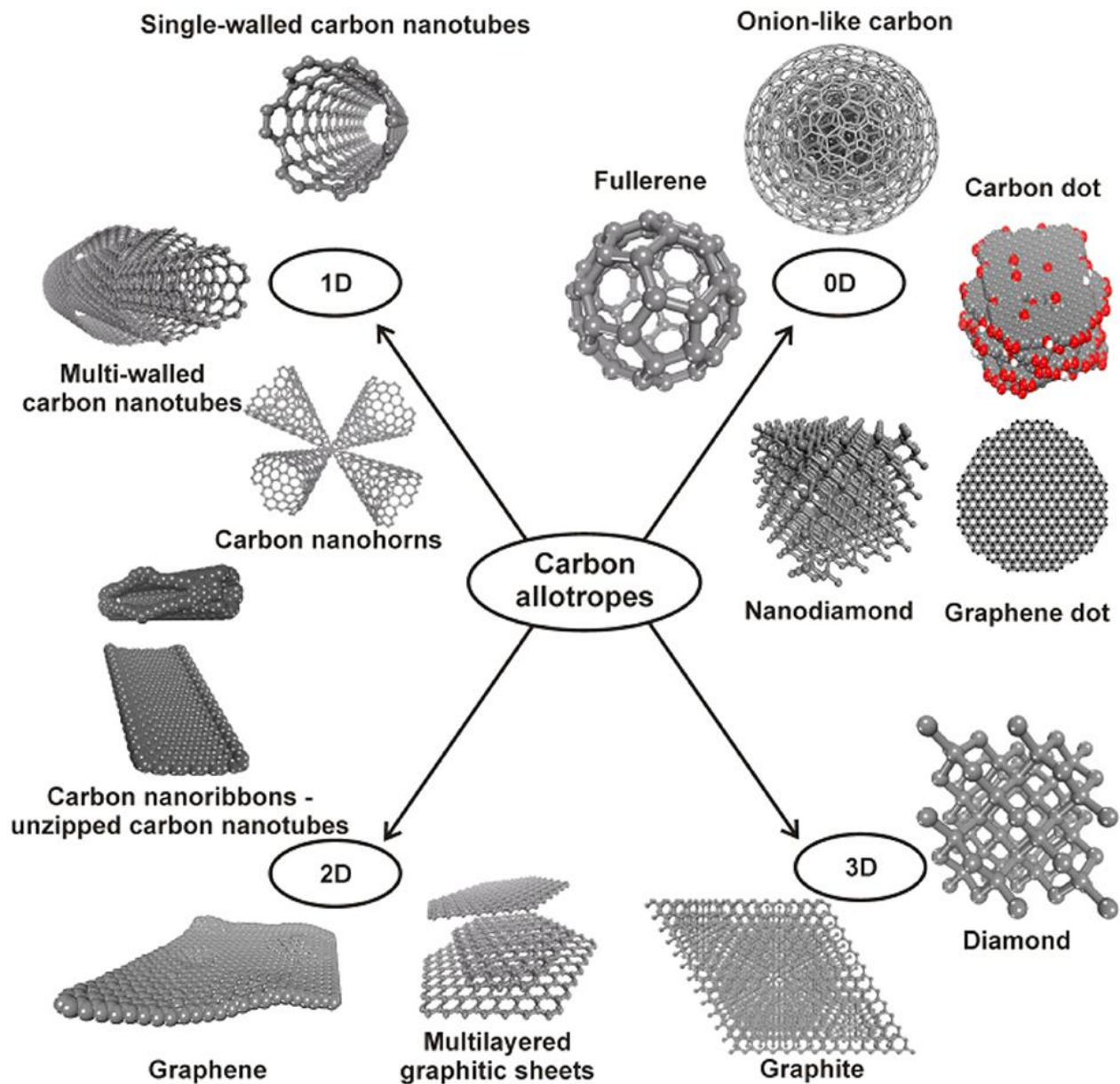


Figure 16 : Carbon-based nanomaterials (Adapted from (Rahmati & Mozafari, 2019))



### 6.2.3 Organic NMs

These NMs are primarily made from organic matter, excluding carbon-based or inorganic-based NMs. The concept of non-covalent (weak) interactions for self-assembly and molecular design helps transform organic NMs into desired structures such as Dendrimers, micelles, liposomes, and ferritin, and other NMs. These NMs are non-toxic, biodegradable, and some NMs such as micelles and liposomes also have a hollow core (Figure 17), which makes them sensitive to thermal and electromagnetic radiation such as heat and light. These distinctive qualities make them an ideal choice for drug delivery. Organic nanoparticles are most extensively used in the biomedical field, such as the drug delivery system, mainly because of targeted drug delivery.

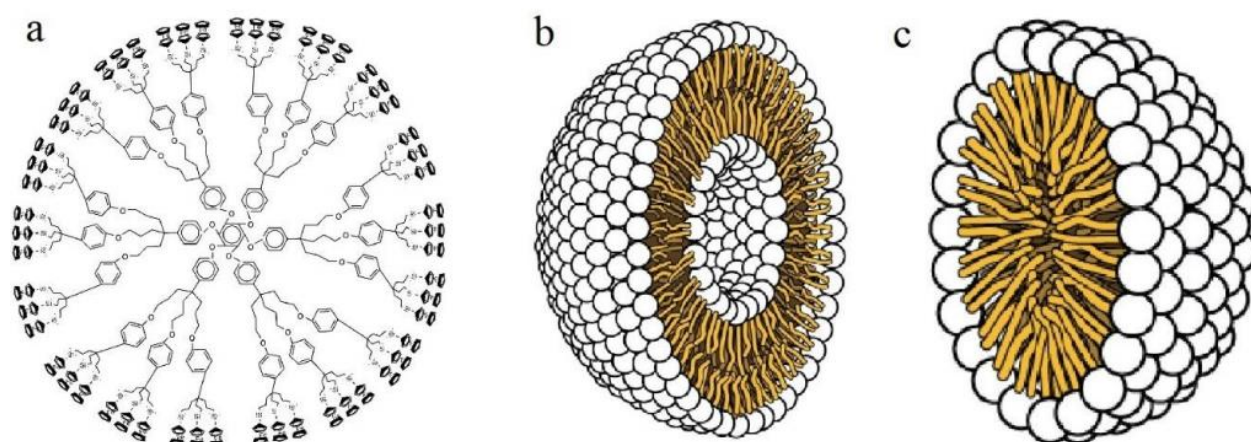


Figure 17: Organic nanoparticles: a – Dendrimers, b – Liposomes, and c – micelles.

### 6.3 Biomedical usage of nanoparticles

The advancement of biomedical research has been based on two dogmas. First, assessment of biological behaviors over large populations. Second, improvement of ill-behaviors by systemic administration of therapeutic treatments. Interestingly nanotechnology significantly contributed to the advancement of both dogmas. In the framework of biology and medicine, nanotechnology underpins materials, devices, and systems whose structure and function are relevant to small scales, from nanometers ( $10^{-9}$  m) to microns ( $10^{-6}$  m) (Whitesides 2003). Living organisms are made up of cells that are usually ten  $\mu\text{m}$  in size. However, the cellular components are much smaller and are in the realm of sub-micron size.

Proteins, the key player of different biological functions, are about 5 nm, equivalent to the size of the smallest fabricated nanoparticles. Interestingly, nanotechnology offers manipulation of the regime of biological systems, which is correlated with both living systems and artificial devices.

The conceptual framework for nano-bio applications can be organized based on two main themes:

1. Nanotechnology allows new ways to understand and detect biological systems both *in vitro* and *in vivo*.
2. Nanotechnology enables new ways to treat diseased cells and cure patients.

For example, nanoscale devices can detect minute alterations in single-cell as well as molecular level. This exquisite sensitivity can be used to interpret single-cell heterogeneity at extremely high throughput, revealing distinguishable hierarchies and cell populations. On the other side, Nanomaterials can be engineered to deliver therapeutics precisely to specific locations while overcoming or avoiding biological obstacles, thus altering the inherent pharmacokinetics and biodistribution of the cargo.

Nanotechnology can be used for various biological applications such as Drug and gene delivery (Dong *et al*, 2018; Pantarotto *et al*, 2003), Tissue engineering (de la Isla *et al*, 2003), Probing of DNA structure (Mahtab *et al*, 1995), Fluorescent biological labels (Chan & Nie, 1998), MRI contrast enhancement (Weissleder *et al*, 1990), Phagokinetic studies (Parak *et al*, 2002), Hyperthermia (Shinkai *et al*, 1999), Purification and isolation of biological molecules and cells (Molday & Mackenzie, 1982) and many more. Several NMs are used for the mentioned functions. Out of several NMs three of the NMs and their biomedical use is described below as a part of this Ph.D. thesis.

### 6.3.1 Gold nanoparticles (AuNPs)

Since long time, gold is used to treat various diseases like rheumatoid arthritis in recent days. Gold-based nanoparticles (AuNPs) are used in several biomedical applications. AuNPs with controlled properties are used in genomics and biosensors, immunoassays and clinical chemistry, photothermolysis of cancer cells and tumors, targeted delivery of drugs and antigens, and optical bioimaging of cells and tissues with state-of-the-art nanophotonic detection systems. These oscillations are known as Plasmon surface resonance. The dominant characteristics of AuNPs include shape-related optoelectronic properties, a large surface-to-volume ratio, excellent biocompatibility, and low toxicity, making them exemplary tools in biomedical applications (Figure 18).

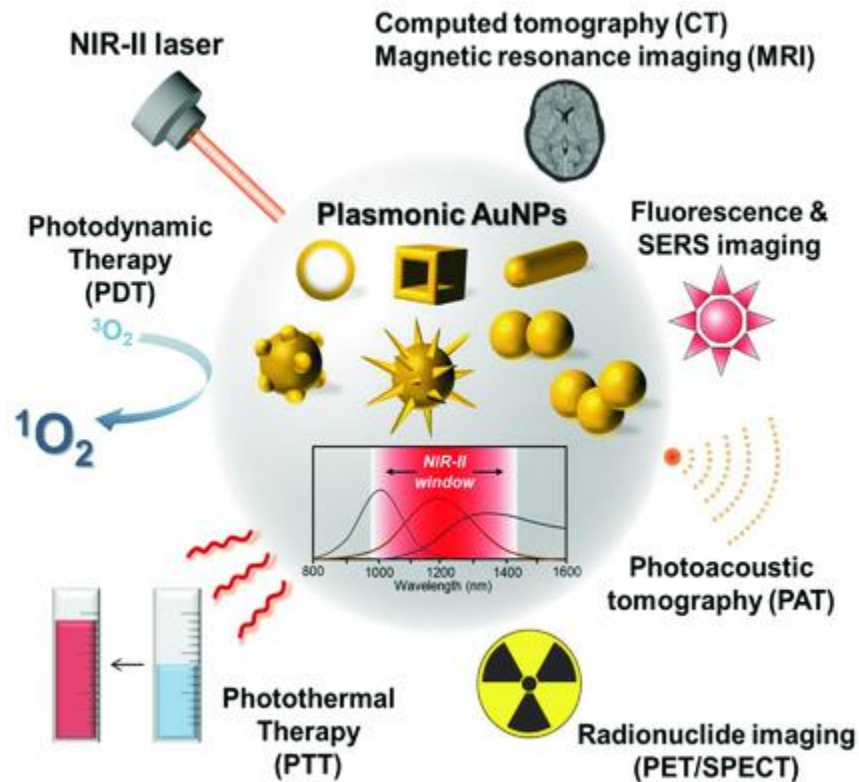


Figure 18: Biomedical applications of AuNPs (Adapted from (Liu *et al*, 2015))

### Photodynamic therapy

Photodynamic therapy (PDT) is a well-known effective treatment for oncological diseases and certain skin or infectious diseases. Effective fluorescence quenching and SPR absorption are the important characteristics of AuNPs used in photodynamic therapy (Wilson, 2008).

### Photothermal therapy

Photothermal cell damage is a promising mechanism in tumor therapy (Kim *et al*, 2018) and the treatment of infectious diseases with minimal invasiveness. Because of the high absorption in the visible or near-IR region, AuNPs receive light and generate heat. The heat causes the death of malignant tumors (Manjunath *et al*, 2017; Narang *et al*, 2015). In addition, AuNPs – antibody conjugates may be used for diagnostic and plasma photothermal therapy (PPTT), known as theranostic. Like PDT, the binding properties of AuNPs play a vital role in the cellular internalization process.

### X-ray radiation therapy

AuNPs are also used to improve X-ray radiation therapy. A challenge in radiation therapy, in general, is that high-dose X-rays damage healthy cells. AuNPs, during X-ray irradiation, can act as dose amplifiers and

/ or generate radicals which damage cancer cells and induce cell apoptosis. This role of AuNPs as radiosensitizers allows a reduction in the dose of X-rays used, with improved therapeutic results (Setyawati *et al*, 2014; Zhang *et al*, 2015).

#### Drug delivery and vaccination

Targeted drug delivery is one of the most promising and actively emerging avenues for the therapeutic use of AuNPs (Duncan *et al*, 2010; Pissuwan *et al*, 2011). Biocompatibility, unique optical, physicochemical properties, low toxicity, controlled disparity, tunable monolayers, functional flexibility, high surface area for loading the density of drugs, and stability make AuNPs an efficient nanocarrier in drug delivery systems (nDDSs). AuNPs are capable of transferring various drugs such as peptides (Lu *et al*, 2013), proteins (Love *et al*, 2015), plasmid DNAs (pDNAs), small interfering RNAs (siRNAs), and chemotherapeutic agents (Liu *et al*, 2015). AuNPs can be used as vaccine delivery vehicles because they are biocompatible and can be used as adjuvants to improve vaccine efficacy by stimulating antigen-presenting cells and ensuring the controlled release of antigens. AuNPs are used to develop HIV (Liu & Chen, 2016), Encephalitis (Zhao *et al*, 2003), Hepatitis (Pilling *et al*, 2002), and other vaccines (Salazar-González *et al*, 2015; Sanchez-Villamil *et al*, 2019).

#### Nano-biosensor

One of the promising purposes of AuNPs is chemical and biological sensing. Inherent characteristics of AuNPs allow them the detection of different metal ions, anions, and molecules. Gold nanotubes attract much attention for biosensing among the various types of AuNPs due to its exceptionally unique optical properties.

### 6.3.2 Lipid nanoparticles (LNs)

Lipids are the inherent components of cell membranes where they provide a basic structural scaffold. Cell membranes are primarily composed of phospholipids and serve as a shield to protect the cell components from the external environment (Simons, 2016).

In recent years, advances in the nanomedicine field demonstrated the utilization of lipid nanoparticles (LNs) in targeted delivery of therapeutic drugs. One of the advantages of LNs is the physiological properties that explain their biocompatibility and biodegradability *in vivo*. LNs are mainly composed of three major parts: a lipid part, a surfactant part, and water. The lipid part can have different forms, such as

phospholipids, free fatty acids, glycolipids, or fatty alcohols. The surfactant part plays a role of a stabilizing agent.

Lipid nanocarrier is generally divided into two types: Solid lipid nanoparticles (SLNs) and Nanostructured Lipid Carriers (NSLC). Solid lipid nanoparticles (SLNs) are solid core lipid nanocarriers that can accommodate both hydrophilic and hydrophobic drugs (Paliwal *et al*, 2020). SLNs act as an alternate solution to conventional colloidal carriers such as polymeric microparticles, nanoparticles, liposomes, and emulsions. The biocompatibility of the lipid matrix is a crucial factor that enables SLNs to be used as drug carriers. SLNs can be manufactured using homogenization techniques, spray congealing methods, and microemulsions. Large surface area, Small in size, High stability than biological liposomes, High drug loading capacity, Less toxic than ceramic or polymer nanoparticles, Readily biodegradable make SLN an excellent drug carrier system. Biomedical applications of some of the SLNs are listed in

Table 5.

SLN composition	Drug	Application
Stearic acid	Rifampicin, isoniazid, pyrazinamide	Mycobacterium Tuberculosis (Pandey & Khuller, 2005)
Stearic acid, soya phosphatidylcholine, and Sodium taurocholate	Ciprofloxacin hydrochloride, tobramycin	Gram-negative bacteria, Gram-positive bacteria and mycoplasma (Jain & Banerjee, 2008)
Soyabean-oil	Doxorubicin Breast cancer	Breast cancer (Wong <i>et al</i> , 2006)
SLN	Tamoxifen, Methotrexate, and camptothecin	Breast cancer (Fontana <i>et al</i> , 2005; Ruckmani <i>et al</i> , 2006)

Table 5: Biomedical application of solid lipid nanoparticles (SLN)

NSLC is formulated from a mixture of solid and liquid lipids, but the particles are in solid-state at body temperature. NSLC manufacturing is mainly based on solidified emulsion (dispersed phase) technology. Distorted lipid structures allow NSLCs to accommodate drug molecules. NSLCs of certain structures can be used for burst drug release by applying the trigger impulse to the matrix to convert in a more ordered structure. (Radtke and Müller, 2001). NSLCs can be used in pharmaceuticals for topical drug delivery, oral and parenteral (subcutaneous or intramuscular, and intravenous) routes. Some examples of biomedical applications of NLCs are listed in

Table 6.

Nanostructured lipid carrier's composition	Application
Phosphatidylcholine, dynasan and flurbiprofen	Sustained release of the anti-inflammatory drug (Bhaskar <i>et al</i> , 2009)
Stearic acid, oleic acid, carbapol and minoxidil	Pharmaceutical, cosmetic and biochemical purposes (Silva <i>et al</i> , 2009)
Fluticasone propionate, glyceryl palmito-stearate, and PEG	Topical corticotherapy (Doktorovová <i>et al</i> , 2010)
Beta-carotene loaded Propylene glycol monostearate	Evaluate the feasibility (Hentschel <i>et al</i> , 2008)
Monostearin and caprylic and capric triglycerides	Improved drug loading capacity and controlled release properties (Hu <i>et al</i> , 2006)
Clozapine, triglycerides (trimyristin, tripalmitin and tristearin), soylécithin 95%, and poloxamer 188)	Improved bioavailability (Venkateswarlu & Manjunath, 2004)

Table 6: Biomedical application of nanostructured lipid carriers (NLC).

LNs such as liposomes and nanoemulsions are lymphotropic due to their lipid nature. Since last decades LNs loaded with a hydrophobic cyanine dye are used for *in vivo* fluorescence imaging. A modified formulation with human-use approved ingredients with broad absorption/emission spectra is designed by CEA-LETI in Grenoble. These newly formulated LNs with unique optical properties are termed as "Lipidots." They are formulated by sonication between a lipid phase, containing glycerides and phospholipids (lecithin), and an aqueous phase containing a hydrophilic surfactant (Poly-Ethylene-Glycol (PEG) (Figure

19). These Lipidots are colloidal in nature and within a size between 50 and 200nm in diameter, depending on the lipid/surfactant ratio used. The viscosity of this nucleus can be adjusted according to its composition, which gives the particle variable rheological properties (Delmas *et al*, 2011).

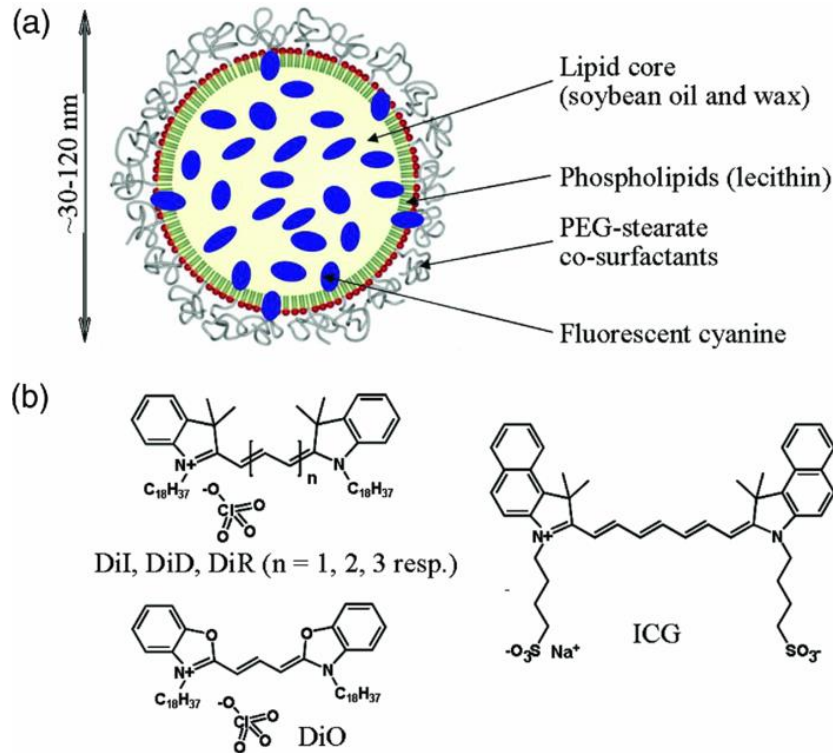


Figure 19: Lipidot structure. (a) Lipidots are dye-loaded oily droplets dispersed in aqueous buffer, whose diameter can be adjusted between 30 and 120 nm. Their fluorescent properties are conferred by lipophilic or amphiphilic cyanine dyes (b), encapsulated in the lipid core, and/or the surfactant layer.

These LNs were primarily used for imaging. These LNs can be labeled with a lipophilic fluorochrome, encapsulated in the core of the particle (Texier *et al*, 2009). Furthermore, LNs are decorated with targeting ligands at their surface, like the graft of cRGD peptide targeting the  $\alpha V\beta 1$  integrins, known as markers of some tumors. The LNs have been used for *in vivo* imaging in mice to monitor targeted therapies (Goutayer *et al*, 2010). Interestingly, these NPs are detectable at very low doses, like 2pmol of particles that are enough to mark the lymph nodes of mice. Using this feature, LNs were used to mark biological fluids, the lymphatic system, and tumors (Gravier *et al*, 2011; Navarro *et al*, 2012a). This allowed non-invasive, real-time imaging of lymphatic vessels in mice *in vivo*. For instance, LNs (50nm) labeled with a hydrophobic cyanine DiD could image the development of lymphatic vessels to study the role of BMP-9 (bone morphogenetic protein 9) in this process (Levet *et al*, 2013). Recently, these LNs have been used for intraoperative fluorescence imaging during the excision of malignant tumors in dogs (Cabon *et al*, 2016).

LN's are also used for the development of new vaccines to deliver protein antigens, including p24 of HIV (Bayon *et al*, 2018; Courant *et al*, 2017)

### 6.3.3 Dendrimer

Dendrimers are unimolecular, monodisperse, micellar macromolecules with a highly branched three-dimensional architecture. Dendrimer configurations are composed of three main components: the core, interior, and the surface (Figure 20). The core governs the 3D architecture of the dendrimer (i.e., spherical, ellipsoid, or cylindrical scaffolds). The interior influences the host-guest property of the dendrimer. Dendrimer surface can be further polymerized or altered with peripheral functional groups. Both the core and the number/type of the internal branching units influence the overall dendrimer morphology. Dendrimers are usually prepared using either a divergent approach or a converging one (Hodge, 1993) with a structure like a tree branching out from the central point. Based on the dendrimers' growth process, these can be classified according to their generation numbers, such as G0.5, G1, G2, G3, G4, and G5. Dendrimeric vectors are most frequently used as parenteral injections, either directly in the tumor tissue or intravenously for systemic delivery (Tomalia *et al*, 2007).

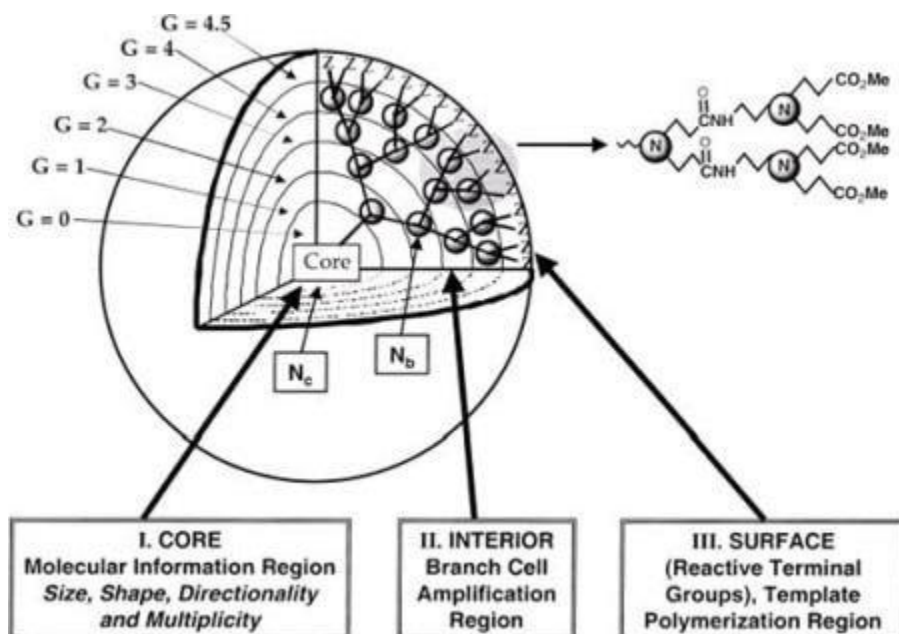


Figure 20 Three dimensional projection of dendrimer core-shell architecture for G=4.5 PAMAM dendrimer with principal architectural components (I) core, (II) interior & (III) surface. (Adapted from (Tripathy & Das, 2013))



Dendrimers used in biomedical research usually contain one or more of the following polymers: poly(amidoamine) (PAMAM), polyamide, poly(L-lysine) (PLL), poly(2,2-bis(hydroxymethyl)propionic acid (bis-MPA), polypropylenimine (PPI), and poly (glycerol succinic acid) (PGLSA-OH) (Figure 21).

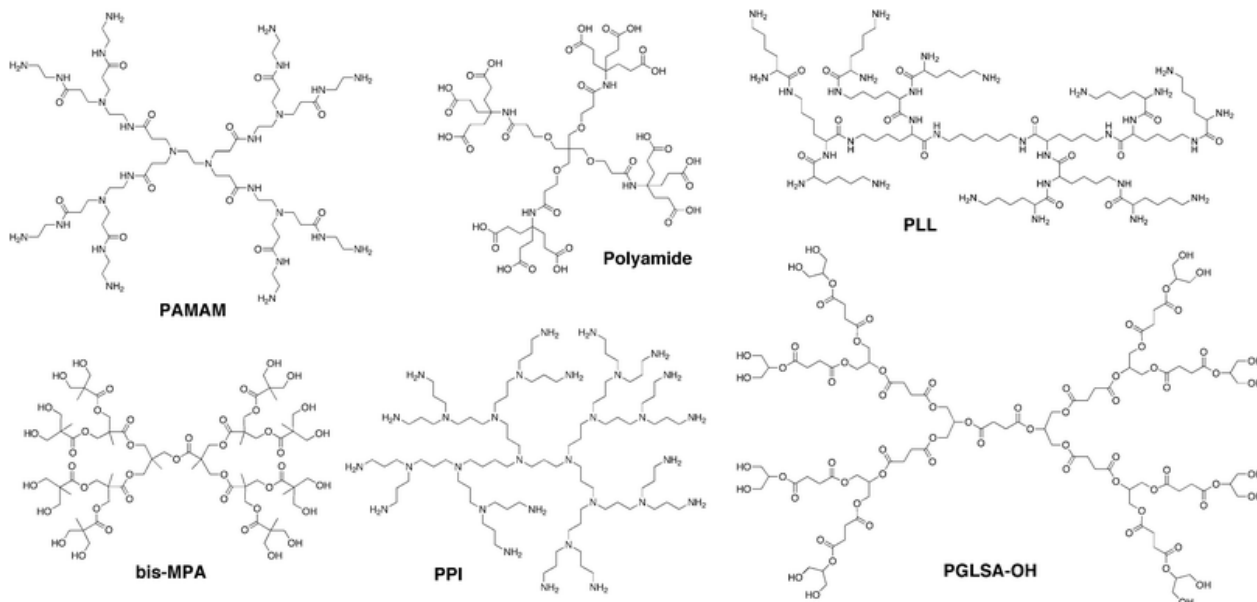


Figure 21: Chemical structures of several commonly used dendrimer (Adapted from (Mintzer & Grinstaff, 2011))

Altogether, dendrimer generation, composition of the core, and peripheral groups play a crucial role in defining the physicochemical properties of dendrimer, which substantially encompasses the biomedical applications of a particular dendrimer molecule.

#### Dendrimers as drug and antiviral agents

Cationic dendrimers with amphiphilic properties are one of the potent antimicrobial agents. In 2000 Cooper et al. synthesized PPI dendrimers with quaternary ammonium groups on the periphery, which showed the antimicrobial activity (Chen *et al*, 2000). Although cationic dendrimer showed notable antimicrobial activity, they all suffer drawbacks due to Cytotoxicity towards eukaryotic cells. Recently, the Grinstaff group designed anionic amphiphilic dendrimers to remove the cationic charge and showed that elimination of positive charge from the dendrimer does not alter their antimicrobial activity(Meyers *et al*, 2008).

Dendrimers are also well studied for their antiviral effects, particularly against HIV-1. VivaGel, a sulfonated polysine dendrimer currently undergoing clinical trials (Mintzer & Grinstaff, 2011). VivaGel is one of the most effective anionic dendrimers used for antiviral purposes.

### Dendrimers as MRI contrast agents

Magnetic resonance imaging has been a commonly used technique for the diagnosis of disease. Dendrimer-based metal chelates function as contrast agents for magnetic resonance imaging. The unique properties of dendrimer make them extremely appropriate image contrast media for MRI (Mintzer & Grinstaff, 2011).

### Dendrimers as transfecting agent

Viral vectors are efficient to induce long-term gene expression as they can be integrated into the cell genome. However, some of these vectors have been associated with a potential oncogenic activation and a significant infection of non-targeted cells hence making them a safety risk in clinical applications, thereby increasing the need for non-viral vectors. Among organic nanocarriers, dendrimer-based vectors have shown multiple advantages to others due to their biological and chemical properties, which provide a suitable and efficient nucleic acid delivery into targeted cells. Currently, several dendrimers polymers have been designed for siRNA delivery, for instance, PAMAM dendrimers, amphiphilic dendrimers (ADs), Poly PPI dendrimers, PLL dendrimers, and many more.

These dendrimers possess a positively charged amine domain at the surface, which facilitates the binding with siRNA molecules, which are negatively charged. Their interior structure keeps tertiary amines that promote the release of siRNA molecules into the cell cytoplasm (Figure 22). This nanovector-based technology showed excellent efficiency in delivering siRNA molecules in both *in vitro* and *in vivo* disease models (Dong *et al.*, 2018; Liu *et al.*, 2014).

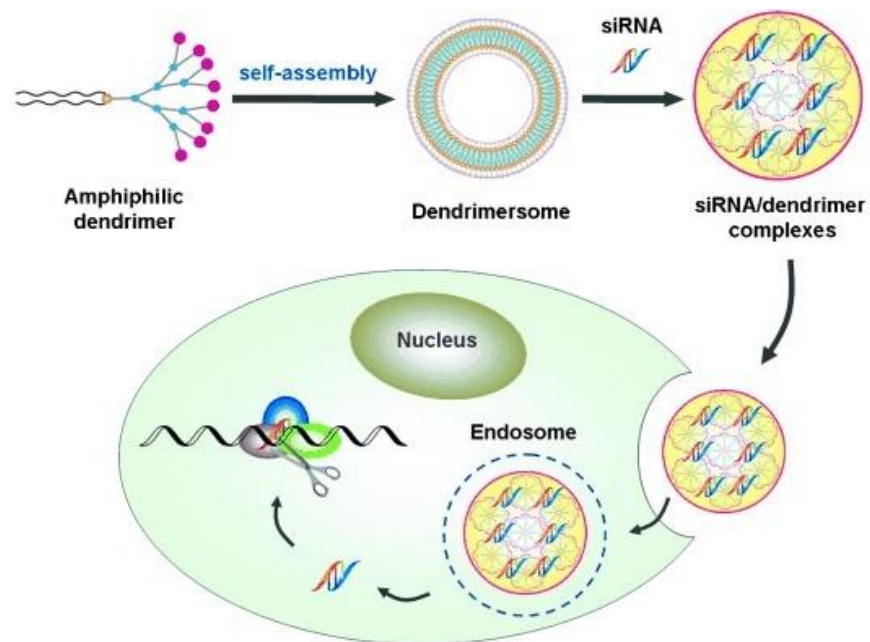


Figure 22:Representation of interaction between amphiphilic dendrimer and siRNA for siRNA delivery (Adapted from (Liu *et al.*, 2014))

#### Dendrimer as an immunomodulatory agent

Modification of six branched anionic Poly-(phosphohydrazone) (PPH) dendrimers, with 12 aminobis (methylene phosphonate) end groups (ABP), dramatically inhibits inflammation and bone erosion in mouse models of experimental arthritis by inhibiting monocyte-derived osteoclasts differentiation and activity (Hayder *et al.*, 2015). These ABP dendrimers have shown immunomodulatory and anti-inflammatory effects on the human immune system, which can be used to treat chronic inflammatory disorders.

#### Miscellaneous dendrimer applications

There are undoubtedly several other areas of biological chemistry where the application of dendrimer systems may be beneficial. Dendrimers can be used in burn treatment (Halkes *et al.*, 2002), prion research (Supattapone *et al.*, 2002), and Photodynamic therapy (Battah *et al.*, 2001) are some of the diverse areas of fascinating ongoing dendrimer research, solubility enhancing agent, bio-sensors, tissue engineering and many more.

## 6.4 Immunotoxicity of nanoparticles

Nanotechnology is applied in many industrial applications and consumer products and is being used for several biomedical applications. In parallel to this technological development, Nanotoxicology has emerged to evaluate safety during industrial processes and the use of products. A functional understanding of the acute and chronic toxicological effects of engineered nanomaterials is currently lacking and may represent a significant limitation to the nanomaterial development and application.

Most of the research on the toxicology of NMs focused on the effects of nanoparticles that inadvertently infiltrate our body.

Immune and inflammatory responses are critical aspects of toxicology studies. Nanoparticles accumulate into cells due to their uptake properties and can provoke immunotoxicity due to increased interaction with immune components and the use of immunostimulatory materials in nano-formulations. For these reasons, Macrophages and Dendritic Cells appear as the most exposed immune cells to the exogenous nanomaterials due to their great capacity in foreign materials engulfment and in their important roles in the regulation of the inflammatory and immune responses.

In contrast to cytotoxicity, screening of immunotoxicity is not well established because of the problems in simulating the complexity of the immunological system *in vitro*, as well as in the extrapolation of *in vitro* and animal data to human reactions. On the other hand, different NMs exhibit different effects on the immune system, which cannot be generalized for all NMs.

Different agencies tried to give a brief guideline for immunotoxicity analysis. For example, according to the Agence Française de Sécurité Sanitaire des Produits de Santé (AFSSAPS), screening of NMs on the basis of immunotoxicity should focus on granulocytes, macrophages, and dendritic cells (DCs), and cytokine production should be considered as one of the readout parameters (Fröhlich, 2015a). Unfortunately, there are no harmonized internationally accepted guidelines until today for determining immunotoxicity.

Literature review showed different *in vitro* assays to ensure the safety of NMs (Elsabahy & Wooley, 2013; Fröhlich, 2015a). Cytokine secretion, chemotaxis, phagocytosis, respiratory burst, Nitric Oxide (NO) generation, functions of dendritic cells, the release of elastase and myeloperoxidase can be assessed to get a preliminary idea about the biosafety of a particular NM.

## 7 Aim of the thesis

To investigate the immunotoxicity of different nanomaterials (NMs) in terms of their effect on cytokine, redox, and metabolic profile of primary immune cells.

## 8 Objectives of the thesis

- Toxicity evaluation of different NMs under investigation on primary macrophages (BMDMs) and dendritic cells (BMDCs).
- Analysis of the effect of different NMs on inflammatory responses on naïve and challenged states of BMDMs and BMDCs.
- Analysis of the effect of different NMs on metabolic profile of naïve and challenged state of BMDMs and BMDCs.
- Investigation on the effect of different NMs on antigen specific T cell response.

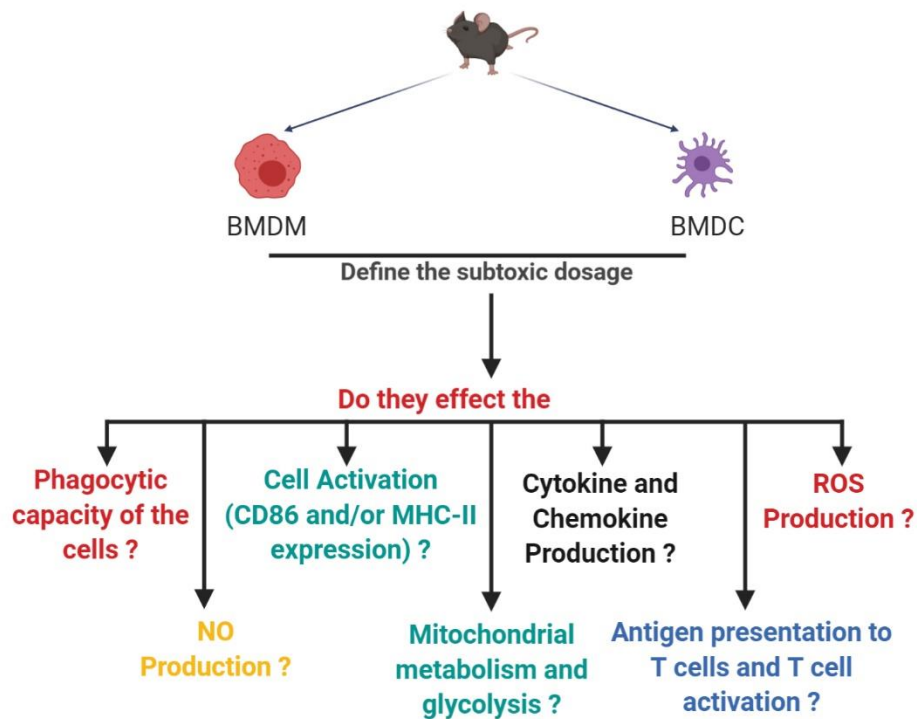


Figure 23: Objectives of the thesis (Created with BioRender.com)

## 9 Results

### 9.1 Impact of Gold nanoparticles on the functions of macrophages and dendritic cells

This part of my thesis was achieved following the “CellNanoTox” FP7 European Project (FP6-NMP-CT-2006-032731), which was designed to enhance the knowledge about the cellular interactions and toxicity of different engineered nanoparticles to assess better the risk of occupational and general population exposure to industrially manufactured nanoparticles. According to the Global Nanomaterials Market Size Report (GVR-4-68038-565-6), the global market size of nanomaterials in 2019 was USD 8.5 billion and is anticipated to rise at a compound annual growth rate (CAGR) of 13.1 percent from 2020 to 2027. Despite having such a promising market growth, the scarcity of toxicology data on engineered NPs has not yet provided appropriate risk assessment. To reduce the level of possible obstruction on Nanomaterials Market growth and research in this field, it is important to identify potential risks from exposure to different NPs and establish a scientifically defensible database for risk assessment purposes.

NP toxicity assessment is highly complex and involves a range of cutting-edge technology, validation skills, and industrial know-how to incorporate basic scientific knowledge and implementation as well as innovation in the field of toxicology. Therefore, the CellNanoTox consortium was made up of 9 partners from 5 countries specialists (<http://www.fp6-cellnanotox.net/>) combining different scientific fields. Our laboratory was in charge of the analysis of the interactions of NP with the immune system. AuNPs were among the studied NPs, and the first results showed AuNPs were not toxic, did not stimulate DCs but could affect their cytokine production in response to LPS stimulation (Villiers *et al*, 2010). To further explore the effects of AuNPs, I participated in analyzing several cellular functions of bone marrow-derived primary macrophages (BMDMs) and dendritic cells (BMDCs). My contribution to the works was focused on the consequences of AuNP exposure to primary macrophages. Furthermore, I have established the experimental conditions to analyze *in vitro* the metabolism of immune cells, either lines or primary cells.

In this study, we have developed a panel of functional *in vitro* tests to assess the impact of AuNPs on different cellular functions. More precisely, I participated in generating research data mainly focused on BMDCs and BMDMs, namely, LDH Assay for toxicity analysis, proinflammatory and Th1/Th2/Th17 cytokine profiling using CBA or ELISA kit, ROS production by using ROS-Glo™ H<sub>2</sub>O<sub>2</sub> Assay, NO production by Griess assay, and metabolic profiling by using Seahorse XF bio Analyser. Phagocytic assay using fluorescently labelled microsphere and confocal microscopy have been performed by former Ph.D. fellow of the lab, Dr. A Gonon. In addition, Dr. E-I Pécheur (researcher at CRCL Lyon) did electronic microscopy. In the lab, Mrs. M Pezet provided expert advice in cell fluorescent imaging, and flow cytometry, Dr. C Villiers and Dr. P-N




Marche designed and supervised the study at different progress levels. I also participated in writing the original draft of the attached manuscript.

Our investigation concluded AuNPs by themselves displayed no significant effect on primary macrophages (M) and DCs functions. However, when exposed to AuNPs, M and DCs responded differently to LPS or IL-4 stimulations. We showed AuNPs altered cytokine and ROS productions differently in M and DCs, whereas NO production by both cells remained unaffected. The metabolic profile underpins all functions of the immune cells and their polarisation. The analysis of the metabolic activity revealed that AuNPs significantly altered mitochondrial respiration and glycolysis of M, while only little effect was seen on DCs. Furthermore, we showed that T cell responses increased when antigen was presented by AuNPs-exposed DCs, leading to stronger Th1, Th2, and Th17 responses.

Our data not only contributed to enrich the immunotoxicological effect of AuNPs but also, this kind of analysis can be extended to a set of NPs of different sizes and different natures.

A paper is published on *Cells* 2021, 10(1), 96; <https://doi.org/10.3390/cells10010096>.

# Impact of Gold Nanoparticles on the Functions of Macrophages and Dendritic Cells

Arindam K. Dey <sup>1,†</sup> , Alexis Gonon <sup>1,†</sup> , Eve-Isabelle Pécheur <sup>2</sup>, Mylène Pezet <sup>1</sup>, Christian Villiers <sup>1</sup> and Patrice N. Marche <sup>1,\*</sup> 

<sup>1</sup> Institute for Advanced Biosciences, UMR CNRS 5309/INSERM U1209, Université Grenoble-Alpes, 38400 Grenoble, France; arindam.dey@inserm.fr (A.K.D.); alexis.gonon@gmail.com (A.G.); mylene.pezet@inserm.fr (M.P.); villiers.christ@gmail.com (C.V.)

<sup>2</sup> Centre de Recherche en Cancérologie de Lyon, UMR CNRS 5286/INSERM U1052, Université de Lyon, 69008 Lyon, France; eve-isabelle.pecheur@inserm.fr

\* Correspondence: patrice.marche@inserm.fr; Tel.: +33-670165352

† A.K.D. and A.G. equally contributed.

**Abstract:** Gold nanoparticles (AuNPs) have demonstrated outstanding performance in many biomedical applications. Their safety is recognised; however, their effects on the immune system remain ill defined. Antigen-presenting cells (APCs) are immune cells specialised in sensing external stimulus and in capturing exogenous materials then delivering signals for the immune responses. We used primary macrophages (Ms) and dendritic cells (DCs) of mice as an APC model. Whereas AuNPs did not alter significantly Ms and DCs functions, the exposure to AuNPs affected differently Ms and DCs in their responses to subsequent stimulations. The secretion of inflammatory molecules like cytokines (IL-6, TNF- $\alpha$ ), chemokine (MCP-1), and reactive oxygen species (ROS) were altered differently in Ms and DCs. Furthermore, the metabolic activity of Ms was affected with the increase of mitochondrial respiration and glycolysis, while only a minor effect was seen on DCs. Antigen presentation to T cells increased when DCs were exposed to AuNPs leading to stronger Th1, Th2, and Th17 responses. In conclusion, our data provide new insights into the complexity of the effects of AuNPs on the immune system. Although AuNPs may be considered as devoid of significant effect, they may induce discrete modifications on some functions that can differ among the immune cells.

**Keywords:** antigen presenting cells; phagocytic cells; immunotoxicity; inflammation; immuno-metabolism



**Citation:** Dey, A.K.; Gonon, A.; Pécheur, E.-I.; Pezet, M.; Villiers, C.; Marche, P.N. Impact of Gold Nanoparticles on the Functions of Macrophages and Dendritic Cells. *Cells* **2021**, *10*, 96. <https://doi.org/10.3390/cells10010096>

Received: 30 November 2020

Accepted: 4 January 2021

Published: 7 January 2021

**Publisher's Note:** MDPI stays neutral with regard to jurisdictional claims in published maps and institutional affiliations.



**Copyright:** © 2021 by the authors. Licensee MDPI, Basel, Switzerland. This article is an open access article distributed under the terms and conditions of the Creative Commons Attribution (CC BY) license (<https://creativecommons.org/licenses/by/4.0/>).

## 1. Introduction

In the past few decades, nanoparticles (NPs) have been introduced in medicine for therapeutic and diagnostic applications. The surface modifications of these nanometric structures, together with the encapsulation of drugs, enable the development of innovative drug carriers or contrast agents for imaging. This field of investigation is of great interest, as NPs might enable the development of targeted therapies, increasing the diffusion and effectiveness of drugs together with facilitated administration and reduced public health costs [1].

Gold is the archetype of materials developed for medical purposes. Indeed, gold-based NPs (AuNPs) are easily synthesised and adjustable in size. Their surface can be covalently-modified and they are resistant to oxidation [2]. All these properties enable the use of AuNPs to deliver different kinds of therapeutic agents [3]. Furthermore, AuNPs have specific optical properties, and can be easily detected and imaged. Based upon these peculiarities, AuNPs have been used as photothermal agents for cancer therapy, which are capable of delivering heat upon surface plasmon oscillation excitation [4]. Despite the wide range of beneficial applications, AuNPs are thought to induce toxic side effects when inhaled or ingested. Thus, it is important to investigate their toxicity and how they can be minimised.



The immune system is specialised in the maintenance of body integrity and comprises an innate and adaptive contribution. The innate immune system is considered as the first line of defence against foreign pathogens [5]. It comprises antigen-presenting cells (APCs), such as macrophages (Ms) and dendritic cells (DCs), both found in the blood, lymphoid organs, and residing in any organs. Ms are a subset of phagocytes of the innate immune system. Their main role is to engulf and digest cellular debris and pathogens taken up from their environment by a mechanism called phagocytosis. They contribute to a rapid and non-specific defence, and are efficient against most pathogens [6]. The DCs are defined as professional APCs [7]. They act at the interface between the innate and adaptive immune systems. After phagocytosis, their main function is to process and present antigens to naive T lymphocytes (LT), associated with class II major histocompatibility complex (MHC-II). This process may initiate the adaptive immune response. Upon activation by a foreign pathogen, DCs secrete a large range of cytokines, implicated in the activation of natural killers or the control of T cell response, for example [8]. The integrity of both these cell populations is necessary to ensure proper responses to infection; they are, thus, likely the most relevant experimental models for the study of the effects of NPs on cell fate.

Both DCs and Ms express toll-like receptors (TLR) that allow them to detect and respond to pathogen-derived molecules [9]. In response to different TLR agonists, as well as cytokines such as IL-4 and IL-13, DCs and Ms transition from a resting to an activated state through a process that involves the induction of expression of genes encoding a broad array of proteins such as cytokines, chemokines, and co-stimulatory molecules. Activation of DCs and Ms in response to particular stimulus requires support from metabolic and bioenergetic resources. Therefore, immuno-metabolism entails all activities and changes that occur in immune cells [10].

Indeed, AuNPs have been found to accumulate in Ms and DCs due to their phagocytic capacity [11], making these cells suitable to investigate the toxic effects of AuNPs. They could engulf a large volume of these particles, and in case AuNPs display high toxicity, the metabolism of Ms and DCs could be severely affected, eventually leading to the alteration of cellular functions.

Up to now, publications dealing with AuNPs toxicity demonstrated that the accumulation of these particles in cells induced low cytotoxicity [12–15]. However, the functional impact of AuNPs exposure on the immune system cells, also defined as immunotoxicity, remains poorly documented.

This paper describes the impact of AuNPs on Ms and DCs metabolism, which could lead to alteration in the respective cell function, and proposes that reprogramming of cell metabolism using AuNPs might be a novel therapeutic approach to treat inflammatory diseases.

For this reason, we analysed whether exposure to sub-toxic doses of AuNPs (10 nm and 50 nm) leads to functional alterations of these cells. We evaluated the effect of AuNPs on the following: (1) phagocytic capacity of Ms and DCs; (2) cell activation; (3) cytokine production; (4) redox profile; (5) metabolic profile, and (6) LT activation by DCs.

## 2. Materials and Methods

### 2.1. Cell Culture

The mouse Ms cell line J774.1A was obtained from the American Type Culture Collection (ATCC™). Cells were cultured in complete Dulbecco's modified Eagle's medium (DMEM) supplemented with 10% foetal bovine serum and 1% penicillin-streptomycin.

The bone marrow (BM) derived dendritic cells (BMDCs) were generated from BM extracted from C57BL/6 mice (Charles River, l'Arbresle, France), as described earlier [16]. Briefly, BM cells were isolated by flushing from the tibia and femurs. Erythrocytes and GR1 (Granulocytic Marker-1) positive cells were removed by magnetic cell sorting using Dynabeads (ThermoFisher, Waltham, MA, USA, cat. no.: 11047) after incubation with Ly-6G/Ly-6C (BD Pharmingen, cat. no.: 553125) and TER-119 (BD Pharmingen, cat. no.: 553672) antibodies, the remaining negatively sorted cells were isolated using Dynabeads isolation kit (ThermoFisher, cat. no.: 11047), and resuspended at  $5 \times 10^5$  cells/mL in complete

Iscove's modified Dulbecco's medium (IMDM) (ThermoFisher, cat. no.: 21980065), supplemented with granulocyte-macrophage colony-stimulating factor (GM-CSF) (PeproTech, London, UK, cat. no.: 315-03), FLT-3L (PeproTech, cat. no.: 250-31L), and IL-6 (PeproTech, cat. no.: 216-16) according to Table 1. The transformation of the progenitors into fully active DCs occurred after 10 days of culture.

**Table 1.** Concentration of granulocyte-macrophage colony-stimulating factor (GM-CSF), FLT-3L, and IL-6 for bone marrow (BM) derived dendritic cells (BMDCs) culture <sup>1</sup>.

		Cells Are Cultured				
		Day 0	Day 3	Day 5	Day 7	Day 10
Cell Concentration		$0.6 \times 10^6/\text{mL}$	$0.5 \times 10^6/\text{mL}$	$0.5 \times 10^6/\text{mL}$	$0.5 \times 10^6/\text{mL}$	According to Cell Plating
Supplement	IL-6	5 ng/mL	2.5 ng/mL	2.5 ng/mL	-	-
	FLT-3	50 ng/mL	40 ng/mL	30 ng/mL	25 ng/mL	25 ng/mL
	GM-CSF	5 ng/mL	5 ng/mL	5 ng/mL	5 ng/mL	5 ng/mL

<sup>1</sup> BMDCs culture: BMDCs were cultured in a 100 mM TC-treated cell culture dish with 15 mL culture media. Varying concentrations of GM-CSF, FLT-3L and IL-6 were added to on day 0, day 3, Day 5, Day 7, and Day 10 to harvest fully differentiated BMDCs in day 11.

The bone marrow-derived macrophages (BMDMs) were generated from the BM from C57BL/6 mice, as described earlier [17]. Erythrocytes were removed by red blood cell (RBC) lysis buffer, and the remaining cells were cultured in complete DMEM medium (ThermoFisher, cat.no:61965026) supplemented, with 20% of L929 conditioned medium (source of M-CSF) for 7 days.

Ovalbumin (OVA)-specific CD4+ T cells were obtained from OT II Mice (Charles River Laboratories, l'Arbresle, France). Briefly, mouse spleen was dissociated in the Roswell Park Memorial Institute (RPMI) medium, and erythrocytes were lysed using RBC lysis buffer. The T cells were isolated by negative selection using Dynabeads<sup>®</sup> Untouched<sup>™</sup> Mouse T Cell Kit (ThermoFisher, cat. no.: 11413D) and resuspended in the culture medium of BMDCs.

## 2.2. Gold Nanoparticles (AuNPs)

BioPure Gold Nanospheres were obtained from Nanocomposix (Nanocomposix, San Diego, CA, USA, cat. no.: AUCB20). These AuNPs were of high quality particles, unagglomerated, monodispersed, extensively purified, and provided sterile and endotoxin free (<5 EU/mL). The zeta potential of these particles were  $+19.7 \pm 0.8$  mV (3 independent measurements at 25 °C) by electrophoretic light scattering (ELS) using a Zeta Sizer Nano ZS instrument (Malvern Panalytical, Malvern, UK) with 1 µg/mL AuNPs dispersion in 1 mM NaCl. The hydrodynamic diameter and polydispersity index (PDI) of these particles were measured by dynamic light scattering (DLS) with a 1 µg/mL AuNPs in complete DMEM medium. The hydrodynamic diameter was  $97.01 \pm 7.29$  nm in DMEM (complete medium with 10% FBS) (Supplementary Table S1). The PDI was  $0.45 \pm 0.009$ .

## 2.3. Incubation with AuNPs

Cells were plated on 12, 24, or 96 well plates from Falcon<sup>®</sup> or Seahorse XFe96 cell culture microplates and exposed to AuNPs at 10 and 50 µg/mL final concentrations for 24 h. This time of exposure was selected because it is actually the longest time of exposure feasible to achieve all the assay time lines without affecting cell viability. Then, the cells were washed and stimulated with lipopolysaccharide (LPS) (Sigma, Saint-Quentin Fallavier, France, cat. no.: L2654) (2 µg/mL) or IL-4 (ThermoFisher, cat. no.: 14-8041-80) (20 ng/mL) for 24 h. The impact of AuNPs on BMDMs and BMDCs was assayed for parameters such as viability, phagocytosis, activation, cytokine secretion, nitric oxide (NO) production, reactive

oxygen species (ROS) production, glycolysis, or mitochondrial metabolism. A graphical representation of all the experiments is presented in Supplementary Figure S1.

#### 2.4. Toxicity Assessment

Cell viability was tested by CytoTox-ONE™ Homogeneous Membrane Integrity Assay (Promega, Charbonnières-les-Bains, France, cat. no.: G7891), according to the manufacturer's optimised protocol. Lysis solution was added to generate full lactic dehydrogenase (LDH) release corresponding to a 100% cell death and used as control. The fluorescence signal was recorded (at 560 nm and 590 nm for excitation and emission, respectively) with a CLARIOstar® Microplate Reader (BMG Labtech, Ortenberg, Germany).

#### 2.5. Confocal Microscopy and Transmission Electron Microscopy (TEM) Analyses

The AuNPs accumulation inside cells was analysed by the reflection of the indicated laser on their surface, using LSM510 Confocor II (Zeiss, Oberkochen, Germany). Cell membrane was visualised using FITC-conjugated cholera toxin (Sigma, cat. no.: C1655). Cell compartments were labelled with Cy3-coupled anti-early endosome antigen 1 (EEA1) (GeneTex, Irvine, CA, USA, cat. no.: GTX109638) and Alexa Fluor 647® coupled anti-lysosomal associated membrane protein 1 (LAMP1) antibodies (Santa Cruz Biotechnology, Heidelberg, Germany, cat. no.: sc-8099). After incubation with AuNPs at the indicated conditions, cells washed with PBS were incubated for 1 h at room temperature in Petri dishes pre-coated with 20 mM polylysine for 24 h.

For TEM, cells were gently washed with PBS and fixed with 1% *v/v* glutaraldehyde in PBS for 1 h at room temperature. They were then post-fixed in 1% *v/v* osmium tetroxide in PBS for 1 h, and processed by ethanol dehydration, followed by embedding in epoxy resin. Observations were performed on a Philips CM120 TEM microscope operated at 80 kV.

#### 2.6. Phagocytosis Assay

The AuNPs exposed J774.1A Ms were incubated with 1 µM-diameter FluoSpheres® Carboxylate-Modified Microspheres (1 µM, ThermoFisher, cat. no.: F8851), at a ratio of 10 microspheres per cell for 6 h at 37 °C in a 5% CO<sub>2</sub> incubator. The cells were analysed for their fluorescence on a BD Accuri™ C6 flow cytometer (BD Biosciences, Claix, France) and FCS Express V6 (De Novo Software).

#### 2.7. Cell Activation

The AuNPs exposed BMDMs and BMDCs were stimulated with 2 µg/mL LPS from *E. coli*, for 24 h at 37 °C with 5% CO<sub>2</sub>. The supernatant was harvested for cytokine immunoassay, and the cells were labelled with antibodies specific for CD11b (Ozyme, Saint Cyr, France, cat. no.: BLE101226) and CD11c (Ozyme, cat. no.: BLE117318), or CD11b (Ozyme, cat. no.: BLE101216) and F4/80 (Ozyme, cat. no.: BLE123152), cell surface markers of BMDCs and BMDMs, respectively, after Fc receptor blocking (BD Pharmingen, Claix, France, cat. no.: 553142) to reduce non-specific binding. To evaluate cellular activation, BMDCs and BMDMs were immunostained with anti-IAb-A<sup>b</sup> (Ozyme, cat. no.: BLE116410) and anti-CD86 (Ozyme, cat. no.: BLE105008) antibodies. In both cases, only live cells were selected by staining with 7-Aminoactinomycin D (7AAD) (negative gating) (BD Biosciences, cat. no.: 559925) and analysed by flow cytometry using BD™ LSR II (BD Biosciences). The proportion of activated cells was quantified using FCS Express V6 (De Novo Software).

#### 2.8. Cytokine Immunoassays

Cytokine production was measured in the supernatant of cell cultures utilising Cytometric Bead Array (CBA) (BD Biosciences, cat. no.: 552364), using a Mouse Inflammation Kit against IL-6, IL-12p70, MCP-1, TNF-α, IL-10, and IFN-γ. The results were acquired by flow cytometry on a BD™ LSR II (BD Biosciences) and analysed with FCAP Array Software v3.0 (BD Biosciences, cat.no: 652099).

### 2.9. The NO and ROS Production

The amounts of NO production by BMDMs and BMDCs were assessed by measuring nitrite concentration in the cell culture media by the Griess assay. An amount of 50  $\mu$ L of cell supernatants was transferred into a 96-well plate, incubated with an equal volume of Sulphanilamide (Sigma, cat. no.: S9251) and N-alpha-naphthyl-ethylenediamine (NED) (Sigma, cat. no.: 222488) solutions, respectively, and was allowed to sit for 10 min in the dark. Then the optical density (OD) of the solution was then measured at 540 nm, using the CLARIOstar<sup>®</sup> Microplate Reader (BMG Labtech). The approximate concentration of nitrite in samples was determined from a standard curve. The ROS production by BMDMs and BMDCs was determined by the ROS-Glo<sup>™</sup> H<sub>2</sub>O<sub>2</sub> Assay kit (Promega, cat. no.: G8821). The cells were cultured at a  $5 \times 10^4$  cells/mL concentration in 96-well plates, exposed to AuNPs 24 h. After that cells were stimulated with 2  $\mu$ g/mL LPS for 18 h. Then, 20  $\mu$ L of H<sub>2</sub>O<sub>2</sub> substrate solution was added for 6 h, followed by addition of 100  $\mu$ L of the ROS-Glo<sup>™</sup> detection solution. After this plate was incubated for 20 min at 22 °C, and luminescence was recorded using the CLARIOstar<sup>®</sup> Microplate Reader. (BMG Labtech).

### 2.10. Metabolic Flux Analysis

Mature BMDCs (at Day 10) were plated at  $1.5 \times 10^5$  cells per well in the Seahorse culture plate (Agilent, cat. no.: 102416-100) pre-coated with Cell-Tak (Sigma, cat. no.: 354240) in complete culture medium supplemented by GM-CSF (5 ng/mL) and flt3L (25 ng/mL). Mature BMDMs (at Day 7) were plated at  $0.8 \times 10^5$  cells per well in the Seahorse culture plate. For both cells types, 1 h after plating, the AuNPs were added. After 24 h of culture, they were washed, and stimulated or not with LPS/IL-4. Then after 24 h, they were either washed with glycostress assay medium [XF base medium supplemented (Agilent, cat. no.: 103575-100) with 1 mM glutamine (Agilent, Santa Clara, CA, USA, cat. no.: 103579-100)) or Mito stress assay medium (XF base medium supplemented with 1 mM pyruvate (Agilent, cat. no.: 103578-100), 2 mM glutamine and 10 mM glucose (Agilent, cat. no.: 103577-100)), and then replenished with the same medium (180  $\mu$ L/well). The cell culture plate was placed into a 37 °C incubator in the absence of CO<sub>2</sub> for 45 min to 1 h before the assay. The Seahorse XFe96 took analyser takes measurements of the extracellular acidification rate (ECAR) and the oxygen consumption rate (OCR) every 6 to 7 min. During the course of experiment, inhibitors were introduced to determine which metabolic parameters were affected because of the AuNPs treatment by measuring the ECAR and OCR. Mitochondrial metabolism of BMDCs and BMDMs was monitored by the mitostress assay. The inhibitors for mitostress assay, added in the listed order, were Oligomycin (Sigma, cat. no.: 75351) (1.5  $\mu$ M—inhibits F0/F1 ATPase), Carbonyl cyanide-p-trifluoromethoxyphenylhydrazone (Sigma, cat. no.: C2920) (1.5  $\mu$ M—uncoupling agent), antimycin A (Sigma, cat. no.: A8674), and rotenone mixture (Sigma, cat. no.: R8875) (1  $\mu$ M—inhibits mitochondrial respiratory complexes 3 and 1, respectively). Glycolysis of BMDCs and BMDMs was monitored by the glycostress assay. For the glycostress assay glucose (10 mM), Oligomycin (1.5  $\mu$ M), and 2-deoxy-D-glucose (2-DG) (Sigma, cat. no.: D8375) (30 mM—inhibits glycolysis) were injected sequentially. For each assay, Hoechst 33342 (ThermoFisher, cat. no.: H21492) was injected at the end, to normalise the data based on cell count. A graphical representation of the experimental design is presented in Supplementary Figure S2.

### 2.11. Antigen Presentation Assay

The AuNPs exposed BMDCs were stimulated with 2  $\mu$ g/mL LPS for 4 h and incubated with 25  $\mu$ g/mL OVA for another 4 h at 37 °C and 5% CO<sub>2</sub>. A total of  $0.4 \times 10^6$  T cells (extracted from OT-II mice and resuspended in the culture medium of BMDCs) were added to  $0.1 \times 10^6$  BMDCs. Co-cultures were incubated for 4 d, and supernatants were then harvested for cytokine immunoassays to measure IFN- $\gamma$  and IL-17 by using the Th1/Th2/Th17 CBA kit (BD Biosciences, cat. no.: 560485), and IL-13 (ThermoFisher, cat.

no.: 88-7137-77) was determined by ELISA. A graphical representation of the experimental design is presented in Supplementary Figure S3.

### 2.12. Statistical Analysis

Results are expressed as mean values  $\pm$  SD. Statistical analysis was performed using Prism version 8.4.2 (GraphPad). Statistically significant differences were assessed by ordinary one-way ANOVA, or repeated measures (RM) ANOVA with Tukey's multiple comparisons test. Significance of the results is indicated according to  $p$ -values as follows: \*  $p \leq 0.05$ , \*\*  $p \leq 0.01$ , \*\*\*  $p \leq 0.001$  and \*\*\*\*  $p \leq 0.0001$ . The  $p$ -value below 0.05 was considered statistically significant.

## 3. Results

### 3.1. Viability of APCs after Exposure to AuNPs

To analyse whether AuNPs are toxic for APCs, dendritic cells (BMDCs) and macrophages (BMDMs and J774.1A) were exposed to different concentrations of AuNPs in vitro. Cell viability was evaluated after 24 h by measuring membrane integrity through the LDH release assay (Figure 1). For concentrations up to 150  $\mu\text{g}/\text{mL}$ , no significant cytotoxicity of AuNPs was observed (Figure 1). For the analysis of the immune cell functions, we later used 50  $\mu\text{g}/\text{mL}$  as the highest concentration of AuNPs. This was due to a constraint in some experimental set up, like in the metabolic analysis, limiting the volume of AuNPs that could be added.

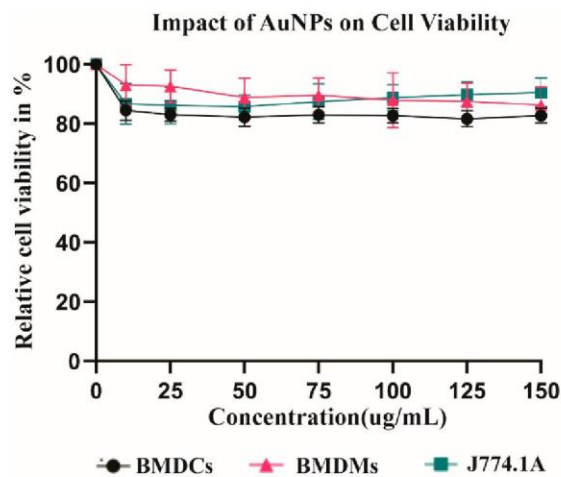


**Figure 1.** Evaluation of cell toxicity after gold nanoparticles (AuNPs) exposure of antigen-presenting cells (APCs). Cell mortality (lactic dehydrogenase (LDH) Assay) of BMDCs, bone marrow-derived macrophages (BMDMs), and J774.1A cells was analysed after exposure to different concentrations of AuNPs for 24 h. Data are normalised to untreated cells (no AuNPs), considered 100% live. The results are the mean and standard deviation of three independent experiments.

### 3.2. The AuNPs Uptake by APCs

To visualise the internalisation of AuNPs by APCs, we first used J774.1A cell line as a model of phagocytic cells. Cells were exposed to 50  $\mu\text{g}/\text{mL}$  of AuNPs for 24 h and observed by confocal microscopy, AuNPs were visualised by light reflection, cellular plasma membranes were stained using FITC labelled cholera toxin. Figure 2A clearly shows the internalisation of AuNPs into J774.1A cells. To more precisely map the sub-cellular compartments of the internalisation, primary phagocytic cells, BMDCs, were exposed to AuNPs for 24 h, then early endosomes and late endosomes were labelled with anti-EEA1 antibodies and anti-LAMP1 antibodies, respectively. Confocal imaging revealed that AuNPs appeared scattered throughout the cell with no specific accumulation with either early or late endosomes (Figure 2B). The intracellular location of AuNPs in

BMDCs was further analysed by electron microscopy, confirming some AuNPs were inside intracellular vesicles (orange arrow) and also that AuNPs accumulated in the cytoplasm (green arrow) or associated to the membrane, probably being internalised (blue arrow) (Figure 2C). Accumulation of AuNPs into phagocytic APCs raises the question of whether their functions could be altered.

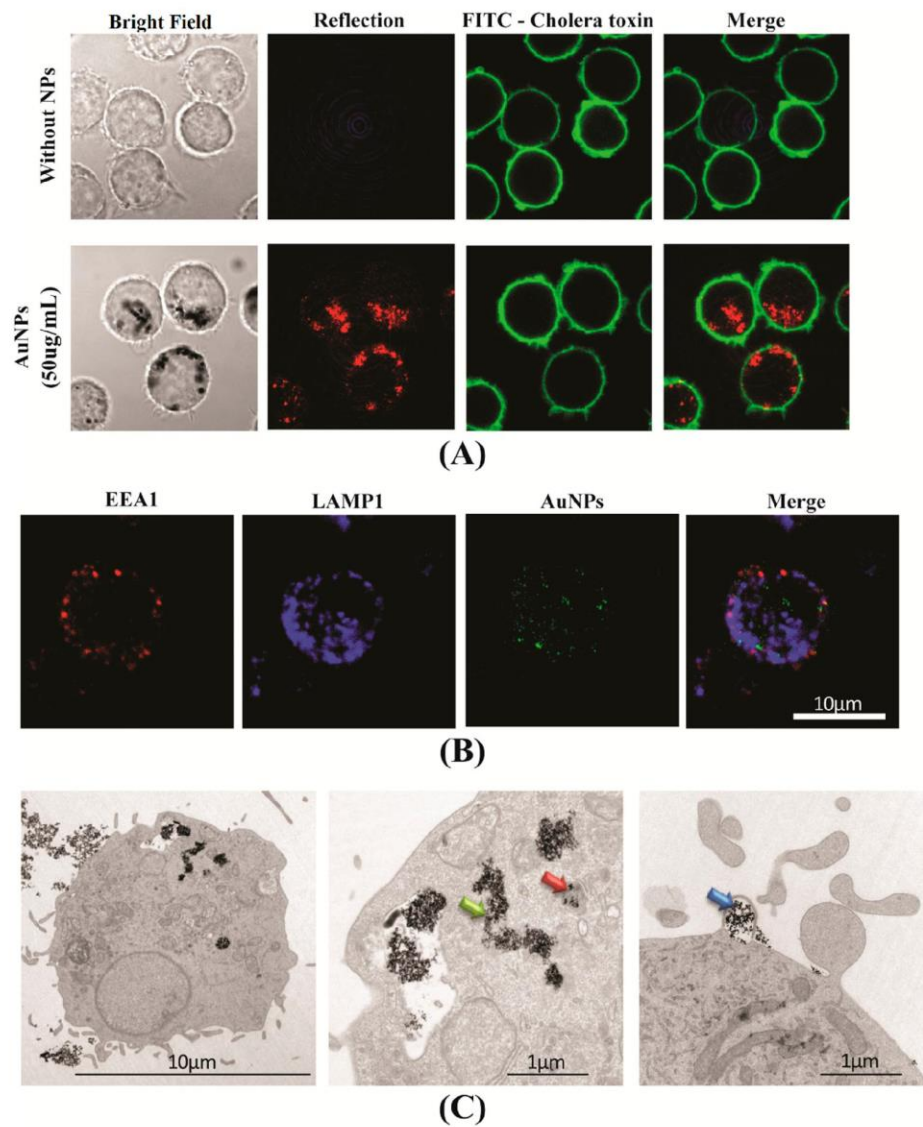


**Figure 2.** Uptake of AuNPs by APCs. **(A,B)** are images of confocal microscopy. **(A)** After exposure of the J774.1A cells to 50 µg/mL AuNPs for 24 h, cell membranes were labelled with FITC-coupled cholera toxin (green), and AuNPs were observed by the reflection using a 560 nm laser (red). **(B)** the BMDCs were exposed to 75 µg/mL AuNPs for 10 min; early (EEA1) and late (LAMP1) endosomes were labelled and AuNPs were observed by the reflection of 488 nm laser. **(C)** The intracellular location of AuNPs (13 µg/mL) in BMDCs was analysed using transmission electron microscopy after a 18-h incubation. The central and right panels represent magnified views of cells. Images are representative of the majority of cells observed.

### 3.3. Phagocytosis Capacity of Macrophages

The J774.1A Ms. are a commonly used model to analyse internalisation processes and phagocytosis. The phagocytic capacity of J774.1A Ms. was evaluated via engulfment of

polystyrene microspheres (1  $\mu\text{M}$ ) coupled with a fluorochrome. After sorting, the number of phagocytosed polystyrene microspheres was counted by confocal microscopy. Different sub-populations could be defined depending on their fluorescence intensity. Furthermore, fluorescence intensity can be correlated to a number of phagocytosed polystyrene microspheres counted by confocal microscopy (Figure 3A). Thus, each peak of the flow cytometry histogram has been assigned to a cell population which has internalised 1, 2, 3, and more microspheres respectively. After exposure to AuNPs, the same analysis was performed (Figure 3B) and showed a moderate increase of phagocytosis at the highest dose of AuNPs that is reflected by a decrease of the number of cells, which did not contain microspheres. In conclusion, the exposure of macrophages to AuNPs does not lead to important change in their subsequent phagocytosis capacity.

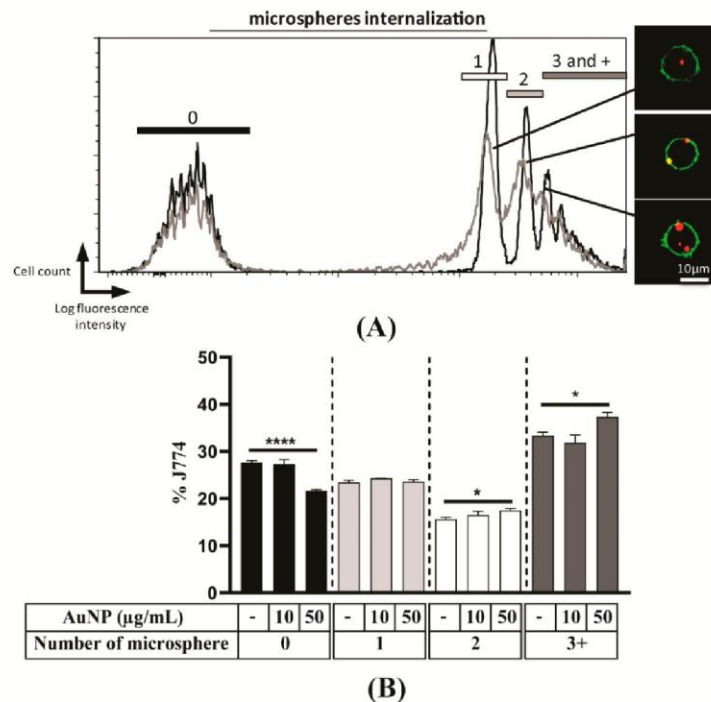


**Figure 3.** Phagocytosis capacity of macrophages. (A) J774.1A were exposed (grey) or not (black) to 50  $\mu\text{g/mL}$  AuNPs for 24 h and incubated with fluorescent microspheres Fluospheres<sup>®</sup> for 6 h, and analysed by flow cytometry. Overlaid histograms are shown. (B) After exposure to different concentrations of AuNPs, the proportion of cells in each peak was analysed. The results are the mean  $\pm$  SD of three independent experiments. Ordinary one-way ANOVA was performed \*  $p \leq 0.05$ , \*\*\*\*  $p \leq 0.0001$ .

#### 3.4. The AuNPs Do Not Impact the Expression of Cell Surface Markers of APCs Activation

The impact of AuNPs on APCs cell activation was analysed using primary BMDCs and BMDMs; being not transformed these cells better reproduce cellular fate than cell lines. After the differentiation of BM cells in the culture, BMDCs and BMDMs were analysed by flow cytometry for the expression of differentiation surface markers. The BMDCs were stained for CD11b and CD11c expressions and BMDMs for CD11b and F4/80 expressions (Supplementary Figure S4). For each cell preparation, live cells were gated by selecting the 7AAD negative cell population, and double-positive cells were gated to analyse the expression of the activation markers CD86 and MHC-II (Figure 4A,B). As expected after the activation of APCs by LPS, the number of activated cells expressing both CD86 and MHC-II increased from 27.57% to 74.97% for BMDCs (Figure 4A), but a negligible change was observed in the case of BMDMs (18.43 to 14.69%) (Figure 4B). Although LPS did not

alter the double- positive cell population in BMDMs, however, in case of BMDMs, CD86 expression significantly increased (43.25 vs. 84.03%) (Supplementary Figure S4). Exposure to increasing concentrations of AuNPs did not yield to the activation of BMDCs, the level of double-positive cells remaining in the same range between 27.57% to 28.26%, but decreased in the case of BMDMs (18.43% vs. 4.39%). These data led us to conclude that AuNPs cannot activate BMDCs but can suppress BMDMs activation. When cells were exposed to AuNPs, their capacity to respond to LPS activation increased for BMDCs (74.97% vs. 83.37%), but remain unchanged for BMDMs (14.69% vs. 12.37%). The AuNPs-mediated modulation of cell surface marker expression is presented in Table 2, and the analysis of flow cytometry data is shown in Supplementary Figure S4. Altogether, these data indicate that exposure to AuNPs affect APCs activation estimated by the expression of cell surface markers.

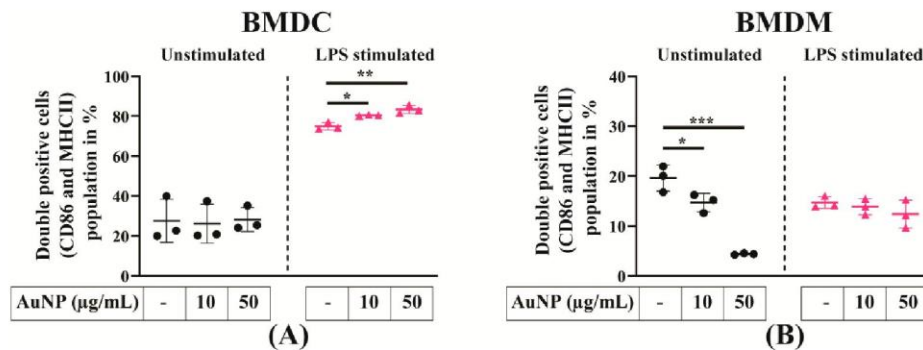


**Figure 4.** Expression of activation surface markers of APCs. (A) Expression of activation markers of BMDCs. (B) Expression of activation markers of BMDMs. APCs are exposed to AuNPs for 24 h, followed by lipopolysaccharide (LPS) stimulation for an additional 24 h. Percentage of double-positive (CD86 and class II major histocompatibility complex (MHC-II)) BMDCs and BMDMs are counted gated on CD11b and Cd11c positive cells for BMDCs and CD11b and F4/80 positive cells for BMDMs and plotted in a bar graph. The results are mean  $\pm$  SD of three independent experiments. Ordinary one-way ANOVA was performed \*  $p \leq 0.05$ , \*\*  $p \leq 0.01$  and \*\*\*  $p \leq 0.001$ .

**Table 2.** Percentage of activated APCs with or without AuNPs treatment <sup>1</sup>.

	BMDCs		BMDMs	
	Unstimulated	LPS Stimulated	Unstimulated	LPS Stimulated
Cells	27.57 $\pm$ 8.80	74.97 $\pm$ 1.54	18.43 $\pm$ 1.64	14.69 $\pm$ 0.93
Cells + AuNP <sub>10</sub> $\mu$ g/mL	26.21 $\pm$ 7.95	80.46 $\pm$ 0.23	14.68 $\pm$ 1.50	13.88 $\pm$ 1.31
Cells + AuNP <sub>50</sub> $\mu$ g/mL	28.26 $\pm$ 4.95	83.37 $\pm$ 1.65	4.39 $\pm$ 0.11	12.37 $\pm$ 2.25

<sup>1</sup> Expression of activation surface marker of APCs. Expression of activation marker of BMDCs and BMDMs after exposure to AuNPs for 24 h, followed by LPS stimulation for an additional 24 h. Percentage of double-positive (CD86 and MHC-II) BMDCs and BMDMs were gated on CD11b and Cd11c positive cells for BMDCs and CD11b and F4/80 positive cells for BMDMs and the data is displayed in tabular form. Results are mean  $\pm$  SD of 3 independent experiments.

### 3.5. The AuNPs Do Not Modify the Secretions of Signalling Factors by APCs

The production of soluble factors, including signalling proteins like cytokines or chemokines and small molecular mediators like NO and ROS, are important features of APCs responses to activation. To determine whether the exposure of APCs to AuNPs could modulate their capacity to secrete cytokines and chemokines, supernatants of BMDCs and BMDMs cultures were collected and quantified for their content in pro-inflammatory (IL-6, TNF- $\alpha$ ), immunoregulatory cytokines (IL-10, IL-12) and chemokine (MCP-1). The AuNPs by themselves did not induce any cytokine and chemokine secretion (Figure 5). As expected, in response to LPS activation, both BMDCs and BMDMs secreted cytokines and chemokines, and their exposure to AuNPs had little impact on their cytokine secretion capacity to APCs. The production of IL-10 by BMDCs reduced at the highest concentration



alter the double- positive cell population in BMDMs, however, in case of BMDMs, CD86 expression significantly increased (43.25 vs. 84.03%) (Supplementary Figure S4). Exposure to increasing concentrations of AuNPs did not yield to the activation of BMDCs, the level of double-positive cells remaining in the same range between 27.57% to 28.26%, but decreased in the case of BMDMs (18.43% vs. 4.39%). These data led us to conclude that AuNPs cannot activate BMDCs but can suppress BMDMs activation. When cells were exposed to AuNPs, their capacity to respond to LPS activation increased for BMDCs (74.97% vs. 83.37%), but remain unchanged for BMDMs (14.69% vs. 12.37%). The AuNPs-mediated modulation of cell surface marker expression is presented in Table 2, and the analysis of flow cytometry data is shown in Supplementary Figure S4. Altogether, these data indicate that exposure to AuNPs affect APCs activation estimated by the expression of cell surface markers.

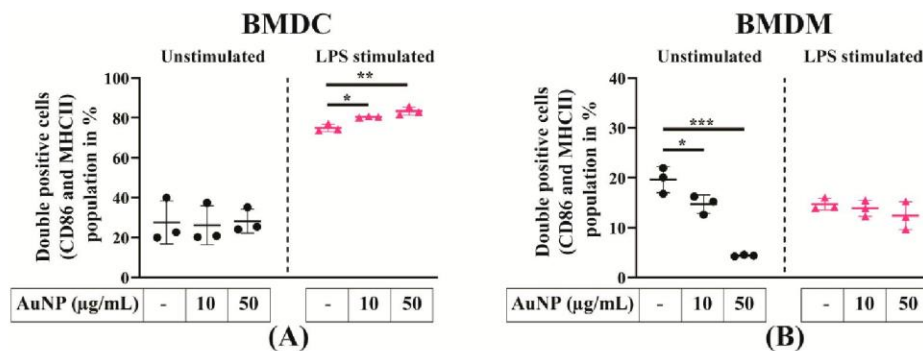


**Figure 4.** Expression of activation surface markers of APCs. **(A)** Expression of activation markers of BMDCs. **(B)** Expression of activation markers of BMDMs. APCs are exposed to AuNPs for 24 h, followed by lipopolysaccharide (LPS) stimulation for an additional 24 h. Percentage of double-positive (CD86 and class II major histocompatibility complex (MHC-II)) BMDCs and BMDMs are counted gated on CD11b and Cd11c positive cells for BMDCs and CD11b and F4/80 positive cells for BMDMs and plotted in a bar graph. The results are mean  $\pm$  SD of three independent experiments. Ordinary one-way ANOVA was performed \*  $p \leq 0.05$ , \*\*  $p \leq 0.01$  and \*\*\*  $p \leq 0.001$ .

**Table 2.** Percentage of activated APCs with or without AuNPs treatment<sup>1</sup>.

	BMDCs		BMDMs	
	Unstimulated	LPS Stimulated	Unstimulated	LPS Stimulated
Cells	27.57 $\pm$ 8.80	74.97 $\pm$ 1.54	18.43 $\pm$ 1.64	14.69 $\pm$ 0.93
Cells + AuNP <sub>10</sub> µg/mL	26.21 $\pm$ 7.95	80.46 $\pm$ 0.23	14.68 $\pm$ 1.50	13.88 $\pm$ 1.31
Cells + AuNP <sub>50</sub> µg/mL	28.26 $\pm$ 4.95	83.37 $\pm$ 1.65	4.39 $\pm$ 0.11	12.37 $\pm$ 2.25

<sup>1</sup> Expression of activation surface marker of APCs. Expression of activation marker of BMDCs and BMDMs after exposure to AuNPs for 24 h, followed by LPS stimulation for an additional 24 h. Percentage of double-positive (CD86 and MHC-II) BMDCs and BMDMs were gated on CD11b and Cd11c positive cells for BMDCs and CD11b and F4/80 positive cells for BMDMs and the data is displayed in tabular form. Results are mean  $\pm$  SD of 3 independent experiments.

### 3.5. The AuNPs Do Not Modify the Secretions of Signalling Factors by APCs

The production of soluble factors, including signalling proteins like cytokines or chemokines and small molecular mediators like NO and ROS, are important features of APCs responses to activation. To determine whether the exposure of APCs to AuNPs could modulate their capacity to secrete cytokines and chemokines, supernatants of BMDCs and BMDMs cultures were collected and quantified for their content in pro-inflammatory (IL-6, TNF- $\alpha$ ), immunoregulatory cytokines (IL-10, IL-12) and chemokine (MCP-1). The AuNPs by themselves did not induce any cytokine and chemokine secretion (Figure 5). As expected, in response to LPS activation, both BMDCs and BMDMs secreted cytokines and chemokines, and their exposure to AuNPs had little impact on their cytokine secretion capacity to APCs. The production of IL-10 by BMDCs reduced at the highest concentration

of AuNPs. The BMDMs showed a little but significant increase of TNF- $\alpha$ , and of MCP-1 only at the highest concentration of AuNPs. In conclusion, AuNPs exposure has little, if any, effect on the capacity of APCs to secrete cytokines or chemokines in response to inflammatory signalling by LPS.

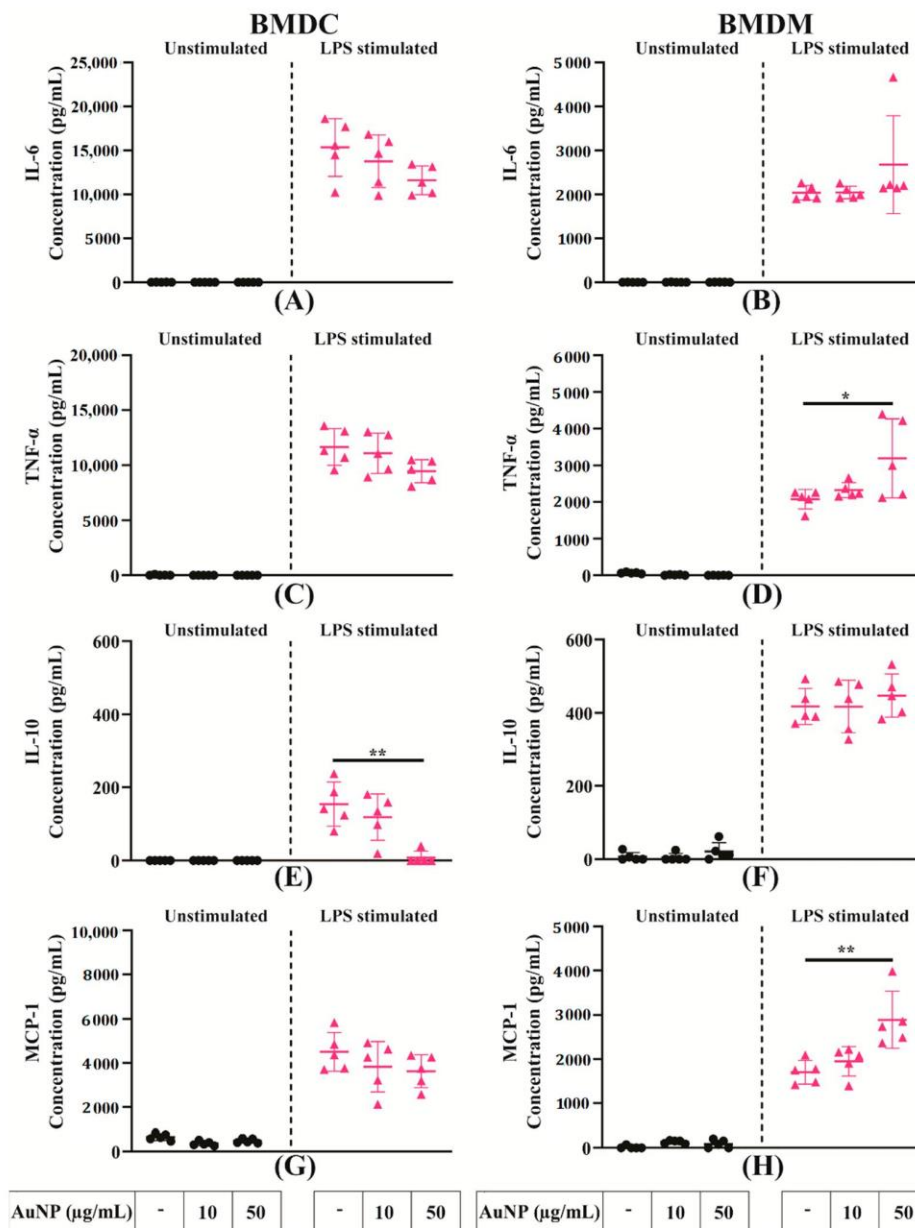


**Figure 5.** Secretion of different signalling factors by activated APCs. (A–H) Relative cytokine and chemokine concentrations in the supernatant of BMDCs and BMDMs exposed to AuNPs and activated by LPS. Results are mean  $\pm$  SD of five independent experiments. Ordinary one-way ANOVA was performed \*  $p \leq 0.05$  and \*\*  $p \leq 0.01$ .

The NO and ROS productions were evaluated in the culture supernatant of APCs cultures with the Griess assay and the quantification of H<sub>2</sub>O<sub>2</sub>, respectively. No indication of NO or ROS production was obtained after exposure of both APCs to AuNPs (Figure 6A–C). After stimulation of LPS, both APCs produced significant quantities of these mediators.

In the case of BMDMs, these productions were not modified by exposure to AuNPs (Figure 6B,D); BMDCs showed a moderate reduction of ROS productions (Figure 6C) with NO production remaining unchanged (Figure 6D). These data indicate that BMDCs and BMDMs are differently affected by AuNPs in their capacity to produce NO and ROS after LPS activation.

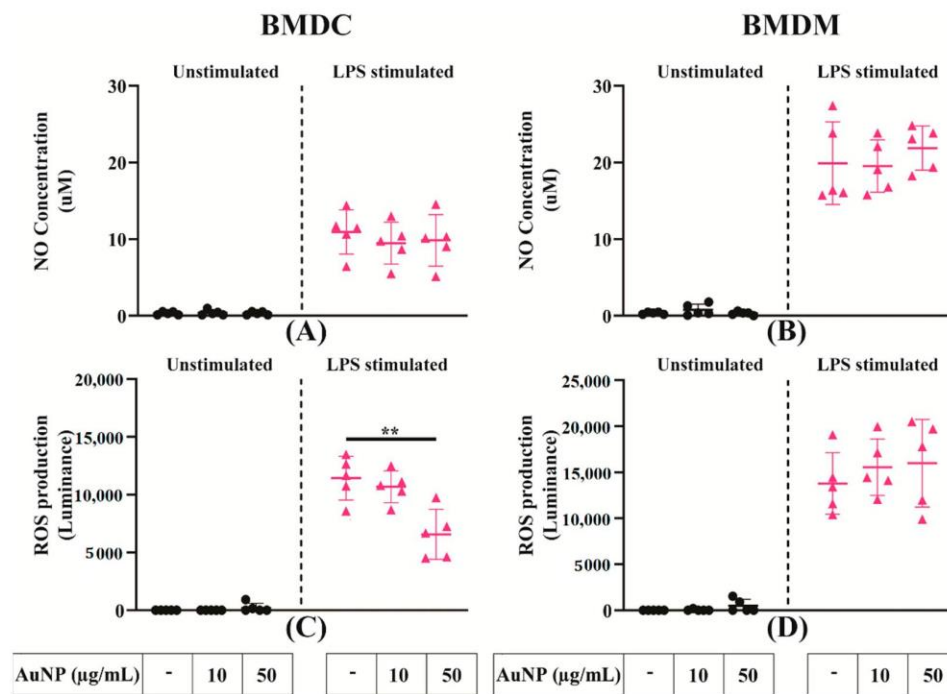


**Figure 6.** Secretion of different signalling factors by activated APCs. (A,B) Relative nitric oxide (NO) concentration in the supernatant of BMDCs and BMDMs exposed to AuNPs and activated by LPS. (C,D) Relative reactive oxygen species (ROS) production by BMDCs and BMDMs exposed to AuNPs and activated by LPS. Results are mean  $\pm$  SD of five independent experiments. Ordinary one-way ANOVA was performed  $** p \leq 0.01$ .

### 3.6. Analysis of the Mitochondrial Metabolism of APCs

Cellular metabolism is of particular interest, considering its implication in many cell functions. Under the influence of their micro-environment, APCs are polarised to achieve distinct functions. For instance, when APCs are challenged with LPS, they polarise towards pro-inflammatory M1 phenotype; conversely, when they are stimulated with IL-4, they develop an anti-inflammatory M2 phenotype. Moreover, it is known that the metabolism of LPS-activated BMDCs and BMDMs relies mainly on glycolysis, whereas cells activated by IL-4 are dependent on mitochondrial metabolism.

To reveal the impact of AuNPs on mitochondrial metabolism of differently polarised cells, the cells were pre-treated with different concentrations of AuNPs, then stimulated with LPS or IL-4 or unstimulated for 24 h. The OCR was measured by the Seahorse XFe96 analyser. As shown in Figure 7A, AuNPs exposure did not induce any alteration of the basal mitochondrial respiratory capacity of BMDCs, activated by LPS or IL-4 or not. Similarly, pre-treatment of AuNPs had no significant effect on the basal respiratory capacity of unstimulated or LPS-stimulated BMDMs; however, IL-4-stimulated BMDMs showed a significant increase of their basal respiration in a concentration-dependent manner (Figure 7B). The AuNPs did not alter proton leakage for BMDCs and BMDMs in the stimulated or unstimulated states (Figure 7C,D).

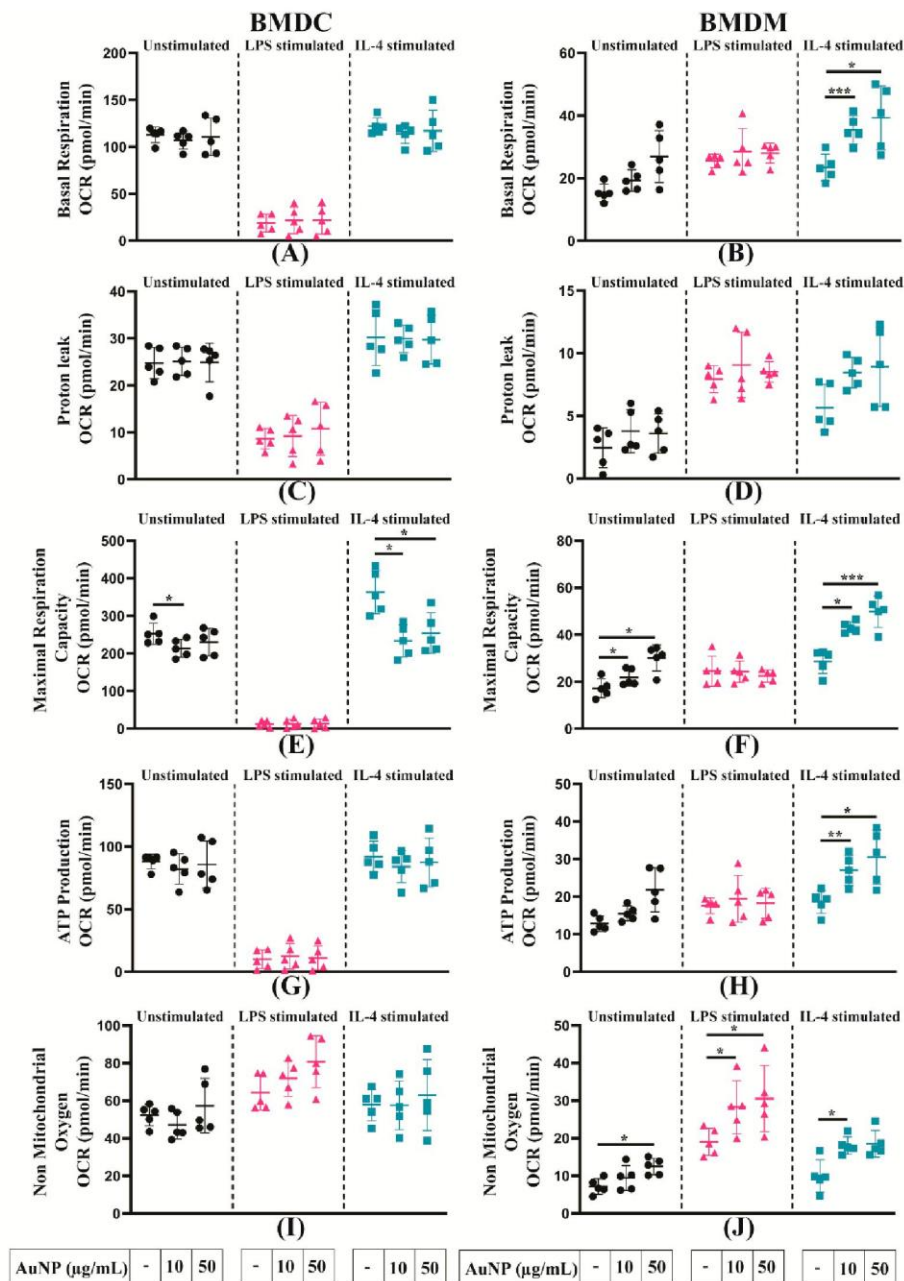


**Figure 7.** Mitochondrial metabolism of APCs activated or not. (A,B) Basal respiration, (C,D) H<sup>+</sup> (Proton) leakage, (E,F) maximal respiration, (G,H) ATP production, (I,J) non-mitochondrial respiration of BMDCs and BMDMs was measured after a 24 h exposure to AuNPs or not stimulated by LPS or IL-4 for another 24 h or not, as indicated in the graphs below. After measuring the oxygen consumption rate (OCR) by using the Seahorse XFe96 analyser, data were normalised based on the cell number by using Hoechst 33342 staining. The results are mean  $\pm$  SD from five independent experiments. RM one-way ANOVA was performed \*  $p \leq 0.05$ , \*\*  $p \leq 0.01$  and \*\*\*  $p \leq 0.001$ .

The maximal respiration capacity decreased after AuNPs exposure of unstimulated BMDCs and, more importantly, in IL-4-stimulated BMDCs (Figure 7E). Of note, LPS stimulation led to a complete abolishment of the maximal respiratory capacity of BMDCs. The behaviour of BMDMs was different, a significant increase in the maximal respiration capacity of unstimulated and IL-4-stimulated BMDMs was observed, while no change

was observed in LPS-stimulated BMDMs (Figure 7F). The analysis of ATP production (Figure 7G,H) showed similar profiles as those observed for basal respiration, with no modification after AuNPs exposure of the stimulated or unstimulated BMDCs, but a significant increase in IL-4-stimulated BMDMs, and no alteration in LPS and unstimulated BMDMs. The non-mitochondrial oxygen consumption of BMDCs was not significantly affected whatever their stimulation status (Figure 7I). Again, BMDMs displayed different reactivity, with an increase in the non-mitochondrial respiratory capacity for all types of BMDMs (Figure 7J).

Furthermore, we measured the spare respiratory capacity, which indicates the cell ability to respond to the increasing demand for ATP during the period of stress. Our results revealed that BMDCs spare respiratory capacity follows the same profile as that of maximal respiratory capacity (Supplementary Figure S5A), which is not observed in BMDMs. However, the results are not conclusive because of high variability (Supplementary Figure S5B). The analysis of coupling efficiency showed that AuNPs did not influence the coupling efficiency of stimulated or unstimulated BMDCs (Supplementary Figure S5C) and BMDMs (Supplementary Figure S5D), indicating there was no leakage of protons, which is essential for driving ATP synthase.

Altogether, these data show that the metabolism of BMDCs and BMDMs are differently affected by the exposure to AuNPs, BMDCs are moderately affected, whereas BMDMs significantly increase their mitochondrial and non-mitochondrial respiratory capacities.

### 3.7. Analysis of the Glycolysis of APCs

The effects of AuNPs exposure on the metabolism of APCs were further investigated by the analysis of their glycolytic activity. The BMDMs and BMDCs were pre-treated with different concentrations of AuNPs, then stimulated with LPS or IL-4 or kept unstimulated for 24 h. The extracellular acidification rate (ECAR) was measured by the seahorse XFe96 analyser. As shown in Figure 8A, AuNPs exposure led to a slight increase of glycolysis in unstimulated BMDCs, whereas stimulated BMDCs displayed high variable levels of glycolysis. All types of BMDMs responded to AuNPs exposure by significant increases in glycolysis (Figure 8B). Figure 8C depicted that pre-treatment with AuNPs increased the glycolytic reserve of LPS stimulated BMDCs but not that of unstimulated and IL-4-stimulated BMDCs. An increase was observed in LPS and IL-4-stimulated BMDMs, but unstimulated cells showed no alteration when exposed to different concentrations of AuNPs (Figure 8D). Overall, AuNPs increased glycolysis dependent energy demand in both BMDCs and BMDMs in a manner dependent on the dose, and on the state of stimulation.

### 3.8. The AuNPs Exposure to BMDCs Increases the Antigen Specific the T Cell Responses

To explore whether alterations of the metabolic profile of APCs impair the activation of T cell, we performed an in vitro antigen presentation assay. Briefly, AuNPs exposed BMDCs were activated with LPS and a model antigen OVA, then co-cultured with LT purified from the spleen of OT-II transgenic mice. The OT-II mice exhibit a transgenic T cell receptor (TCR), which recognises OVA peptide presented by APCs on MHC-II IAb; consequently, all LT from these mice are specific to OVA. After 4 days, the supernatant of the co-cultures was collected and the fate of LT was evaluated with regard to the cytokines secreted: gamma interferon (IFN- $\gamma$ ) as the major effector of Th1 response, IL-13 and IL-4 for Th2 response and IL-17 as representative of Th17 response. These cytokine secretions were analysed by the CBA. Figure 9 shows the quantification of these cytokines for a representative experiment. The AuNPs by themselves did not induce cytokine secretion by LT. Additionally, LDH mediated toxicity analysis showed AuNPs did not directly induced T cell death (Supplementary Figure S6). The production of IFN- $\gamma$ , IL-13, and IL-17 significantly increased when BMDCs were exposed to a high concentration of AuNPs (50  $\mu\text{g}/\text{mL}$ ). Altogether, these data showed AuNPs exposure increased BMDCs capacity to activate antigen specific responses of all T cells, i.e., Th1, Th2, Th17.

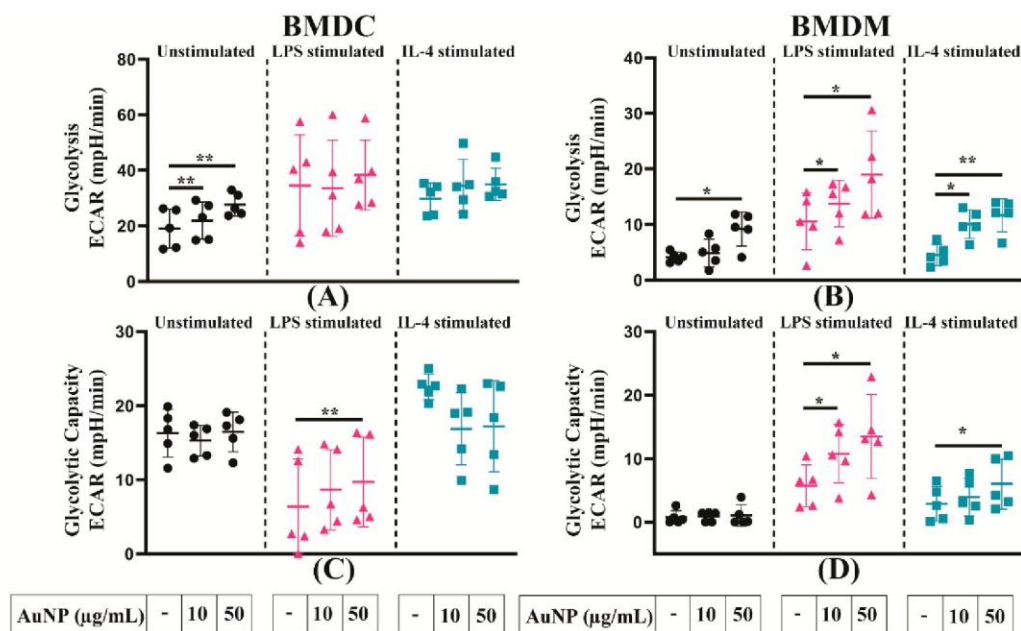


**Figure 8.** Glycolysis of APCs activated or not. (A,B) Glycolysis, (C,D) glycolytic Capacity of BMDCs and BMDMs were evaluated after a 24 h exposure to AuNPs or not and after stimulation or not by LPS or IL-4 for another 24 h, as indicated in the graphs below. After measuring the extracellular acidification rate (ECAR) using the Seahorse XF analyser, the data were normalised based on the cell number by using Hoechst 33342 staining. The results are mean  $\pm$  SD of five independent experiments. RM one-way ANOVA was performed \*  $p \leq 0.05$  and \*\*  $p \leq 0.01$ .

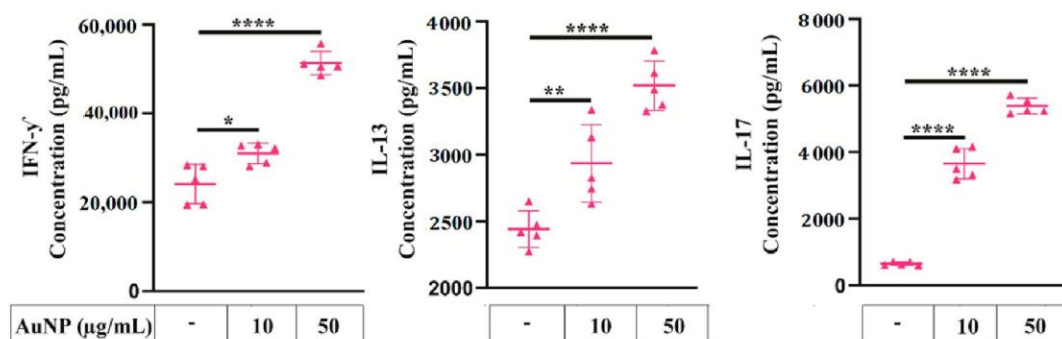


**Figure 9.** Antigen-specific T-cell responses. [A] OT-II T cells were co-cultured with AuNPs exposed/ovalbumin (OVA) loaded/LPS activated BMDCs for 4 days. T cell cytokine production is shown. In the absence of OVA antigen, the concentrations of IFN- $\gamma$ , IL-13, and IL-17 produced by T cells are 186, 35, and 623 pg/mL, respectively (data not shown), and in the absence of OVA antigen but the presence of AuNPs, the concentrations of IFN- $\gamma$ , IL-13, and IL-17 produced by T cells are 90 pg/mL, 24 pg/mL, and 381 pg/mL, respectively (data not shown). The results are mean  $\pm$  SD of five independent experiments. Ordinary one-way ANOVA was performed \*  $p \leq 0.05$ , \*\*  $p \leq 0.01$  and \*\*\*\*  $p \leq 0.0001$ .

#### 4. Discussion

Gold salts have long been used to treat various diseases such as rheumatoid arthritis and tuberculosis [18]. Today, AuNPs are widely used in targeted drug delivery, cell imaging, cancer diagnostics, and treatments [1]. The effectiveness of these particles depends on their ability to target specific cells followed by their internalisation. The nanometric size of AuNPs plays a critical role in their internalisation; 50 nm AuNPs have been shown to be

the most efficiently internalised by cells [19]. As these nanoparticles are internalised and accumulated inside cells, they may interfere with the cellular fate and functions. This issue is especially important concerning the immune system, because of the capacity of some cells of this system to actively capture extracellular materials and control immune responses by the delivery of inflammatory signals for stimulation and orientation of antigen presentation, leading to specific immune responses. A precise knowledge of the effects of AuNPs on APCs, including macrophages (Ms) and dendritic cells (DCs), provides a valuable insight into the biological consequences of AuNPs exposures and to define putative adverse effects. It is yet well established that NPs immunotoxicity should be tested on APCs [20,21], because these cells are involved in nonspecific innate defences, as well as in specific immune responses. Furthermore, DCs play a critical role as a bridge between innate and adaptive immune systems by initiating the T cell-mediated response [22]. Therefore, perturbation of the functions of these cells may result in altered immune response in NP-exposed individuals. In consequence, Ms and DCs appear to be appropriate tools for discriminating between NPs that interfere with the immune system or not. The current work provides a comparative study of the influence of AuNPs at subtoxic concentration on two primary professional phagocytic cells derived from the bone marrow of mice, BMDCs and BMDMs. Their activities and characteristics: phagocytosis, cell activation, cytokine secretions, redox status together with their ability to present antigens was analysed in detail. In addition, we provide a study of the metabolic activity, pointing at different influences of AuNPs on mitochondrial metabolism and glycolysis of BMDCs and BMDMs.

The phagocytic capacity of APCs leads to the accumulation of NP inside cells, therefore it is important to investigate the sub cellular localisation of AuNPs in APCs. Accumulation of AuNPs inside intracellular vesicles of the J774.A1 Ms cell line [23] and, more precisely, in the lysosome of the raw 264.7 Ms cell line [24], has been shown by TEM and confocal microscopy. In the present study, we demonstrate the presence of AuNPs in early (EEA1+) and late (LAMP1+) endosomes of APCs by confocal microscopy. In addition to AuNPs identified in EEA1 and LAMP1 vesicles, aggregated clusters of AuNPs were observed in the cytosol of APCs using confocal microscopy and more precisely with TEM.

One of the key properties of APCs is their ability to engulf foreign material by phagocytosis. The exposure to 10 nm AuNPs was shown to significantly reduce the phagocytic capacity of Raw 264.7 Ms cell line and BMDMs [25]. In the present study, we show that the phagocytic capacity of the J774.1A Ms cell line is not impaired after 24 h exposure with AuNPs. A possible explanation for these different effects could be that different cell lines of Ms were used and/or related to the nature of the phagocytosis assay that is based on the use of *E. coli* [25] and of polystyrene beads in our study.

Accumulation of nanoparticle inside the APCs could be an important perturbation for the activation state of the cells. Cell interaction with nanoparticle may hinder their activation state which could be evaluated by the cell surface expression of CD86 and MHC-II. We found that AuNPs did not activate the BMDCs by themselves but increase the response of BMDCs to LPS. This finding is consistent with previous studies showing the increased expression of MHC-II [14] and CD86 [26]. Interestingly, BMDMs display a different behaviour: treatment with AuNPs mildly reduced the expression of activation markers in a dose dependent manner. However, AuNPs treated BMDMs did not show any alteration of the expression of activation markers upon LPS stimulation, which may be due to the saturation of CD86 and MHC-II expression. However, in the case of BMDMs an increase of CD86 expression upon LPS stimulation is more evident than both the CD86 and MHC-II expression level.

Upon activation, APCs secrete several immune-regulatory molecules. We showed that AuNPs by themselves did not fuel any cytokine secretion. These data are in the direct line of previous studies on DCs [14] and on Ms [25], indicating that AuNPs did not promote production of TNF- $\alpha$ , IL-6 and IL-10. These findings were also validated by other previous publications in various models [24,27]. However, we see a mild increase in TNF- $\alpha$  and

MCP-1 production in AuNPs-treated BMDMs upon LPS stimulation at a high concentration (50 µg/mL).

We observed that AuNPs neither induced NO and ROS production in unstimulated BMDMs nor altered their production after LPS stimulation. This is consistent with previous findings [27]. Concerning BMDCs, we have seen a significant reduction of ROS production after LPS activation but only at high concentration of AuNPs, while NO production remains unchanged.

Generally, NMs that do not induce inflammatory response are considered as safe. However, there are evidences that NMs might alter the function of immune cells by inducing alterations in metabolic pathways [28,29]. To evaluate the effect of AuNPs on the metabolism of BMDMs and BMDCs, we stimulated them either with either LPS or IL-4 as representatives of different microenvironments, which may affect cellular functions. For example, conventional activation of pro-inflammatory cells by LPS facilitate inflammation and participate to the host defence against various kinds of microbial threats. On the other hand, alternative activation by IL4 induced anti-inflammatory cells, potent suppressors and controllers of ongoing immune responses. Such stimulated cells exhibit a distinguishable regulation of their metabolism: LPS-activated proinflammatory cells undergoing a metabolic switch to enhance glycolysis [30,31]. Alternatively, IL-4 stimulated cells rely on both fatty acid oxidation (FAO) and mitochondrial oxidative phosphorylation (OXPHOS) for sustained energy [10]. Thus, altered metabolism is not only a key feature of stimulated cell function but also a prerequisite for a proper response to immune stimuli. The analysis of mitochondrial metabolism and glycolysis showed that AuNPs did not to alter the basal mitochondrial respiration of BMDCs but increased it for BMDMs. The possible explanation for this phenomenon is the different phagocytic capacity of these cells. Indeed, it has been established that the phagocytic index of Ms is higher than that of DCs [32], thereby enabling accumulation of a large quantities of AuNPs in BMDMs, and increasing the basal respiration to meet the endogenous ATP demand of the cell. Unaltered proton leakage in BMDCs and BMDMs suggests that AuNPs did not induce any mitochondrial damage in these cells. Measurement of ATP production shows that pre-treatment with AuNPs did not alter the ATP production of BMDCs but increased it in BMDMs, which is consistent with basal respiration.

The basal respiration rate does not accurately reflect the ability of cellular respiration to respond to increased energy demand. As such, estimating the maximum capacity of substrate oxidation can be extremely valuable for the discovery of mechanisms by which AuNPs could affect cell metabolism.

Conversely, spare respiratory capacity indicates the reserve capacity of a cell to respond to an increased ATP demand and withstand periods of stress. Here, we show that pre-treatment with AuNPs significantly decreases the maximal and spare respiratory capacities of unstimulated and IL-4-stimulated BMDCs (cells, largely dependent on mitochondrial metabolism), but increases them significantly in unstimulated and IL-4-stimulated BMDMs. The increase of these two parameters in BMDMs can be explained by the increase in basal respiration as well as ATP production due to the increase in cellular energy demand. However, a significant decrease of both these parameters in BMDCs shows the impact of AuNPs on BMDCs. The possible explanation for this could be either alteration of the mitochondrial content and cristae density or alteration of the respiratory substrate transport system or alteration of the respiratory chain complex activity or a combination of these parameters [33]. Benjamin et al. have already hypothesised that AuNPs dependent alteration of innate immune memory in human monocytes might be explained by alterations in metabolic pathways [34]. Here, we confirm that AuNPs alter the metabolic response of BMDMs in response to secondary stimuli (LPS/IL-4).

To be activated, T cells have to recognise the antigen presented by MHC-II molecules and to be stimulated by CD86 accessory molecules, which are both expressed at the surface of DCs, in the context of an inflammatory signal. We observed that BMDCs challenged by LPS as inflammatory signal showed an increased expression of CD86 and MHC-II



molecules when they have been exposed to AuNPs. We investigated the impact of BMDCs on T cell antigen responses by the analysis of the secreted cytokines. A significant increase of IFN- $\gamma$ , IL-13, and IL-17 productions, reflecting Th1, Th2, and Th17 cell polarisation, could be correlated with the activation of the BMDCs seen by high CD86 and MHC-II expression levels. A study with 50 nm AuNPs reported the induction of a Th17 response in humans, but no significant change in Th1 and Th2 responses [35]. This difference can be explained by the cellular model, the surface coating of AuNPs, the maturation, and activation states of DCs and the routes of antigen uptake. Interestingly, the fact that increase T cell responses to antigen affects Th1, Th2, and Th17 subsets of T cells may preserve the balance between pro-inflammatory and anti-inflammatory responses.

In conclusion, our study shows that Ms and DCs respond differently when exposed to AuNPs. Therefore, it is mandatory to take both cell types into account when conducting immunotoxicity testing.

**Supplementary Materials:** The following are available online at <https://www.mdpi.com/2073-4409/10/1/96/s1>, Table S1: Hydrodynamic diameter of AuNPs, Figure S1: Experimental scheme of AuNPs, Figure S2: Experimental scheme for metabolic flux analysis, Figure S3: Schematic representation of Antigen presentation assay, Figure S4: Expression of activation surface marker of APC, Figure S5: Effect of AuNPs on Spare respiratory capacity and Coupling Efficiency (%) of activated or un activated BMDMs and BMDCs, Figure S6: Evaluation of cell toxicity after AuNPs exposure of T cells.

**Author Contributions:** Conceptualisation, C.V. and P.N.M.; Data curation, A.K.D., A.G., E.-I.P. and M.P.; Formal analysis, A.K.D., A.G. and E.-I.P.; Funding acquisition, P.N.M.; Methodology, A.K.D., E.-I.P., M.P. and C.V.; Supervision, P.N.M.; Validation, C.V. and P.N.M.; Writing—original draft, A.K.D., A.G. and P.N.M.; Writing—review & editing, C.V. All authors have read and agreed to the published version of the manuscript.

**Funding:** This work was supported by institutional grants from Institut National de la Santé et de la Recherche Médicale (INSERM) and was initiated during “CellNanoTox” FP6 project (NMP4-CT-2006-032731).

**Institutional Review Board Statement:** Not applicable.

**Informed Consent Statement:** Not applicable.

**Data Availability Statement:** Not applicable.

**Acknowledgments:** The authors acknowledge the staff of the animal facility of IAB, Christine Charrat for technical support, Sandrine Blanchet for her expertise in SeaHorse analysis, Zuzana Macek-Jilkova for stimulating discussions, Adrien Nougarede for expertise in DLS. Alexis Gonon was supported by a PhD fellowship from ARC3 action of the Rhone-Alpes region. A.K.D. was supported by a PhD fellowship from the European Union’s Horizon 2020 project “NEWDEAL” (grant agreement No. 720905).

**Conflicts of Interest:** The authors declare no conflict of interest. The funders had no role in the design of the study; in the collection, analyses, or interpretation of data; in the writing of the manuscript, or in the decision to publish the results.

## References

1. Ashraf, S.; Pelaz, B.; del Pino, P.; Carril, M.; Escudero, A.; Parak, W.J.; Soliman, M.G.; Zhang, Q.; Carrillo-Carrion, C. Gold-Based Nanomaterials for Applications in Nanomedicine. *Top. Curr. Chem.* **2016**, *370*, 169–202. [[CrossRef](#)] [[PubMed](#)]
2. Khlebtsov, B.; Panfilova, E.; Khanadeev, V.; Bibikova, O.; Terentyuk, G.; Ivanov, A.; Rummyantseva, V.; Shilov, I.; Ryabova, A.; Loshchenov, V.; et al. Nanocomposites containing silica-coated gold-silver nanocages and Yb-2,4-dimethoxyhematoporphyrin: Multifunctional capability of IR-luminescence detection, photosensitization, and photothermal therapy. *ACS Nano* **2011**, *5*, 7077–7089. [[CrossRef](#)] [[PubMed](#)]
3. Farooq, M.U.; Novosad, V.; Rozhkova, E.A.; Wali, H.; Ali, A.; Fateh, A.A.; Neogi, P.B.; Neogi, A.; Wang, Z. Gold Nanoparticles-enabled Efficient Dual Delivery of Anticancer Therapeutics to HeLa Cells. *Sci. Rep.* **2018**, *8*, 2907. [[CrossRef](#)] [[PubMed](#)]
4. Hwang, S.; Nam, J.; Jung, S.; Song, J.; Doh, H.; Kim, S. Gold nanoparticle-mediated photothermal therapy: Current status and future perspective. *Nanomedicine* **2014**, *9*, 2003–2022. [[CrossRef](#)] [[PubMed](#)]

5. Trombetta, E.S.; Mellman, I. Cell biology of antigen processing in vitro and in vivo. *Annu. Rev. Immunol.* **2005**, *23*, 975–1028. [[CrossRef](#)] [[PubMed](#)]
6. Klopffleisch, R. Macrophage reaction against biomaterials in the mouse model—Phenotypes, functions and markers. *Acta Biomater.* **2016**, *43*, 3–13. [[CrossRef](#)]
7. Banchereau, J.; Briere, F.; Caux, C.; Davoust, J.; Lebecque, S.; Liu, Y.J.; Pulendran, B.; Palucka, K. Immunobiology of dendritic cells. *Annu. Rev. Immunol.* **2000**, *18*, 767–811. [[CrossRef](#)]
8. Blanco, P.; Palucka, A.K.; Pascual, V.; Banchereau, J. Dendritic cells and cytokines in human inflammatory and autoimmune diseases. *Cytokine Growth Factor Rev.* **2008**, *19*, 41–52. [[CrossRef](#)]
9. Takeda, K.; Akira, S. Toll-like receptors in innate immunity. *Int. Immunol.* **2005**, *17*, 1–14. [[CrossRef](#)]
10. O’Neill, L.A.; Kishton, R.J.; Rathmell, J. A guide to immunometabolism for immunologists. *Nat. Rev. Immunol.* **2016**, *16*, 553–565. [[CrossRef](#)]
11. Hussain, S.; Vanoirbeek, J.A.; Hoet, P.H. Interactions of nanomaterials with the immune system. *Wiley Interdiscip. Rev. Nanomed. Nanobiotechnol.* **2012**, *4*, 169–183. [[CrossRef](#)] [[PubMed](#)]
12. Alkilany, A.M.; Murphy, C.J. Toxicity and cellular uptake of gold nanoparticles: What we have learned so far? *J. Nanopart. Res.* **2010**, *12*, 2313–2333. [[CrossRef](#)]
13. Rambanapasi, C.; Zeevaert, J.R.; Buntting, H.; Bester, C.; Kotze, D.; Hayeshi, R.; Grobler, A. Bioaccumulation and Subchronic Toxicity of 14 nm Gold Nanoparticles in Rats. *Molecules* **2016**, *21*, 763. [[CrossRef](#)]
14. Villiers, C.; Freitas, H.; Couderc, R.; Villiers, M.B.; Marche, P. Analysis of the toxicity of gold nano particles on the immune system: Effect on dendritic cell functions. *J. Nanopart. Res.* **2010**, *12*, 55–60. [[CrossRef](#)] [[PubMed](#)]
15. Fratoddi, I.; Venditti, I.; Cametti, C.; Russo, M.V. How toxic are gold nanoparticles? The state-of-the-art. *Nano Res.* **2015**, *8*, 1771–1799. [[CrossRef](#)]
16. Faure, M.; Villiers, C.L.; Marche, P.N. Normal differentiation and functions of mouse dendritic cells derived from RAG-deficient bone marrow progenitors. *Cell Immunol.* **2004**, *228*, 8–14. [[CrossRef](#)] [[PubMed](#)]
17. Chen, J.; Ellert-Miklaszewska, A.; Garofalo, S.; Dey, A.K.; Tang, J.; Jiang, Y.; Clément, F.; Marche, P.N.; Liu, X.; Kaminska, B.; et al. Synthesis and use of an amphiphilic dendrimer for siRNA delivery into primary immune cells. *Nat. Protoc.* **2021**, *16*, 327–351. [[CrossRef](#)] [[PubMed](#)]
18. Norn, S.; Permin, H.; Kruse, P.R.; Kruse, E. History of gold—with danish contribution to tuberculosis and rheumatoid arthritis. *Dan. Med. Arbog* **2011**, *39*, 59–80.
19. Chithrani, B.D.; Ghazani, A.A.; Chan, W.C. Determining the size and shape dependence of gold nanoparticle uptake into mammalian cells. *Nano Lett.* **2006**, *6*, 662–668. [[CrossRef](#)]
20. Dobrovolskaia, M.A.; Shurin, M.; Shvedova, A.A. Current understanding of interactions between nanoparticles and the immune system. *Toxicol. Appl. Pharmacol.* **2016**, *299*, 78–89. [[CrossRef](#)]
21. Fröhlich, E. Value of phagocyte function screening for immunotoxicity of nanoparticles in vivo. *Int. J. Nanomed.* **2015**, *10*, 3761–3778. [[CrossRef](#)] [[PubMed](#)]
22. Tai, Y.; Wang, Q.; Korner, H.; Zhang, L.; Wei, W. Molecular Mechanisms of T Cells Activation by Dendritic Cells in Autoimmune Diseases. *Front. Pharmacol.* **2018**, *9*, 642. [[CrossRef](#)] [[PubMed](#)]
23. Walkey, C.D.; Olsen, J.B.; Guo, H.; Emili, A.; Chan, W.C. Nanoparticle size and surface chemistry determine serum protein adsorption and macrophage uptake. *J. Am. Chem. Soc.* **2012**, *134*, 2139–2147. [[CrossRef](#)] [[PubMed](#)]
24. Shukla, R.; Bansal, V.; Chaudhary, M.; Basu, A.; Bhonde, R.R.; Sastry, M. Biocompatibility of gold nanoparticles and their endocytotic fate inside the cellular compartment: A microscopic overview. *Langmuir* **2005**, *21*, 10644–10654. [[CrossRef](#)]
25. Bancos, S.; Stevens, D.L.; Tyner, K.M. Effect of silica and gold nanoparticles on macrophage proliferation, activation markers, cytokine production, and phagocytosis in vitro. *Int. J. Nanomed.* **2015**, *10*, 183–206. [[CrossRef](#)]
26. Ye, F.; Vallhov, H.; Qin, J.; Daskalaki, E.; Sugunan, A.; Toprak, M.S.; Fornara, A.; Gabriellson, S.; Scheynius, A.; Muhammed, M. Synthesis of high aspect ratio gold nanorods and their effects on human antigen presenting dendritic cells. *Int. J. Nanotechnol.* **2011**, *8*, 631–652. [[CrossRef](#)]
27. Zhang, Q.; Hitchins, V.M.; Schrand, A.M.; Hussain, S.M.; Goering, P.L. Uptake of gold nanoparticles in murine macrophage cells without cytotoxicity or production of pro-inflammatory mediators. *Nanotoxicology* **2011**, *5*, 284–295. [[CrossRef](#)]
28. Dalzon, B.; Torres, A.; Diemer, H.; Ravanel, S.; Collin-Faure, V.; Pernet-Gallay, K.; Jouneau, P.-H.; Bourguignon, J.; Cianféroni, S.; Carrière, M.; et al. How reversible are the effects of silver nanoparticles on macrophages? A proteomic-instructed view. *Environ. Sci. Nano* **2019**, *6*, 3133–3157. [[CrossRef](#)]
29. Saborano, R.; Wongpinyochit, T.; Totten, J.D.; Johnston, B.F.; Seib, F.P.; Duarte, I.F. Metabolic Reprogramming of Macrophages Exposed to Silk, Poly(lactic-co-glycolic acid), and Silica Nanoparticles. *Adv. Healthc. Mater.* **2017**, *6*, 1601240. [[CrossRef](#)]
30. Everts, B.; Amiel, E.; van der Windt, G.J.; Freitas, T.C.; Chott, R.; Yarasheski, K.E.; Pearce, E.L.; Pearce, E.J. Commitment to glycolysis sustains survival of NO-producing inflammatory dendritic cells. *Blood* **2012**, *120*, 1422–1431. [[CrossRef](#)]
31. Van den Bossche, J.; Baardman, J.; de Winther, M.P. Metabolic Characterization of Polarized M1 and M2 Bone Marrow-derived Macrophages Using Real-time Extracellular Flux Analysis. *J. Vis. Exp.* **2015**. [[CrossRef](#)] [[PubMed](#)]
32. Kiama, S.G.; Cochand, L.; Karlsson, L.; Nicod, L.P.; Gehr, P. Evaluation of phagocytic activity in human monocyte-derived dendritic cells. *J. Aerosol. Med.* **2001**, *14*, 289–299. [[CrossRef](#)] [[PubMed](#)]

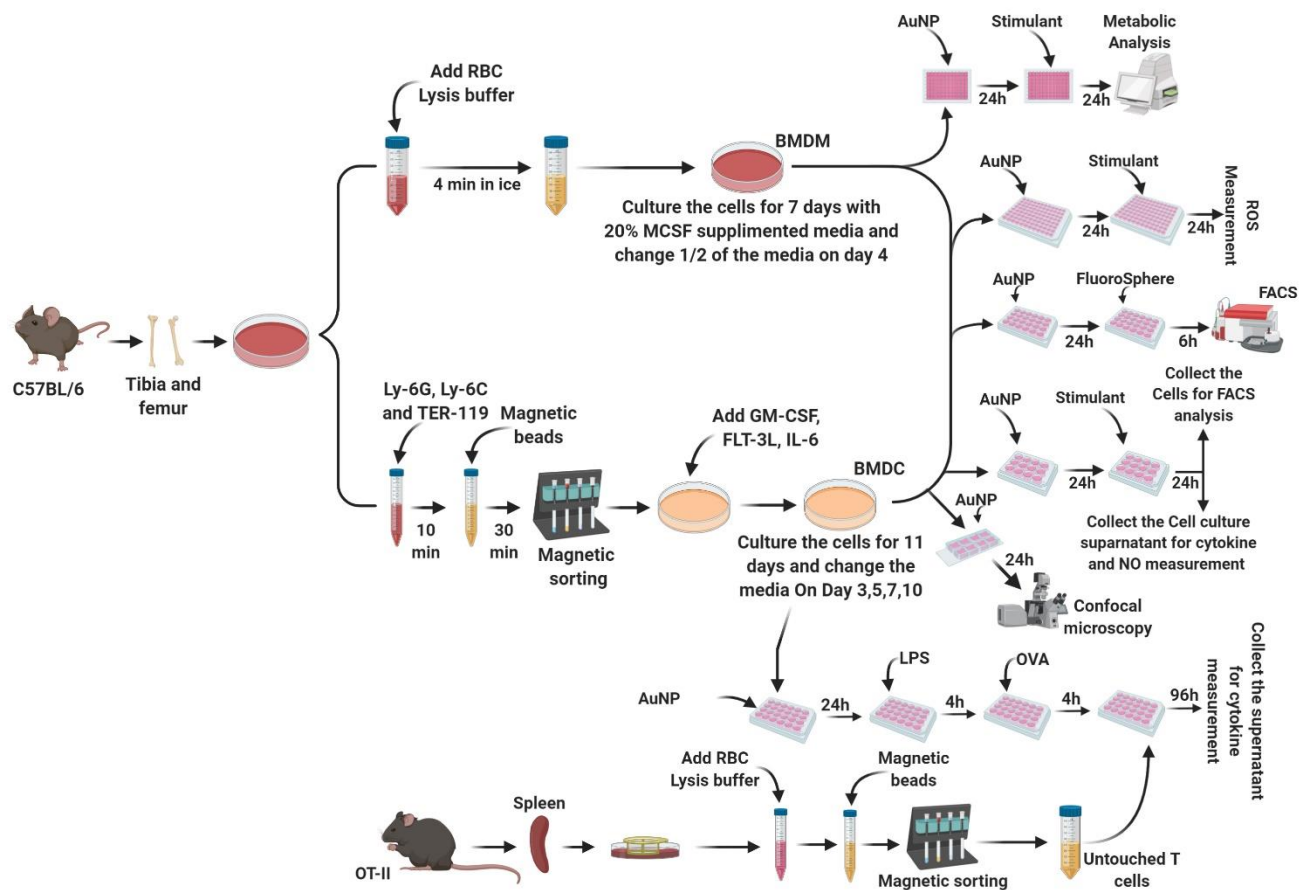
33. Divakaruni, A.S.; Paradyse, A.; Ferrick, D.A.; Murphy, A.N.; Jastroch, M. Analysis and interpretation of microplate-based oxygen consumption and pH data. *Methods Enzymol.* **2014**, *547*, 309–354. [[CrossRef](#)] [[PubMed](#)]
34. Swartzwelter, B.J.; Barbero, F.; Verde, A.; Mangini, M.; Pirozzi, M.; De Luca, A.C.; Pantes, V.F.; Leite, L.C.C.; Italiani, P.; Boraschi, D. Gold Nanoparticles Modulate BCG-Induced Innate Immune Memory in Human Monocytes by Shifting the Memory Response towards Tolerance. *Cells* **2020**, *9*, 284. [[CrossRef](#)] [[PubMed](#)]
35. Tomic, S.; Ethokic, J.; Vasilijic, S.; Ogrinc, N.; Rudolf, R.; Pelicon, P.; Vucevic, D.; Milosavljevic, P.; Jankovic, S.; Anzel, I.; et al. Size-dependent effects of gold nanoparticles uptake on maturation and antitumor functions of human dendritic cells in vitro. *PLoS ONE* **2014**, *9*, e96584. [[CrossRef](#)] [[PubMed](#)]

Supplementary Table 1. Hydrodynamic diameter of AuNPs

	Water	DMEM
Hydrodynamic diameter	24.43 ± 0.34 nm	97.01 ± 7.29
Pdl	0.20 ± 0.01	0.45 ± 0.009

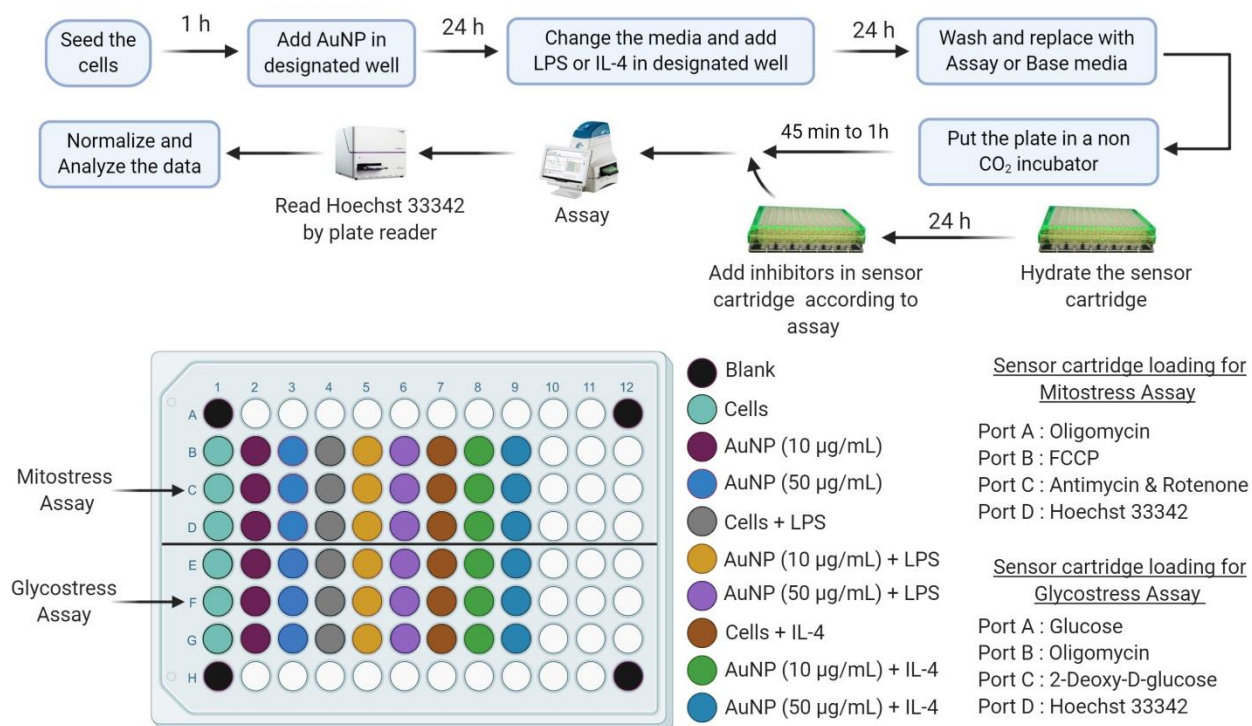
Supplementary Table 1. Hydrodynamic diameter of AuNPs. The hydrodynamic diameter and polydispersity index (Pdl) of the AuNPs were measured by dynamic light scattering (DLS) with a 1 µg/mL AuNPs dispersion in complete DMEM media (In presence of 10% FBS) and H<sub>2</sub>O. Each measurement was performed in three replications at 25°C.

Supplementary Figure 1. Experimental scheme of AuNPs



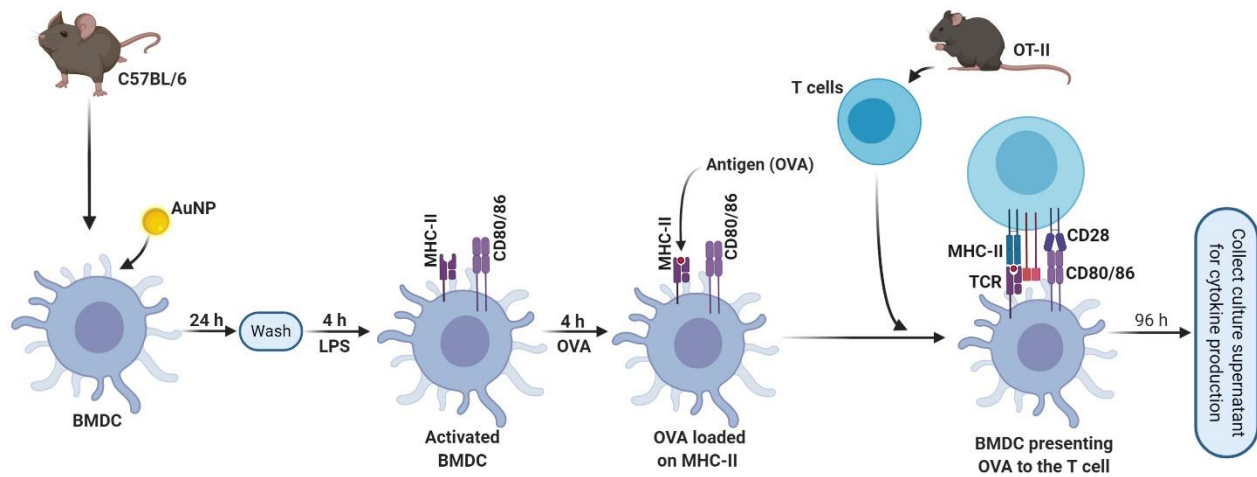
Supplementary Figure 1. Experimental scheme of AuNPs: BMDCs and BMDMs were cultured from mouse bone marrow for 11 and 7 days respectively. After harvesting, the cells were seeded either in 12, 24 or 96 wells plates from Falcon® or Seahorse XFe96 cell culture with AuNPs at 10 and or 50 µg/mL final concentrations. After 24 h of culture, cells were washed and stimulated with LPS or IL-4 for 24 h and downstream experiments were conducted according to the protocol.

Supplementary Figure 2.: Experimental scheme for metabolic flux analysis.



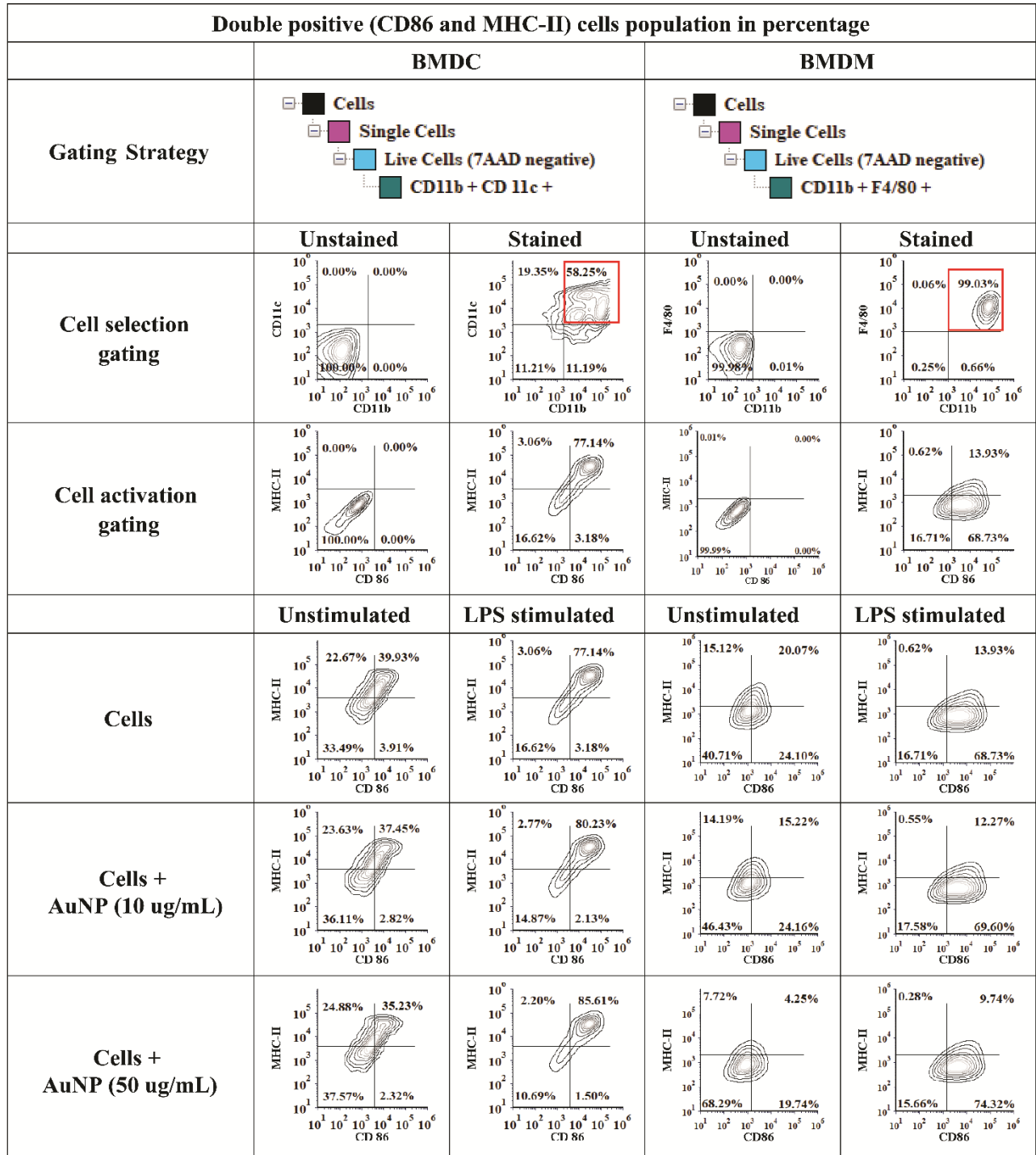
Supplementary Figure 2.: Experimental design of metabolic flux analysis: Mature BMDCs and BMDMs were seeded in Seahorse culture plate. 1 h after plating, cells were treated with AuNPs. After 24 h of culture, cells were washed and left unstimulated or stimulated with LPS/IL-4 for 24 h and the metabolic analysis is done using a Seahorse bio analyzer using the mitostress and glycostress assay protocol.

Supplementary Figure 3. Schematic representation of Antigen presentation assay.



Supplementary Figure 3. Schematic representation of Antigen presentation assay: AuNPs exposed BMDCs were stimulated with  $2\mu\text{g}/\text{mL}$  LPS for 4h and incubated with  $25\mu\text{g}/\text{mL}$  OVA for additional 4 h at  $37^\circ\text{C}$  and 5%  $\text{CO}_2$ .  $0.4 \times 10^6$  T cells were added to  $0.1 \times 10^6$  BMDCs, at a ratio of 1 BMDCs for 4 T cells. Co-cultures were incubated for 4 days, and then supernatants were harvested for cytokine immunoassays.

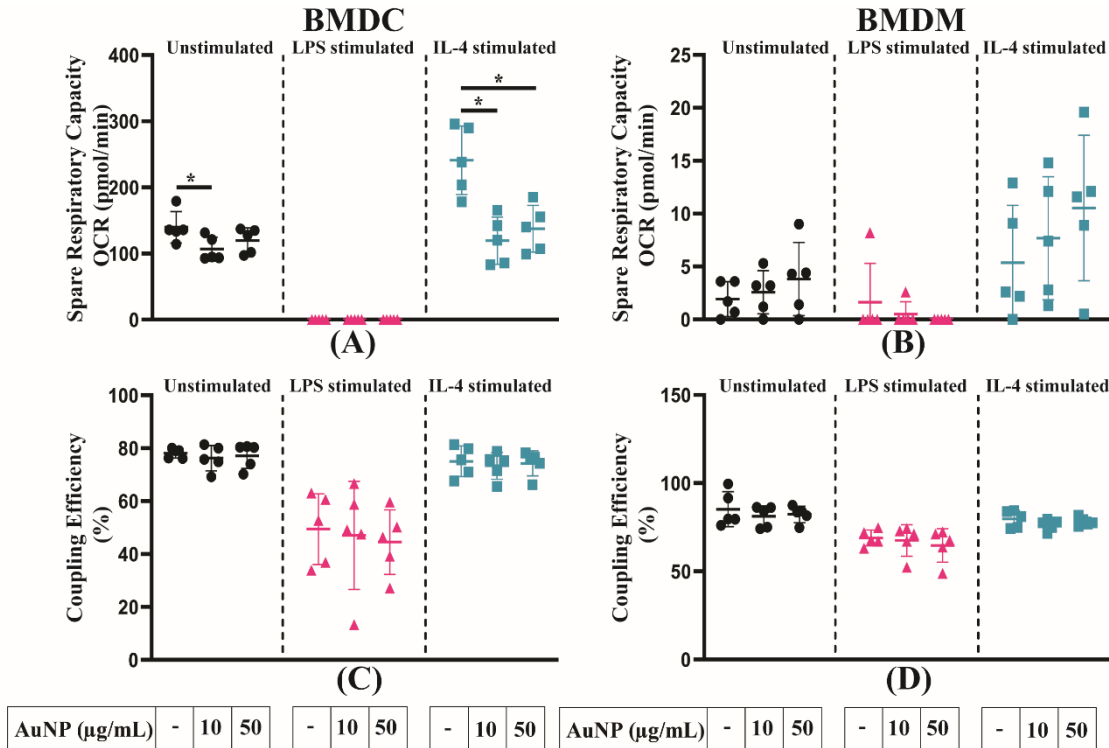
Supplementary Figure 4. Expression of activation surface marker of APC.



Supplementary Figure 4. Expression of activation marker of BMDCs and BMDMs after exposure to AuNPs for 24 h, followed by LPS stimulation for an additional 24 h. Percentage of double-positive (CD86 and MHC-II) BMDCs and BMDMs were gated on CD11b and Cd11c positive cells for BMDCs and CD11b and F4/80 positive cells for BMDMs and contour graph was displayed. The results are one representative of one of three independent experiments.

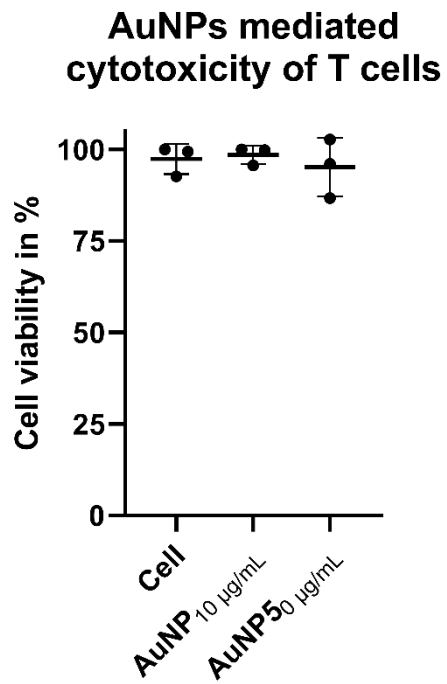


Supplementary Figure 5. Effect of AuNPs on Spare respiratory capacity and Coupling Efficiency (%) of activated or un activated BMDMs and BMDCs.



Supplementary Figure 5. Effect of AuNPs on Spare respiratory capacity and Coupling Efficiency (%) of activated or not activated BMDMs and BMDCs. [A, B, C, D] Spare respiratory capacity and coupling efficiency (%). The BMDCs and BMDMs were exposed to AuNPs for 24 h and activated by LPS or IL-4 for another 24 h. After measuring the OCR using the Seahorse XF analyser, data were normalised based on the cell number by using Hoechst 33342 staining. Results are mean +/- SD of 5 independent experiments. RM one-way ANOVA was performed \*p < 0.05.

Supplementary Figure 6. Evaluation of cell toxicity after AuNPs exposure of T cells.



Supplementary Figure 7. Evaluation of cell toxicity after AuNPs exposure of T cells. T cells were extracted from mouse spleen using Dynabeads® Untouched™ Mouse T Cell Kit. Cells were seeded with CD3<sup>+</sup>/28<sup>+</sup> beads and either treated with 10 and 50 µg/mL of AuNPs or remain untreated. T cell mortality (LDH Assay) was analysed after 24 h. Results are the mean and standard deviation of 3 independent experiments.

## 9.2 Impact of Lipid nanoparticles on the functions of macrophages and dendritic Cells

Many innovations for drug delivery have been generated by nanotechnology, thus paving the way for the proposals of new therapies. Lipid Nano Carriers attracted a lot of interest in the development of potent delivery systems. In this context, I was engaged in the 'NEWDEAL' European project, funded by the "Horizon 2020 research and innovation program" of the European Union (agreement No 720905). The purpose of this project was to develop innovative therapy against chronic disease in the call that excluded cancers and infectious diseases. NEWDEAL was proposing to develop lipid nanocarriers to deliver new anti-inflammatory agents, consisting of siRNA interfering with the expression of the JAK kinases, as new treatments for inflammatory bowel disease (IBD). IBD is an immune-mediated chronic intestinal condition that involves chronic inflammation of all or part of the digestive tract. The two conditions of IBD, Crohn's disease and ulcerative colitis are characterized by chronic inflammation of the gastrointestinal (GI) tract. Although several drugs are available to treat IBD, but the major drawbacks of current therapies are (1) Lack of Efficacy, (2) Tolerability, and (3) Convenience. In an attempt to address the demands of current IBD therapies, two approaches are addressed in this project

1. Specific inhibition of JAK1 by means of siRNA and RNAi interference.
2. Delivery of the siRNA by combining innovative nanostructured lipid carriers.

To achieve the goal of the project, NEWDEAL consortium is created with 11 partners, including academic laboratories and industries coming from 5 different countries. The entire "NEWDEAL" program is divided into 6 work packages (WPs) to execute the project (Figure 24).

- WP1 focuses on the screening, validation, and production of siRNA targeting JAK1
- WP2 focuses on product development & scale-up (WP2)
- WP3, WP4, WP5 focus on the efficacy and safety evaluation of the NEW DEAL therapeutic solution
- WP6 focuses on regulatory aspects, providing guidance, and collect all necessary data to constitute an IMPD file for phase 1 studies and generate a clinical development plan.

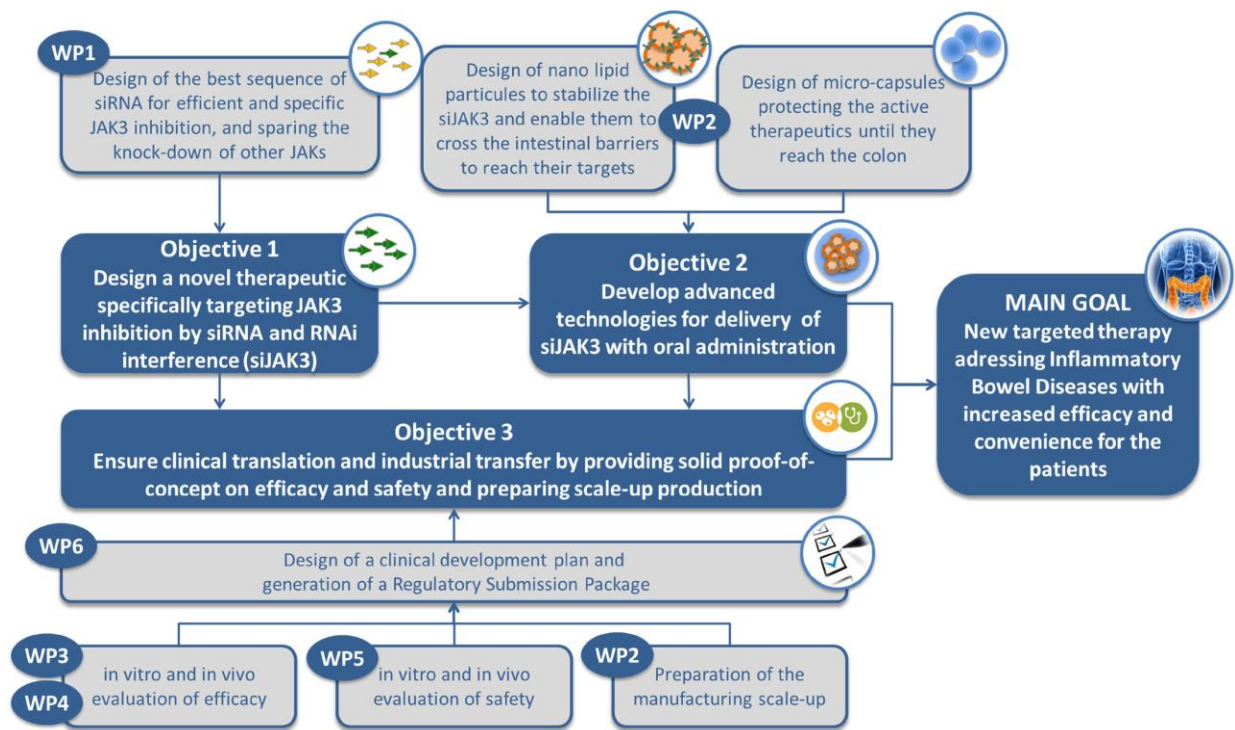


Figure 24: NEW DEAL global methodology (Reused from "NEWDEAL" project proposal)

As a part of the "NEWDEAL" project, our team participated in WP1, WP4, and WP5. The main objectives of the participating WP are

- WP1: to rapidly identify in-vitro, the best siRNA sequence that can efficiently and precisely (without off-target effects) downregulate JAK expression.
- WP4: to demonstrate the efficacy of JAK targeting using siRNA loaded NLCs in experimental models of intestinal inflammation.
- WP 5: to properly assess safety for correct validation of all products generated in WP1 and WP2, as well as to contribute to the standardization of nanotechnology, specifically in its application to healthcare and Pharma sectors.

I have been actively involved in these three WP, but for simplicity, only the data from WP5 concerning the toxicity evaluation of the lipid nanocarrier is exposed in this thesis.

Our lab had to test the immunotoxicity of the lipid nanocarriers used to deliver therapeutic siRNA. Interestingly, previously works with neutral lipidic nanocarriers NLC have shown the absence of toxicity and pro-inflammatory effects on immune cells (Courand et al; Bayon et al). However, to deliver siRNA,

cationic lipidic nanocarriers CLC) have been selected because of their property to associate tightly with nucleic acids. However, the introduction of charges on the lipidic carriers led to some effects on MDC. Therefore, the accessibility to both NLC and CLC allowed us investigating how to reduce or abolish the effects on immunotoxicity of positive charge on the lipid carriers.

The study analysis was conducted using BMDCs and BMDMs as immune cell model system. We followed the same optimized scheme of experiments done for AuNPs. Finally, to establish the effect of charge, we reversed the positive charge on the CLC by using negatively charged siRNA. For this purpose, all-star negative control siRNA (siAS) was used at different N/P ratios (the ratio of positively-charged amine groups of dendrimer (N = nitrogen) to negatively-charged phosphate (P) groups of nucleic acid) and complexed with CLC. After complexation, the zeta potential of the CLC/siAS complex was measured in 1 mM NaCl. We also performed the analysis of different cellular functions such as cytokine productions, NO production, metabolic flux analysis on BMDMs after reversing the charge. This "charge reversal study" is presented in a format of an article, which will be submitted for publication entitled "**Tuning the immunostimulation properties of cationic lipid nanocarriers for nucleic acid delivery.**" In this manuscript, I actively participated in producing all the data related to cellular function analysis and writing the original draft of the manuscript. The study was achieved in collaborating with CEA-LETI at Grenoble with Dr. A Nougarede, M Escudé, Dr. D Jary, Dr. F. Navarro) as partners who produced and fully characterized NLC and CLC. Dr. F Clément provides advice is siRNA handling, Dr. C Fournier in metabolism analysis, and Dr. E Jouvin-Marche in immunology. The study was designed by PN Marche.

The outcome of this "charge reversing experiment" improve the knowledge about the effect of the positive charge in the course of different drug designing experiments.

## Tuning the immunostimulation properties of cationic lipid nanocarriers for nucleic acid delivery

Arindam K Dey<sup>1,2</sup>, Adrien Nougarede<sup>1,3</sup>, Flora Clement<sup>1,2,4</sup>, Carole Fournier<sup>1,2</sup>, Evelyne Jouvin-Marche<sup>1,2</sup>, Marie Escudé<sup>1,3</sup>, Dorothée Jary<sup>1,3</sup>, Fabrice P. Navarro<sup>1,3</sup> and Patrice N Marche<sup>1,2\*</sup>.

<sup>1</sup> Université Grenoble-Alpes, Institute for Advanced Biosciences, 38700 La Tronche, France

<sup>2</sup> Research Center Inserm U1209, CNRS UMR5309, 38700 La Tronche, France

<sup>3</sup> Division for biology and healthcare technologies, CEA, LETI, MINATEC Campus, 38054 Grenoble, France

<sup>4</sup> CEA, INSERM, BIG-BGE, 38054 Grenoble, France

\* Corresponding author [patrice.marche@inserm.fr](mailto:patrice.marche@inserm.fr)

### Abstract

Non-viral systems, such as lipid nanoparticles, have emerged as reliable methods to enable nucleic acid intracellular delivery. Lipid nanoparticles are currently in use for drug delivery. The use of cationic lipids in the formulation of lipid nanoparticles enable to form complexes with nucleic acid cargo and facilitate their uptake by target cells. However, due to their small size and highly charged nature, these nanocarriers systems can interact *in vivo* with antigen-presenting cells (APCs), such as dendritic cells (DCs) and macrophages. As this might prove to be a safety concern for the development of therapies based on lipid nanocarriers, we sought to understand how they could affect APCs physiology. In the present study, we investigated the cellular and metabolic response of primary macrophages or DCs exposed to the neutral or cationic variant of the same lipid nanoparticle formulation. We demonstrated that macrophages were the most affected cells and that the cationic nanocarrier has a more substantial impact on their physiology, dependent on the positive surface charge. Our study provides a first model explaining the impact of charged lipid biomaterials on immune cells, and demonstrate that we can prevent the main adverse effects observed by finely tuning the load of nucleic acid cargo. Finally, we bring rational to calibrate the nucleic acid load of cationic lipid nanocarriers depending on whether immunostimulation is desirable with the intended therapeutic application, for instance, gene delivery or mRNA vaccines.

Key words: Nanostructured lipid carrier, Antigen presenting cells, nucleic acid delivery, toxicity, surface charge

## Introduction

In recent years, advances in nanotechnology field have demonstrated their potentials for precision medicine. For instance, lipid nanocarriers can be used for targeted delivery of therapeutic molecules, increasing their bioavailability and pharmacokinetic properties beyond the Lipinski rules [1]. Indeed, the development of nucleic acid therapeutics has long been hampered by the inherent hydrophilic nature, large size and poor membrane permeability of nucleic acids. Lipid nanocarriers can offer a very potent alternative to viral-mediated nucleic acid delivery, with a broad range of applications such as RNAi therapy or RNA-based vaccines, through the intracellular delivery respectively of short interfering RNA (siRNA) or messenger RNA (mRNA) [2].

One of the main advantages associated with lipid nanocarriers is their ease of manufacture and biocompatibility, enabling their use *in vivo* for human therapy [3]. Lipid nanocarriers are made of two major components: a lipid phase, and a water-phase containing surfactants. While the lipid phase can incorporate a variety of lipids such as phospholipids, free fatty acids, glycolipids or fatty alcohols, the surfactant phase plays a role of a stabilizing agent [4].

Lipid nanocarriers are generally divided into liposomes or nanoparticles, the latter which could be solid lipid nanoparticles (SLN) with a solid core and Nanostructured Lipid Carriers (NSLC) featuring a core with a mixture of solid and molten lipids. Over liposomes, NSLC offer the significant improvements in stability and allows better interaction with the immune system [5].

By incorporating cationic lipids in their formulation, NSLC are able to bind their negatively-charged nucleic acid cargo through electrostatic interactions. NSLC are able to protect bound nucleic acid from degradation and promote cellular uptake, as cytosolic availability is a prerequisite for therapeutic siRNA or mRNA biological activity.

However, nanoparticle based carriers, according to their characteristics (i.e. size and surface charge), can have immunomodulatory effects by interacting with APCs [6]; especially dendritic cells and macrophages for which they can alter the secretion of pro-inflammatory cytokines [7]. In addition, integrating cues from the microenvironment, including exposure to nanoparticles, can drive distinct macrophage or dendritic cell fates and functions through the activation of different metabolic pathways. For example, while lipopolysaccharide (LPS)-stimulated classically activated proinflammatory macrophages (M1) rely on glycolysis, interleukin (IL)-4 stimulated alternatively activated anti-inflammatory macrophages (M2) mainly utilize fatty acid oxidation and oxidative phosphorylation (OXPHOS) [8]. Besides, exposition to

cationic lipid particles has been shown previously to induce the expression of two co-stimulatory molecules, CD80 and CD86, in bone marrow derived dendritic cells (BMDCs) without inducing the secretion of pro-inflammatory cytokines [9]. Moreover, how the positive charge of lipid particles modulates the metabolic fitness of APCs and how this is related to the cellular function have not yet been elucidated. As the positive charge of lipid nanocarriers plays an important function both for nucleic acid delivery and immunogenicity [10], a precise tuning of the surface charge is required whether immunostimulation is required or to be avoided for a given therapeutic application. Therefore, understanding the impact of positively charged particles on immunogenicity and particularly on APCs metabolism, fate and cytokine secretion is crucial.

In the present study, we analyzed the effect of NLCs surface charge on primary APCs using BMDCs and bone marrow derived macrophages (BMDMs), as cellular models. We evaluated the impact of neutral lipid carrier (NLCs) and cationic lipid carrier (CLCs) on the secretion of different signaling factors and on mitochondrial metabolism and glycolysis. Furthermore, after complexing CLCs with negatively charged siRNA we reversed the charge on CLCs and we evaluated the effect of different charges on cell function.

## Materials and Methods

### Cell culture

Murine macrophage cell line (J774.1A) was purchased from ATCC, cells were cultured in Dulbecco's modified Eagle's medium (DMEM) supplemented with 10% fetal bovine serum and 1% penicillin-streptomycin.

As previously described [11], bone marrow derived dendritic cells (BMDCs) were generated from the bone marrow extracted from C57BL/6 mice (Charles River, l'Arbresle, France). Bone marrow cells were isolated by flushing from the tibia and femurs. Erythrocytes and GR1 positives cells were removed by incubating with Ly-6G/ Ly-6C (BD Pharmingen, #553125) and TER-119 (BD Pharmingen, #553672) antibodies, and the remaining negatively sorted cells were isolated using Dynabeads isolation kit (ThermoFisher, #11047) by magnetic cell sorting, then the remaining negatively sorted cells were resuspended at  $5 \times 10^5$  cells/ml in complete Iscove's modified Dulbecco's medium (IMDM) supplemented with GM-CSF (Peprotech, #315-03), FLT-3L (Peprotech, #250-31L) and IL-6 (Peprotech, #216-16) according to Table 1. Transformation of the progenitors into fully active dendritic cells (DCs) was performed over a 10 days' timeframe.



Bone marrow derived macrophages (BMDMs) were also generated from bone marrow extracted from C57BL/6 mice. Erythrocytes were removed by RBC lysis buffer, and the remaining cells were cultured in complete DMEM medium with 20% L929 (Sigma, #85011425) conditioned medium (source of macrophage-colony stimulating factor (M-CSF)) for 7 days.

### Cationic and neutral lipid nano carriers

NLCs and CLCs were prepared as previously described [12]. Briefly, for NLCs, a lipid phase was prepared containing triglycerides (Suppocire NB, Gattefossé; Super Refined soybean oil, Croda Uniqema), phospholipids (Lipoid S75-3, Lipoid), fusogenic lipid DOPE (1,2-dioleoyl-sn-glycero-3-phosphoethanolamine, Avanti Polar Lipids). For CLCs, the same lipid phase supplemented with the cationic lipid DOTAP (1,2-dioleoyl-3-trimethylammonium-propane chloride, Avanti Polar Lipids) was used. When indicated, Dil lipophilic dye (D282, Thermofisher) was added to the lipid phase to enable fluorescence detection of NLCs. A second aqueous phase containing the PEGylated surfactant PEG40-Stearate (Myrj S40, Croda Uniqema) was prepared in PBS (#806552, Sigma). Both lipid and aqueous phases were mixed together through high frequency sonication. Lipid nanoparticles are purified by dialysis in 100 volumes of LNP Buffer: 154 mM NaCl, 10 mM HEPES, pH7.4 using endotoxin-free ultra-pure water (TMS-011-A, Sigma) using 12-14 kDa MW cut-off membranes (ZelluTrans/Roth T3). Finally, the LNP solution was sterilized by filtration through a 0.22 µm Millipore membrane.

### Nanoparticle uptake assay

For nanoparticle uptake assays,  $0.5 \times 10^5$  cells/mL BMDCs and BMDMs were seeded in a 4-well Lab-Tek chambered coverslip. After 24 h of growth, cells were incubated with both CLCs and NLCs Dil-labeled nanocarriers for 24 h at 37°C with 5% CO<sub>2</sub> and performed live imaging. Nanocarrier accumulation inside cells was monitored by microscopy using a spinning disk confocal microscope (Andromeda, TILL-FEI). Dil-labeled nanocarriers were visualized using the lipophilic dye excitation wavelength of 514 nm while plasma membranes were labelled with FITC conjugated cholera toxin (Sigma, C1655) and visualized at the excitation wavelength of 488 nm. After acquisition images were processed in Icy 2.0.3.0 software and spectral deconvolution was performed using NIS 5.20.01 software.

### Physical characterisation of NLCs

The hydrodynamic diameter and polydispersity index (PDI) of the NLCs were determined by dynamic light scattering (DLS) and the zeta potential was determined by electrophoretic light scattering (ELS) using a Zeta Sizer Nano ZS instrument (Malvern). The hydrodynamic diameter and PDI were measured with a 1 mg/mL NLCs dispersion in PBS while Zeta potential was measured with a 1 mg/mL NLCs dispersion in 1 mM NaCl. Each assay was performed in three replications at 25°C.

### Complexation of CLCs nanocarrier with Nucleic acid (NA)

Complexation of CLCs with model NA, all-star negative control siRNA (siAS) was carried out in PBS. The required volume for siAS was calculated according to the desired N/P ratios at a constant concentration of the CLCs nanocarrier (100 µg/mL). CLCs carrier and diluted siAS were gently homogenized by pipetting and kept for 10 minutes at room temperature before immediate use for downstream experiments.

### Incubation with nanoparticles

For cell culture 12, 24 and 96 cell culture microplates manufactured by Falcon® or Seahorse XFe96 were used. Cells were seeded at a concentration of  $10^6$  cells/mL and cultured for 24 h. An incubation of 24 h with NLCs or CLCs at concentration ranging from 20 to 100 µg/mL was performed. Cells were subsequently washed and stimulated with LPS (2 µg/mL) or IL-4 (20 ng/mL) for another 24 h. Finally, the impact of the two nanocarriers on BMDMs and BMDCs was assayed using various parameter, such as: viability, phagocytosis, activation, cytokine secretion, nitric oxide (NO) production, reactive oxygen species (ROS) production and glycolysis or mitochondrial metabolism.

### Toxicity assessment

Toxicity was measured by quantifying the cell viability using the CytoTox-ONE™ Homogeneous Membrane Integrity Assay kit (Promega, G7891) according to the manufacturer protocol. Briefly, lysis solution (2 µl of Lysis Solution per 100 µl original volume) as a positive control for lactate dehydrogenase (LDH) release. A volume of 100 µL of CytoTox-ONE™ reagent was added to each well, before homogeneization on a shaker for 30 seconds and followed by an incubation for another 10 minutes in the dark. After that stop solution (50 µL) was added to each well and the plate was placed on the shaker for another 10 second. Finally,

there fluorescence was recorded at an excitation wavelength of 560 nm and an emission wavelength of 590 nm using a CLARIOstar® Microplate Reader (BMG LABTECH).

### Phagocytosis assay

Nanocarrier-exposed macrophages (BMDMs and J774.1A) and BMDCs were incubated at a ratio of 10 microspheres per cell for 6 h with 1.0 µm FluoSpheres® Carboxylate-Modified Microspheres (ThermoFisher, F8851) labelled with a red fluorescent dye (580 nm excitation and 605 nm emission). Cells were analyzed by flow cytometry with an Accuri C6 instrument (Becton-Dickinson) and the analysis was performed by the FCS Express V5 software (De Novo Software).

### Cell activation

Nanocarrier exposed BMDCs and BMDMs were stimulated for 24 h using 2 µg/mL Lipopolysaccharide (LPS) from E. Coli. Supernatants were collected for downstream cytokine immunoassay. The cells were labelled with antibodies specific for CD11b (Ozyme, BLE101226) and CD11c (Ozyme, BLE117318) or CD11b (Ozyme, BLE101216) and F4/80 (Ozyme, BLE123152) cell surface markers of BMDCs and BMDMs respectively after blocking the Fc receptor (BD Pharmingen, 553142) to reduce nonspecific binding. To evaluate the cell activation BMDCs and BMDMs were stained with anti-IAb (Ozyme, BLE116410) and CD86 (Ozyme, BLE105008) antibodies. In both cases, live cells were selected by negative 7-Aminoactinomycin D (7AAD) (BD Pharmingen, 559925) staining and analyzed by flow cytometry using a LSR II instrument (Becton-Dickinson). The proportion of activated cells was quantified using FCS Express V5 software.

### Cytokine immunoassays

Cytokine production was measured from cell culture supernatants with Cytometric Bead Array (CBA) (BD Pharmingen, 552364) using mouse inflammation kit against IL-6, IL-12p70, MCP-1, TNFα, IL-10, and IFNγ. Results were acquired by flow cytometry using a BD LSR II instrument and analyzed with FCAP Array Software v3.0 (BD Pharmingen, 652099).

## NO and ROS Production

NO produced by BMDMs and BMDCs were determined by measuring nitrite concentration in cell culture media by Griess assay. Briefly, 50  $\mu\text{L}$  of cell supernatant was transferred to a 96-well plate and incubated with equal volume of Sulphanilamide (Sigma, S9251) and N-alpha-naphthyl-ethylenediamine (NED) (Sigma, 222488) solutions respectively for 10 min each, protected from light. Optical density (OD) was measured at 540 nm using a CLARIOstar<sup>®</sup> Microplate Reader and sample nitrite concentration was determined using a standard curve. ROS production by BMDMs and BMDCs was determined by ROS-Glo<sup>™</sup> H<sub>2</sub>O<sub>2</sub> Assay kit (Promega, G8821). The cells were cultured at  $5 \times 10^4$  cell/mL concentration in a 96-well plate, exposed to nanocarriers for 24 h and stimulated with 2  $\mu\text{g}/\text{mL}$  of LPS. A volume of 20  $\mu\text{L}$  of H<sub>2</sub>O<sub>2</sub> substrate solution was added to each well 6 h prior ROS production measurement. ROS production measurement was performed by adding 100  $\mu\text{L}$  of ROS-Glo<sup>™</sup> Detection solution per well, before 20 min of incubation at 22°C followed by luminescence using a CLARIOstar<sup>®</sup> Microplate Reader.

## Metabolic flux analysis

For mature BMDCs (on day 10)  $1.5 \times 10^5$  cells per well were seeded in Seahorse culture plate (Agilent, 102416-100) precoated with Cell-Tak (Corning, 354240) to enable BMDCs adherence, in complete culture media supplemented with GM-CSF (5 ng /mL) and flt3L (25 ng/ mL). For mature BMDMs (on day 7)  $0.8 \times 10^5$  cells per well were seeded in Seahorse culture plate. In the case of BMDCs at day 11 and for BMDMs, 1 h after plating (on day 7), cells were treated with nanocarriers. After 24 h of incubations with the nanocarriers, cells were washed and stimulated when indicated with LPS/IL-4. After 24 h of stimulation, cells were either washed and incubated at 37°C for 1 h without CO<sub>2</sub> with either Glycolysis stress assay medium, composed of XF base medium supplemented (Agilent, 103575-100); with 1 mM glutamine (Agilent, 103579-100); or Mitochondrial stress assay medium, composed of XF base medium supplemented with 1 mM pyruvate (Agilent, 103578-100), 2 mM glutamine, and 10 mM glucose (Agilent, 103577-100). A Seahorse XFe96 instrument was used to measure the extracellular acidification rate (ECAR) and the oxygen consumption rate (OCR) every 6 minutes. Over the course of analysis, inhibitors were added as internal controls to determine which parameters in metabolism were affected from nanocarrier exposure. The inhibitors for Mitochondrial stress assay, added in the listed order, were Oligomycin (Sigma, #75351) at 1.5  $\mu\text{M}$ , Carbonyl cyanide-p-trifluoromethoxyphenylhydrazone (Sigma, C2920) at 1.5, antimycin A (Sigma, A8674) and rotenone (Sigma, R8875) mixture at 1  $\mu\text{M}$  each. In the case of Glycolysis stress assay glucose at 10 mM, Oligomycin at 1.5  $\mu\text{M}$ , and 2-deoxy-D-glucose (Sigma,

D8375) at 30 mM were injected sequentially. For the two assays, Hoechst 33342 (ThermoFisher, H21492) was added at the end of the experiment to normalize the data based on cell count. A graphical representation of the experiment design is presented in Supplementary Figure 3,7.

### Statistical analysis

Results are expressed as mean values  $\pm$  SD. Statistical analysis was performed using Graph Pad Prism version 8.4.2. Statistical significance was assessed by between two groups by one-way ANOVA or ANOVA with Tukey's correction for multiple comparisons. P-values below 0.05 were considered as significant, and indicated as following: \*P  $\leq$  0.05, \*\*P  $\leq$  0.01, \*\*\*P  $\leq$  0.001, \*\*\*\*P  $\leq$  0.0001.

## Result

### Neutral and Cationic lipid carriers do not induce cell toxicity and are efficiently internalized by APCs

We first investigated whether exposure of NLCs and CLCs is toxic for APCs *in vitro*, using a macrophage cell line (J774.1A) or primary untransformed cells extracted from bone marrow: macrophages (BMDMs) and dendritic cells (BMDCs). Cells were exposed to NLCs and CLCs with concentrations ranging from 0 to 250  $\mu$ g/mL and toxicity was measured using CytoTox-ONE Homogenous Membrane Integrity Assay kit (Figure 1A). Among all the tested cells, BMDCs was most susceptible to both NLCs and CLCs exposure, but none of the cells exhibited more than 20 percent cytotoxicity. Therefore, we chose for subsequent experiments 20 and 100  $\mu$ g/mL as low and high standard doses without adverse effects, i.e. higher than 80% of cell viability after a 24 h incubation.

Next, we assayed the internalization and cellular localization of both NLCs and CLCs by BMDCs and BMDMs. Both nanocarriers were internalized into the cytoplasm of BMDCs (Figure 1B) and BMDMs (Figure 1C) within a 24 h timeframe. Therefore, we can conclude from these first experiments on the absence of toxicity of these two nanocarriers up to a 260  $\mu$ g/mL concentration, while they are both efficiently internalized by APCs.

### NLCs and CLCs are internalized by APCs without affecting their phagocytic capacity

Accumulation of nanocarriers into phagocytic APC opens the question whether their functions could be altered, such as phagocytosis which is one of the main features of APC. The phagocytic capacity of BMDC or BMDM was assessed by counting the number of engulfed microspheres per cells by flow cytometry. This parameter was not altered by either the neutral or the cationic nanocarrier supporting that the phagocytic capacity of both APC cells was not modified by any type of nanocarrier (Figure 2A to 2D). Moreover, we noticed that the phagocytic capacity of BMDM was 20% higher than for BMDC (Figure 2B and 2D).

We also verified the impact of the nanocarriers on the phagocytic capacity of J774.1A, a well characterized macrophage cell line for phagocytosis analysis [13]. Similarly, we did not observe a significant change in phagocytic capacity between the nanocarrier treated cells or control cells. These results obtained with the J774.1A cell line were consistent with what we observed in the primary cells (Supplementary Figure 1A and B), although we observed a difference in the phagocytic capacity between J774.1A cell line and primary macrophage cells (BMDMs).

### CLCs, but NLCs, can increase LPS activation of BMDMs

Next, we took advantage of the BMDCs and BMDMs models, which are primary non-transformed cells reproducing physiological immune cell responses *ex vivo* to study the impact of both the nanocarriers on APCs activation.

BMDCs were identified by CD11b and CD11c expression [14] whereas BMDMs were marked by CD11b and F4/80 expression [15] (see gating strategy in Supplementary Figure 2). Activation of BMDCs and BMDMs was evaluated by the frequency of CD86 and MHC-II double positive cells. After LPS stimulation, the frequency of CD86<sup>+</sup> MHC-II<sup>+</sup> BMDCs increased from 27.83% to 75.9% (Figure 3A) while no significative changes were observed in BMDMs) (Figure 3B).

Exposure to increasing concentrations of NLCs or CLCs did not significantly alter LPS-induced double expression of CD86 and MHC-II in BMDCs. In case of BMDMs activation, CD86 and MHC-II double positive cell percentage was not altered when exposed to NLCs but significantly decreased when exposed the CLCs from 19.6% to 9.79%. In the case of unactivated BMDMs, the percentage of CD86 positive cell remains unaltered when exposed to NLCs (Supplementary table 2). Altogether, these data highlight that both nanocarriers do not activate BMDCs but the CLCs slightly alter the activation of BMDMs. BMDCs exposure

to both nanocarriers, maintained their capacity to respond to LPS activation. However, in the case of BMDMs, CLCs exposure significantly increased the percentage of activated BMDMs from 14.69% to 29.76%, while it remained similar with the NLCs (Figure 3B). This suggests that exposure to nanocarriers alone is not sufficient to activate both BMDCs and BMDMs, however, in LPS-stimulated BMDMs, the exposure to CLCs increased the frequency of CD86<sup>+</sup> MHCII<sup>+</sup> activated cells. nanocarriers is not sufficient to activate both BMDCs and BMDMs although CLCs exposure enhanced the ability of BMDMs to respond to LPS stimulation.

### CLCs and NLCs can alter the production of signal molecules of APCs

The capacity to produce different soluble factors, including signaling proteins like cytokines or chemokines and other small molecular mediators like NO and ROS is a hallmark of APCs activation.

Having demonstrated that exposure to a CLCs could alter the activation of BMDMs in response to LPS, we wondered what would be the impact of both nanocarriers on cytokine secretion. We observed that both nanocarriers did not induce cytokine secretion in unstimulated BMDCs and BMDMs (Figure 4A to 4D, left panel), although exposure to CLCs, but NLCs, significantly increased the production of the MCP-1 chemokine in both unstimulated BMDCs and BMDMs (Figure 4E and 4F, left panel).

Upon LPS stimulation of APCs, NLCs exposure did not alter IL-6 production by both BMDCs and BMDMs. However, exposure to CLCs significantly increased IL-6 production by BMDMs (Figure 4B, right panel) but not by BMDCs (Figure 4A, right panel). In the case of BMDCs, both NLCs and CLCs increased TNF- $\alpha$  production at 100  $\mu\text{g}/\text{mL}$  (Figure 4C, right panel). For BMDMs, TNF- $\alpha$  production was only increased at 100  $\mu\text{g}/\text{mL}$  of CLCs but not for NLCs (Figure 4D, right panel). We also observed that treatment with CLCs but not NLCs significantly increased MCP-1 production in both stimulated BMDCs and BMDMs (Figure 4E and 4F, right panel).

Two other important secretory molecules, NO and ROS productions were evaluated from the culture supernatant of APCs by griess assay or H<sub>2</sub>O<sub>2</sub> quantification respectively. In absence of LPS stimulation, we did not observe a production of NO by BMDCs and BMDMs in response to both nanocarriers (Figure 4G and 4H, left panel) although ROS production was detected by BMDCs at 100  $\mu\text{g}/\text{mL}$  but and not in BMDMs (Figure 4I and 4J, left panel). In LPS stimulated conditions, both NLCs and CLCs decreased NO production by BMDCs at 100  $\mu\text{g}/\text{mL}$  (Figure 4G, right panel), while CLCs at 100  $\mu\text{g}/\text{mL}$  was responsible for increasing NO production in BMDMs (Figure 4H, right panel). After stimulation by LPS, both APCs produced increased

quantities of mediators, but ROS production which was not significantly altered by exposure of BMDCs and BMDMs to both nanocarriers (Figure 4I and 4J, right panel). These results indicate that BMDCs and BMDMs are differently affected by neutral or cationic nanocarriers regarding their capacity to produce NO and ROS, depending on activation stimuli.

Overall, both nanocarriers have an influence on signal molecule secretion, although limited to a slight increase in MCP-1 secretion (CLCs only) for both unstimulated APCs and in ROS production (CLCs and NLCs) for unstimulated BMDCs only. In activated BMDMs, CLCs increased IL-6, TNF- $\alpha$ , MCP-1 secretion and NO production. We can therefore conclude that the cationic charge of CLCs might be responsible for increased adverse effects on APCs physiology and the secretion of signaling molecules.

### NLCs and CLCs have a significant impact on the mitochondrial metabolism of BMDMs but BMDCs

As cellular metabolism plays a key role in different functions of APC, we sought to determine the effect of differentially charged lipid nanocarriers on mitochondrial metabolism. For instance, pro-inflammatory stimuli by LPS is known to triggers a metabolic switch that would enhance glycolysis, whereas enhanced fatty acid oxidation (FAO) and mitochondrial oxidative phosphorylation (OXPHOS) is a hallmark of IL-4-induced anti-inflammatory activity in immune cells. To analyze the impact of neutral and cationic nanocarriers on mitochondrial metabolism, APCs cells were first treated with different concentrations of both nanocarriers for 24 h, then stimulated with either LPS or IL-4 for 24 h before measuring the oxygen consumption rate (OCR), using the experimental setup detailed in Supplementary Figure 3.

Upon exposition to both nanocarriers, no alteration in the basal respiration, maximal respiration capacity, spare respiratory capacity, non-mitochondrial oxygen consumption and coupling efficiency (Supplementary Figure 4A, 4C, 4E, 5A, 5C) proton leak or ATP production (Figure 5A and 5C) in unstimulated or stimulated BMDCs were found.

In BMDMs, exposure to both nanocarriers increased basal respiration and non-mitochondrial oxygen consumption of unstimulated cells at 100  $\mu\text{g}/\text{mL}$ , as well as the non-mitochondrial oxygen consumption of LPS-stimulated cells treated with the NLCs (Supplementary Figure 4B, 5B). Treatment with 100  $\mu\text{g}/\text{mL}$  of CLCs increased significantly the proton leak, ATP production, Basal respiration, maximal respiration capacity, spare respiratory capacity and non-mitochondrial oxygen consumption (Figure 5B and 5D, Supplementary Figure 4B, 4D, 4F, 5B) in unstimulated or IL-4 stimulated BMDMs whereas the NLCs did



only slightly increase basal respiration and non-mitochondrial oxygen consumption (Supplementary Figure 4A and 5A).

Of note, both nanocarriers did not impaired the coupling efficiency of unstimulated or stimulated BMDMs (Supplementary Figure 5B).

As a whole, our results demonstrate that the CLCs has a more important effect on BMDMs metabolism compared to the NLCs, while both nanocarriers have very little effect on the metabolism of BMDCs.

### NLCs and CLCs alter the glycolysis of BMDMs and not of BMDCs

Considering the alterations of the mitochondrial metabolism induced by the CLCs and to a lesser extent the NLCs, we sought to investigate their effects on the glycolytic profile of APCs as LPS stimulated cells are mostly dependent on glycolysis. To evaluate the different glycolytic parameters of BMDCs and BMDMs, cells were first pre-treated with different concentrations of both nanocarriers, and then stimulated with LPS or IL-4 for 24 hours. After stimulation, the extracellular acidification rate (ECAR) was measured using the glycolysis stress assay in order to assess glycolysis and glycolytic capacity.

Unlike for BMDCs that did not showed any alteration in glycolysis (Figure 5E) or glycolytic capacity (Supplementary Figure 6A), in BMDMs glycolysis (Figure 5F) and glycolytic capacity (Supplementary Figure 6B), were increased in both unstimulated and stimulated conditions when exposed to 100  $\mu\text{g}/\text{mL}$  of CLCs. However, exposition to the NLCs did not induce any alteration in glycolysis or glycolytic capacity in BMDMs, independently of stimulating conditions (Figure 5F and Supplementary Figure 6B).

The combination of these results revealed that the cationic but not the neutral lipid nanocarriers at the highest concentration alter the glycolytic profile in BMDMs. On the other hand, both nanocarriers have no effect on glycolysis in BMDCs.

### Reversing the surface charge with a nucleic acid cargo prevent adverse effects of cationic lipid nanocarriers on APCs

As previous experiments combined pointed out that at 100  $\mu\text{g}/\text{mL}$  CLCs had a more dramatic effect on BMDMs physiology, than a NLCs, we wondered if the surface charge alone could explain the differences observed.

This led us to investigate whether we could reverse the phenotype observed on APCs by reversing the surface charge of the CLCs with a nucleic acid cargo, here a negative control siRNA (siAS). We used different surface charges by finely tuning the ratio of the positively-charged amine groups of CLCs nanocarriers (N =  $\text{NH}^{3+}$  group) relative to the negatively-charged phosphate groups (P) from each phosphodiester bonds within the nucleic acid sequence, hence called N/P ratio. After complexation between siRNA and CLCs nanocarrier, the zeta potential and hydrodynamic diameter these nanocomplexes was measured. Naked CLCs showed a zeta potential of  $45.80 \pm 3.8$  mV while increasing amounts of the nucleic acid cargo and thus decreasing the N/P ratio lead to lower the zeta potential values down to  $-9.97 \pm 0.94$  mV, while naked NLCs was measured at  $-16.50 \pm 0.53$  mV (Figure 6A). Of note, the complexation of CLCs with different quantities of siRNA did not altered significantly the size of the nanocomplexes (Figure 6B).

Using different N/P ratios, we generated nanocarriers with different zeta potentials that we used to investigate their effects on BMDMs functions. BMDMs were exposed to 100  $\mu\text{g}/\text{mL}$  of CLCs nanocarrier, CLCs-siRNA nanocomplexes at N/P 8 to N/P 1 or NLCs nanocarrier. The culture supernatants were collected and the secretion of pro-inflammatory cytokines (IL-6,  $\text{TNF}\alpha$ ) or chemokine (MCP-1) was quantified by immunoassay. IL-6 and  $\text{TNF}\alpha$  productions by LPS-stimulated BMDMs were correlated to the zeta potential of the nanocarriers they were exposed to (Figure 6C and 6D), i.e. the productions were maximum with CLCs and decreased when CLCs are complexed to siRNA reaching at N/P ratio 1 a similar level than the one obtained with NLCs. The production of NO and MCP-1 by LPS-activated BMDMs did also decrease with lower N/P ratios but to a lesser extent than for IL-6 and  $\text{TNF}\alpha$  (Figure 6E and Supplementary Figure 8A).

To analyze the effect of the surface charge on glycolysis, we measured ECAR in BMDMs exposed to nanocomplexes at different N/P ratios and then stimulated or not with LPS. Both unstimulated and LPS-stimulated BMDMs showed decrease in both glycolysis and glycolytic capacities with decreasing zeta potential, and almost down to the same values than that of the NLCs for the unstimulated cells (Figure 6F and Supplementary figure 8B).

Next, we analyzed the effect of the surface charge on the mitochondrial metabolism of BMDMs, by measuring the OCR in BMDMs exposed to nanocomplexes at different N/P ratios and then stimulated or not with IL-4. The exposure to differently charged nanocarrier showed a decrease in basal respiration, maximal respiration capacity, ATP production, spare respiratory capacity, and proton leak correlated with a decrease in zeta potential in both unstimulated and IL-4 stimulated BMDMs (Figure 6G to 6J and Supplementary Figure 8C). However, the effect of differently charged nanocarriers on both unstimulated

and IL-4 stimulated BMDMs was not statistically significant for non-mitochondrial oxygen consumption and percentage of coupling efficiency (Supplementary Figure 8D and 8E).

Altogether, these results revealed that decreasing zeta potential, hence the surface charge of the CLCs was able to reverse their effect on the different cellular functions of primary BMDMs upon both pro- and anti-inflammatory stimulations. In addition, using a range of N/P ratios representing the surface charge of the nanocarriers, we demonstrated that the alteration of the BMDMs physiology was proportional to the overall surface charge of nucleic acid-loaded lipid nanoparticles.

## Discussion

Lipid nanocarriers are promising nanodelivery systems for imaging [16], nucleic acids delivery [17], siRNA transfection [18], drug delivery [19], adjuvant delivery system [5] and other biomedical applications. However, the potential reaction of the host immune system to those nanoparticles constitutes a major challenge in using different NLCs in biomedical science. Nanoparticles composed of cationic lipids have a strong capacity for binding and condensing nucleic acid by electrostatic interactions, and deliver the payload across cellular membranes within the target cell cytoplasm [20]. While siRNA off-target effects have been extensively studied, it is crucial to consider the side effects and toxicity of nanocarriers themselves, which remained to be more deeply characterized from immunological point of view.

Our current study revealed that BMDCs and BMDMs responded differently when treated with differently charged NLCs. In case of BMDMs we demonstrated that CLCs at high concentration provoked an enhanced immune response by increasing the production of different secretory molecules including IL-6, TNF- $\alpha$ , MCP-1, upon LPS stimulation while NLCs did not. However, we observe a reduction in TNF- $\alpha$  secretion by NLCs and CLCs exposed LPS-stimulated BMDCs.

To assess the influence of NLCs on the metabolism of BMDMs and BMDCs, we activated these cells with either LPS or IL-4. While LPS-activated pro-inflammatory cells undergoing a metabolic switch to enhanced glycolysis [21, 22], IL-4 induced alternatively activated cells toward and anti-inflammatory response, which would then rely mostly on fatty acid oxidation (FAO) and mitochondrial oxidative phosphorylation (OXPHOS) [23]. As a result, altered metabolism is not only a characteristic of macrophages cell function, it is also a prerequisite for a proper response to an immune stimulus. In our study, we showed that both

nanocarriers did not alter the basal mitochondrial respiration of BMDCs, but in the case of BMDMs basal respiration did increase when exposed to the highest concentration used (100 µg/mL) with the two NLCs.

Globally, in unstimulated BMDCs and BMDMs, nanocarriers had very few effects on cellular production of soluble factors *in vitro*. While no metabolic changes were observed in BMDCs; BMDMs showed a positive charge specific increase of glycolysis and mitochondrial respiration. Previous studies have shown a positive association between the glycolytic and the secretory activities in macrophages, however this was evaluated under LPS stimulation [22]. In unstimulated conditions with CLCs exposure, we do not observe this coupling, maybe because the CLCs-induced increase of glycolysis is not high enough to drive secretory adaptations as observed in CLCs-treated BMDMs under LPS stimulation. It is noteworthy that LPS activated BMDMs rely on mitochondrial respiration. These results obtained *in vitro* let us suppose that positively charged lipid carriers *in vivo* would not greatly affect the basal level of unstimulated DCs or macrophage secretory activity, hence avoiding unintended immune responses (suppression or activation) and subsequent harmful outcomes (cancer or autoimmunity).

Under LPS stimulation, CLCs exposed BMDCs and BMDMs increase their production of MCP-1. MCP-1 is responsible for monocytes/macrophages migration and their infiltration in tissues [24]. MCP-1 has been described as a pro-inflammatory chemokine associated with rheumatoid arthritis (RA) [25] or allergic asthma development [26]. Therefore, *in vivo* administration of CLCs might increase MCP-1 production facilitating the emigration of immature myeloid cells at the site of exposure. Then, immature myeloid cells may acquire pro-inflammatory or anti-inflammatory properties under the influence of the inflammatory condition of the tissue. Pro-inflammatory behavior associated with M1 activation may lead to an imbalance in M1/M2 ratio promoting osteoclastogenesis in RA [27]. Anti-inflammatory behavior associated with M2 activation impairs T-cell response [28], leading to neoangiogenesis [29, 30] and stimulates tumor growth [31].

In our study, we have seen that the alteration of cellular function of APCs was predominantly linked with a CLCs (+45.8 mV). Therefore, we further studied the effect of the charge of the nanocarrier using BMDMs as cellular model since these cells appeared the most affected by the exposure to CLCs. We could modify the surface charge of the CLCs by the binding of negatively charged siRNA at different N/P ratios. We observed that the increase of the production of secretory molecules (IL-6, TNF-α, MCP-1 and NO) was proportional to the surface charge of the lipid nanocarriers. In parallel, metabolic parameters, including basal respiration, maximal respiration capacity, ATP production, spare respiratory capacity and proton leak, were also modulated accordingly to the charge of the lipid nanocarriers. These results show that the

effects of positively charged nanocarriers, like CLCs, can be reversed by the complexation of negatively charged ligands, such as RNA, proportionally to the charge of resulting nanocarrier.

Several studies reported some effect of the charge of nanoparticles on cell behavior. For instance, N-Arginine-N-octyl chitosan (AOCS) is used to synthesize pH-sensitive charge-reversal lysosomolytic nanocarriers (ANLC), which could reduce the potential toxicity of the nanocarrier as well as the increase drug delivery efficiency [32]. In addition, Chen and coworkers showed that charge-reversal nanocarriers enhanced gene delivery to the tumor site [33]. Furthermore, Han and colleagues demonstrated that the use of chitosan and the pH-responsive charge-reversible polymer enhanced the siRNA delivery [34]. Here, our results highlight that fine tuning of the surface charge of cationic lipid nanocarriers with an oppositely charged biomaterial, for instance nucleic acid, could prevent immunostimulation properties of the cationic carrier and has to be kept in mind for the future use of such carriers for therapeutic applications. Overall, using the same cationic lipid nanocarrier with tunable surface charge, we propose that positive charge is one of the major factor responsible for the alteration of the immune response.

## Conclusion

In conclusion, both BMDCs and BMDMs responded differently when exposed to the cationic or neutral variation of the same lipid nanocarrier formulation. Therefore, it is highly relevant to include both cell types in case of the analysis of immunotoxicity. We demonstrated that both nanocarriers, at low concentration, did not significantly alter several functions of both APCs. However, the cationic nanocarrier, at highest concentration, induced alterations of some functions of APCs. We demonstrated that this effect on APCs was dependent to the positive surface charge of the lipid carrier that could be offset by loading nucleic acid cargo that mediated reversal of charge. Finally, we propose that tuning the nucleic acid load, hence the surface charge of lipid nanocarriers is critical to their use for therapy, and prevent the alteration of immune cell response to stimuli.

## Abbreviations

APCs	antigen presenting cells
BMDCs	bone marrow derived dendritic cells
BMDMs	bone marrow derived macrophages
CLCs	cationic lipid carrier
CD	cluster of differentiation
ECAR	extracellular acidification rate
IL	interleukin
LPS	lipopolysaccharide
LC	lipid nanocarrier
OCR	oxygen consumption rate
OXPPOS	oxidative phosphorylation
NSLC	nanostructured lipid carrier
NLCs	neutral lipid carrier
NP	nano particles
ROS	reactive oxygen species
RA	rheumatoid arthritis
SLN	solid lipid nanoparticles
TNF	tumor necrosis factor
TLR	toll like receptor

## Funding Statement

This project has received funding from the European Union's Horizon 2020 research and innovation program H2020 "NEWDEAL" (grant agreement No. 720905). AD, AN and FC were supported by a fellowship from H2020 NEWDEAL project.

## Disclaimer

This publication reflects only the author's view and the Commission is not responsible for any use that may be made of the information it contains.

### *Figure Legends*

Figure 1 - Neutral and Cationic lipid nanocarriers do not induce cell toxicity but are efficiently internalized by APC.

(A) Cell viability (LDH release Assay) of BMDCs, BMDMs and J774.1A was analyzed after exposure to different concentration of NLCs and CLCs nanocarriers for 24 h. Data is displayed as mean  $\pm$  SD and is normalized to the untreated cells ( $N = 3$  independent experiments). (B) Confocal microscopy analysis of NLCs and CLCs uptake in (B) BMDCs and (C) BMDMs. After APCs exposure to 100  $\mu\text{g}/\text{ml}$  of NLCs or CLCs nanocarriers for 24 h, cell membranes were labeled with FITC-cholera toxin (green) and NLCs and CLCs are observed by excitation of Dil fluorescent dye (red). Images were acquired using confocal spinning-disk microscope. The images displayed were representative of the majority of cells observed.

Figure 2 - Phagocytic capacity of APCs exposed to neutral or cationic lipid nanocarriers

BMDCs and BMDMs were exposed to NLCs and CLCs nanocarriers at 20 and 100  $\mu\text{g}/\text{mL}$  for 24 h, then incubated with fluorescent microspheres for 6 h, and subsequently analyzed by flow cytometry. The repartition of the cells in the 1<sup>st</sup>, 2<sup>nd</sup>, 3<sup>rd</sup> and 4<sup>th</sup> peak corresponds to 0, 1, 2 and 3 or more beads internalization, respectively. Overlaid histograms are shown in (A) for BMDCs and (C) for BMDMs. The proportion of cells in each peak was analyzed (B) for BMDCs and (D) for BMDMs. Data is displayed as mean  $\pm$  SD ( $N = 3$  independent experiments).

Figure 3 - Expression of activation surface marker in APCs following exposure to neutral or cationic lipid nanocarriers

BMDCs (A) and BMDMs (B) were exposed to NLCs or CLCs lipid nanocarriers for 24 h, followed by LPS stimulation for additional 24 h. Percentage of double positive (CD86 and MHC-II) BMDCs and CD86 positive BMDMs were determined, with a gating on CD11b and Cd11c positive cells for BMDCs and CD11b and F4/80 positive cells for BMDMs. Data is displayed as mean  $\pm$  SD ( $N = 3$  independent experiments) and statistical significance between nanocarrier treated or untreated groups was performed by one-way ANOVA test using Tukey's multiple comparisons test. \* $P \leq 0.05$ ; \*\*\* $P \leq 0.001$ ; \*\*\*\* $P \leq 0.0001$ .

Figure 4 - Secretions of signalling factors by APCs in response to neutral or cationic lipid nanocarriers

Relative cytokine and chemokine concentration in the supernatant of BMDCs and BMDMs exposed to NLCs or CLCs and activated or not by LPS was determined by immunoassay. Secretion of the IL-6 cytokine (**A**) in BMDCs and (**B**) in BDDMs; the TNF $\alpha$  cytokine (**C**) in BMDCs and (**D**) in BMDMs; the chemokine MCP-1 (**E**) in BMDCs and (**F**) in BMDMs. Relative NO concentration in the supernatant of BMDCs (**G**) and BMDMs (**H**) cells exposed to NLCs or CLCs and activated or not by LPS was determined by griess assay. ROS production by BMDCs (**I**) and BMDMs (**J**) cells exposed to NLCs or CLCs and activated or not by LPS was determined by ROS-Glo™ H<sub>2</sub>O<sub>2</sub> Assay. Data is displayed as mean  $\pm$  SD ( $N = 4$  independent experiments) and statistical significance between nanocarrier treated or untreated groups was performed by one-way ANOVA test using Tukey's multiple comparisons test. \* $P \leq 0.05$ ; \*\* $P \leq 0.01$ ; \*\*\* $P \leq 0.001$ ; \*\*\*\* $P \leq 0.0001$ .

Figure 5 – Mitochondrial metabolism in naïve, pro-inflammatory or anti-inflammatory activated APCs in response to neutral or cationic lipid nanocarriers

(**A, B**) Proton leak, (**C, D**) ATP production, (**E, F**) Glycolysis in BMDCs and BMDMs respectively were measured after exposure to CLCs or NLCs for 24 h and activated by LPS or IL-4 for another 24 h. Oxygen consumption rate (OCR) and Extracellular acidification rate (ECAR) were quantified using a Seahorse XF analyser. Data was normalized by cell number based on cell count (Hoechst 33342 staining) and is displayed as mean  $\pm$  SD ( $N = 4$  independent experiments). Statistical significance between nanocarrier treated or untreated groups was performed by one-way ANOVA test using Tukey's multiple comparisons test. \*\* $P \leq 0.01$ ; \*\*\* $P \leq 0.001$ ; \*\*\*\* $P \leq 0.0001$ .

Figure 6 - Reversing the surface charge with a nucleic acid cargo prevent adverse effects of cationic lipid nanocarrier on APCs

(**A**) Zeta potential measurement of CLCs complexes with siRNA at different N/P ratios was performed on a zeta sizer instrument by electrophoretic light scattering in 1 mM NaCl. (**B**) Hydrodynamic diameter of CLCs complexes with siRNA at different N/P ratios was measured on a zeta sizer instrument by dynamic light scattering in PBS buffer. (**C**) IL-6 and (**D**) TNF $\alpha$  secretion was quantified from the supernatant of BMDMs exposed to 100  $\mu$ g/mL of CLCs complexes with siRNA at different N/P ratios and activated or not by LPS. (**E**) NO concentration in the supernatant of BMDMs exposed to 100  $\mu$ g/mL of CLCs complexes with siRNA at different N/P ratios and activated or not by LPS was determined by Griess assay. (**F**) Glycolysis in BMDMs exposed to 100  $\mu$ g/mL of CLCs complexes with siRNA at different N/P ratios and activated or not by LPS



was determined by ECAR. **(G)** Basal respiration **(H)** ATP production, **(I)** Maximal respiration capacity and **(J)** Spare respiratory capacity in BMDMs exposed to 100 µg/mL of CLCs alone or complexes with siRNA at different N/P ratios and activated or not by IL-4 was determined by OCR. Oxygen consumption rate (OCR) and Extracellular acidification rate (ECAR) were quantified using a Seahorse XF analyser. Data was normalized by cell number based on cell count (Hoechst 33342 staining) and is displayed as mean ± SD (*N* = 4 or 6 independent experiments). Statistical significance between nanocarrier treated or untreated groups was performed by one-way ANOVA test using Tukey's multiple comparisons test. \**P* ≤ 0.05; \*\**P* ≤ 0.01; \*\*\**P* ≤ 0.001; \*\*\*\**P* ≤ 0.0001.

#### Supplementary Figure 1 - Phagocytosis capacity of macrophage cell line J774.1A

J774.1A cells were exposed to NLCs and CLCs nanocarriers at 100 µg/mL for 24 h, then incubated with fluorescent microspheres for 6 h, and subsequently analyzed by flow cytometry. The repartition of the cells in the 1<sup>st</sup>, 2<sup>nd</sup>, 3<sup>rd</sup> and 4<sup>th</sup> peak corresponds to 0, 1, 2 and 3 or more beads internalization, respectively. Overlaid histograms are shown in **(A)** The proportion of cells in each peak was analysed **(B)**. Data is displayed as mean ± SD (*N* = 3 independent experiments).

#### Supplementary Figure 2 - Expression of activation surface marker in APCs

The expression of activation marker for BMDCs and BMDMs was quantified by flow cytometry after exposure to neutral or cationic lipid nanocarrier for 24 h, followed by LPS stimulation for additional 24 h when indicated. The percentage of double positive (CD86 and MHC-II) BMDCs and BMDMs were gated on CD11b and Cd11c positive cells for BMDCs and CD11b and F4/80 positive cells for BMDMs and contour graph was displayed. The results are representative one of the three independent experiment.

#### Supplementary Figure 3 - Experimental design of metabolic flux analysis

Mature BMDCs and BMDMs were seeded on a Seahorse culture plate. One hour after plating, cells were treated with the different nanocarriers. After 24 h of culture, cells were washed and when indicated stimulated with LPS or IL-4 for 24 h. The metabolic analysis was performed using a Seahorse bio-analyzer using the mitochondrial stress and glycolysis stress assay protocol, with the corresponding chemical inhibitors.

Supplementary Figure 4 – Basal respiration, Maximal respiration capacity, and Spare respiratory capacity of naïve, classically activated or alternatively activated APCs in response to neutral or cationic lipid nanocarriers

**(A, B)** Basal respiration, **(C, D)** Maximal respiration capacity, **(E, F)** Spare respiratory capacity of BMDCs and BMDMs respectively were measured after exposure to cationic or neutral lipid nanocarriers for 24 h and activated by LPS or IL-4 for another 24 h. Oxygen consumption rate (OCR) was quantified using a Seahorse XF analyser. Data was normalized by cell number based on cell count (Hoechst 33342 staining) and is displayed as mean  $\pm$  SD ( $N = 4$  independent experiments). Statistical significance between nanocarrier treated or untreated groups was performed by one-way ANOVA test using Tukey's multiple comparisons test. \* $P \leq 0.05$ ; \*\* $P \leq 0.01$ ; \*\*\* $P \leq 0.001$ ; \*\*\*\* $P \leq 0.0001$ .

Supplementary Figure 5 – Non-mitochondrial oxygen consumption and Percentage of coupling efficiency of naïve, classically activated or alternatively activated APCs in response to neutral or cationic lipid nanocarriers

**(A, B)** Non-mitochondrial oxygen consumption, **(C, D)** Percentage of coupling efficiency of BMDCs and BMDMs respectively were measured after exposure to cationic or neutral lipid nanocarriers for 24 h and activated by LPS or IL-4 for another 24 h. Oxygen consumption rate (OCR) was quantified using a Seahorse XF analyser. Data was normalized by cell number based on cell count (Hoechst 33342 staining) and is displayed as mean  $\pm$  SD ( $N = 4$  independent experiments). Statistical significance between nanocarrier treated or untreated groups was performed by one-way ANOVA test using Tukey's multiple comparisons test. \* $P \leq 0.05$ ; \*\* $P \leq 0.01$ ; \*\*\* $P \leq 0.001$ ; \*\*\*\* $P \leq 0.0001$ .

Supplementary Figure 6 - Glycolytic capacity of naïve, naïve, classically activated or alternatively activated APCs in response to neutral or cationic lipid nanocarriers

Glycolytic capacity **(A)** in BMDCs and **(B)** in BMDMs were evaluated after exposure to cationic or neutral lipid nanocarriers for 24 h and activated by LPS or IL-4 for another 24 h. Extracellular acidification rate (ECAR) was quantified using a Seahorse XF analyser. Data was normalized by cell number based on cell count (Hoechst 33342 staining) and is displayed as mean  $\pm$  SD ( $N = 4$  independent

experiments). Statistical significance between nanocarrier treated or untreated groups was performed by one-way ANOVA test using Tukey's multiple comparisons test.  $^{**}P \leq 0.01$ ;  $^{***}P \leq 0.001$ ;  $^{****}P \leq 0.0001$ .

Supplementary Figure 7 - Experimental design of metabolic flux analysis for reversal of nanocarrier surface charge

Mature BMDCs and BMDMs were seeded in Seahorse culture plate. One hour after plating, cells were treated with the different nanocarriers, and when indicated with nanocarriers/siRNA nanocomplexes at the corresponding N/P ratios. After 24 h of culture, cells were washed and when indicated stimulated with LPS or IL-4 for 24 h. The metabolic analysis was performed using a Seahorse bio-analyzer using the mitochondrial stress and glycolysis stress assay protocol, with the corresponding chemical inhibitors.

Supplementary Figure 8 - Effect of the surface charge of cationic lipid nanocarriers on different cellular functions and metabolism of BMDMs

**(A)** MCP-1 production was quantified from the supernatant of BMDMs exposed to 100  $\mu\text{g}/\text{mL}$  of CLCs complexes with siRNA at different N/P ratios and activated or not by LPS. **(B)** Glycolytic capacity in BMDMs exposed to 100  $\mu\text{g}/\text{mL}$  of CLCs complexes with siRNA at different N/P ratios and activated or not by LPS was determined by ECAR. **(C)** Proton leak **(D)** Non-mitochondrial oxygen consumption, **(E)** percentage of coupling efficiency in BMDMs exposed to 100  $\mu\text{g}/\text{mL}$  of CLCs complexes with siRNA at different N/P ratios and activated or not by IL-4 was determined by OCR. Oxygen consumption rate (OCR) and Extracellular acidification rate (ECAR) were quantified using a Seahorse XF analyser. Data was normalized by cell number based on cell count (Hoechst 33342 staining) and is displayed as mean  $\pm$  SD ( $N = 3$  independent experiments). Statistical significance between nanocarrier treated or untreated groups was performed by one-way ANOVA test using Tukey's multiple comparisons test.  $^{*}P \leq 0.05$ ;  $^{**}P \leq 0.01$ ;  $^{***}P \leq 0.001$ ;  $^{****}P \leq 0.0001$ .

## References

- [1] N. Yousefi, N. Tufenkji, Probing the Interaction between Nanoparticles and Lipid Membranes by Quartz Crystal Microbalance with Dissipation Monitoring, *Front Chem* 4 (2016) 46.
- [2] H.Y. Xue, P. Guo, W.C. Wen, H.L. Wong, Lipid-Based Nanocarriers for RNA Delivery, *Curr Pharm Des* 21(22) (2015) 3140-7.
- [3] S. Chira, C.S. Jackson, I. Oprea, F. Ozturk, M.S. Pepper, I. Diaconu, C. Braicu, L.Z. Raduly, G.A. Calin, I. Berindan-Neagoe, Progresses towards safe and efficient gene therapy vectors, *Oncotarget* 6(31) (2015) 30675-703.
- [4] A. Gordillo-Galeano, C.E. Mora-Huertas, Solid lipid nanoparticles and nanostructured lipid carriers: A review emphasizing on particle structure and drug release, *Eur J Pharm Biopharm* 133 (2018) 285-308.
- [5] E. Bayon, J. Morlieras, N. Dereuddre-Bosquet, A. Gonon, L. Gosse, T. Courant, R. Le Grand, P.N. Marche, F.P. Navarro, Overcoming immunogenicity issues of HIV p24 antigen by the use of innovative nanostructured lipid carriers as delivery systems: evidences in mice and non-human primates, *npj Vaccines* 3(1) (2018) 46.
- [6] Y. Liu, J. Hardie, X. Zhang, V.M. Rotello, Effects of engineered nanoparticles on the innate immune system, *Semin Immunol* 34 (2017) 25-32.
- [7] C. Villiers, H. Freitas, R. Couderc, M.B. Villiers, P. Marche, Analysis of the toxicity of gold nano particles on the immune system: effect on dendritic cell functions, *J Nanopart Res* 12(1) (2010) 55-60.
- [8] M.I. Stunault, G. Bories, R.R. Guinamard, S. Ivanov, Metabolism Plays a Key Role during Macrophage Activation, *Mediators of Inflammation* 2018 (2018) 2426138.
- [9] D.P. Vangasseri, Z. Cui, W. Chen, D.A. Hokey, L.D. Faló, Jr., L. Huang, Immunostimulation of dendritic cells by cationic liposomes, *Mol Membr Biol* 23(5) (2006) 385-95.
- [10] X. Chen, L. Liu, C. Jiang, Charge-reversal nanoparticles: novel targeted drug delivery carriers, *Acta Pharm Sin B* 6(4) (2016) 261-7.
- [11] M. Faure, C.L. Villiers, P.N. Marche, Normal differentiation and functions of mouse dendritic cells derived from RAG-deficient bone marrow progenitors, *Cell Immunol* 228(1) (2004) 8-14.
- [12] T. Courant, E. Bayon, H.L. Reynaud-Dougier, C. Villiers, M. Menneteau, P.N. Marche, F.P. Navarro, Tailoring nanostructured lipid carriers for the delivery of protein antigens: Physicochemical properties versus immunogenicity studies, *Biomaterials* 136 (2017) 29-42.
- [13] Y. Luo, E. Cook, B.C. Fries, A. Casadevall, Phagocytic efficacy of macrophage-like cells as a function of cell cycle and Fc $\gamma$  receptors (Fc $\gamma$ R) and complement receptor (CR)3 expression, *Clin Exp Immunol* 145(2) (2006) 380-387.
- [14] H. Li, G.X. Zhang, Y. Chen, H. Xu, D.C. Fitzgerald, Z. Zhao, A. Rostami, CD11c+CD11b+ dendritic cells play an important role in intravenous tolerance and the suppression of experimental autoimmune encephalomyelitis, *J Immunol* 181(4) (2008) 2483-93.
- [15] X. Zhang, R. Goncalves, D.M. Mosser, The isolation and characterization of murine macrophages, *Curr Protoc Immunol Chapter 14* (2008) Unit 14.1.
- [16] F.P. Navarro, F. Mittler, M. Berger, V. Jossierand, J. Gravier, F. Vinet, I. Texier, Cell tolerability and biodistribution in mice of indocyanine green-loaded lipid nanoparticles, *J Biomed Nanotechnol* 8(4) (2012) 594-604.
- [17] A. Hibbitts, A. Lucía, I. Serrano-Sevilla, L. De Matteis, M. McArthur, J.M. de la Fuente, J.A. Aínsa, F. Navarro, Co-delivery of free vancomycin and transcription factor decoy-nanostructured lipid carriers can enhance inhibition of methicillin resistant *Staphylococcus aureus* (MRSA), *PLOS ONE* 14(9) (2019) e0220684.
- [18] Ö. Tezgel, A. Szarpak-Jankowska, A. Arnould, R. Auzély-Velty, I. Texier, Chitosan-lipid nanoparticles (CS-LNPs): Application to siRNA delivery, *Journal of Colloid and Interface Science* 510 (2018) 45-56.

- [19] D. Hinger, F. Navarro, A. Käch, J.S. Thomann, F. Mittler, A.C. Couffin, C. Maake, Photoinduced effects of m-tetrahydroxyphenylchlorin loaded lipid nanoemulsions on multicellular tumor spheroids, *J Nanobiotechnology* 14(1) (2016) 68.
- [20] A. Elouahabi, J.-M. Ruyschaert, Formation and Intracellular Trafficking of Lipoplexes and Polyplexes, *Molecular Therapy* 11(3) (2005) 336-347.
- [21] J. Van den Bossche, J. Baardman, M.P. de Winther, Metabolic Characterization of Polarized M1 and M2 Bone Marrow-derived Macrophages Using Real-time Extracellular Flux Analysis, *J Vis Exp* (105) (2015).
- [22] B. Kelly, L.A.J. O'Neill, Metabolic reprogramming in macrophages and dendritic cells in innate immunity, *Cell Res* 25(7) (2015) 771-784.
- [23] L.A. O'Neill, E.J. Pearce, Immunometabolism governs dendritic cell and macrophage function, *J Exp Med* 213(1) (2016) 15-23.
- [24] S.L. Deshmane, S. Kremlev, S. Amini, B.E. Sawaya, Monocyte chemoattractant protein-1 (MCP-1): an overview, *J Interferon Cytokine Res* 29(6) (2009) 313-326.
- [25] S. Rantapää-Dahlqvist, K. Boman, A. Tarkowski, G. Hallmans, Up regulation of monocyte chemoattractant protein-1 expression in anti-citrulline antibody and immunoglobulin M rheumatoid factor positive subjects precedes onset of inflammatory response and development of overt rheumatoid arthritis, *Annals of the Rheumatic Diseases* 66(1) (2007) 121.
- [26] W.K. Ip, C.K. Wong, C.W.K. Lam, Interleukin (IL)-4 and IL-13 up-regulate monocyte chemoattractant protein-1 expression in human bronchial epithelial cells: involvement of p38 mitogen-activated protein kinase, extracellular signal-regulated kinase 1/2 and Janus kinase-2 but not c-Jun NH2-terminal kinase 1/2 signalling pathways, *Clinical & Experimental Immunology* 145(1) (2006) 162-172.
- [27] S. Fukui, N. Iwamoto, A. Takatani, T. Igawa, T. Shimizu, M. Umeda, A. Nishino, Y. Horai, Y. Hirai, T. Koga, S.-Y. Kawashiri, M. Tamai, K. Ichinose, H. Nakamura, T. Origuchi, R. Masuyama, K. Kosai, K. Yanagihara, A. Kawakami, M1 and M2 Monocytes in Rheumatoid Arthritis: A Contribution of Imbalance of M1/M2 Monocytes to Osteoclastogenesis, *Frontiers in immunology* 8 (2018) 1958-1958.
- [28] S.M. Moghimi, A.C. Hunter, T.L. Andresen, Factors Controlling Nanoparticle Pharmacokinetics: An Integrated Analysis and Perspective, *Annual Review of Pharmacology and Toxicology* 52(1) (2012) 481-503.
- [29] S.W. Jones, R.A. Roberts, G.R. Robbins, J.L. Perry, M.P. Kai, K. Chen, T. Bo, M.E. Napier, J.P.Y. Ting, J.M. DeSimone, J.E. Bear, Nanoparticle clearance is governed by Th1/Th2 immunity and strain background, *The Journal of Clinical Investigation* 123(7) (2013) 3061-3073.
- [30] S.H. Burnett, E.J. Kershen, J. Zhang, L. Zeng, S.C. Straley, A.M. Kaplan, D.A. Cohen, Conditional macrophage ablation in transgenic mice expressing a Fas-based suicide gene, *Journal of Leukocyte Biology* 75(4) (2004) 612-623.
- [31] R. Rajan, M.K. Sabnani, V. Mavinkurve, H. Shmeeda, H. Mansouri, S. Bonkougou, A.D. Le, L.M. Wood, A.A. Gabizon, N.M. La-Beck, Liposome-induced immunosuppression and tumor growth is mediated by macrophages and mitigated by liposome-encapsulated alendronate, *Journal of Controlled Release* 271 (2018) 139-148.
- [32] M. Sun, J. Li, C. Zhang, Y. Xie, H. Qiao, Z. Su, D. Oupicky, Q. Ping, Arginine-Modified Nanostructured Lipid Carriers with Charge-Reversal and pH-Sensitive Membranolytic Properties for Anticancer Drug Delivery, *Adv Healthc Mater* 6(8) (2017).
- [33] X. Chen, L. Liu, C. Jiang, Charge-reversal nanoparticles: novel targeted drug delivery carriers, *Acta Pharm Sin B* 6(4) (2016) 261-267.
- [34] L. Han, J. Zhao, X. Zhang, W. Cao, X. Hu, G. Zou, X. Duan, X.J. Liang, Enhanced siRNA delivery and silencing gold-chitosan nanosystem with surface charge-reversal polymer assembly and good biocompatibility, *ACS Nano* 6(8) (2012) 7340-51.

**Tables:**

**Table 1: Concentration of GM-CSF, FLT-3L and IL-6 for BMDCs culture.**

Cells are cultured 100 mm TC-treated Cell Culture Dish with 15 mL culture media						
		Day 0	Day 3	Day 5	Day 7	Day 10
Cell Concentration		0.6 * 10 <sup>6</sup> /mL	0.5 * 10 <sup>6</sup> /mL	0.5 * 10 <sup>6</sup> /mL	0.5 * 10 <sup>6</sup> /mL	According to cell plating
Supplement	IL-6	5 ng /mL	2.5 ng /mL	2.5 ng /mL	-	-
	FLT-3	50 ng /mL	40 ng /mL	30 ng /mL	25 ng /mL	25 ng /mL
	GM-CSF	5 ng /mL				

**Table 2: Percentage of Activated APCs with or without NLCs treatment.**

Double positive (CD86 and MHC-II) cells population percentage (mean ± SD)				
	BMDCs		BMDMs	
	Unstimulated	LPS stimulated	Unstimulated	LPS stimulated
Cells	27.83 ± 8.58	75.9 ± 1.62	19.6 ± 2.13	14.69 ± 0.93
Cells + NLCs 20 ug/mL	28.61 ± 12.22	80.51 ± 2.97	19.98 ± 1.92	16.32 ± 2.35
Cells + NLCs 100 ug/mL	29.3 ± 11.21	71.38 ± 4.85	16.3 ± 1.90	18.1 ± 1.05
Cells + CLCs 20 ug/mL	28.97 ± 7.79	79.57 ± 4.27	20.61 ± 3.39	25.84 ± 0.98
Cells + CLCs 100 ug/mL	27.74 ± 6.37	79.91 ± 2.39	9.79 ± 3.07	29.76 ± 2.45

## Figures

Figure 1

Neutral and Cationic lipid nanocarriers do not induce cell toxicity but are efficiently internalized by APCs

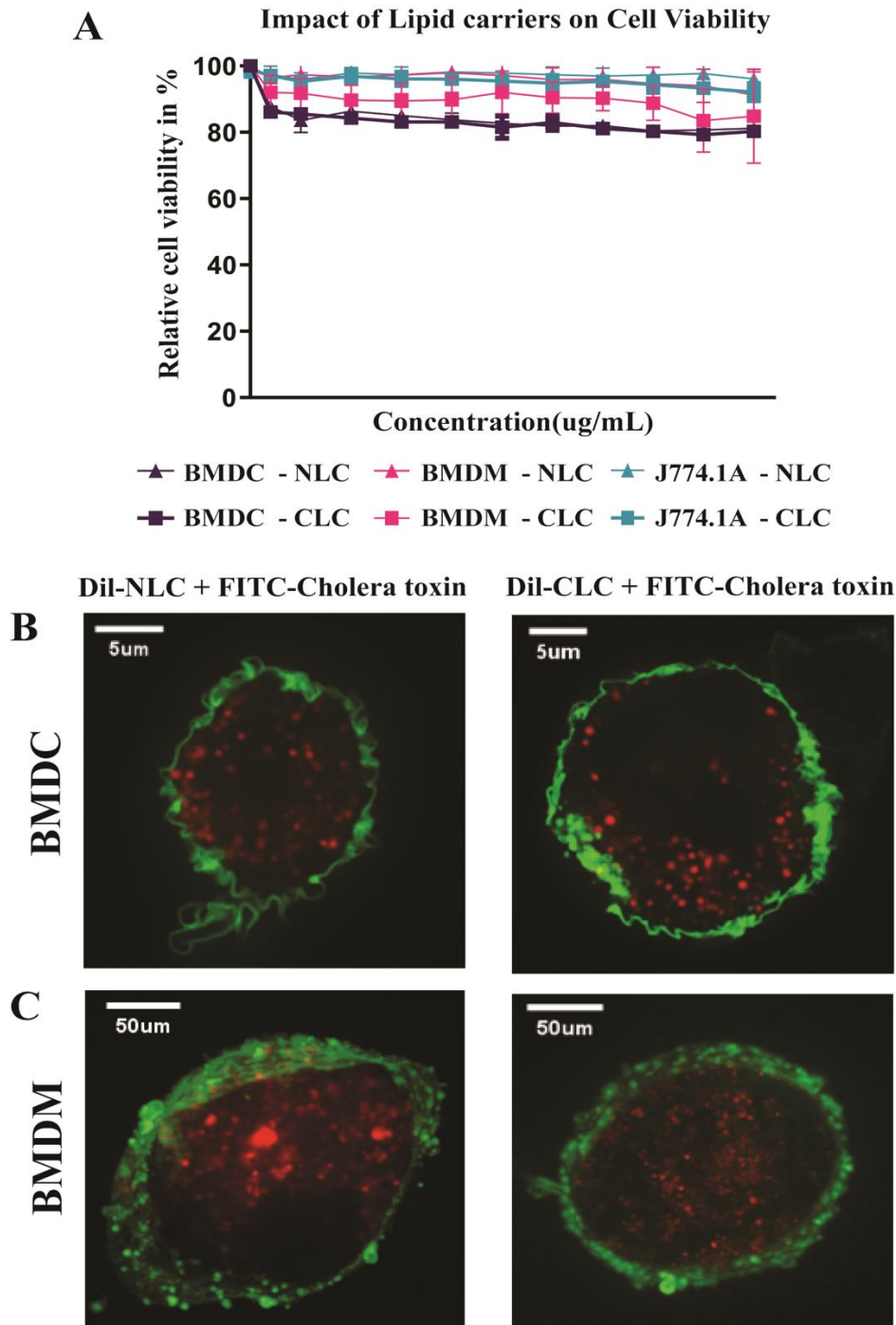


Figure 2

Phagocytic capacity of APCs exposed to neutral or cationic lipid nanocarriers

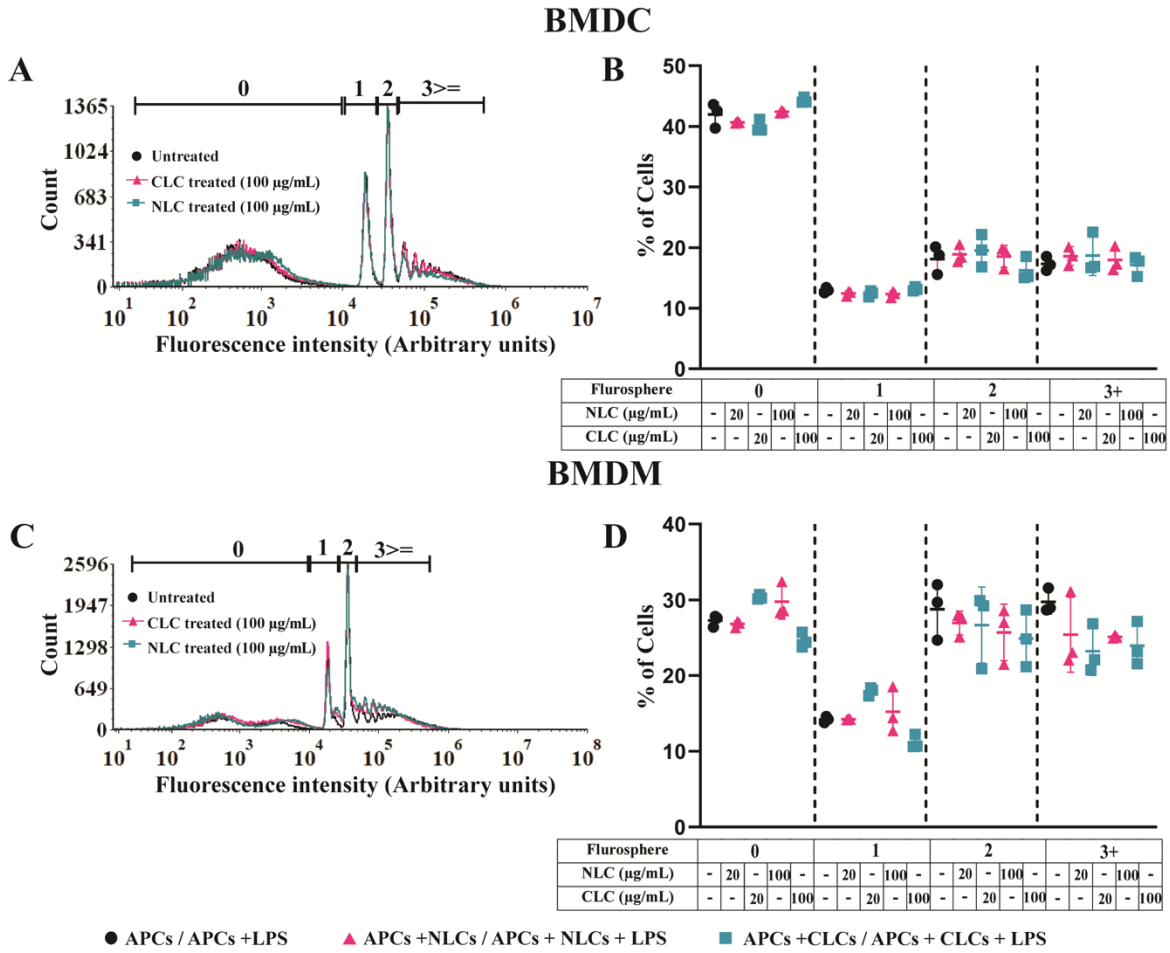




Figure 3

Expression of activation surface marker in APCs following exposure to neutral or cationic lipid nanocarriers

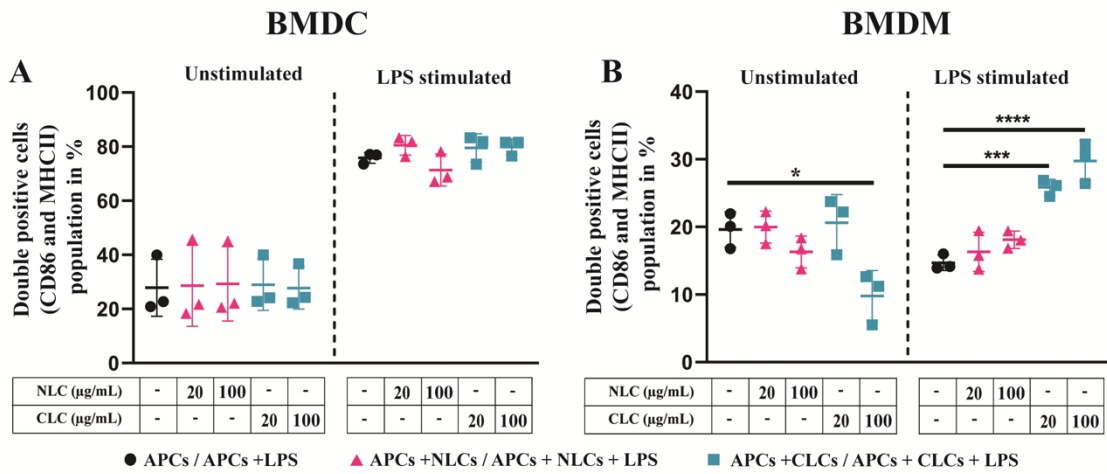


Figure 4

Secretions of signalling factors by APCs in response to neutral or cationic lipid nanocarriers

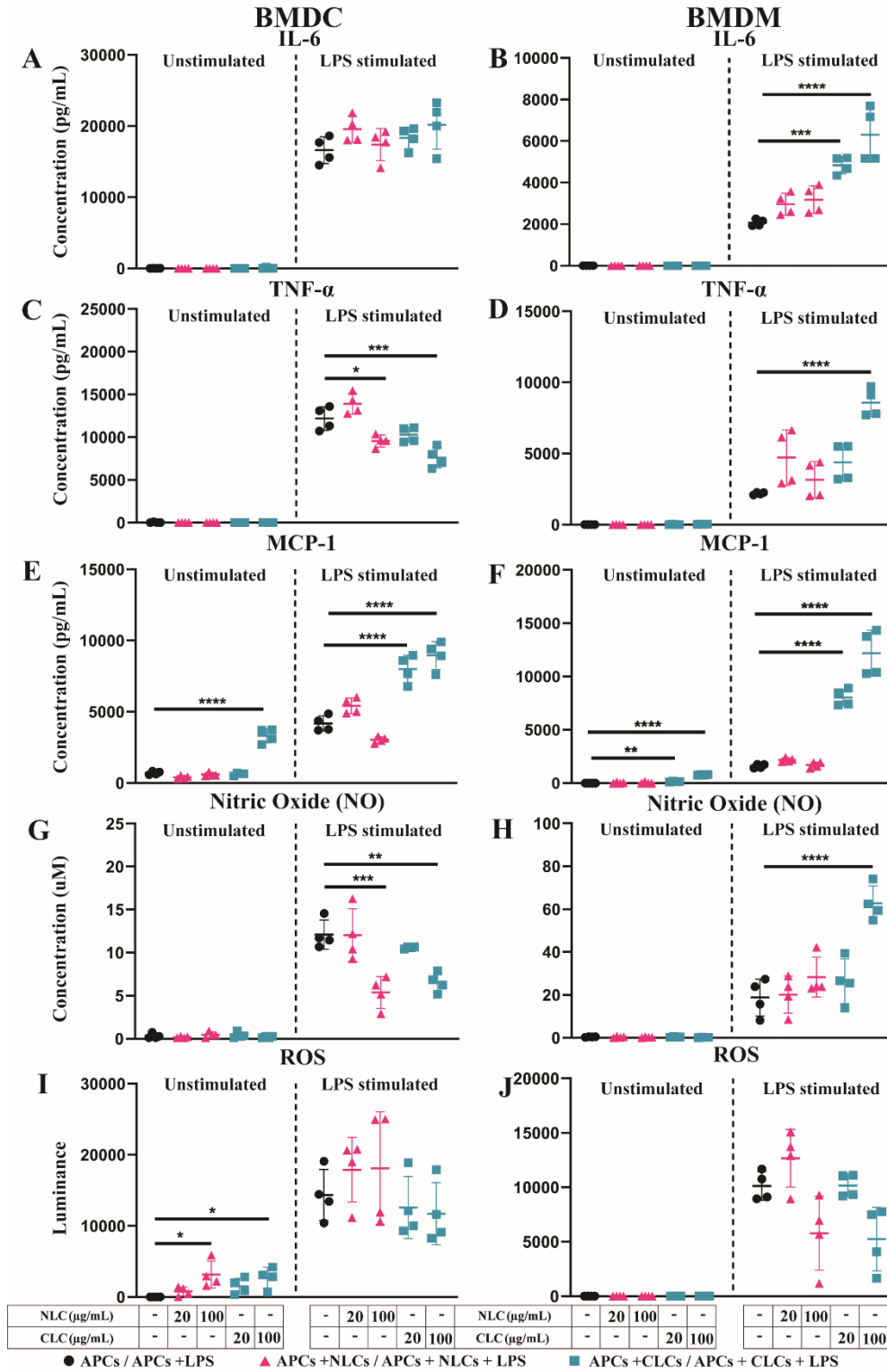


Figure 5

Mitochondrial metabolism in naïve, classically activated or alternatively activated APCs in response to neutral or cationic lipid nanocarriers

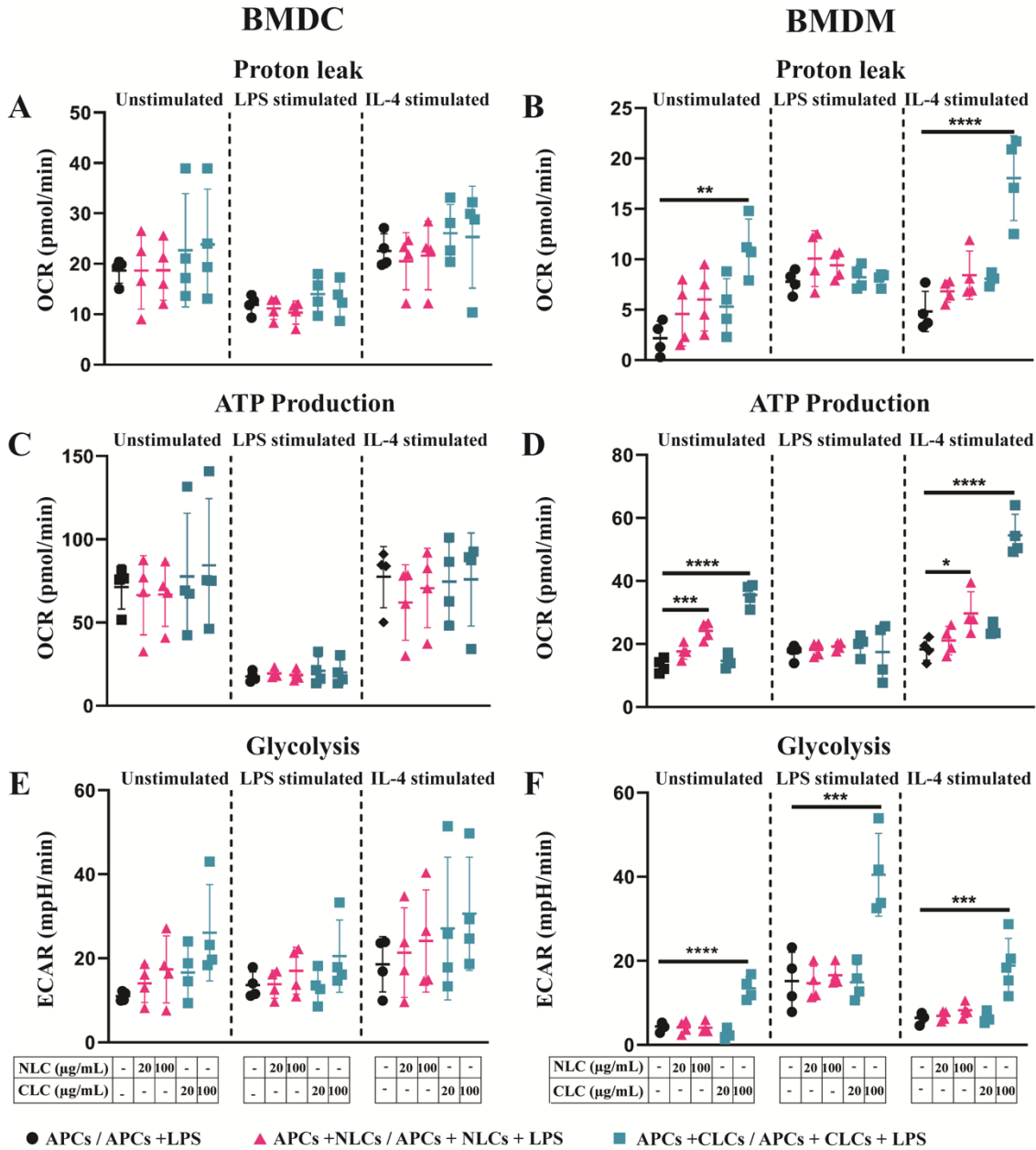
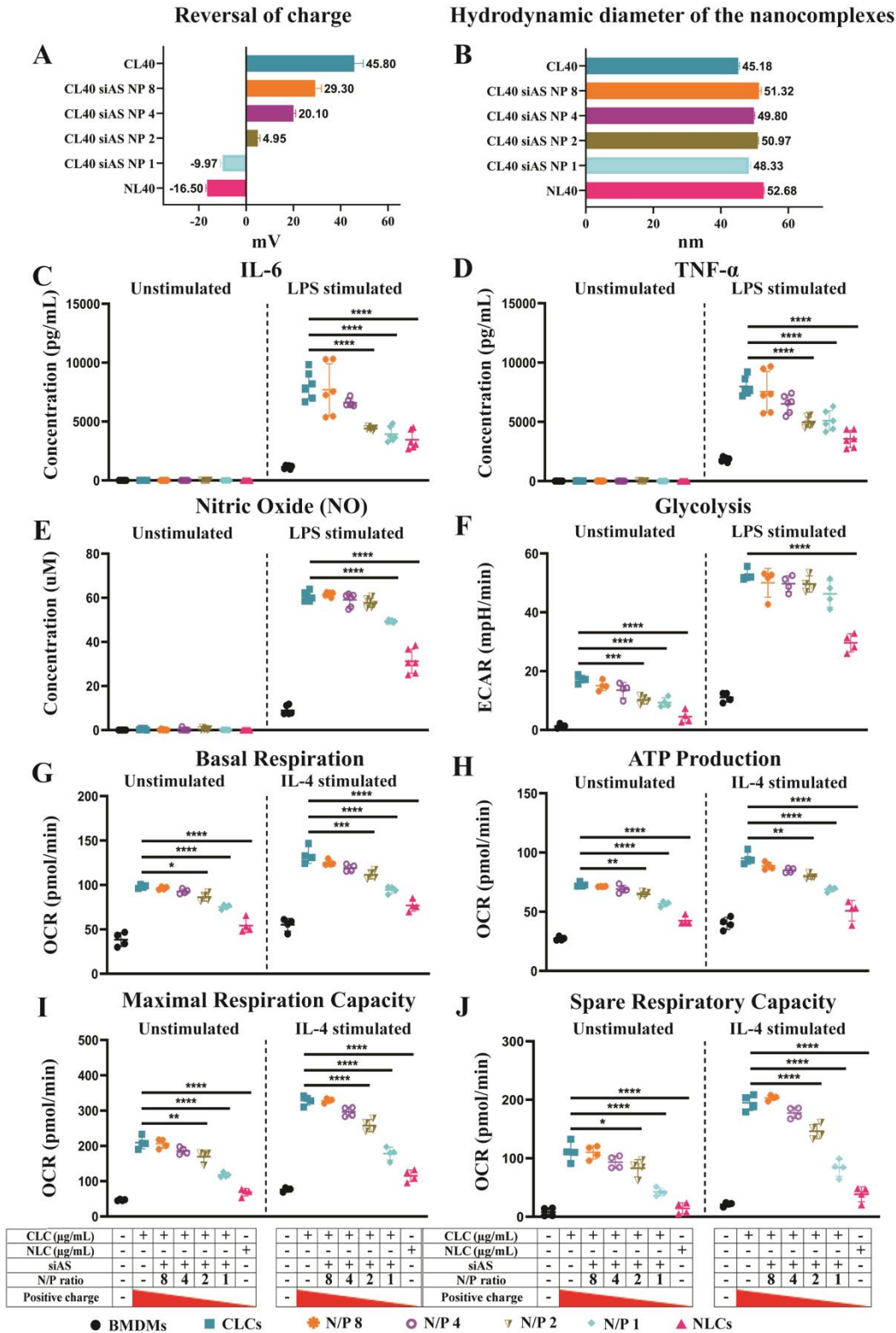


Figure 6

Reversing the surface charge with a nucleic acid cargo prevent adverse effects of cationic lipid nanocarrier on APCs



Supplementary figures

Figure 1

Phagocytosis capacity of macrophage cell line J774.1A

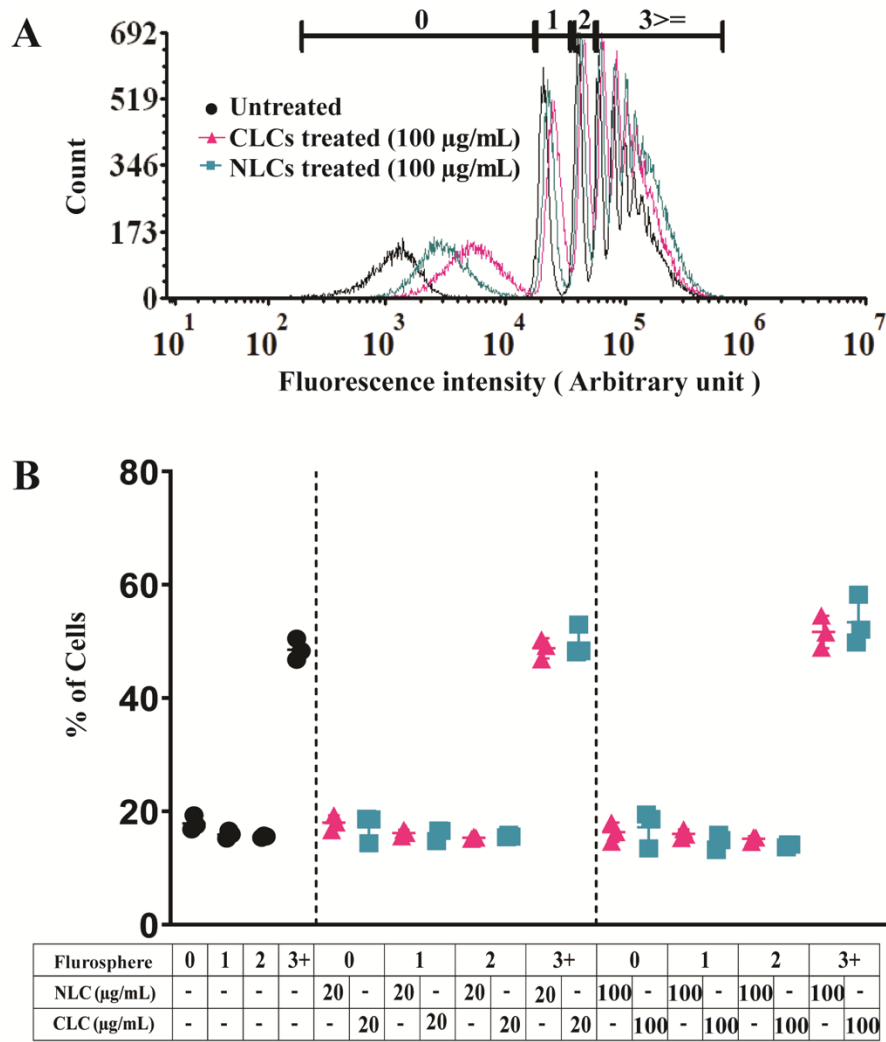


Figure 2

Expression of activation surface marker in APC

**Double positive (CD86 and MHC-II) cells population in percentage**

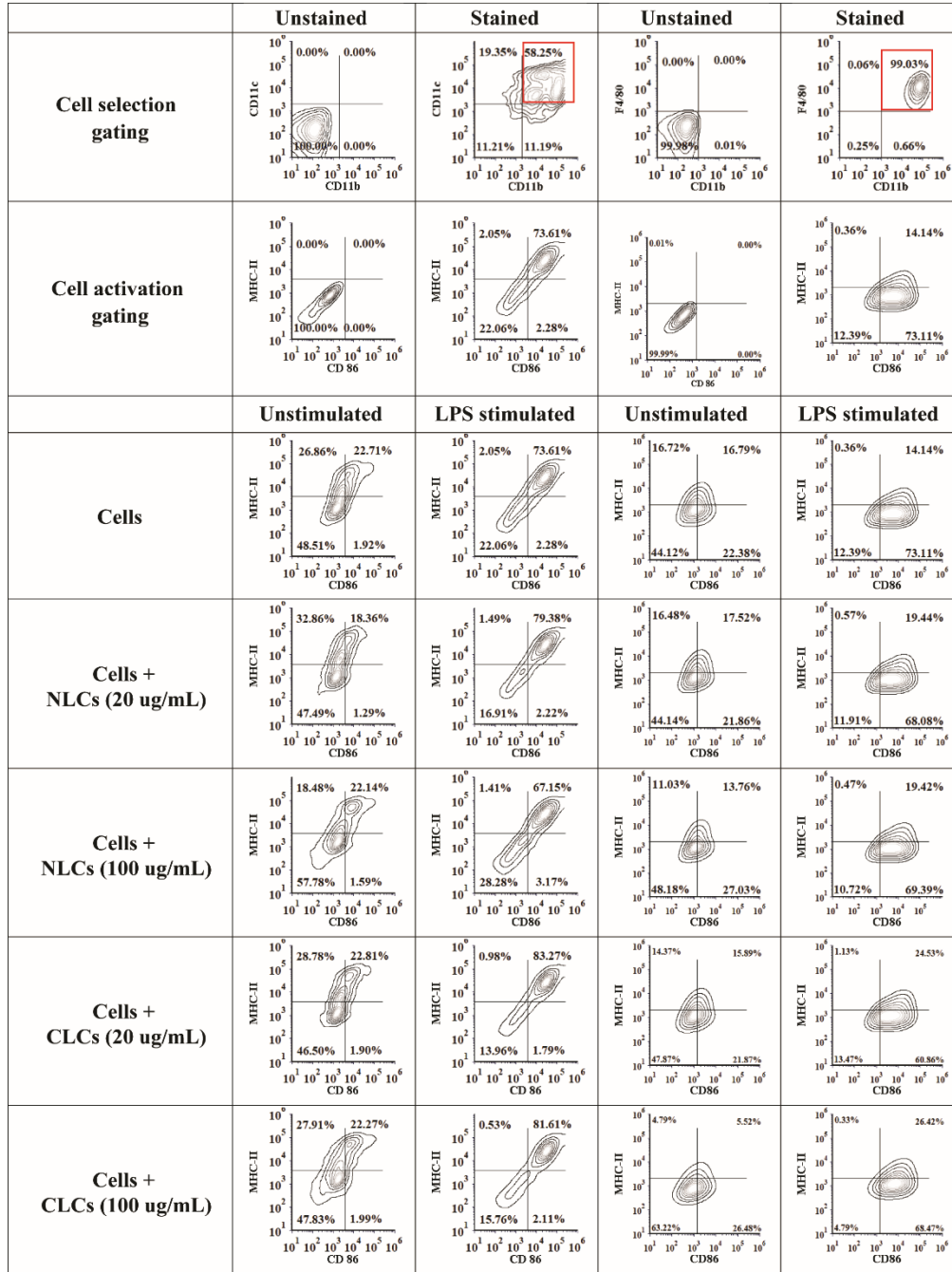


Figure 3

Experimental design of metabolic flux analysis

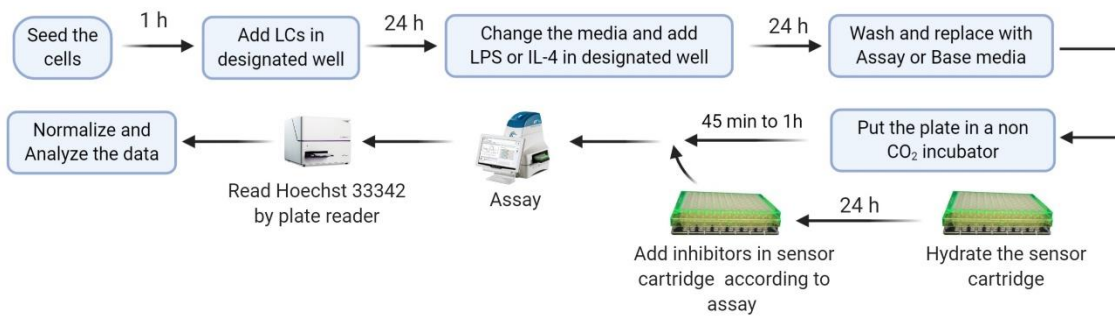


Figure 4

Basal respiration, Maximal respiration capacity, and Spare respiratory capacity of naïve, classically activated or alternatively activated APCs in response to neutral or cationic lipid nanocarriers

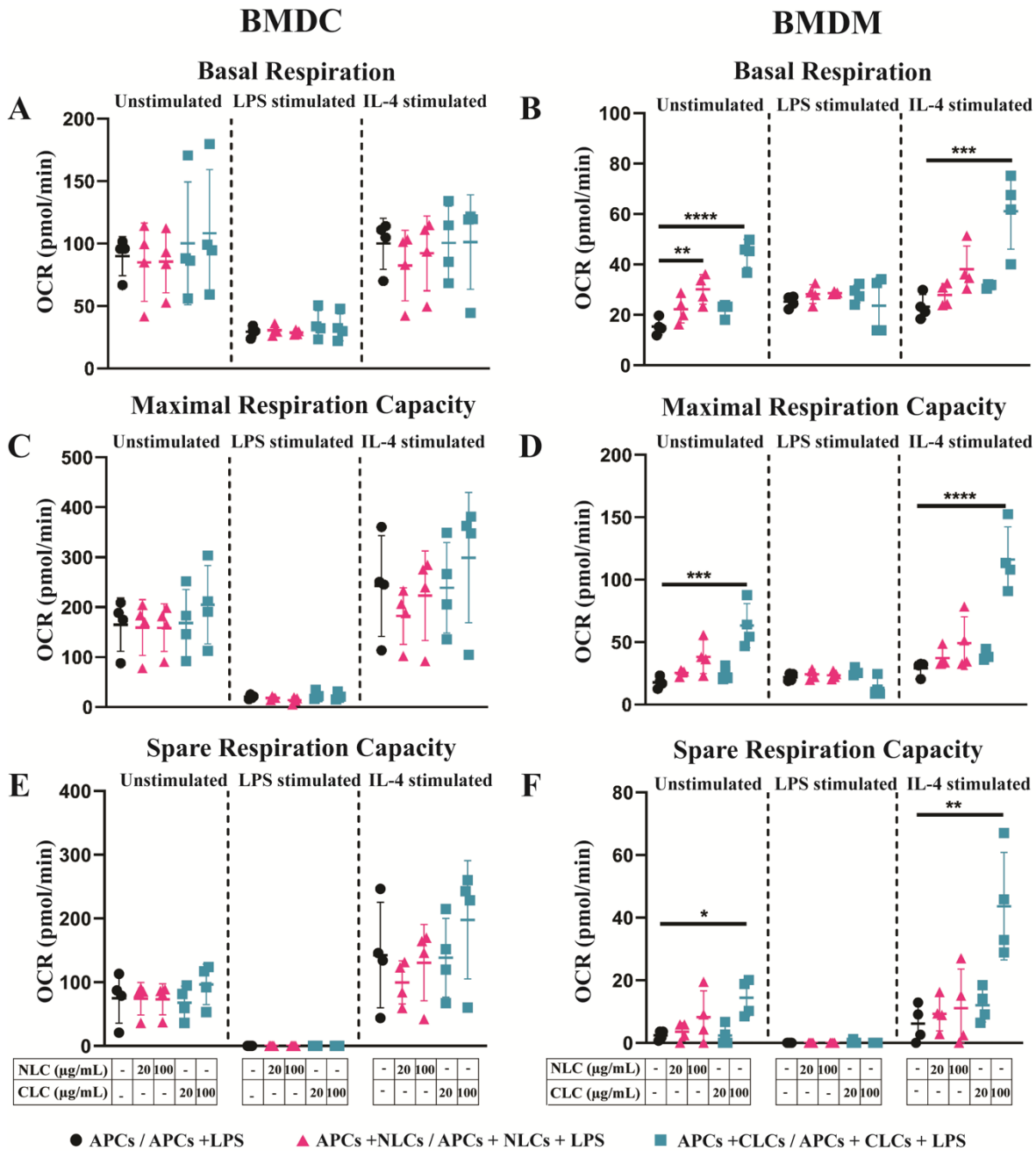




Figure 5

Non-mitochondrial oxygen consumption and Percentage of coupling efficiency of naïve, classically activated or alternatively activated APCs in response to neutral or cationic lipid nanocarriers

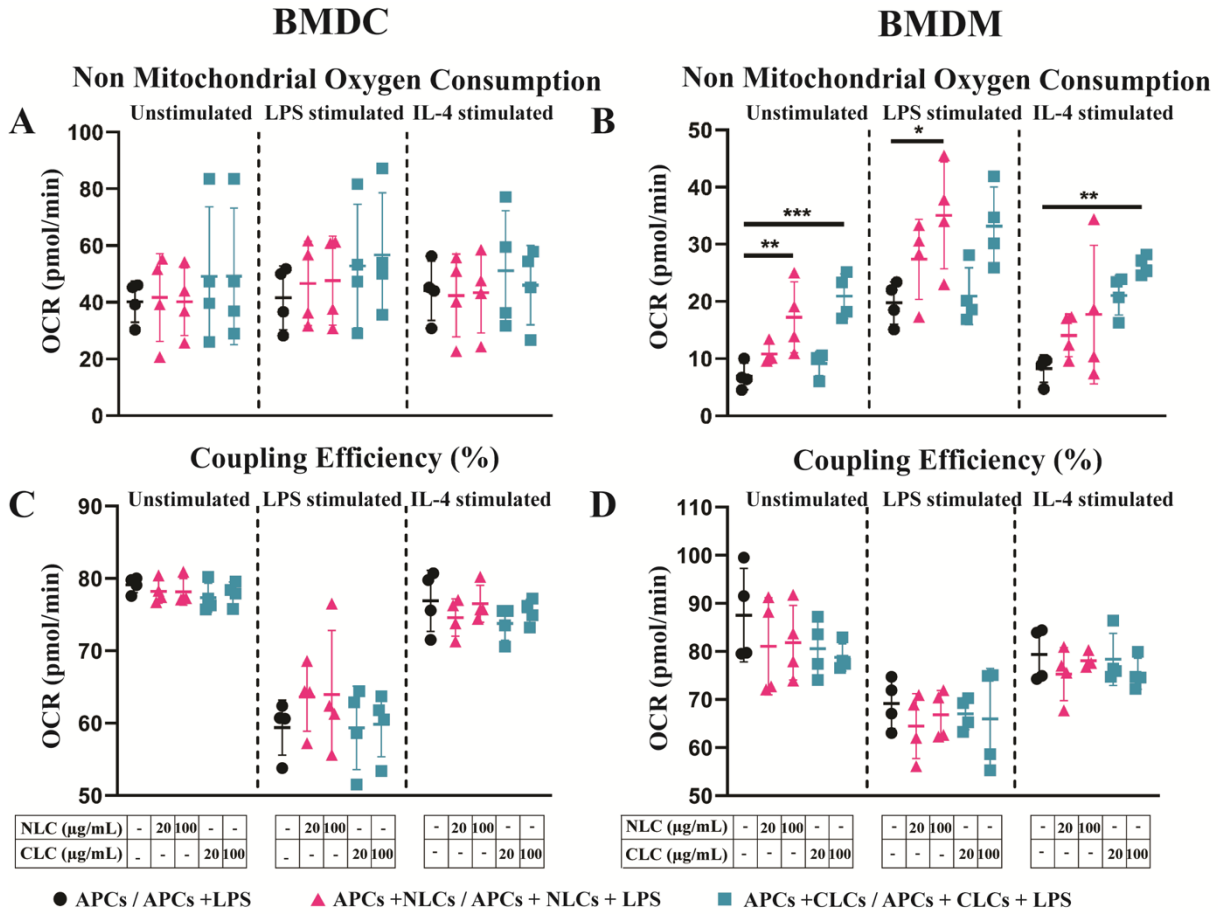


Figure 6

Glycolytic capacity of naïve, naïve, classically activated or alternatively activated APCs in response to neutral or cationic lipid nanocarriers

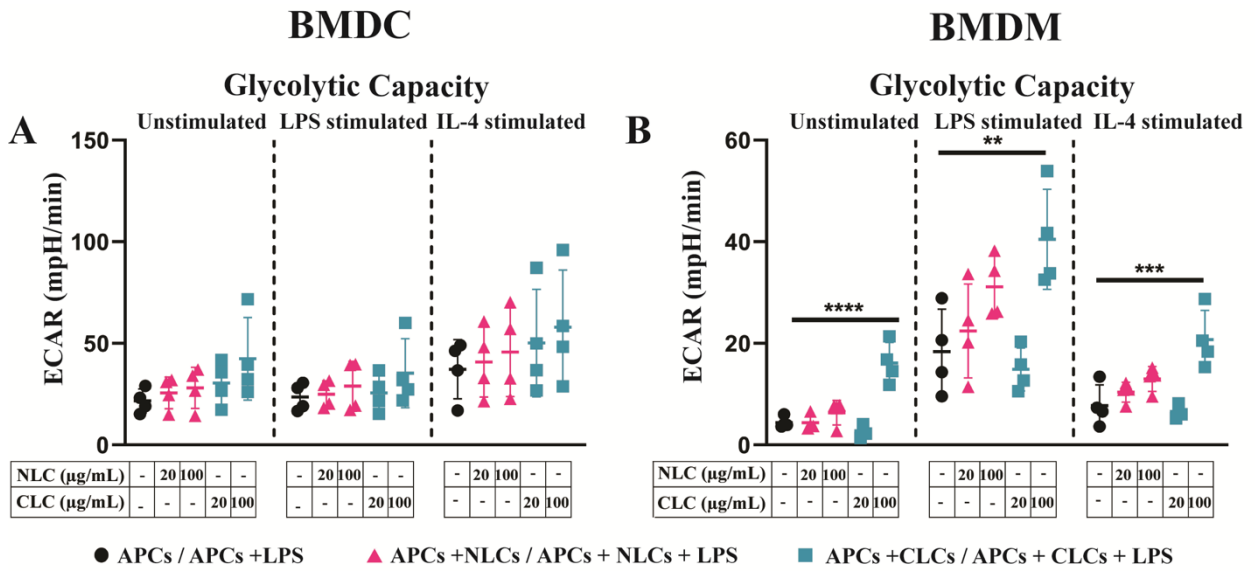


Figure 7

Experimental design of metabolic flux analysis for reversal of nanocarriers surface charge

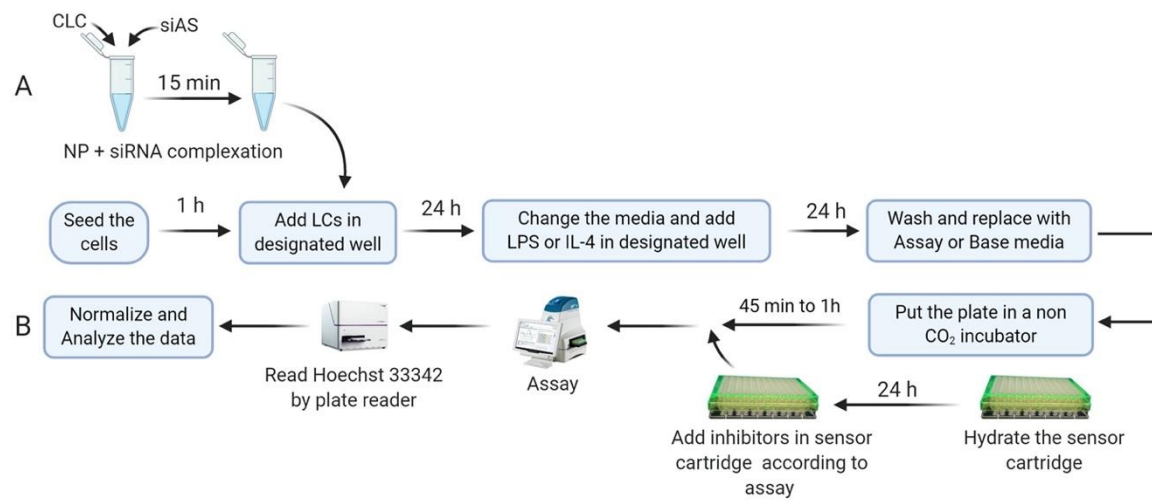
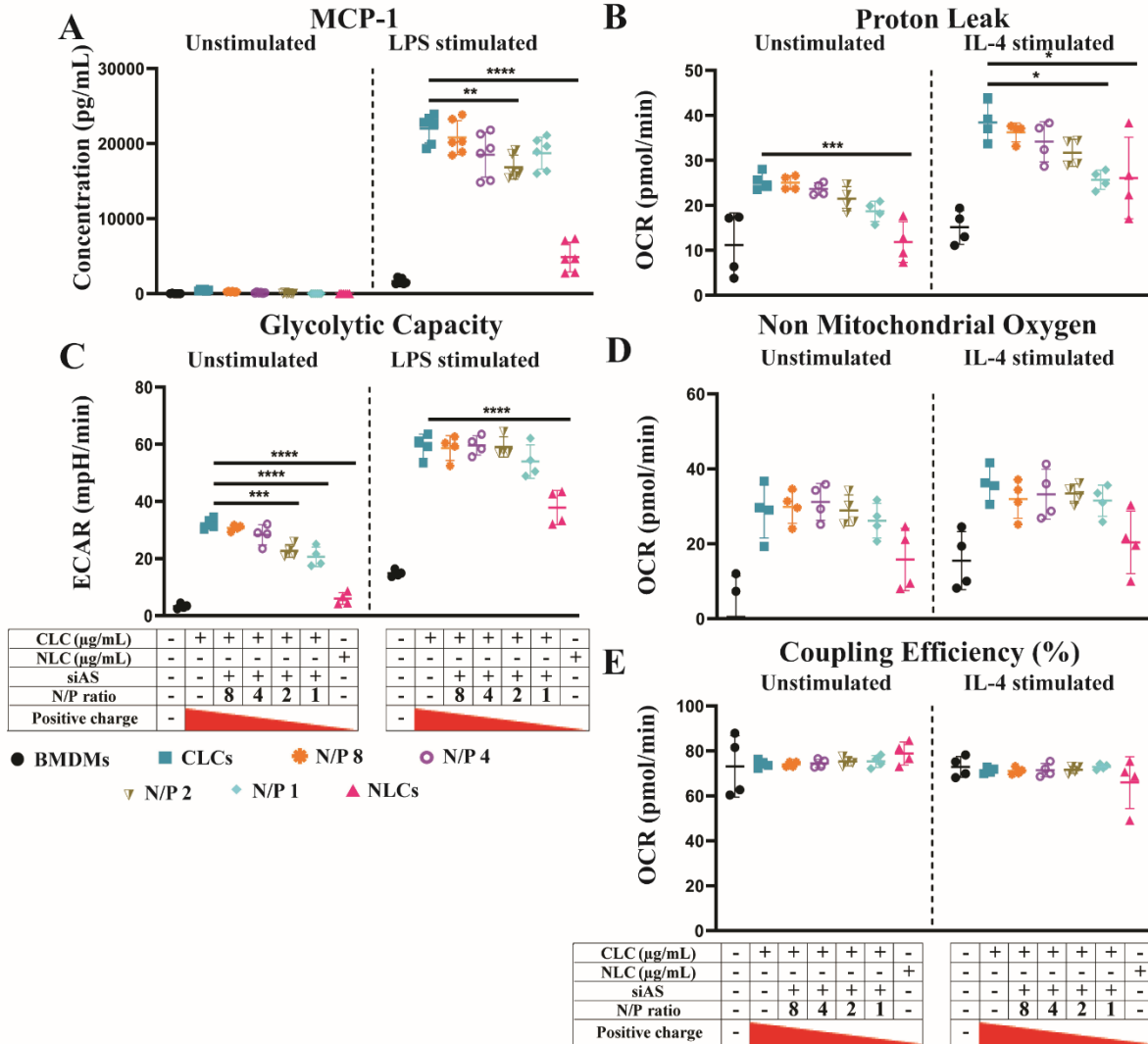


Figure 8

Effect of the net surface charge of cationic lipid nanocarriers on different cellular functions and metabolism of BMDMs



### 9.3 Impact of Amphiphilic dendrimers on the functions of macrophages and dendritic cells

In this project, several targeted drug delivery nanosystems (nDDSs) have been initially proposed to transport identified immunomodulators to the tumor in the attempt to reactivate innate immunity by stimulating various components of the immune system. This strategy of immunotherapy of cancers is promising; however, its efficacy has to be evaluated along with its safety as early as possible from the beginning of the development in order to select desired future candidates. The works presented below were achieved in the frame of an EuroNanoMed international program supporting the development of different nDDSs to modulate immune cells associated with brain tumors, including microglia/macrophage, lymphocytes, and natural killer (NK) cell. Glioblastoma (GBM) is a hyper-aggressive brain tumor associated with short life expectancy, and current therapeutic means are poorly efficacious. Immunotherapy is considered the most promising approach to successfully cure and remove cancer due to a persistent and significant antitumor response mediated by effective immunomodulatory agents.

However, an advance in immunotherapy in the treatment of GBM involves a safe and convenient-to-use system that can deliver immunomodulators to tumor lesions. In order to address GBM with immunotherapy, the "NanoGlio" project was designed to develop nanotechnology-based systems for the targeted delivery of immunomodulating agents with an aim of developing and validating novel immunotherapeutic approaches to GBM.

To achieve this goal, different nDDSs were produced by partners using lipid, polymers, and dendrimers nanoformulations; then, the most promising candidates have been selected to be tested for anticancer activity in patient-derived xenograft models. In order to realize the project, NanoGlio project consortium has been built with 7 partners coming from 5 different countries. The work was subdivided into 6 WPs. As a part of the "NanoGlio project", I participated in WP 4 "Toxicity assay and cellular uptake mechanism." WP 4 aimed to evaluate the toxicity and their potential immune-inflammatory effects of the loaded and empty nDDSs in order to decide, at an early stage, on whether a nDDSs is suitable for further cellular or animal studies. Specific objectives of this WP included:

- 1) *in vitro* evaluation of the cell toxicity,
- 2) determination of the immune-inflammatory responses of exposed cells and *in vivo* evaluation of toxicity.

These works were divided into two tasks, which altogether, gathered a panel of *in vitro* assays allowing rapid screening of nDDSs candidates for their nontoxicity and the absence of proinflammatory property in order to retain those presenting less risk for *in vivo* trials.

Task 4.1: *In vitro* toxicity assay of all the nDDSs has been performed using cells from various origins, including A549 (lung), Caco-2 (colon), and HepG2 (liver). In parallel, we used cell lines specialized in the internalization of foreign materials (nDDSs): THP-1 and U937 (human) and J774 (mice). Toxicity exhibited by different nDDSs on mentioned cell lines was monitored by LDH release assay and 7AAD/Annexin V. The aim of Task 4.1 is to choose the most suitable nDDSs for further experiments (Figure 25). For simplicity of the thesis, results from Task 4.1 is not shown here. But LDH assay and 7AAD/Annexin V assay suggested amphiphilic dendrimer designed by Dr. ling’s laboratory in Aix-Marseille Université as the most suitable nDDSs for further toxicity analysis.

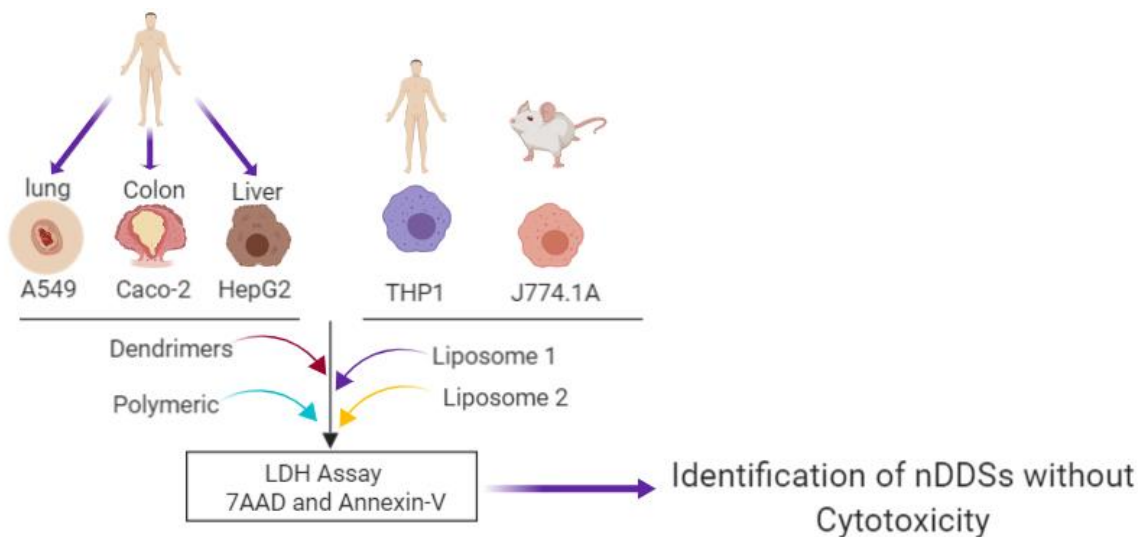


Figure 25: Identification of nDDSs without cytotoxicity.

Task 4.2: In task 4.2, we analysed the immunotoxicity exhibited by dendrimer in detail using the same experimental scheme developed during the immunotoxicity analysis of AuNPs. The outcome of task 4.2 encouraged us to write two manuscripts titled as

- 1) Synthesis and use of an amphiphilic dendrimer for siRNA delivery into primary immune cells.
- 2) Amphiphilic dendrimers: A potentially nontoxic siRNA delivery agent

The first article entitled “Synthesis and use of an amphiphilic dendrimer for siRNA delivery into primary immune cells” has already been accepted in “Nature Protocols” (NP-P200172B). This article aims to provide detailed protocols showing the high performance of amphiphilic dendrimer (AD) for siRNA delivery to a wide range of cell types, including highly challenging primary immune cells, such as human peripheral blood mononuclear cells (PBMCs), human B- and T-lymphocytes, NK cells (human and mouse), primary bone marrow-derived macrophages and primary microglial cells (rat and mouse). I contributed to this particular article in providing a proficient method for the transfection of primary mouse macrophages (BMDMs) by delivering ADs loaded with JAK1 siRNA as an example.

### 9.3.1 Synthesis and use of an amphiphilic dendrimer for siRNA delivery into primary immune cells

siRNA mediated gene manipulation of immune cells is important for both basic immunological studies and therapeutic applications. However, **siRNA delivery is challenging because primary immune cells are often sensitive to the standard transfection reagents and generate immune responses**. To address these problems, Dr. Ling’s team has developed an innovative amphiphilic dendrimer, which exhibits particularly high performance for siRNA delivery to a wide range of cell types. Notably, this dendrimer is able to form small and stable nanoparticles with siRNA, thus protecting the siRNA from degradation and facilitating cellular uptake of siRNA. The subsequent siRNA-mediated gene silencing is specific and effective at both the mRNA and protein levels, leading to consequential biological effects. Remarkably, this dendrimer does not induce apparent cellular toxicity or non-specific immune responses under experimental conditions. This article provides a detailed protocol describing the amphiphilic dendrimer mediated siRNA delivery in human peripheral blood mononuclear cells (PBMCs), human B- and T-lymphocytes, NK cells (human and mouse), **primary bone marrow-derived macrophages (BMDMs)**, and primary microglial cells (rat and mouse). The paper is already published on *Nature Protocols* volume 16, pages327–351(2021). DOI: <https://doi.org/10.1038/s41596-020-00418-9>

In the second manuscript entitled “Amphiphilic dendrimers: A potentially nontoxic siRNA delivery agent,” I contributed to generate most of the immunotoxicity experiments except the western blotting and *in vivo* CAM experiment. This manuscript is still under process and waiting for the expert reviews of other participants in the project framework.



# Synthesis and use of an amphiphilic dendrimer for siRNA delivery into primary immune cells

Jiaxuan Chen<sup>1,2</sup>, Aleksandra Ellert-Miklaszewska<sup>3</sup>, Stefano Garofalo<sup>4</sup>, Arindam K. Dey<sup>5</sup>, Jingjie Tang<sup>1</sup>, Yifan Jiang<sup>1</sup>, Flora Clément<sup>5</sup>, Patrice N. Marche<sup>5</sup>, Xiaoxuan Liu<sup>2</sup>, Bozena Kaminska<sup>3</sup>, Angela Santoni<sup>6</sup>, Cristina Limatola<sup>4,6</sup>, John J. Rossi<sup>7</sup>, Jiehua Zhou<sup>7</sup>✉ and Ling Peng<sup>1</sup>✉

Using siRNAs to genetically manipulate immune cells is important to both basic immunological studies and therapeutic applications. However, siRNA delivery is challenging because primary immune cells are often sensitive to the delivery materials and generate immune responses. We have recently developed an amphiphilic dendrimer that is able to deliver siRNA to a variety of cells, including primary immune cells. We provide here a protocol for the synthesis of this dendrimer, as well as siRNA delivery to immune cells such as primary T and B cells, natural killer cells, macrophages, and primary microglia. The dendrimer synthesis entails straightforward click coupling followed by an amidation reaction, and the siRNA delivery protocol requires simple mixing of the siRNA and dendrimer in buffer, with subsequent application to the primary immune cells to achieve effective and functional siRNA delivery. This dendrimer-mediated siRNA delivery largely outperforms the standard electroporation technique, opening a new avenue for functional and therapeutic studies of the immune system. The whole protocol encompasses the dendrimer synthesis, which takes 10 days; the primary immune cell preparation, which takes 3–10 d, depending on the tissue source and cell type; the dendrimer-mediated siRNA delivery; and subsequent functional assays, which take an additional 3–6 d.

## Introduction

RNA interference (RNAi) is a powerful tool for manipulation of gene expression in basic research and an emerging therapeutic strategy to treat various diseases<sup>1,2</sup>. The power of RNAi lies in its ability to potently and specifically silence any gene of interest with small interfering RNAs (siRNAs), enabling functional study of the target gene and/or effective inhibition of the disease-associated gene for therapeutic intervention. The breakthrough success of RNAi therapeutics came in 2018, when Patisiran (Alnylam Pharmaceuticals) became the first siRNA drug approved by the USA Federal Drug Administration (FDA; ref. <sup>3</sup>). In addition, the recent success of cancer immunotherapy has fueled a tremendous interest in genetic manipulation of immune cells using siRNAs to address basic immunological questions and for potential therapeutic applications<sup>4,5</sup>. However, the major obstacle in implementing RNAi in those cells has been poor delivery of the siRNA<sup>6,7</sup>, in particular in primary immune cells such as lymphocytes (B cells, T cells, natural killer (NK) cells), mononuclear phagocytes (monocytes, macrophages, microglia, dendritic cells), and granulocytes (neutrophils, eosinophils, basophils). This is because siRNA molecules are hydrophilic and highly negatively charged and cannot readily cross cell membranes to reach the RNAi machinery within the cytoplasm for gene silencing. In addition, naked siRNA is not stable and can be rapidly degraded by enzymes such as nucleases. If administered at high concentrations, naked siRNA will often generate off-target effects and activate innate immunity<sup>8,9</sup>, which may induce severe adverse effects. In addition, siRNA can induce the activation of the innate immune response through various possible pathways, such as Toll-like receptors (TLR3, TLR7/8), double-stranded RNA (dsRNA)-dependent protein kinase (PKR) and retinoic acid-inducible gene-I (RAI1)<sup>10</sup>. Although using modified siRNA chemistry and

<sup>1</sup>Aix-Marseille Université, Center Interdisciplinaire de Nanoscience de Marseille, UMR 7325, Equipe Labellisée Ligue Contre le Cancer, CNRS, Marseille, France. <sup>2</sup>State Key Laboratory of Natural Medicines and Jiangsu Key Laboratory of Drug Discovery for Metabolic Diseases, Center of Drug Discovery, Center of Advanced Pharmaceutics and Biomaterials, China Pharmaceutical University, Nanjing, P. R. China. <sup>3</sup>Laboratory of Molecular Neurobiology, Neurobiology Center, Nencki Institute of Experimental Biology of the Polish Academy of Sciences, Warsaw, Poland. <sup>4</sup>Department of Physiology and Pharmacology, Sapienza University of Rome, Rome, Italy. <sup>5</sup>Institute for Advanced Biosciences, University Grenoble-Alpes, Inserm U1209, CNRS 5309, La Tronche, France. <sup>6</sup>IRCCS Neuromed, Pozzilli, Italy. <sup>7</sup>Department of Molecular and Cellular Biology, Beckman Research Institute, City of Hope Medical Center, Monrovia, CA, USA. ✉e-mail: [jh.zhou@hitgen.com](mailto:jh.zhou@hitgen.com); [ling.peng@univ-amu.fr](mailto:ling.peng@univ-amu.fr)



optimized siRNA sequences can stabilize siRNA and lessen the unwanted effects<sup>10</sup>, siRNA delivery to primary immune cells remains a special challenge. Immune cells such as T lymphocytes and NK cells are small, with limited cytoplasm. Macrophages, dendritic cells, and microglia, as professional phagocytes, are endowed with many potent degradative enzymes that can disrupt nucleic acid integrity and make gene transfer into these cells an inefficient process<sup>11</sup>. In addition, primary immune cells are often sensitive to the delivery materials, generating nonspecific immune responses. On the other hand, most common methods that are used to deliver siRNA to primary immune cells and that do not require any additional carriers—such as electroporation and nucleofection—lead to excessive cell death and low transfection efficiency and hence are unsuitable for general applications in either basic or translational research. Consequently, there is a high demand for safe and effective delivery systems that are able to protect siRNA from degradation, deliver it to the target cells, and ultimately achieve gene silencing to facilitate genetic manipulation of immune cells for functional and therapeutic studies.

Both viral and nonviral delivery vectors have been explored for siRNA delivery<sup>6,7</sup>, in particular to immune cells<sup>5,11–14</sup>. Viral delivery is more effective; however, increasing concerns over the immunogenicity and safety of viral vectors have driven the development and improvement of non-viral delivery systems. Non-viral vectors offer more-flexible options, with lipid and polymer vectors being the most commonly used. For example, the first human trial of siRNA therapeutics used a polymer vector<sup>15</sup>, whereas the first FDA-approved siRNA drug, Patisiran, uses a lipid nanoparticle (LNP) delivery formulation. Although some well-studied lipid and polymer vectors perform well for the majority of established immortalized cells, they have marginal efficacy in siRNA delivery to primary immune cells and often induce nonspecific immune responses.

To circumvent these problems, we have been developing innovative amphiphilic dendrimers for effective siRNA delivery. The rationale behind these dendrimer vectors is that they combine the multivalent cooperativity of dendritic polymer vectors with the self-assembly property of lipid vectors, hence capitalizing on the advantageous delivery characteristics of both lipid and polymer vectors—while overcoming their limitations—for more effective and potent siRNA delivery<sup>16–21</sup>. One of these dendrimers, AD (Fig. 1), exhibits particularly high performance for siRNA delivery to a wide range of cell types, including highly challenging primary immune cells, such as human peripheral blood mononuclear cells (PBMCs), human B and T lymphocytes, NK cells (human and mouse), primary monocyte-derived macrophages and primary microglial cells (rat and mouse)<sup>17,20,21</sup>. Notably, this AD dendrimer is able to form small and stable nanoparticles with siRNA, thus protecting the siRNA from degradation and facilitating its cellular uptake<sup>17,20</sup>. The subsequent siRNA-mediated gene silencing is specific and effective at both the mRNA and protein levels, leading to consequential biological effects. Remarkably, this dendrimer does not induce apparent cellular toxicity or nonspecific immune responses under experimental conditions. Consequently, it constitutes a promising tool for siRNA delivery to immune cells and provides a new outlook for functional and therapeutic studies of the immune system.

We provide here the procedures for the robust synthesis of this dendrimer, AD, and the AD-mediated delivery of siRNA to immune cells using primary T cells, natural killer cells, macrophages, and microglial cells as the model cells. The dendrimer synthesis is easy to follow and reproduce. In addition, the final purification of the dendrimer AD is achieved through simple dialysis in water, giving AD in high yield and purity. Most importantly, the formation of the siRNA–dendrimer complexes requires only simple mixing of the siRNA with AD in solution at room temperature (25 °C). The complexes can then be readily applied to the immune cells, such as T lymphocytes, B lymphocytes, monocytes/macrophages, brain innate immune cells (microglia), and NK cells, for transfection and gene silencing assays.

### Overview of the procedure

In this protocol, we first describe the synthesis and molecular characterization of the dendrimer AD. Using 21/21-mer siRNAs and 27/29-mer Dicer-substrate siRNAs (DsiRNAs)<sup>22,23</sup> as examples, we explain the procedure and the conditions for AD-mediated transfection assays to deliver siRNA to primary immune cells (T cells, NK cells, macrophages, and microglia) in various plate formats and the subsequent validation of gene knockdown. Typically, the chemical synthesis of AD takes 10 d, including purification. The whole transfection procedure—from cell seeding, preparation of the siRNA–AD complexes, and cell transfection to validation tests and functional assays—takes 7 d. Time

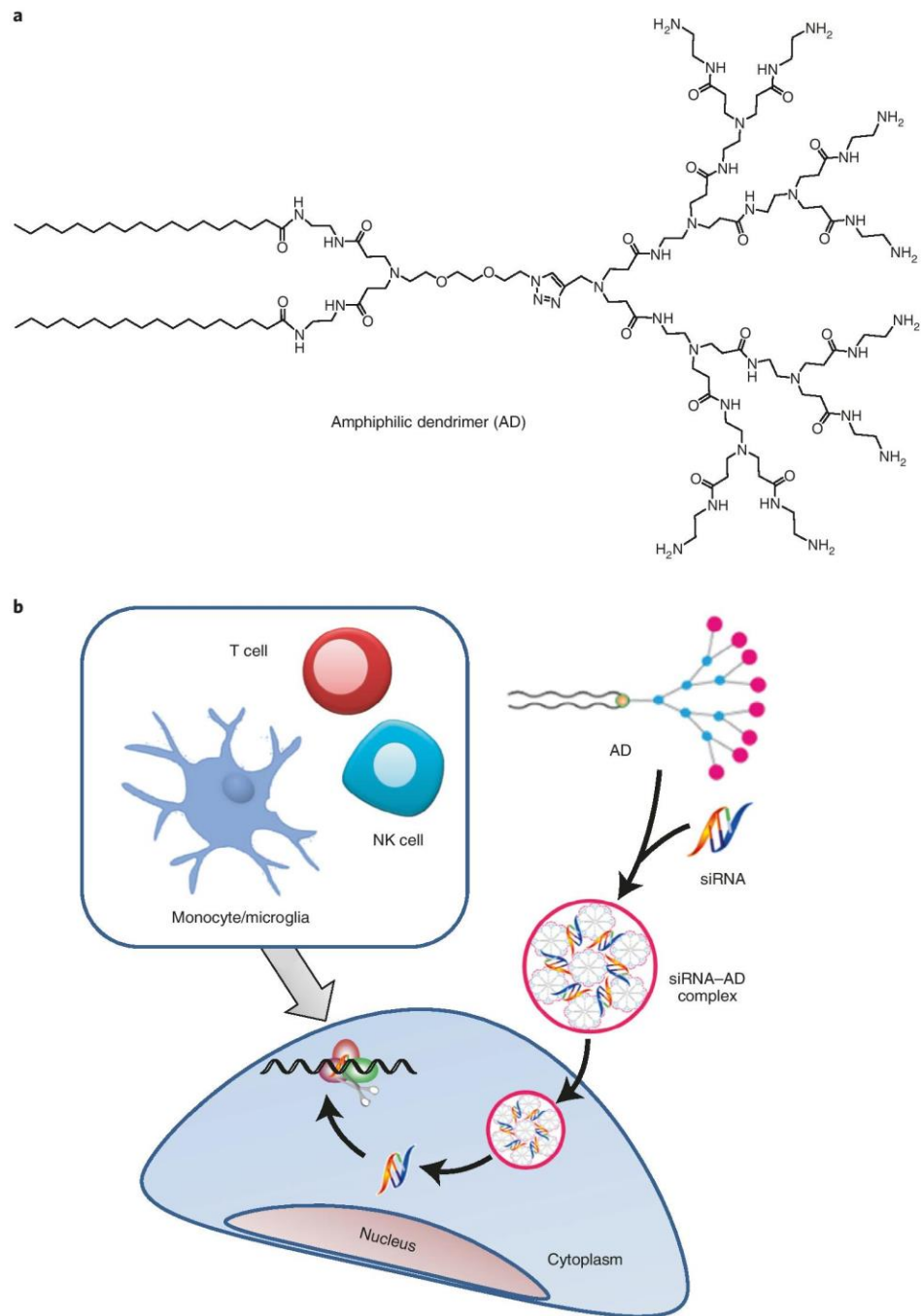


**Fig. 1 | Schematic presentation of siRNA delivery mediated by the amphiphilic dendrimer AD. a**, The molecular structure of AD. **b**, Diagram showing AD-mediated siRNA delivery to various immune cells, including T cells, microglia, and NK cells. The pink dots in the AD structure represent amine terminals, the blue dots represent the amidoamine backbone branching tertiary amine functions and the yellow dot represents the AD's triazole ring. Adapted with permission from ref. <sup>17</sup>, Wiley, and ref. <sup>20</sup>, *Nanomedicine* (as agreed by Future Medicine Ltd.).

frames for preparation of primary cell cultures can vary, as described in the Supplementary Methods. Details of the isolation and maintenance and/or expansion of primary immune cells are also provided in the Supplementary Methods.

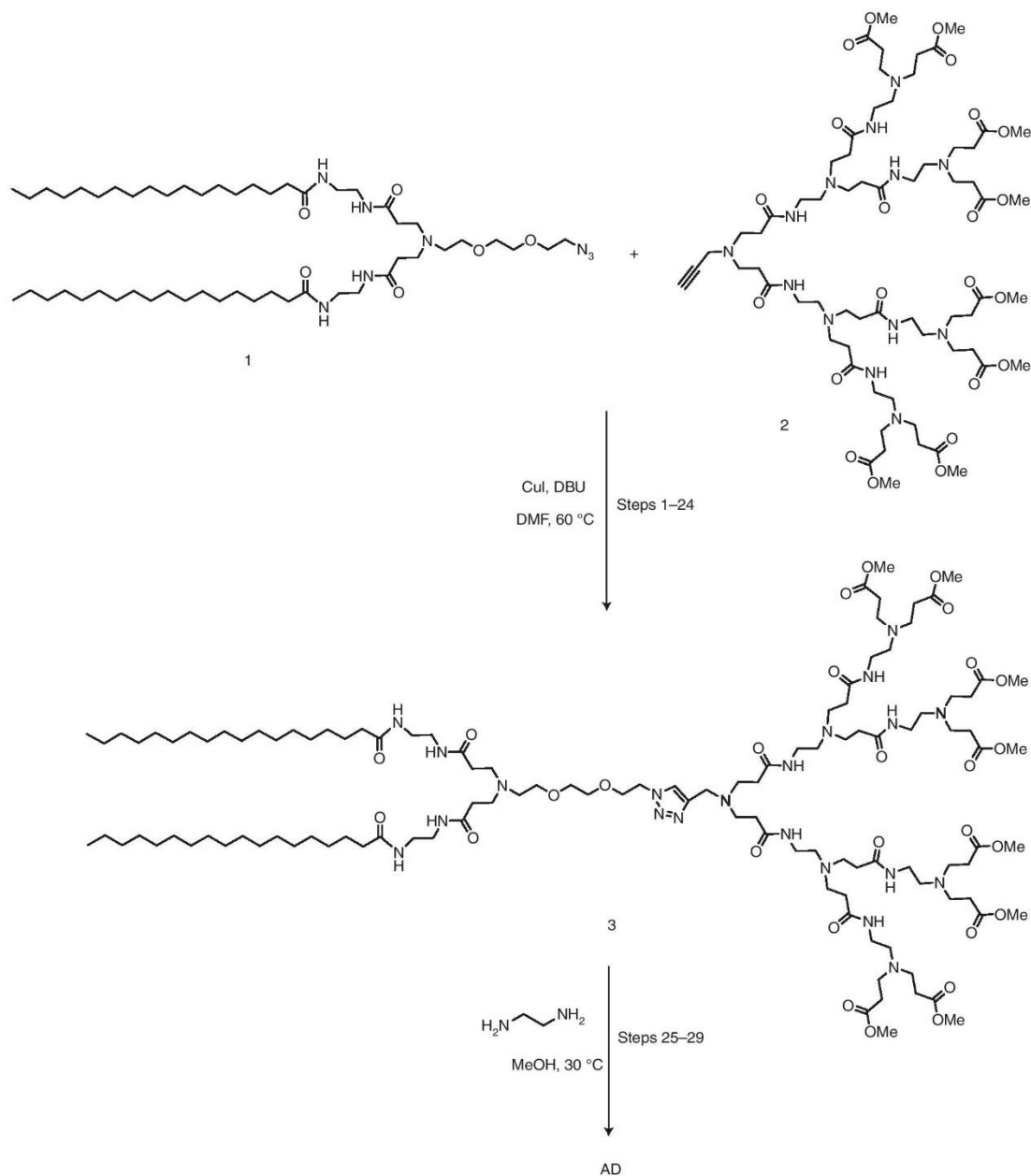


**Fig. 2 |** Chemical synthesis of the amphiphilic dendrimer AD. Adapted with permission from ref. <sup>17</sup>, Wiley.

### Experimental design

#### Chemical synthesis

Synthesis of AD is achieved by coupling the hydrophobic chain **1** and the hydrophilic PAMAM dendron **2** via ‘click’ reaction using copper-catalyzed azide–alkyne cycloadditions (CuAACs), followed by amidation with ethylenediamine (EDA) (Fig. 2). The starting materials **1** and **2** can be easily prepared using well-established protocols<sup>16,17</sup>. However, **1** is poorly soluble in dimethylformamide (DMF), so it is necessary to raise the reaction temperature to 60 °C to solubilize **1** and drive the reaction to completion, thus producing **3** in high yield. It is also critical to keep the amounts of **1** and **2** at a molar ratio of 1:1.05 for the click reaction, because it is difficult to separate the remaining excess **1** and/or **2** from the product **3** if the reaction is performed without respecting the

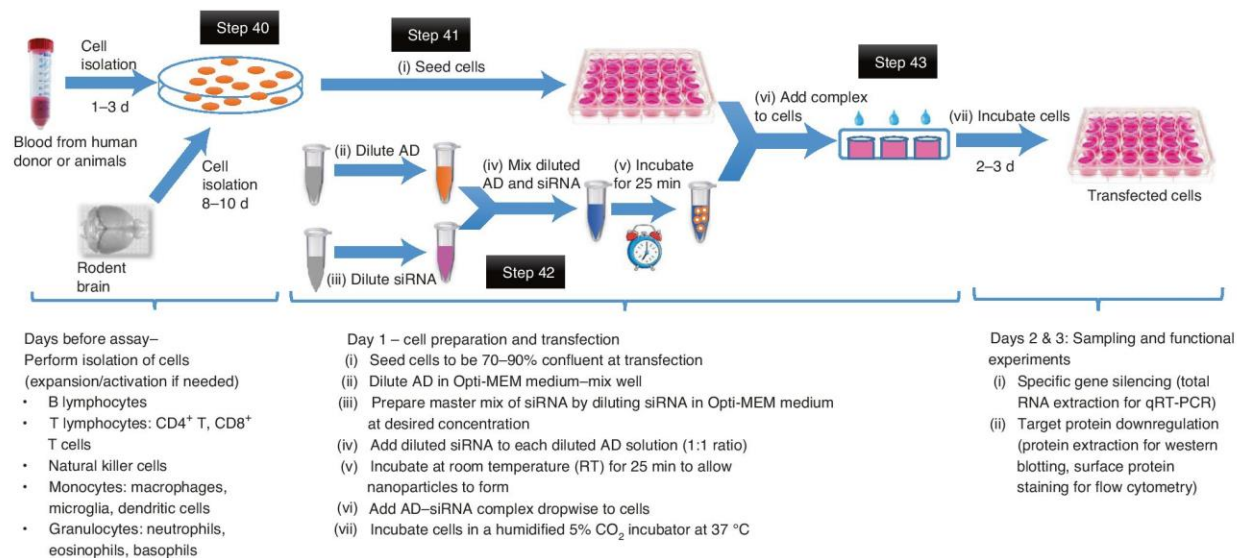


**Fig. 3 | Experimental outline.** A schematic illustrating dendrimer-mediated siRNA transfection of primary cells.

stoichiometry. For the amidation reaction, the amount and concentration of EDA must be controlled in order to maximally suppress the retro-Michael side reaction and cyclization by-products<sup>24–26</sup>. Different from our previously published protocol<sup>17</sup>, here we use MeOH instead of MeOH/CH<sub>2</sub>Cl<sub>2</sub> as solvent for the amidation. This is because CH<sub>2</sub>Cl<sub>2</sub> can react with EDA to generate oligomeric impurities<sup>27</sup> and at the same time increase the formation of cyclization at the dendrimer terminals. The optimized conditions therefore enable more reliable amidation. The final dendrimer, AD, is purified using dialysis against water and obtained as a pale powder after lyophilization.

#### Formation of the siRNA–AD complexes

As shown in Fig. 3, the siRNA–dendrimer complexes are formulated by simply adding the siRNA solution to the dendrimer solution at 25 °C in DPBS buffer or serum-free Opti-MEM, followed by gentle vortexing and incubation. The complexes are then applied to the primary immune cell culture. It is preferable to use a freshly prepared solution of siRNA–AD complexes for transfection.

#### Calculation of the ratio of siRNA to the dendrimer AD in a transfection assay

The formulation of siRNA–dendrimer complexes depends critically on the dendrimer-to-RNA charge ratio (N/P ratio). It is calculated as [total terminal amino groups in the cationic dendrimer]/[total phosphates in the siRNA]. We always calculate the amount of AD according to the amount of siRNA in the final volume of cell culture media and the N/P ratio, as follows:

$$\text{Amount of AD} = (\text{amount of siRNA}) \times (\text{number of phosphates in siRNA}) \times (N/P \text{ ratio}) / (\text{number of amino groups in AD})$$

In our previous work, we established an optimal N/P ratio of either 5 or 10 for AD-mediated siRNA delivery to immune cells, including PBMC–CD4<sup>+</sup> T cells, natural killer cells, macrophages, and microglial cells. In Table 1, we present the steps for AD-mediated transfection of an siRNA or a Dicer-substrate siRNA (DsiRNA) in various plate formats. Unlike a conventional siRNA duplex, which is composed of sense and antisense 21-mer oligonucleotides, the DsiRNA used in this protocol, also called 27/29-mer DsiRNA, contains a 27-mer sense oligonucleotide and a 29-mer antisense oligonucleotide. Such DsiRNAs have been demonstrated to enhance RNAi potency and efficacy<sup>22,23</sup>. As an example, in a 24-well plate format, with 500 μL of cell culture medium in each well, and using a 21/21-mer siRNA or a 27/29-mer DsiRNA at a 50 nM concentration, the amount of AD with eight terminal amino groups is calculated at an N/P ratio of 5 as follows:

$$\text{For a 21/21-mer siRNA, the amount of AD} = (50 \text{ nM} \times 500 \text{ } \mu\text{L}) \times (21 + 21) \times (5) / (8) = 656.25 \text{ pmol}$$

**Table 1 | Summary of the volumes of reagents required for dendrimer-mediated transfection of 21/21 mer siRNA or 27/29 mer DsiRNA in various plate formats**

Step	Component	96-well	24-well	12-well	6-well
i	Experimental cells (number)	$2 \times 10^4$ to $4 \times 10^4$	$1 \times 10^5$ to $5 \times 10^5$	$0.2 \times 10^6$ to $1 \times 10^6$	$0.5 \times 10^6$ to $2 \times 10^6$
	Cell culture medium (volume)	80 $\mu$ L	400 $\mu$ L	800 $\mu$ L	2,000 $\mu$ L
ii	Opti-MEM medium (if 21/21-mer siRNA is used)	9.45 $\mu$ L	47.27 $\mu$ L	94.53 $\mu$ L	236.35 $\mu$ L
	Amphiphilic dendrimer (AD) 21/21-mer siRNA (240 $\mu$ M stock solution)	0.55 $\mu$ L	2.73 $\mu$ L	5.47 $\mu$ L	13.65 $\mu$ L
	Here, N/P ratio = 5 as an example 27/29-mer DsiRNA	0.73 $\mu$ L	3.65 $\mu$ L	7.3 $\mu$ L	18.25 $\mu$ L
iii	Opti-MEM medium	9.5 $\mu$ L	47.5 $\mu$ L	95 $\mu$ L	237.5 $\mu$ L
	siRNA (10 $\mu$ M stock solution of siRNA); 50 nM as working concentration	0.5 $\mu$ L	2.5 $\mu$ L	5 $\mu$ L	12.5 $\mu$ L
iv	Diluted AD (step ii, final 50 $\mu$ L) + diluted siRNA (step iii, final 50 $\mu$ L) solution	20 $\mu$ L	100 $\mu$ L	200 $\mu$ L	500 $\mu$ L
v	Incubate at room temperature for 25 min to allow nanoparticles to form.				
vi	Final volume: step i cell culture + step iv complex	100 $\mu$ L	500 $\mu$ L	1,000 $\mu$ L	2,500 $\mu$ L
vii	Incubate cells in a humidified 5% CO <sub>2</sub> incubator at 37 °C				

N/P ratio is defined as [total end amines in cationic dendrimer] / [phosphates in siRNA] Example is for 50 nM siRNA and an N/P ratio = 5.

For a 27/29-mer DsiRNA, the amount of AD =  $(50 \text{ nM} \times 500 \mu\text{L}) \times (27+29) \times (5) / (8) = 875 \text{ pmol}$

Consequently, 2.73 or 3.65  $\mu$ L of 240  $\mu$ M AD stock solution is needed for transfection of a 21-mer siRNA or a 27-mer DsiRNA, respectively, in a 24-well plate.

**siRNA delivery and testing efficacy of gene silencing**

For siRNA delivery using dendrimer AD, the prepared stock solution containing the siRNA–AD complexes is added to primary immune cells in an appropriate dilution to reach the required final siRNA concentration. The effects of the transfection procedure on gene and protein expression are analyzed after 2 or 3 d by quantitative real-time PCR (qRT-PCR) and western blot (WB) or FACS, respectively. Several key controls should be included in the experimental design: (i) cells without any siRNA–AD transfection (as a mock control); (ii) cells transfected with an unrelated or scrambled siRNA–AD complex (as a negative control); and (iii) cells transfected with the experimental siRNA using a commercial transfecting agent (as a positive control or as a comparison control). By including these controls and comparing their effects on target gene and protein expression, the AD-mediated delivery and siRNA-mediated knockdown activity is defined and validated. Generally, siRNAs serving as negative controls that do not target any human or animal genome can be purchased from commercial vendors with the validation test in which the negative control siRNA has been functionally proven to have no substantial effect on cell proliferation, viability or morphology (<https://www.thermofisher.com/us/en/home/life-science/rnai/synthetic-rnai-analysis/controls-for-rnai-experiments.html#2>).

**Validation and applications**

To demonstrate the validation and application of siRNA delivery to immune cells using the dendrimer AD, we have selected four examples (Fig. 4) in which AD has been used to successfully deliver (i) anti-HIV siRNAs into primary CD4<sup>+</sup> T cells for efficient suppression of HIV-1 replication<sup>17</sup>; (ii) an anti-NKG2D siRNA into NK cells to reduce their cytotoxic activity toward tumor cells and motor neurons in a model of amyotrophic lateral sclerosis (ALS)<sup>21</sup>; (iii) an siRNA targeting the *JAK1* gene in primary mouse macrophages to regulate their inflammatory activities; and (iv) an siRNA targeting the transcription regulator ID1 in microglia for functional exploration of ID1<sup>20</sup>.

**Limitations**

This protocol provides a reliable and easy-to-use transfection agent, AD, for siRNA delivery to various primary immune cells. It will be important to determine whether the chemical composition of

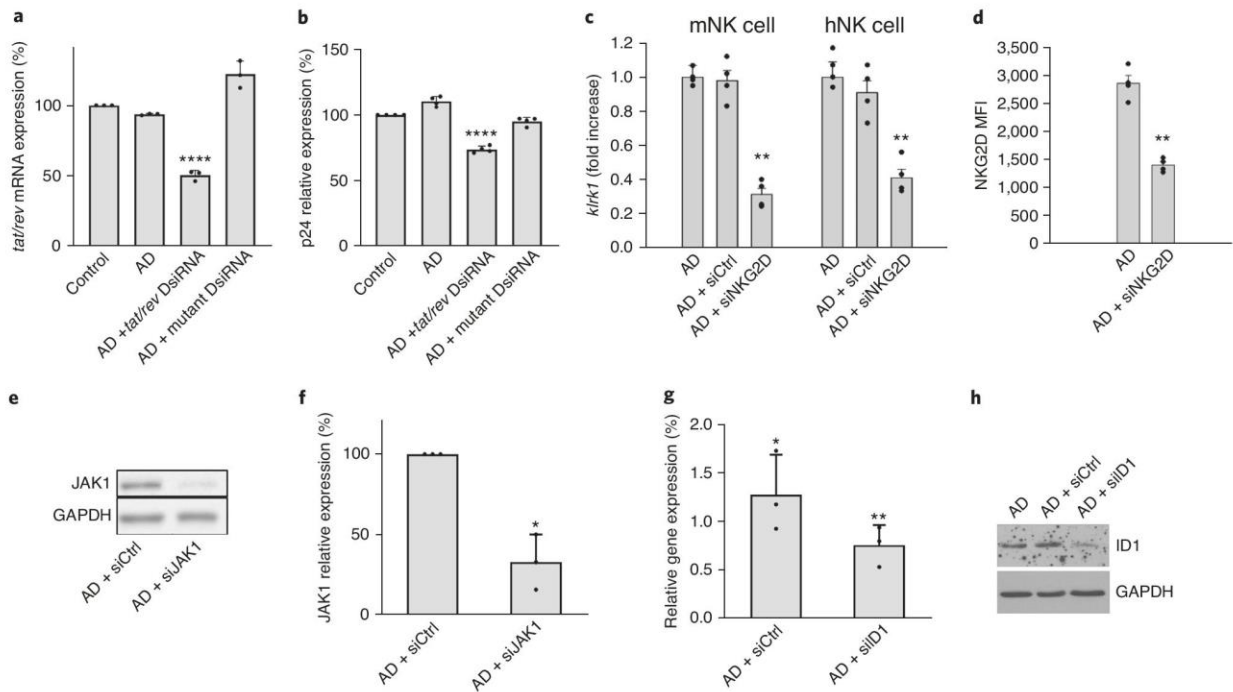


**Fig. 4 | Functional siRNA delivery mediated by AD in various primary immune cells. a, b,** AD-mediated anti-HIV siRNA delivery in human primary CD4<sup>+</sup> T lymphocytes. Downregulation of *tat/rev* mRNA expression as measured by RT-qPCR (**a**;  $n = 3$ , data are expressed as mean  $\pm$  SD, \*\*\*\* $P \leq 0.0001$  versus control, one-way ANOVA) and effective inhibition of HIV-1 replication with 50 nM DsiRNA and AD at an N/P ratio of 5 (**b**). Viral loading was assessed using HIV-1 p24 antigen ELISA assay at 3 d of post-treatment. PBMC-CD4<sup>+</sup> T cells were infected by NL4-3 virus (multiplicity of infection (MOI): 0.001) for 5 d before transfection. ( $n = 4$ , data are expressed as mean  $\pm$  SD, \*\*\*\* $P \leq 0.0001$  versus control, one-way ANOVA). The control is cells alone without any treatment. All measurements were taken from distinct samples. Statistical significance was assessed by one-way ANOVA for parametrical data as indicated by GraphPad Prism v. 8.0. **c, d,** AD-mediated siRNA delivery in murine (m) and human (h) primary NK cells. **c,** RT-PCR of *klrk1* gene in murine (left) and human (right) NK cells treated with siRNA and AD at an N/P ratio of 5 ( $n = 4$ , data are expressed as mean  $\pm$  SEM, \*\* $P < 0.001$  versus empty AD, one-way ANOVA). **d,** Detection of NKG2D protein in murine NK cells transfected with the complexes of anti-NKG2D or scrambled siRNA with AD at an N/P ratio of 10. Protein expression was assessed by FACS 48 h after transfection ( $n = 4$ , data are expressed as mean  $\pm$  SEM, \*\*\* $P < 0.001$  versus empty AD, one-way ANOVA). All measurements were taken from distinct samples. Statistical significance was assessed by one-way ANOVA for parametrical data, as indicated; Holm-Sidak test was used as a post hoc test; Mann-Whitney rank and Shapiro-Wilk tests for non-parametrical data, followed by Tukey's post hoc tests. For multiple comparisons, multiplicity-adjusted  $P$  values are indicated in the corresponding figures. Statistical analyses comprising calculation of degrees of freedom were done using Sigma Plot v. 12.5. **e, f,** AD-mediated siRNA delivery in mouse bone marrow-derived primary macrophages (BMDMs). **e,** Detection of JAK1 protein in macrophages transfected with anti-JAK1 (siJAK1) or control siRNA (siCtrl). Transfection was done with 50 nM siRNA and AD at an N/P ratio of 5. Protein expression was assessed by WB 48 h after transfection with antibodies specific to JAK1 or specific to GAPDH as a standard for protein expression. **f,** Quantification of JAK1 expression from WB. All measurements were taken from distinct samples. A significant reduction of JAK1 expression, with a mean at 67% of specific decrease after transfection with siJAK1-AD in comparison with siCtrl-AD, was evaluated by paired Student's  $t$ -test ( $n = 3$ , \* $P \leq 0.05$ ) using Graph Pad Prism v. 8.4.2. **g, h,** AD-mediated siRNA delivery in rat primary microglia. The levels of mRNA (**g**) and protein (**h**) were analyzed 72 h post-transfection using qPCR and WB, respectively. Specific siRNA-AD complexes effectively silence the glioma-conditioned medium (GCM)-induced expression of the *id1* gene in primary rat microglia. Rat microglia were transfected with AD alone, complexes of AD with the control siRNA (siCtrl-AD) or complexes of AD with the *id1*-targeting siRNA (siID1-AD) and then stimulated with GCM. The two siRNAs at a work concentration of 12.5 nM were complexed with AD at N/P ratios of 10 and 12.5 nM, respectively. Gene expression is presented as fold change relative to the treatment with AD alone ( $n = 3$ , mean  $\pm$  SD). All measurements were taken from distinct samples. Statistically significant differences between cultures treated with siID1-AD and siCtrl-AD were evaluated by the paired Student's  $t$ -test using GraphPad Prism v. 6.04. \* $P < 0.05$ ; \*\* $P < 0.01$ . In WB evaluation, detection of GAPDH confirmed equal protein loading. hNK, human NK cell; MFI, mean fluorescence intensity; mNK, murine NK cell; siCtrl, siRNA control; siJAK1, siRNA targeting JAK1; siID1, siRNA targeting *id1*; siNKG2D, siRNA targeting NKG2D. **a, b,** adapted with permission from ref. <sup>17</sup>, Wiley. **c, d,** adapted with permission from ref. <sup>21</sup>, Springer Nature America, Inc. **g, h,** adapted with permission from ref. <sup>20</sup>, Nanomedicine (as agreed by Future Medicine Ltd).

AD, or the size and surface charge of the siRNA-AD complexes, affects the efficacy of siRNA delivery and gene expression interference in various types of immune cells. Furthermore, detailed biodistribution studies in ex vivo white blood cells (WBCs) or in vivo animal models may be necessary to establish how cells at the different anatomic sites of the body would be exposed to the siRNA-AD complexes. In addition, cell-specific targeting strategies can be developed for AD with the goal of targeting immune cell subsets for specific siRNA delivery<sup>19</sup>. We are actively working in this direction.

Materials

**Biological materials**

- **Blood !CAUTION** The research involves blood specimens from anonymous human subjects with no identifiers of age, race, ethnicity, or gender. Use of such specimens does not need to be approved nor does it need to undergo continuing review by the institutional review board (IRB) at the authors' institute (J.H.Z. and J.J.R., City of Hope, ref. no. 97071/075546). Human tissue was obtained and used in accordance with the Declaration of Helsinki, and the human subjects Ethical Committee of Sapienza University approved the selection process and technical procedures (ref. no. 3314/25.09.14; protocol no. 1186/14). For human samples, blood should be obtained according to a protocol approved by the relevant ethical committee and after obtaining written, informed consent from subjects. All blood samples should be treated as infectious materials.
- **Rats and mice !CAUTION** All experiments involving animals must be approved by your institutional animal care and use committee (IACUC) and performed in accordance with IACUC-approved protocols. All animal care and procedures were performed according to protocols reviewed and approved by the relevant IACUC. The experiments described in this work were approved by the Italian Ministry of Health (authorization no. 78/2017-PR) in accordance with the guidelines on the ethical use of animals from the European Community Council Directive of September 22, 2010 (2010/63/EU) and from the Italian D.Leg 26/2014. All possible efforts were made to minimize animal suffering and to reduce the number of animals used per condition by calculating the necessary sample size before performing the experiments.
- C57BL/6J mice (Charles River, cat. no. C57BL/6 JFEMELLES PF3, RRID: IMSR\_JAX:000664)
- HIV-1 isolate (HIV-1 IIIB and Bal; NIH AIDS Research and Reference Reagent Program, Division of AIDS, cat. nos. 398 (IIIB) and 510 (Bal), respectively) **!CAUTION** HIV-1 is a class 2/3 human pathogen and should be handled in a biosafety level (BSL)3-level facility.
- L929 cell line from mouse (ECACC, cat. no. 85011425) **!CAUTION** The cell lines used in your research should be regularly checked to ensure they are authentic and are not infected with mycoplasma. Our cell lines were checked regularly using a MycoAlert Mycoplasma Detection Kit (Lonza, cat. no. LT07-318) or a Universal Mycoplasma Detection Kit (ATCC, cat. no. 30-1012K). Cell lines that were contaminated with mycoplasma were discarded or treated with Plasmocin (Invivogen, cat. no. antmpt-1) or BM-Cyclin (Sigma, cat. no. 10799050001) **▲CRITICAL** L929 is a fibroblast cell line. These cells produce natural M-CSF (macrophage colony-stimulating factor), which is essential for the maturation of mouse bone marrow cells to macrophages. The use of L929-conditioned medium for mouse macrophage culture is well documented in the literature<sup>28</sup>.

**Reagents**

**General reagents !CAUTION** Because most of the chemicals and organic solvents used for dendrimer synthesis are potentially hazardous to human health, we recommend performing the click reaction and the amidation reaction, as well as the handling of organic solvents, inside an efficient chemical fume hood while wearing personal protective equipment (lab coat, gloves, and goggles) to prevent exposure.

- 1** and **2** should be synthesized according to the reported protocols<sup>16,17</sup>
- *N,N*-Dimethylformamide (DMF; Sigma-Aldrich, cat. no. 227056)
  - Dichloromethane (CH<sub>2</sub>Cl<sub>2</sub>; Sigma-Aldrich, cat. no. 32222-M)
  - Methanol (MeOH; Sigma-Aldrich, cat. no. 179337)
  - Triethylamine (TEA; Sigma-Aldrich, cat. no. 471283)
  - Copper(I) iodide (CuI; Sigma-Aldrich, cat. no. 215554)
  - 1,8-Diazabicyclo[5.4.0]undec-7-ene (DBU; Sigma-Aldrich, cat. no. 139009)
  - Sodium sulfate anhydrous (Na<sub>2</sub>SO<sub>4</sub>; Sigma-Aldrich, cat. no. 798592)
  - Magnesium sulfate monohydrate (MgSO<sub>4</sub> · H<sub>2</sub>O; Sigma-Aldrich, cat. no. 434183)
  - Ammonium chloride (NH<sub>4</sub>Cl; Sigma-Aldrich, cat. no. 213330)
  - Sodium bicarbonate (NaHCO<sub>3</sub>; Sigma-Aldrich, cat. no. S6014)
  - Sodium chloride (NaCl; Sigma-Aldrich, cat. no. S9888)
  - Silica gel for flash chromatography (Sigma-Aldrich, cat. no. 227196)
  - Ethylenediamine (EDA; Merck, cat. no. S7392647 745) **!CAUTION** To ensure the purity of the reagent, the EDA should be distilled before use<sup>29</sup>.
  - Chloroform-d (99.8 atom % D; Sigma-Aldrich, cat. no. 416754)
  - β-Glycerophosphate (Applichem, cat. no. A2253.0100)
  - Sodium orthovanadate (Sigma-Aldrich, cat. no. S6508)

**Table 2 | Custom siRNA sequences**

siRNA	Sense (5'-3')	Antisense (5'-3')
HIV-1 <i>tat/rev</i> site I 27 mer DsiRNA (viral RNA)	GCG GAG ACA GCG ACG AAG AGC UCA UCA	UGA UGA GCU CUU CGU CGC UGU CUC CGC dTdT
Human CD4 21-mer siRNA	GAU CAA GAG ACU CCU CAG U dGdA	ACU GAG GAG UCU CUU GAU C dTdG
Human CD4 27-mer DsiRNA	GAU CAA GAG ACU CCU CAG UGA GAA G	CUU CUC ACU GAG GAG UCU CUU GAU <b>CU</b> G-3' (2'-OMe modified U is bold)
Mouse <i>JAK1</i> 21-mer siRNA	GAA UAA AUG CAG UAU CUA AAU	<b>P</b> -UUA GAU ACU GCA UUU AUU CGG (a phosphate is added in 5' and is bold)

**Table 3 | Primers for qRT-PCR analysis**

Name	Sequence (5'-3')
HIV-1 <i>tat/rev</i> forward primer	GGC GTT ACT CGA CAG AGG AG
HIV-1 <i>tat/rev</i> reverse primer	TGC TTT GAT AGA GAA GCT TGA TG
Human CD4 forward primer	GCT GGA ATC CAA CAT CAA GG
Human CD4 reverse primer	CTT CTG AAA CCG GTG AGG AC
Human GAPDH forward primer	CAT TGA CCT CAA CTA CAT G
Human GAPDH reverse primer	TCT CCA TGG TGG TGA AGA C
Rat ID1 forward primer	AGTCTGAAGTCGCGACCGCC
Rat ID1 reverse primer	CTGGAACACATGCCGCTCGG
NKG2D forward primer	TACTGTGGCCCATGTCTTAA
NKG2D reverse primer	CTTTCAGAAGGCTGGCATT
18S RNA forward primer	CGGACATCTAAGGGCATCACA
18SRNA reverse primer	AACGAACGAGACTCTGGCATG

- Triton X-100 (Sigma-Aldrich, cat. no. T8787)
- Glycerol (Sigma-Aldrich, cat. no. G7757)
- Leupeptin hydrochloride (Sigma-Aldrich, cat. no. L9783)
- Aprotinin (Sigma-Aldrich, cat. no. A1153)
- Benzamidine hydrochloride (Sigma-Aldrich, cat. no. B6506)
- Dithiothreitol (DTT; Thermo Fisher Scientific, cat. no. R0861)
- Bromophenol Blue sodium salt (Sigma-Aldrich, cat. no. B5525)
- Tween 20 (Sigma-Aldrich, cat. no. P7949)
- Argon (Linde, Argon 5.0 Instrument)
- Liquid nitrogen (Linde)
- Sodium acetate (anhydrous; Sigma-Aldrich, cat. no. S2889)
- Glacial acetic acid (Sigma-Aldrich, cat. no. 1.00066)
- EDTA (0.5 M, pH 8; Thermo Fisher Scientific, cat. no. AM9260G)

#### Cell culture and biological reagents

- Universal negative siRNA controls (Integrated DNA Technologies, cat. nos. 51-01-14-03 (negative control DsiRNA) and 51-01-19-08 (scrambled negative control DsiRNA)) **▲ CRITICAL** It is critical to have an appropriate negative control against which one can compare experimental results in gene silencing and functional studies using siRNA or DsiRNA duplexes. A scrambled siRNA does not target any part of the human, mouse, or rat transcriptomes.
- Custom-made siRNAs (Integrated DNA Technologies, Table 2) **▲ CRITICAL** It is critical to select an optimal siRNA sequence for effective gene silencing. According to our previous experience, we designed one 21-mer siRNA and one 27-mer DsiRNA per target sequence with appropriate 3'-overhangs and chemical modifications.
- Rat ID1 siRNA (ON-TARGETplus SMART pool; Dharmacon, cat. no: L-080165-02-0005)
- Custom primers for qRT-PCR analysis (Integrated DNA Technologies or Genescript; Table 3)



- Negative-control siRNA that does not target any human, mouse, or rat gene products (ON-TARGETplus non-targeting pool; Dharmacon, cat. no: D-001810-10-05)
- Negative-control siRNA (AllStars; Qiagen, cat. no. 1027281)
- Milli-Q ultrapure water (Millipore)
- Opti-MEM medium (Gibco, cat. no 31985-047)
- Dulbecco's PBS without calcium and magnesium (DPBS<sup>-</sup>; Corning, cat. no. 21-031-cv)
- Phosphate-buffered saline (PBS; Thermo Fisher Scientific, cat. no 20012-027)
- Dulbecco's PBS with calcium and magnesium (DPBS<sup>+</sup>; Thermo Fisher Scientific, cat. no.14040091)
- Ficoll (Sigma-Aldrich (Milan, Italy)
- Trypsin inhibitor (Sigma-Aldrich, cat. no. T6522)
- DNase (Sigma-Aldrich, cat. no. DN25)
- RPMI 1640 (Corning, cat. no. 15-040-cv)
- RPMI 1640 with GlutaMAX (Gibco, cat. No 61870036)
- Skim milk powder (non-fat) (Merck, cat. no. 70166)
- DMEM with GlutaMAX, high glucose (Thermo Fisher Scientific, cat. no 31966-021, 61965026)
- MEM non-essential amino acids solution (100×; Thermo Fisher Scientific, cat. no.11140050)
- Sodium pyruvate (100 mM; Thermo Fisher Scientific, cat. no. 11360070)
- 2-Mercaptoethanol (50 mM; Thermo Fisher Scientific, cat. no. 31350010)
- HEPES (1 M; Thermo Fisher Scientific, cat. no. 11360070)
- Fetal bovine serum (FBS; Gibco, cat. nos. 10082-147 and 10270-106) **▲ CRITICAL** Because the specific FBS plays an important role in the differentiation and growth of a particular cell type, it is essential to consider a specific FBS for a particular primary cell culture.
- L-Glutamine (200 mM, 100×; Irvine Scientific, cat. no. 9317-100 mL)
- Penicillin–streptomycin (10,000 units of penicillin per mL; 10,000 µg of streptomycin per mL; Gibco, cat. no. 15140-122-100 mL)
- Phytohemagglutinin-L (PHA; Roche, cat. no. 11 249 738 001)
- Recombinant interleukin-2 (IL-2, Teceleukin; Hoffmann–La Roche, cat. no. Ro 23-6019)
- Trypan blue stain (0.4% (wt/vol); Invitrogen, cat. no. T10282)
- **! CAUTION** RoboSep Buffer is a potential irritant to the eyes, respiratory system, and skin. Wear suitable protective clothing, glasses, and gloves.
- TRIzol (Thermo Fisher Scientific, cat. no. 15596026) **! CAUTION** TRIzol is harmful upon inhalation or contact with skin and is toxic if swallowed. It is an irritant to the eyes. There is evidence of a carcinogenic effect. Wear suitable protective clothing, glasses, and gloves and use in a fume hood. This material and its container must be disposed of as hazardous waste.
- Chloroform/isopropanol 24:1 solution (Sigma, cat. no. C0549) **! CAUTION** Chloroform/isopropanol 24:1 solution is harmful upon inhalation or contact with skin and is toxic if swallowed. It is an irritant to the eyes. There is evidence of a carcinogenic effect. Work under a fume hood and wear suitable protective clothing, glasses, and gloves. This material and its container must be disposed of as hazardous waste.
- Glycogen (Roche, cat. no. 10 901 393 001)
- RNA isolation Kit (RNeasy Mini Kit; Qiagen, cat. no. 74104)
- QuantiNova Reverse Transcription kit (Qiagen, cat. no. 205411) or SuperScript III Reverse Transcriptase (Thermo Fisher Scientific, cat. no 18080-044) and a set of dNTPs (Promega, cat. no U1330)
- SsoAdvanced Universal SYBR Green Supermix (Bio-Rad, cat. no. 172-5271) or Fast SYBR Green Master Mix (Applied Biosystems, cat. no 4385612)
- Pacific Blue–conjugated CD4 antibody (clone RPA-T4) (BD Biosciences, cat. no. 558116; RRID: [AB\\_397037](#))
- ID1 antibody (clone B-8) (Santa Cruz Biotechnology, cat. no. sc-133104; RRID: [AB\\_2122863](#))
- GAPDH antibody (Millipore, cat. no. MAB374; RRID: [AB\\_2107445](#))
- Anti-mouse IgG (H+L) antibody peroxidase-conjugated, made in horse (Vector Laboratories, cat. no. PI-2000; RRID: [AB\\_2336177](#))
- JAK1 rabbit mAb antibody (Cell Signaling Technology, cat. no 3332; RRID: [AB\\_2128499](#))
- Arginase-1 rabbit mAb antibody (Cell Signaling Technology, cat. no. 93668S; RRID: [AB\\_2800207](#))
- α/β-Tubulin antibody (Cell Signaling Technology, cat. no. 2148S; RRID: [AB\\_2288042](#))
- NKG2D antibody (eBioscience, cat. no. PE 12-5882-82; RRID: [AB\\_465996](#))
- Fixation/Permeabilization Solution Kit (BD Biosciences, cat. no. 554714) **! CAUTION** There is limited evidence of a carcinogenic effect. The solution may cause sensitization if it comes into contact with the skin. Work under a fume hood and wear suitable protective clothing and gloves.

- Alliance HIV-1 p24 Antigen ELISA Kit (PerkinElmer, cat. No. NEK050A001KT)
- Recombinant interleukin-15 (IL-15; eBioscience)
- BCA Protein Assay Kit (Thermo Scientific Scientific, cat. no. 23225)
- **! CAUTION** The gel is harmful upon inhalation, swallowing, or contact with eyes or skin. It contains material that may cause damage to the kidneys, nervous system, liver, upper respiratory tract, and skin.
- Tris (BioShop, cat. no. TRS001)
- Glycine (BioShop, cat. no. GLN001)
- Bovine serum albumin (BSA; Sigma-Aldrich, cat. No. 9048-46-8)
- Sodium dodecyl sulfate (SDS; Sigma-Aldrich, cat. no. L3771) **! CAUTION** SDS is harmful if inhaled and may cause damage to the upper respiratory tract.
- SDS-PAGE precast gel (4–15%; Bio-Rad, cat. no. 64280120)
- Pre-stained protein markers for SDS-PAGE electrophoresis (Thermo Fisher Scientific)
- SuperSignal West Pico Chemiluminescent Substrate (Thermo Fisher Scientific) or similar reagent containing (horseradish peroxidase) HRP substrate for chemiluminescent protein detection in WB analysis
- SuperSignal West Femto Maximum Sensitivity Substrate (Thermo Fisher Scientific, cat no. 34095)
- RIPA Buffer (Sigma, cat. no. R0278)
- NuPAGE Sample Reducing Agent (10×; Thermo Fisher Scientific, cat. no. NP0004)
- NuPAGE LDS Sample Buffer (4×; Thermo Fisher Scientific, cat. no. NP0007)
- cOmplete, Mini Protease Inhibitor Cocktail (Roche, cat. no. 04693124001)
- Accutase (Biowest, cat. no. L0950)
- Sodium acetate (anhydrous) (Sigma-Aldrich, cat. no. S2889)
- Glacial acetic acid (Sigma-Aldrich, cat. no. 1.00066)
- EDTA (0.5 M, pH 8) (Thermo Fisher Scientific, cat. no. AM9260G)

### Equipment

- Round-bottom flasks (250, 100, 50, and 25 mL; Synthware)
- Dialysis tubing, benzoylated (MWCO: 2000; Sigma-Aldrich, cat. no. D7884-10FT)
- Dialysis tubing closures (Sigma-Aldrich, cat. no. Z371068)
- Non-woven compresses (Nessicare, cat. no. CNST-300D)
- Nitrocellulose membrane (Hybond ECL; Amersham)
- Rotary evaporator (Heidolph)
- Water bath
- Oil bath
- Magnetic stirrer (IKA)
- Stainless-steel needle (0.80 × 120 mm; Sterican, cat. no. 466 5643)
- Silica gel plates for thin-layer chromatography (TLC; Merck, cat. no. 1.0554.0001)
- NMR spectrometer (JEOL, model no. 400M or Bruker, model no. 500M)
- NMR tube (5 mm; Wilmad)
- MS-ESI instrument (Waters)
- FTIR spectrometer (Bruker)
- BSL3 laboratory **! CAUTION** HIV-1 is a class 3 human pathogen, and all the HIV-1-related procedures (HIV-1 infection, cell transfection, and isolation of samples) should be carried out in a BSL3 level facility.
- EasySep Magnet (StemCell Technologies, cat. no. 18000)
- Flash chromatography column
- Countess II FL Automated Cell Counter (Invitrogen, cat. no. AMQAF1000)
- Nucleocounter (ChemoMetec, cat. no. NC-100)
- Cell culture flasks with vent cap (25 and 75 cm<sup>2</sup>)
- Falcon (not TC-treated) bacteriological Petri dish (100 × 15 mm; Corning, cat. no. 351029)
- Centrifuge tubes (15 and 50 mL)
- Screw-cap microtubes (1.5 and 2 mL)
- Safe-Lock microcentrifuge tubes (1.7 mL; Eppendorf)
- Falcon polystyrene round-bottom tubes (14 mL)
- Round-bottom cytometer tubes (5 mL)
- Flat-bottom tissue culture plates (6, 24, 12, 48, and 96 wells)

- Round-bottom tissue culture test plates (96 wells; Corning, cat. no. CLS3367)
- Sterile disposable pipettes (5, 10, and 25 mL)
- Disposable glass Pasteur pipettes
- Nuclease-free tips (0.5–10, 2–20, 20–200, 100–1,000  $\mu$ L)
- Pipettes (0.5–10, 2–20, 20–200, 100–1,000  $\mu$ L)
- Multichannel pipette (50–200, 100–1,000  $\mu$ L)
- Benchtop centrifuge with sealed buckets and plate carriers (Eppendorf, model no. 5810R, 5424, or 5425)
- Mini vortex (Thermolyne, maxi Mix plus) or similar
- Microbiological safety cabinet
- Plate shaker
- CO<sub>2</sub> cell culture incubator (Thermo Fisher Scientific)
- Hemocytometer (Thermo Fisher Scientific, cat. no. 0267110)
- NanoDrop microvolume spectrophotometer (Thermo Fisher Scientific, model no. 2000)
- Optical microscope (Nikon Eclipse, model no. TE2000-S)
- Confocal microscope (Zeiss, model no. LSM880)
- ELISA microplate reader (with kinetic reading capabilities) (BioTek, model no. Cytation 5 Cell Imaging Multi-Mode Reader, or Molecular Devices, model no. SpectraMax iD5) or similar
- Multicolor flow cytometer (BD Biosciences, LSRFortessa model)
- Real-time PCR instrument (Bio-Rad, model no. CFX96 Touch Real-Time PCR Detection System)
- Thermocycler (Mastercycler gradient; Eppendorf)
- MACS separators for magnetic cell isolation (Miltenyi Biotec)
- Large (LS) columns for magnetic cell isolation (Miltenyi Biotec)
- Protein electrophoresis and wet electroblotting system (Bio-Rad, Mini Trans-Blot Electrophoretic Transfer Cell) with power supply
- X-ray film processor (Fuji, model no. FPM 800A) or chemiluminescence detection system (Bio-Rad, ChemiDoc model)
- Parafilm
- Separating funnel
- Fritted filter funnel
- Dialysis tube
- Lyophilizer
- Plastic foam (Dominique Dutscher, cat. no. 040666)
- Aluminum foil (Sodipro, cat. no. 60110)
- Duran bottle (100 ml)
- 0.20- $\mu$ m filter

### Reagent setup

#### siRNAs

Resuspend siRNAs (double-stranded RNA duplexes) in sterile, double-distilled, nuclease-free water as a 500  $\mu$ M stock solution. Before transfection, dilute siRNA stock solution with 1 $\times$  DPBS solution to 10  $\mu$ M for the transfection assay. siRNA stocks can be stored in aliquots at  $-20$  °C for up to 4 weeks or at  $-80$  °C for up to 6 months. **!CAUTION** Because freeze–thaw cycles can degrade RNA, store the RNA solution in 40- $\mu$ L aliquots.

#### Labeling buffer

Supplement 1 $\times$  DPBS with 1.0% (vol/vol) FBS. This buffer can be stored at 4 °C for up to 2 months.

#### IL-2 medium

Supplement RPMI 1640 culture medium with 100  $\mu$ L/mL IL-2. This medium can be stored at 4 °C for up to 2 weeks.

#### BMDM cell culture basic medium

Supplement high-glucose DMEM containing GlutaMAX with penicillin–streptomycin (100 units per mL penicillin; 100  $\mu$ g per mL streptomycin), 1.0% (vol/vol) non-essential amino acids solution, 1.0 mM sodium pyruvate, 1.0 % (vol/vol) HEPES, 0.25 mM 2-mercaptoethanol, and 10% (vol/vol) heat inactivated FBS. This medium can be stored at 4 °C for up to 4 weeks. Supplement BMDM

(bone-marrow-derived primary macrophage) cell culture medium with 20% (vol/vol) L929-conditioned medium just before adding to cell culture and use immediately. **!CAUTION** PMSF is unstable in aqueous solutions.

#### Sample loading buffer (1×)

The final composition of this buffer is 60 mM Tris-HCl, pH 6.8, 2.0% (wt/vol) SDS, 10% (vol/vol) glycerol, 0.5 mM DTT, 0.01% (wt/vol) bromophenol blue. Prepare as 4× concentrate without DTT and store at room temperature for up to several months. Before use, add 4× concentrated DTT (i.e., 2 mM) to 4× concentrate stock to get 4× sample loading buffer with DTT. **!CAUTION** DTT and SDS powder are hazardous. Prepare solution in a ventilated fume hood. SDS can precipitate from the solution over time. Warm the buffer for 3–5 min to at least 55 °C to dissolve the SDS.

#### Running buffer for SDS-PAGE (1×)

This buffer is 25 mM Tris, 192 mM glycine, and 0.1% (wt/vol) SDS, pH ~8.6. **!CAUTION** SDS powder is hazardous. Prepare solution in a ventilated fume hood. This buffer can be stored at 4 °C for up to 8 weeks.

#### Electrophoretic transfer buffer (1×)

This buffer is 25 mM Tris, 192 mM glycine, 0.05% (wt/vol) SDS, and 20% (vol/vol) methanol. **!CAUTION** SDS powder is hazardous. Prepare solution in a ventilated fume hood. Methanol is a hazardous chemical that is highly flammable and toxic. It must be used by people that have been properly trained in its handling in a ventilated fume hood.

#### Tris-buffered saline (1×)

Tris-buffered saline (TBS) is 25 mM Tris, 130 mM NaCl, pH 7.6. TBS can be stored at room temperature for several months.

#### Membrane wash buffer (TBS-T)

Combine 1× TBS with 0.1% (vol/vol) Tween 20. This buffer can be stored at 4 °C for up to 8 weeks.

#### Blocking buffer

Dissolve 5.0 g skim milk powder (non-fat) in 100 mL TBS-T. Prepare freshly before use. Alternatively, blocking buffer can be prepared with 5.0 g of BSA in 100 mL of TBS-T.

#### Equipment setup

##### qRT-PCR system

Configure as follows: 10 min setup time per plate per parameter; 1.5- to 2-h run time.

##### Flow cytometry

Configure as follows: 30-min pre-clean time; 15 min per parameter setup time; 30–60 min run time (will vary according to the number of samples); 30-min cleaning time.

##### ELISA microplate reader

Configure as follows: 15-min run time; 30-s time interval to read at 490-nm wavelength.

##### Chemiluminescence detection instrument (X-ray film processor or chemiluminescence detection system)

Configure as follows: 10-min pre-warming time; 5- to 30-min signal acquisition time.

## Procedure

### Synthesis of **3** ● **Timing 5 h**

- 1 Weigh 95 mg (0.102 mmol) of **1** in a 25-mL round-bottom flask.
- 2 Weigh and add 5.7 mg (0.030 mmol) CuI to the round-bottom flask.  
**!CAUTION** The CuI is easily oxidized; weigh it quickly.
- 3 Add a magnetic stir bar, cap the flask with a rubber septum and wrap it with Parafilm.
- 4 Create a vacuum inside the round-bottom flask and flush with argon from a balloon.  
**▲ CRITICAL STEP** Because the Cu<sup>+</sup> is easily oxidized, the argon protection is mandatory.

- 5 Inject a solution of 143 mg (0.10 mmol) **2** in 5.0 mL of DMF into the round-bottom flask through a stainless-steel needle.
- 6 Inject 70  $\mu$ L DBU through a stainless-steel needle into the round-bottom flask while stirring.
- 7 Place the flask in a preheated oil bath (60 °C) on a hot-plate magnetic stirrer and stir the reaction solution for 90 min under argon atmosphere.
- 8 Monitor the progress of the reaction by taking a 0.05-mL aliquot via a stainless-steel needle and running TLC using silica-gel-coated plates and MeOH/CH<sub>2</sub>Cl<sub>2</sub> 1:9 (vol/vol). (*R<sub>f</sub>* is 0.6 for **1** (starting material). Detect the eluted product and the starting material by I<sub>2</sub> (ref. <sup>30</sup>). *R<sub>f</sub>*, the retention factor in chromatography, is defined as the distance traveled by the compound divided by the distance traveled by the solvent.
- 9 After completion of the reaction, which generally takes 90 min, remove the stopper and the magnetic stir bar.

**? TROUBLESHOOTING**

- 10 Remove the DMF with a rotary evaporator at ~30 °C in a water bath.
- 11 Pour 15 mL CH<sub>2</sub>Cl<sub>2</sub> into the round-bottom flask.
- 12 Transfer the mixed solution to a 125-mL separating funnel and subsequently add 15 mL saturated NH<sub>4</sub>Cl solution.
- 13 Gently shake the mixed solution and let it sit for 5 min until a clear layer appears.
- 14 Open the valve of the separating funnel and collect the lower organic phase (CH<sub>2</sub>Cl<sub>2</sub> layer) into a 250-mL conical flask.
- 15 Extract the aqueous phase three times with 15 mL CH<sub>2</sub>Cl<sub>2</sub> each time and combine the organic phases.
- 16 Transfer the CH<sub>2</sub>Cl<sub>2</sub> layer to a 125-mL separating funnel and then wash the organic phase twice with 15 mL saturated NH<sub>4</sub>Cl solution, twice with 15 mL saturated NaHCO<sub>3</sub> solution, and once with 20 mL of saturated sodium chloride solution.
- 17 Collect the CH<sub>2</sub>Cl<sub>2</sub> layer into a 250-mL conical flask and dry the layer by adding anhydrous Na<sub>2</sub>SO<sub>4</sub> until the powder stops aggregating.
- 18 Gently shake the solution by hand and filter it using a fritted filter funnel under vacuum into a 250-mL round-bottom flask.
- 19 Remove the solvent with a rotary evaporator at ~30 °C in a water bath.
- 20 Dissolve the residue in 1.0 mL of MeOH/CH<sub>2</sub>Cl<sub>2</sub> 1:9 (vol/vol).
- 21 Purify the compound by flash column chromatography (diameter of the column is 2.4 cm, and height of the silica gel in the column is 20 cm), using MeOH/CH<sub>2</sub>Cl<sub>2</sub> 1:9 (vol/vol) to remove the impurities and unreacted starting materials, and then MeOH/CH<sub>2</sub>Cl<sub>2</sub> 1:9 (vol/vol) with 1% (vol/vol) TEA to elute the product.
- 22 Collect eluents in 15-mL fractions using 20-mL test tubes. Analyze the collected fractions by TLC using MeOH/CH<sub>2</sub>Cl<sub>2</sub> 1:9 (vol/vol) as the eluent.
- 23 Pool the pure fractions into a new 100-mL round-bottom flask. Evaporate the solvents with a rotary evaporator at ~30 °C in a water bath.
- 24 Remove the residual solvent under high vacuum overnight. Weigh the pure **3** and calculate its yield.

■ **PAUSE POINT** Compound **3** can be stored at –20 °C for a week.

**? TROUBLESHOOTING**

**Synthesis of AD ● Timing 10 d**

- 25 Weigh 110 mg (0.046 mmol) of **3** in a 25-mL round-bottom flask.
- 26 Add a magnetic stir bar, cap with a rubber septum, and wrap the flask with Parafilm.
- 27 Create a vacuum inside the round-bottom flask and flush with argon from a balloon.  
▲ **CRITICAL STEP** Because there are amine functionalities in the reaction, the argon protection is mandatory.
- 28 Inject 4.0 mL of MeOH into the round-bottom flask through a stainless-steel needle.  
**? TROUBLESHOOTING**
- 29 Wrap the round-bottom flask in black paper to protect the reaction from light.  
▲ **CRITICAL STEP** Because there are amine functionalities in the reaction, we advise protecting the reaction from light to avoid unnecessary by-products.
- 30 Inject 4.0 mL (60 mmol) of EDA drop by drop while stirring.
- 31 Place the flask in a preheated oil bath (30 °C) on a hot-plate magnetic stirrer and stir the reaction solution for 72 h under argon atmosphere.

- 32 Monitor the progress of the reaction by taking a 0.05-mL aliquot of via a stainless-steel needle and running infrared spectroscopy (IR) (look for disappearance of the peak at  $1,750\text{ cm}^{-1}$ , which corresponds to the carbonyl function in the ester group).
- 33 After completion of the reaction, which generally takes 72 h, remove the stopper and the magnetic stir bar. Evaporate the MeOH and excess EDA with a rotary evaporator at  $\sim 30\text{ }^{\circ}\text{C}$  in a water bath.
- 34 Dissolve the residue in 3.0 mL ultrapure water.
- 35 Transfer the solution to a dialysis tube (MW = 2,000). Before transferring the liquid, clamp one side of the tubing with a dialysis tubing closure. After filling the tubing, close it with a dialysis tubing closure that has a piece of plastic foam tied to it. Suspend the tube in a separate 2-liter glass beaker filled with ultrapure water and containing a magnetic stirrer.
- ▲ CRITICAL STEP** The pore size of the dialysis tubing must be selected according to the molecular weight of the product. Typically, the product is subjected to three rounds of dialysis and lyophilization to ensure its purity. The NMR spectrum is used to monitor the purity. The volume of product solution may increase to at most 2 times during the dialysis. We advise using a larger than needed amount of dialysis tube.
- 36 Dialyze the contents for 8 h at room temperature with stirring. Replace the ultrapure water every hour to remove the EDA.
- 37 Transfer the contents of the dialysis tube to new 15-mL Falcon tubes ( $\sim 5\text{ mL}$  per tube). Wrap the tubes with aluminum foil to protect the sample from light exposure and fasten with a rubber band.
- 38 Freeze the samples by keeping them immersed for 5 min in a tank of liquid nitrogen fitted with a tube rack. Transfer the frozen samples to a lyophilizer and dry them for 1 d.
- 39 Dissolve the lyophilisates in 3.0 mL ultrapure water and repeat Steps 35–38 twice to obtain pure AD, which appears as a white to a faint-colored foam-like solid after lyophilization.
- ! CAUTION** Because freezing and thawing repeatedly (freeze–thaw cycles) can degrade AD, store the AD solution in 40- $\mu\text{L}$  aliquots.
- ▲ CRITICAL STEP** To remove water completely, a lyophilization procedure is required. If there is still water/ice in the product after lyophilization, dissolve the product in ultrapure water again and repeat Step 38.
- PAUSE POINT** Dried AD can be stored at  $-20\text{ }^{\circ}\text{C}$  for months. Alternatively resuspend the AD in sterile, double-distilled, nuclease-free water as a 2.0 mM stock solution, which can be stored in aliquots at  $-80\text{ }^{\circ}\text{C}$  for up to 12 months. Before using in transfection, dilute with  $1\times$  DPBS to 240  $\mu\text{M}$ . Diluted AD can be stored in aliquots at  $-20\text{ }^{\circ}\text{C}$  for up to 4 weeks.

#### AD-mediated siRNA transfection into HIV-1-infected $\text{CD4}^+$ T cells ● Timing ~3 d

- 40 *Counting the HIV-1-infected  $\text{CD4}^+$  T cells.* A schematic of the dendrimer-mediated siRNA delivery to HIV-1-infected primary human  $\text{CD4}^+$  T cells is shown in Fig. 5. Grow  $\text{CD4}^+$  T cells and challenge with HIV-1 as outlined in the Supplementary Methods. Wash off the free virus, and after the last wash, pipette off the supernatant, loosen the cell pellet by adding 1.0 mL DPBS, and gently resuspend the cells with the 1.0-mL pipette. Mix 10  $\mu\text{L}$  cells with 10  $\mu\text{L}$  of 0.4% (wt/vol) trypan blue stain and count the cells (e.g., in a hemocytometer). Count unstained cells as live cells and determine the cell density. Take the desired amount of cells and add IL-2 medium to adjust the density as desired.
- ▲ CRITICAL STEP** Cell viability is calculated as the number of viable cells divided by the total number of cells within the grids on the hemocytometer. If cells take up trypan blue (turn blue), they are considered non-viable. Long processing time and poor technique may adversely affect cell viability.
- 41 *Seeding the HIV-1-infected  $\text{CD4}^+$  T cells.* Using a 24-well plate format as an example, seed 400  $\mu\text{L}$  of cells at  $5\times 10^5$  cells per mL into each well ( $2\times 10^5$  cells per well). Incubate the cells at  $37\text{ }^{\circ}\text{C}$  in a humidified incubator under 5%  $\text{CO}_2$ .
- 42 *Formation of the siRNA–AD complex.* As shown in Table 1, calculate the total amounts of AD and HIV-1 *tat/rev* siRNA using the formula provided in the ‘Experimental design’ section and taking into account the number of samples to be transfected. Dilute the AD stock solution (240  $\mu\text{M}$  in DPBS buffer from Step 39) with Opti-MEM medium and mix well by pipetting up and down for 15 s (Fig. 3, ii). Dilute the siRNA solution (10  $\mu\text{M}$  stock solution in DPBS) with Opti-MEM medium and mix well by pipetting up and down for 15 s (Fig. 3, iii). Add the diluted siRNA solution to the diluted AD solution and mix well by pipetting up and down for 20 s (Fig. 3, iv). Incubate the mixture for 25 min at room temperature to allow the nanoparticles to form (Fig. 3, v). For a 24-well-plate format, mix 50  $\mu\text{L}$  of AD (from ii) and 50  $\mu\text{L}$  of diluted siRNA (from iii) to get a 100- $\mu\text{L}$  total volume of complexes.

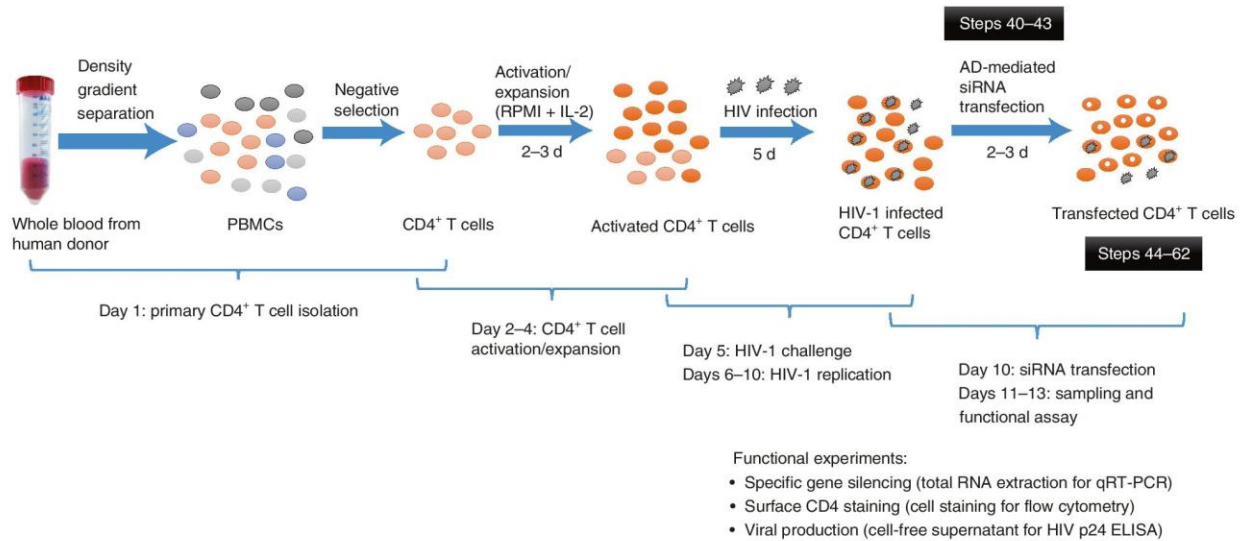


**Fig. 5 | Experimental outline.** A schematic illustrating dendrimer-mediated siRNA delivery to HIV-1-infected primary human CD4<sup>+</sup> T cells.

- 43 *AD-mediated siRNA transfection* Gently mix the complexes by pipetting up and down. Carefully distribute the solution containing the siRNA-AD complexes drop by drop into each well and mix by gently rocking the plate back and forth (step vi in Fig. 3). Incubate the cells at 37 °C in a humidified incubator under 5% CO<sub>2</sub> for 24–72 h (step vii in Fig. 3) before further functional assays.  
**▲ CRITICAL STEP** Proceed to complex addition immediately, once the complex is formed. Evenly distribute the complex onto the cells and do not vigorously mix the complex with the cells.

**Functional evaluation of the gene silencing and anti-HIV activity ● Timing -3 d**

- 44 Using a 1-mL pipette, carefully transfer the HIV-1-infected CD4<sup>+</sup> T cells from the wells of the 24-well plate to 1.7-mL Eppendorf Safe-Lock microcentrifuge tubes. Centrifuge at 400g for 5 min at room temperature and gently transfer the cell-free supernatant to a new 1.7-mL tube. Store the supernatant at -80 °C until the p24 ELISA test (Steps 54–62). Cells can be used for either total RNA extraction (Steps 45–47) or antibody staining (Steps 51–53) as described below.  
**▲ CRITICAL STEP** After centrifugation, the HIV-1-infected cells are concentrated at the bottom of the tube. For aspiration, tilt the tube and place the tip of the aspirator on the wall of the tube, well above the cell pellet, to avoid loss of cells.
- 45 *Determination of siRNA-mediated silencing of target genes by qRT-PCR assay (Steps 45–50).* Total RNA extraction by TRIzol reagent: Add an appropriate amount of TRIzol reagent and lyse the cells by gently pipetting up and down for 15 s. Incubate the homogenized samples for 5 min at room temperature to permit the complete dissociation of nucleoprotein complexes. Add 0.2 mL of chloroform/isopropanol 24:1 solution per 1 mL of TRIzol reagent. Vortex the tubes vigorously for 15 s and incubate them for 3 min at room temperature. Centrifuge the samples at >12,000g for 15 min at 2–8 °C. Carefully transfer the clear upper aqueous phase to a new 1.7-mL tube. The volume of this phase is ~60% of the volume of TRIzol reagent used for homogenization.  
**▲ CRITICAL STEP** One milliliter of TRIzol reagent is enough for up to 10<sup>7</sup> cells. To limit biohazard use and improve total RNA extraction, 0.5 mL of TRIzol reagent is used for 1 well of a 24-well plate.
- 46 Precipitate the RNA by mixing with 0.5 mL of isopropanol per 1.0 mL of TRIzol reagent used for the initial homogenization. Incubate the samples at room temperature for 10 min and centrifuge at no more than 12,000g for 20 min at 2–8 °C.  
**▲ CRITICAL STEP** Before precipitating the RNA with isopropanol, add 5–10 µg RNase-free glycogen as carrier to the aqueous phase to improve RNA recovery.
- 47 Wash the RNA pellet once with at least 1.0 mL of 75% (vol/vol) ethanol per 1.0 mL of TRIzol reagent used for the initial homogenization. Centrifuge at no more than 7,500g for 5 min at 2–8 °C. Remove and discard the ethanol and dry the pellet for 5 min.

- 48 Dissolve the RNA in 20  $\mu\text{L}$  of RNase-free water and quantify the RNA concentration using a NanoDrop microvolume spectrophotometer.
- 49 *cDNA synthesis*. Equilibrate the QuantiNova Reverse Transcription Kit reagents to room temperature before use. As recommended by the manufacturer, combine 0.5–1.0  $\mu\text{g}$  of total RNA with the other reaction components in a 20- $\mu\text{L}$  reaction on ice. Mix thoroughly by pipetting up and down several times. Incubate the complete reaction mix in a thermal cycler, following the manufacturer's protocol.
- 50 *Real-time qPCR*. Thaw SsoAdvanced Universal SYBR Green Supermix (2 $\times$ ) (or Fast SYBR Green Master Mix) and gene-specific primers to room temperature. Determine the number of PCR reactions to use based on the total number of samples plus standards and controls. For a 20- $\mu\text{L}$  PCR reaction, combine 10  $\mu\text{L}$  of SYBR Green Supermix (2 $\times$ ), 2.0  $\mu\text{L}$  of cDNA, gene-specific forward and reverse primers (400  $\mu\text{M}$  working concentration; Table 3; HIV-1 *tat/rev* primer set for target gene; GAPDH primer set for housekeeping gene), and nuclease-free water on the ice. Mix thoroughly to ensure homogeneity and dispense into the wells of a PCR plate. Program the thermal cycling protocol into the real-time PCR instrument according to the manufacturer's instructions (see 'Equipment setup' section).
- ▲ CRITICAL STEP** Set up a no-RT control with the same amount of total RNA but no reverse transcriptase and a no-template control (use the same volume of water) for accurate detection of genomic DNA amplicons. The volume of cDNA synthesis reaction used must not exceed 10% of the qPCR volume. For optimal results, assemble the reaction components on ice.
- ? TROUBLESHOOTING**
- 51 *Determination of anti-HIV-1 (CD4 or HIV-1 *tat/rev*) siRNA-mediated knockdown of target protein by flow cytometry (Steps 51–54)*. Cell-surface staining with anti-CD4 antibody: In the case when CD4 siRNA is used for the transfection experiment, the surface CD4 receptor can be assayed by flow cytometry. After 2–3 d of transfection, wash the pelleted cells from Step 44 twice with 500  $\mu\text{L}$  of DPBS buffer as described in Step 40. Resuspend the cell pellet with 50  $\mu\text{L}$  of labeling buffer for each tube. Add the Pacific Blue-conjugated anti-CD4 antibody (5  $\mu\text{L}$  per 1 million cells) and gently mix by pipetting up and down for 15 s. Wrap the tubes in aluminum foil and incubate at room temperature for 30 min. Add 1.0 mL of labeling buffer to each tube and centrifuge the tubes at 400g for 5 min at room temperature. Discard the supernatants.
- 52 *Fixation of HIV-1-infected CD4<sup>+</sup> T cells*: Loosen the cell pellets and add 250  $\mu\text{L}$  of BD Cytotfix/Cytoperm solution (from the Fixation/Permeabilization Solution Kit). Incubate in the dark at 4  $^{\circ}\text{C}$  for 20 min. Add 1.0 mL of BD Perm/Wash buffer to the tube and centrifuge the tubes at 400g for 5 min at room temperature. Discard the supernatants and resuspend cell pellets in 350  $\mu\text{L}$  of labeling buffer. Store the samples at 4  $^{\circ}\text{C}$  in the dark while setting up the flow cytometry with non-stained control (cells alone without anti-CD4 antibody). Proper fluorescence compensation controls will be used to correct for possible emission spectra overlap if applied.
- 53 *Flow cytometry analysis*: Proceed to acquisition of experimental data (surface CD4 expression level) by flow cytometry (see 'Equipment setup' section for flow cytometer settings).
- 54 *Determination of siRNA-mediated HIV-1 suppression by HIV-1 p24 ELISA (Steps 54–62)*. Equilibrate kit reagents (HIV-1 p24 antibody-coated microplate, 5% Triton X-100, Detector antibody, Streptavidin-HRP diluent, Streptavidin-HRP concentrate, substrate diluent, OPD tablets) to room temperature before use. Dilute 20 $\times$  plate wash concentrate to 1 $\times$  with distilled, deionized water and determine the number of antibody-coated strips to use based on the total number of samples plus standards.
- 55 Prepare p24 standards using the positive control provided by the kit as a virology quality assurance, which covers six concentrations from 4,000 pg/mL to 12.5 pg/mL.
- 56 Prepare the samples by diluting the cell-free supernatant from Step 44 with RPMI 1640 medium to the appropriate concentration.
- ▲ CRITICAL STEP** We recommend setting up a pre-test with non-transfected samples. This will help to determine the dilution ratio of the supernatant. If the supernatant is too diluted, the readout will be negative; if the supernatant is too concentrated, the readout will be saturated.
- 57 Label the ELISA plate and add 20  $\mu\text{L}$  of Triton X-100 to all wells except the substrate blank, to which no substrate is added.
- 58 Add 200  $\mu\text{L}$  of standards, negative control (RPMI 1640 medium), or diluted samples to the appropriate wells. Seal the plate and incubate for 2 h at 37  $^{\circ}\text{C}$ .
- 59 Wash the plate in a cell washer. Add 100  $\mu\text{L}$  of detector antibody to all wells except the blank. Seal the plate and incubate for 1 h at 37  $^{\circ}\text{C}$ .



- 60 Wash the plate in the cell washer. Add 100  $\mu\text{L}$  of (Streptavidin-HRP 1:100 working dilution to all wells except the blank. Seal the plate and incubate for 0.5 h at room temperature
- 61 Wash the plate in the cell washer. Add 100  $\mu\text{L}$  of OPD substrate solution (from the HIV-1 p24 ELISA kit) to all wells, except the blank. Seal the plate and incubate for 0.5 h at room temperature.  
**▲ CRITICAL STEP** Add one OPD tablet to 11 mL of substrate diluent (from the HIV-1 p24 ELISA kit) and protect from light. OPD should be freshly made and used.
- 62 Stop the reaction by adding 100  $\mu\text{L}$  of stop solution (from the kit) to all wells. Immediately read the plate at 490 nm on a preconfigured plate reader (see the 'Equipment setup' section).  
**? TROUBLESHOOTING**

**AD-mediated siRNA transfection into NK cells ● Timing ~3 d**

**▲ CRITICAL** The same procedure also applies to human NK cells.

- 63 Isolate and sort NK cells from mouse spleen as described in the Supplementary Methods. On the experimental day, when the cells are sorted, count the NK cells with a hemocytometer. Add IL-15 medium to adjust the concentration as desired.
- 64 Seeding NK cells: As an example, for a 24-well-plate format, seed 1.0 mL of cells at  $5 \times 10^5$  cells into each well. Incubate the cells at 37 °C in a humidified incubator under 5%  $\text{CO}_2$  for 24 h.
- 65 Formation of the NKG2D siRNA-AD complex: Follow the procedure as described for  $\text{CD4}^+$  T cells (Step 42).
- 66 AD-mediated siRNA transfection: Follow the procedure as described for  $\text{CD4}^+$  T cells (Step 43).

**Functional evaluation of NKG2D gene silencing in NK cells ● Timing ~12 h**

- 67 Use a 1.0-mL pipette to carefully transfer the transfected NK cells (Step 66) from the wells to 1.7-mL Eppendorf Safe-Lock microcentrifuge tubes. Centrifuge at 400g for 5 min at room temperature and proceed to total RNA extraction or antibody staining as described below.  
**▲ CRITICAL STEP** After centrifugation, the NK cells will be concentrated at the bottom of the tube. For aspiration, tilt the tube and place the tip of the aspirator on the wall of the tube, well above the cell pellet, to avoid loss of cells.
- 68 *Determination of siRNA-mediated silencing of the target gene by qRT-PCR assay (Steps 68–70)*. RNA isolation: Follow the procedure as described for  $\text{CD4}^+$  T cells (Steps 45–47) or, alternatively, follow the manufacturer's instructions for the RNeasy Mini Kit.
- 69 Elute the RNA with RNase-free water and quantify the RNA concentration using a NanoDrop microvolume spectrophotometer.
- 70 cDNA synthesis and qRT-PCR: Follow the procedure as described for  $\text{CD4}^+$  T cells (Steps 49 & 50), using NKG2D primers (Table 3).
- 71 *Determination of siRNA-mediated knockdown of NKG2D protein by flow cytometry (Steps 71–73)*. In the case that NKG2D siRNA is used for the transfection experiment, surface expression of the NKG2D receptor can be assayed by flow cytometry. To stain the cell surface with anti-NKG2D antibody, after 2–3 d of transfection, wash the cells from Step 67 twice with 500  $\mu\text{L}$  of DPBS buffer. Resuspend the cell pellet with 50  $\mu\text{L}$  of labeling buffer for each tube. Add the fluorescent dye-labeled anti-NKG2D antibody (0.25  $\mu\text{g}/\text{test}$ ) and gently mix by pipetting up and down for 15 s. Wrap the tubes in aluminum foil and incubate at room temperature for 30 min. Add 1.0 mL of labeling buffer to each tube and centrifuge the tubes at 400g for 5 min at room temperature. Discard the supernatants.
- 72 Fixation of NK cells: Loosen the cell pellets and add 250  $\mu\text{L}$  of BD Cytofix/Cytoperm solution (from the Fixation/Permeabilization Solution Kit). Incubate in the dark at 4 °C for 20 min. Add 1 mL of BD Perm/Wash buffer to the tube and centrifuge the tubes at 400g for 5 min at room temperature. Discard the supernatants and resuspend the cell pellets in 350  $\mu\text{L}$  of labeling buffer. Store the samples at 4 °C in the dark while setting up the flow cytometry with non-stained control cells.
- 73 Flow cytometry analysis: Proceed to acquisition of experimental data (surface NKG2D expression level) by flow cytometry (see 'Equipment setup' section for flow cytometer setup).

**AD-mediated siRNA transfection into primary mouse macrophages (BMDMs)**

**● Timing ~3 d**

- 74 Detaching the BMDMs from Petri dish and cell counting: Isolate BMDMs as described in the Supplementary Methods. On day 7, wash the cells with 5 mL of DPBS and then add 2 mL of Accutase for 5 min at 37 °C in the incubator. Recover the cells by flushing the culture Petri dish and

- collect in a 50-mL conical tube containing 5 mL BMDM cell culture basic medium as described in the 'Reagent setup' section. Centrifuge at 150g for 5 min at room temperature. Aspirate the supernatant, resuspend the cells in BMDM cell culture basic medium, and count the number of cells using a Countess II FL Automated Cell Counter and Trypan blue as a viability dye.
- 75 Seeding of macrophages: Seed  $1 \times 10^6$  cells per well in 1 mL BMDM cell culture basic medium in a 12-well-plate format. Incubate the cells at 37 °C in a humidified incubator under 5% CO<sub>2</sub> for 1 h to allow the cells to attach to the plate. After 1 h, centrifuge the plate at 150g for 5 min at room temperature, remove the medium, and refill with 800 µL of OPTI-MEM medium.
  - 76 Formation of the siRNA-AD complex: Follow the procedure with *JAK1* siRNA as described for CD4<sup>+</sup> T cells (Step 42).
  - 77 AD-mediated siRNA transfection: Gently mix the complexes by pipetting up and down. Carefully add the solution containing the siRNA-AD complexes dropwise to the cells and gently rock the Petri dish for 10 s to homogenize the siRNA-AD complex dispersion on the cells. Incubate the cells at 37 °C in a humidified incubator under 5% CO<sub>2</sub> for 8 h. Then centrifuge the plate at 150g for 5 min at room temperature, remove the OPTI-MEM, and replace it with BMDM cell culture basic medium. Incubate for another 40 h before further functional assays.

### Functional evaluation of *JAK1* gene silencing in primary macrophages ● Timing -3 d

- 78 Wash the cell monolayer (from Step 77) once with ice-cold DPBS<sup>+</sup>. For protein isolation, add 1 tablet of cOmplete, Mini Protease Inhibitor Cocktail in 10 mL of RIPA buffer to prepare the cell lysis buffer and add 150 µL of cell lysis buffer per well to evenly cover the plate well surface.
    - ▲ **CRITICAL STEP** When collecting cell lysates for protein analyses, keep the culture plate and tubes on ice.
    - **PAUSE POINT** At this stage, the culture plate can be stored at -20 °C until required for further processing for WB analysis.
  - 79 Determine siRNA-mediated knockdown of target protein in macrophages by WB (Steps 79–84). Remove the cell lysates from -20 °C, defrost them on ice, and centrifuge at 15,000–20,000g for 15 min at 4 °C. Transfer the supernatants to fresh tubes and discard the pellets.
  - 80 Determine the protein concentration with the BCA Protein Assay Kit, adjust the concentration in each sample to an equal value (e.g., 0.5 µg/mL), and add an appropriate volume of 4× LDS buffer and 10× sample reducing buffer. Boil at 95 °C for 10 min to denature the proteins.
- ? TROUBLESHOOTING**
- 81 Mount the precast SDS-PAGE (4–15%) gels in the electrophoresis system and add the running buffer for SDS-PAGE. Load equal amounts of protein (e.g., 10 µg) into the wells of the gel along with the pre-stained protein marker. Run the gel for the initial 10 min at 80 V and then increase the voltage to 120–170 V and continue for 1–1.5 h until the protein samples are resolved in the gel.
  - 82 Transfer the proteins from the gel to a nitrocellulose membrane in electrophoretic transfer buffer at 100 V for 60 min.
  - 83 Block the membranes in blocking buffer for 1 h at room temperature and incubate overnight at 2–8 °C with primary anti-JAK1 antibodies diluted at 1:1,000, or anti-GAPDH antibodies diluted at 1:2,000, in 5% BSA in TBS-T. The primary antibody reaction is followed by several TBS-T washes, and then by incubation with the peroxidase-conjugated secondary antibody diluted at 1:10,000 for 1 h.
  - 84 Detect the immunocomplexes using a chemiluminescence detection kit and instrument of choice. SuperSignal West Pico Chemiluminescent Substrate was used to detect housekeeping proteins, and SuperSignal West Femto Maximum Sensitivity Substrate was used for JAK1 detection. Estimate the molecular weight of the detected proteins according to pre-stained protein markers.
- ? TROUBLESHOOTING**

### AD-mediated siRNA transfection into primary microglia ● Timing 3–5 d

- 85 Isolate and culture primary microglia from newborn pups as described in the Supplementary Methods
- 86 Seeding of microglia cells: Using a 24-well-plate format as an example, seed  $1 \times 10^5$  cells per well in 0.5 mL culture medium. Incubate the cells at 37 °C in a humidified incubator under 5% CO<sub>2</sub> for 48 h to reach quiescence.
- 87 Formation of the siRNA-AD complex: Follow the procedure as described for CD4<sup>+</sup> T cells (Step 42) using rat ID1 siRNAs.
- 88 AD-mediated siRNA transfection: Follow the procedure as described for CD4<sup>+</sup> T cells (Step 43).

**Functional evaluation of *Id1* gene silencing in primary microglia culture** ● **Timing 3–4 d**

89 Wash the cell monolayer (Step 88) twice with ice-cold DPBS. For total RNA extraction, follow the procedure as described for CD4<sup>+</sup> T cells (Steps 45–47) or, alternatively, the manufacturer’s instructions for the RNA isolation kit. For protein isolation, scrape the cells into the cell lysis buffer containing phosphatase and protease inhibitors. Add a sufficient volume of the cell lysis buffer to evenly cover the plate well surface (e.g., add 50 µL to each well of a 24-well plate). Transfer the lysate to a microcentrifuge tube and store the lysates at –80 °C until required for further processing for WB analysis.

**▲ CRITICAL STEP** When collecting cell lysates for protein analyses, keep the culture plate and tubes on ice.

90 *Determination of siRNA-mediated silencing of the target gene by qRT-PCR assay (Steps 90 & 91).* Dissolve the RNA in RNase-free water and quantify the RNA concentration using a NanoDrop microvolume spectrophotometer.

91 cDNA synthesis and qRT-PCR: Follow the procedure as described for CD4<sup>+</sup> T cells (Steps 49 & 50). Use rat ID1 and 18S RNA primers (Table 3).

**? TROUBLESHOOTING**

92 *Determination of siRNA-mediated knockdown of target protein in microglia by WB (Steps 92–97).* Remove the cell lysates (Step 89) from –80 °C, defrost them on ice, and centrifuge at 16,000g for 15 min at 4 °C. Transfer the supernatant to a fresh tube and discard the pellet.

93 Determine the protein concentration with the Protein Assay Kit, adjust the concentration in each sample to an equal value (e.g., 0.5 µg/mL) using cell lysis buffer, and add an appropriate volume of 4× sample loading buffer with DTT to get a 1× concentration. Boil at 98 °C for 5 min to denature the proteins.

94 Mount the precast SDS-PAGE (4–15%) gels in the electrophoresis system and add the running buffer for SDS-PAGE. Load equal amounts of protein (e.g., 20 µg) into the wells of the gel, along with the pre-stained protein marker. Run the gel for the initial 10 min at 50 V and then increase the voltage to 100–150 V and continue for 1–1.5 h until the protein samples are resolved in the gel.

95 Transfer the proteins from the gel to the nitrocellulose membrane in electrophoretic transfer buffer at 400 mA for 75 min.

96 Block the membranes in blocking buffer for 1 h and incubate for 2 h at room temperature or overnight at 2–8 °C with primary antibodies (anti rat ID1 antibody diluted to 1:1,000 or anti-GAPDH antibody diluted to 1:25,000) in 5% BSA in TBS-T. The primary antibody reaction is followed by incubation with the peroxidase-conjugated anti-mouse IgG antibody diluted to 1:10,000 for 1 h.

97 Detect the immunocomplexes using a chemiluminescence detection kit (e.g., SuperSignal West Pico Chemiluminescent Substrate) and instrument of choice. Estimate the molecular weight of the detected proteins according to pre-stained protein markers.

**? TROUBLESHOOTING**

**Troubleshooting**

Troubleshooting advice can be found in Table 4.

**Table 4 | Troubleshooting table**

Step	Problem	Possible reason	Solution
9	Incomplete reaction	The Cul is oxidized or inactivated	Ensure proper argon protection before and during the whole reaction
24	Low isolated yield for <b>3</b>	Starting material <b>1</b> or <b>2</b> is stuck on the wall of the vial	Ensure proper mixing of all the reagents. During the argon flushing procedure, flush with argon gently
		Product is stuck on the silica gel	Increase the polarity of the eluent or increase the percentage of TEA in eluent
28	Residual TEA in <b>3</b>	TEA has a high boiling point and may be encapsulated within the dendrimer <b>3</b>	Dissolve the product in CH <sub>2</sub> Cl <sub>2</sub> and wash it using saturated NaCl solution. Collect the organic phase and then remove CH <sub>2</sub> Cl <sub>2</sub> to obtain the pure product
	<b>3</b> is not well dissolved in methanol	Poor solubility in pure MeOH	<b>3</b> is soluble in the mixed solvent of MeOH and EDA

Table continued

Table 4 (continued)

Step	Problem	Possible reason	Solution
50	Suboptimal siRNA knockdown efficiency	Poor delivery or suboptimal N/P ratio	The formation of siRNA-dendrimer complexes depends critically on the dendrimer-to-RNA charge ratio, which is defined as the 'N/P ratio'. Ensure an optimal N/P ratio is used for effective delivery and release of siRNA
	No significant siRNA knockdown efficiency	Poor total RNA quality	Total RNA extraction from HIV-1-infected primary CD4 <sup>+</sup> T cells may be challenging. After resuspending cell pellets in TRIzol solution, add 1 $\mu$ L glycogen to improve RNA precipitation. Ensure the ratio of 260 nm/280 nm of total RNA is >2.0 for RNA measurement using a NanoDrop microvolume spectrophotometer
62	False-positive signal shown in no-RT control sample	Genomic DNA contamination	Ensure that the DNase treatment is effective and complete
	HIV p24 ELISA readout is too high or too low to see	Improper sample dilution	Ensure proper sample dilution by setting up a pre-test with non-transfected samples. This will help to determine the dilution ratio. If the supernatant is too diluted, the readout will be negative; if the supernatant is too concentrated, the readout will be saturated
80	Low protein yield	Insufficient number of cells for transfection or insufficient quantity of proteins to be detected by WB	Increase the number of seeded cells and control cell viability. If cell mortality is observed, adjust the method of cell collection to more gentle and rapid handling
84	Inefficient WB detection	Quantity of loaded proteins is too low, inefficient transfer to the membrane, or failure in antibody detection	Increase the quantity of proteins loaded on the gels. Control transfer efficacy with a well-established protein that can be used as an internal control. Change the antibody source
91	Low RNA yield	Insufficient number of cells for transfection, improper collection of cell lysates, or improper handling of RNA samples	Check the number of seeded cells and the condition of cells in culture (e.g., cell viability). Use a quick but gentler method for all washing steps during collection of cell lysates, avoiding scratching or disturbing of cell monolayer. Ensure that RNA isolation is performed quickly, with the use of RNase-free water, and that isolated RNA is handled on ice, with caution to avoid its degradation, which may be caused by contamination with RNases
	Suboptimal knockdown efficiency	siRNA concentration is too low for selected target gene or there were technical problems with qPCR detection	Increase siRNA concentration up to 25 nM, shorten or extend incubation time with AD complexes. A precise measurement of RNA concentration before the reverse-transcription stage and use of an appropriate endogenous control gene ( <i>18SRNA</i> , <i>GAPDH</i> ) in qPCR are required for accurate evaluation of gene expression changes
97	Low protein yield	Insufficient number of cells for transfection or improper collection of cell lysates	Check the number of seeded cells and the condition of cells in culture (e.g., cell viability). Use a quick but gentler method for all washing steps during collection of cell lysates, avoiding scratching or disturbing of cell monolayer
	Suboptimal knockdown efficiency	siRNA concentration is too low, time point for the evaluation of the expression levels of selected target gene was not optimal, or unequal amounts of protein samples were loaded on the gel	Increase siRNA concentration up to 25 nM, shorten or extend incubation time with AD complexes. Perform detection of a control, endogenous protein (e.g., actin, <i>GAPDH</i> ) to ensure equal protein loading in each sample
	No or poor-quality chemiluminescence signal in WB	Inefficient transfer of proteins from the gels to nitrocellulose or antibody failure	Stain gels after transfer to ensure a complete protein transfer. Check whether a primary antibody is validated for use in WB and check that the appropriate secondary antibody was used for detection
	Nonspecific signal on the blots	Nonspecific binding of primary antibody to the nitrocellulose membrane	Extend incubation of the membranes in a blocking buffer for 3-4 h or increase dilution of primary antibody

## Timing

Steps 1–24, 0.5 h for setup, 1.5 h for the reaction, 3 h for workup and purification: 5 h  
Steps 25–39, 0.5 h for setup, 72 h for the reaction, 6 d for purification: 10 d  
Steps 40–43, 1 h for seeding the HIV-1-infected CD4<sup>+</sup> T cells, 1.5 h for forming the siRNA–AD complex, and 2–3 d for the complex-mediated gene silencing and HIV-1 suppression: 4 d  
Steps 44–62, 4 h for collecting the cell-free supernatant, collecting cells, and isolating total RNA; 4 h for cDNA synthesis and qRT-PCR assay; 4 h for surface CD4<sup>+</sup> staining and flow cytometry analysis; and 6 h for HIV-1 p24 ELISA assay: ~3 d  
Steps 63–66, 5 h for sorting NK cells from mouse spleen, cell counting and seeding, 1 d for resting of NK cells in medium supplemented with IL-15, 1.5 h for formulating the siRNA–AD complex, and 2 d for the complex-mediated gene silencing and functional studies: 3 d  
Steps 67–73, 4 h for cell collection and total RNA extraction, 4 h for cDNA synthesis and qRT-PCR assay, and 4 h for flow cytometry analysis: 12 h  
Steps 74–77, 1.5 h for detaching the BMDM from Petri dish, cell counting, and seeding them in a 12-well plate; 1 h for formation of the siRNA–AD complex; and 2 d for the complex-mediated gene silencing: 3 d  
Steps 78–84, 1 h for collecting cell lysates and preparing protein samples, 6 h for SDS-PAGE and electrophoretic transfer, 16 h for protein detection by WB: 3 d  
Steps 85–88, 1.5 h for separation of microglia from monolayer mixed glial culture, cell counting, and seeding; 1–2 d for resting of the microglia culture; 1.5 h for formulation of the siRNA–AD complex; and 2–3 d for the complex-siRNA mediated gene silencing and functional studies: 3–5 d  
Steps 89–97, 3 h for collecting cell lysates and extracting total RNA or preparing protein samples, 4 h for cDNA synthesis and qRT-PCR assay, 6 h for SDS-PAGE and electrophoretic transfer, 4–16 h for protein detection by WB: 3 d

## Anticipated results

The synthesis of AD started with 95 mg (0.102 mmol) of **1**, which delivered 108 mg of the pure compound **3** as a colorless solid with a yield of 73%. Further transformation of **3** produced 118 mg of the pure product AD as a faint-colored foam-like solid at 96% yield. Detailed analytical data for AD are provided in Supplementary Figs. 1–4 and the Supplementary Results (Analytical Data of Dendrimers).

AD-mediated siRNA delivery in primary T cells was performed in HIV-1-infected human primary PBMC–CD4<sup>+</sup> T cells using DsiRNAs to target CD4 and HIV-1 *tat/rev*<sup>17</sup>. CD4 is the primary receptor for HIV-1, and transient knockdown of this receptor blocks HIV-1 entry<sup>31</sup>, whereas HIV-1 Tat and Rev are essential positive regulators of viral gene expression<sup>32</sup>. Using AD as the siRNA delivery vehicle, a substantial decrease of CD4 expression was achieved at both the mRNA and protein levels in T cells<sup>17</sup>. In addition, a considerable reduction in HIV-1 *tat/rev* mRNA (50–70%) was observed in the PBMC–CD4<sup>+</sup> T cells (Fig. 4a), leading to a significant reduction of viral infection (Fig. 4b). AD alone or a control DsiRNA–AD complex did not generate any silencing effect (Fig. 4a), nor affect the cell viability (Supplementary Fig. 5a)<sup>17</sup>. When we compared AD to commercially available vectors, we found that Lipofectamine RNAiMAX (lipo) was unable to deliver the siRNA effectively (Supplementary Fig. 5b), whereas Trans IT-TKO (TKO) exhibited notable toxicity<sup>17</sup>. These results demonstrate the excellent siRNA delivery ability of AD, which opens up a new avenue for siRNA delivery to T cells and also for adoptive T cell therapy.

AD-mediated siRNA delivery in NK cells was carried out in both murine NK cells collected from mouse spleen and human NK cells purified from the blood of healthy donors, using an siRNA specifically targeting the natural-killer receptor group 2, member D (NKG2D). NKG2D is an activating receptor expressed on the membrane of NK cells that triggers their cytotoxic function when it recognizes ligands expressed by a target cell such as a cancer cell<sup>33</sup>. The NKG2D receptor is involved in the cytotoxic function of NK cells against motor neurons<sup>21</sup>. The delivery of AD loaded with NKG2D-specific siRNA occurs 6 h after transfection, as shown using siRNA labeled with a fluorescent dye<sup>21</sup>. AD-mediated siRNA transfection reduced the *NKG2D* mRNA by ~60–70% in both human and murine NK cells, and the protein level by ~50–60% in murine NK cells, as indicated by qPCR and FACS analysis (Fig. 4c,d). The reduction of NKG2D receptor expression reduced the cytotoxic activity of NK cells against motor neurons and tumor cells<sup>21</sup>. Empty AD or AD loaded with scrambled siRNA did not affect the NKG2D expression in NK cells (Fig. 4c,d), nor the viability of NK

cells (Supplementary Fig. 6a)<sup>21</sup>. In addition, the commercial vector Lipofectamine (lipo) was unable to deliver the siRNA in NK cells (Supplementary Fig. 6b). Taken together, these results demonstrate the excellent performance of AD in delivering siRNA to NK cells. The successful AD-mediated siRNA delivery to primary NK cells corroborated the role of NKG2D in the cytotoxic activity of NK cells against tumor cells and motor neurons in neurodegenerative diseases. This opens up the possibility of modifying the functional activation state of NK cells and may provide a new therapeutic approach in different diseases.

AD-mediated siRNA delivery in primary macrophages has been studied using a specific siRNA targeting Janus Kinase 1 (*JAK1*) in mouse primary macrophages originating from the bone marrow (BMDMs). *JAK1* is a protein kinase that is associated with several cytokine or interferon receptors, thus playing an important role in inflammatory responses. Inhibition of *JAK1* activity has been found valuable in the treatments of several diseases, including rheumatoid arthritis<sup>34</sup>, inflammatory bowel disease<sup>35</sup>, and alopecia areata<sup>36</sup>. Reduction of *JAK1* expression in macrophages, in order to restrict their pro-inflammatory activity, remains a challenging issue. Using AD as the vector for the delivery of *JAK1*-specific siRNA to mouse primary macrophages resulted in a significant reduction of *JAK1* protein expression, which was estimated to be 67% of the normal expression by WB analysis 48 h post-transfection with an N/P ratio of 5:1 (Fig. 4e,f). In addition, a high proportion of cells survived the treatment with AD (Supplementary Fig. 7a), and the primary macrophages remained unpolarized upon treatment with AD and AD-complexed control siRNA (Supplementary Fig. 7b). By contrast, commercial vectors such as Lipofectamine RNAiMAX (lipo) did not decrease *JAK1* protein expression levels (Supplementary Fig. 7c). Delivery of *JAK1*-specific siRNA to primary macrophages using AD as a transfection reagent promises to treat various *JAK1*-dependent disease conditions. The capacity in the modulation of *JAK1* activity in primary inflammatory cells such as macrophages opens a new window to intervene in treatment for inflammatory diseases.

Importantly, AD enabled effective siRNA delivery to primary microglial cells at a low siRNA concentration (12.5 nM) and had no effect either on the cell morphology or on the expression of inflammatory and pro-invasive response genes in these cells<sup>20</sup>. AD did not affect the basal function or immune gene expression in primary microglial cells<sup>20</sup>. Microglial cells treated with AD alone or AD complexed with control siRNA retained their ability to proliferate (Supplementary Fig. 8a) and remained unpolarized (Supplementary Fig. 8b,c), and their responses to stimuli were unaffected<sup>20</sup>. By contrast, viral vectors, such as a lentiviral vector carrying an shRNA, and nonviral vectors, such as Viromer (Supplementary Fig. 8b) or Lipofectamine, induced strong inflammatory effects in primary microglia cultures<sup>20,37</sup>. We used AD to deliver an siRNA targeting the transcription regulator ID1 in rat microglial cells. ID1 controls the proliferation and differentiation of many cells, and has been hypothesized to act as a master switch in microglia activation by glioma-derived factors and as a suppressor of anti-tumor immune responses via inhibition of myeloid cell maturation<sup>38,39</sup>. Treatment of the primary microglia with the siRNA-AD complexes triggered effective downregulation of the target *id1* mRNA and its protein product, resulting in ~40–60% of gene silencing as analyzed by qRT-PCR and WB at 72 h post-transfection (Fig. 4g,h)<sup>20</sup>. Knockdown of the transcription regulator ID1 in microglia led to significant changes in gene expression, for example, downregulation of cell cycle-related genes and upregulation of genes associated with the immune response, as demonstrated by RNA sequencing<sup>20</sup>. This enabled us to explore for the first time the functions of ID1 in glioma-stimulated microglia and specifically identify the role of ID1 in tumor-induced immunosuppression<sup>20</sup>.

Collectively, all these results demonstrate the excellent performance of AD for efficient and non-toxic siRNA delivery to primary immune cells. AD therefore constitutes the long-searched-for transfection reagent with the potential to deliver siRNA safely and effectively for the purpose of functional study and therapeutic applications in immune cells.

### Reporting Summary

Further information on research design is available in the Nature Research Reporting Summary linked to this article.

### References

1. Wilson, R. C. & Doudna, J. A. Molecular mechanisms of RNA interference. *Annu. Rev. Biophys.* **42**, 217–239 (2013).
2. Kim, D. & Rossi, J. RNAi mechanisms and applications. *Biotechniques* **44**, 613–616 (2008).

3. Setten, R. L., Rossi, J. J. & Han, S. P. The current state and future directions of RNAi-based therapeutics. *Nat. Rev. Drug Discov.* **18**, 421–446 (2019).
4. Sioud, M. Releasing the immune system brakes using siRNAs enhances cancer immunotherapy. *Cancers (Basel)* **11**, 176 (2019).
5. Riley, R. S., June, C. H., Langer, R. & Mitchell, M. J. Delivery technologies for cancer immunotherapy. *Nat. Rev. Drug Discov.* **18**, 175–196 (2019).
6. Kanasty, R., Dorkin, J. R., Vegas, A. & Anderson, D. Delivery materials for siRNA therapeutics. *Nat. Mater.* **12**, 967–977 (2013).
7. Whitehead, K. A., Langer, R. & Anderson, D. G. Knocking down barriers: advances in siRNA delivery. *Nat. Rev. Drug Discov.* **8**, 129–138 (2009).
8. Judge, A. D. et al. Sequence-dependent stimulation of the mammalian innate immune response by synthetic siRNA. *Nat. Biotechnol.* **23**, 457–462 (2005).
9. Judge, A. & MacLachlan, I. Overcoming the innate immune response to small interfering RNA. *Hum. Gene Ther.* **19**, 111–124 (2008).
10. Whitehead, K. A., Dahlman, J. E., Langer, R. S. & Anderson, D. G. Silencing or stimulation? siRNA delivery and the immune system. *Annu. Rev. Chem. Biomol. Eng.* **2**, 77–96 (2011).
11. Zhang, X., Edwards, J. P. & Mosser, D. M. The expression of exogenous genes in macrophages: obstacles and opportunities. *Methods Mol. Biol.* **531**, 123–143 (2009).
12. Freeley, M. & Long, A. Advances in siRNA delivery to T-cells: potential clinical applications for inflammatory disease, cancer and infection. *Biochem. J.* **455**, 133–147 (2013).
13. Nakamura, T. et al. Small-sized, stable lipid nanoparticle for the efficient delivery of siRNA to human immune cell lines. *Sci. Rep.* **6**, 37849 (2016).
14. Nakamura, T., Yamada, K., Fujiwara, Y., Sato, Y. & Harashima, H. Reducing the cytotoxicity of lipid nanoparticles associated with a fusogenic cationic lipid in a natural killer cell line by introducing a polycation-based siRNA core. *Mol. Pharmaceutics* **15**, 2142–2150 (2018).
15. Davis, M. E. et al. Evidence of RNAi in humans from systemically administered siRNA via targeted nanoparticles. *Nature* **464**, 1067–1070 (2010).
16. Yu, T. et al. An amphiphilic dendrimer for effective delivery of small interfering RNA and gene silencing in vitro and in vivo. *Angew. Chem. Int. Ed. Engl.* **51**, 8478–8484 (2012).
17. Liu, X. X. et al. Adaptive amphiphilic dendrimer-based nanoassemblies as robust and versatile siRNA delivery systems. *Angew. Chem. Int. Ed. Engl.* **53**, 11822–11827 (2014).
18. Chen, C. et al. Mastering dendrimer self-assembly for efficient siRNA delivery: from conceptual design to in vivo efficient gene silencing. *Small* **12**, 3667–3676 (2016).
19. Dong, Y. et al. A dual targeting dendrimer-mediated siRNA Delivery system for effective gene silencing in cancer therapy. *J. Am. Chem. Soc.* **140**, 16264–16274 (2018).
20. Ellert-Miklaszewska, A. et al. Efficient and innocuous delivery of small interfering RNA to microglia using an amphiphilic dendrimer nanovector. *Nanomedicine (Lond.)* **14**, 2441–2458 (2019).
21. Garofalo, S. et al. Natural killer cells modulate motor neuron-immune cell cross talk in models of amyotrophic lateral sclerosis. *Nat. Commun.* **11**, 1773 (2020).
22. Kim, D. H. et al. Synthetic dsRNA Dicer substrates enhance RNAi potency and efficacy. *Nat. Biotechnol.* **23**, 222–226 (2005).
23. Amarzguioui, M. et al. Rational design and in vitro and in vivo delivery of Dicer substrate siRNA. *Nat. Protoc.* **1**, 508–517 (2006).
24. Tomalia, D. A. et al. A new class of polymers - starburst-dendritic macromolecules. *Polym. J.* **17**, 117–132 (1985).
25. Peterson, J., Allikmaa, V., Subbi, J., Pehk, T. & Lopp, M. Structural deviations in poly(amidoamine) dendrimers: a MALDI-TOF MS analysis. *Eur. Polym. J.* **39**, 33–42 (2003).
26. van Dongen, M. A., Desai, A., Orr, B. G., Baker, J. R. & Holl, M. M. B. Quantitative analysis of generation and branch defects in G5 poly(amidoamine) dendrimer. *Polymer* **54**, 4126–4133 (2013).
27. Rastogi, A. & Nayan, R. Studies on copper (II) complexes of some polyaza macrocycles derived from 1, 2-diaminoethane. *J. Coord. Chem.* **62**, 3366–3376 (2009).
28. Trouplin, V. et al. Bone marrow-derived macrophage production. *J. Vis. Exp.* **2013**, e50966 (2013).
29. Armarego, W. L. F. & Perrin, D. D. *Purification of Laboratory Chemicals* (Butterworth Heinemann, 1996).
30. Vogel, A. I., Furniss, B. S., Hannaford, A. J., Smith, P. W. & Tatchell, A. R. *Vogel's Textbook of Practical Organic Chemistry* (Longman Scientific & Technical, 1989).
31. Fauci, A. S. The human immunodeficiency virus: infectivity and mechanisms of pathogenesis. *Science* **239**, 617–622 (1988).
32. Frankel, A. D. & Young, J. A. HIV-1: fifteen proteins and an RNA. *Annu. Rev. Biochem.* **67**, 1–25 (1998).
33. Molfetta, R., Quatrini, L., Santoni, A. & Paolini, R. Regulation of NKG2D-dependent NK cell functions: the yin and the yang of receptor endocytosis. *Int. J. Mol. Sci.* **18**, 1677 (2017).
34. Malemud, C. J. The role of the JAK/STAT signal pathway in rheumatoid arthritis. *Ther. Adv. Musculoskelet. Dis.* **10**, 117–127 (2018).
35. De Vries, L. C. S., Wildenberg, M. E., De Jonge, W. J. & D'Haens, G. R. The future of Janus kinase inhibitors in inflammatory bowel disease. *J. Crohns Colitis* **11**, 885–893 (2017).
36. Triyangkulsri, K. & Suchonwanit, P. Role of Janus kinase inhibitors in the treatment of alopecia areata. *Drug Des. Devel. Ther.* **12**, 2323–2335 (2018).

37. Guo, X. et al. Transfection reagent Lipofectamine triggers type I interferon signaling activation in macrophages. *Immunol. Cell Biol.* **97**, 92–96 (2019).
38. Papaspyridonos, M. et al. Id1 suppresses anti-tumour immune responses and promotes tumour progression by impairing myeloid cell maturation. *Nat. Commun.* **6**, 6840 (2015).
39. Zebedee, Z. & Hara, E. Id proteins in cell cycle control and cellular senescence. *Oncogene* **20**, 8317–8325 (2001).

### Acknowledgements

This work was supported by La Ligue Nationale Contre le Cancer (EL2016.LNCC/LPP to L.P.); the NIH (grants R01AI29329, R01AI42552, and R01HL07470 to J.J.R., as well as grant P30CA033572 for City of Hope Core Facility support); National Science Centre Poland (no. 2017/25/B/NZ3/02483 to A.E.-M.); the French National Research Agency and the Italian Ministry of Health under the frame of the Era-Net EURONANOMED European Research projects ‘NANOGLIO’ (L.P., A.S., C.L., P.N.M.), ‘TARBRAINFEKT’ (L.P.) and ‘NAN-4-TUM’ (L.P.); the China Scholarship Council (J.C., J.T.) and Bourse Eiffel du Campus France (J.C.); the Italian Association for Cancer Research (AIRC) (IG 2015 and IG 2019 to C.L.; 22329 2018 to S.G.); and the Italian Research Foundation for ALS (AriSLA) (Pilot NKINALS 2019 to S.G.). This project has received funding from the European Union’s Horizon 2020 research and innovation program H2020 NMBP ‘SAFE-N-MEDTECH’ (L.P.; under grant agreement no. 814607) and ‘NEWDEAL’ (A.D., F.C., P.N.M.; under grant agreement no. 720905). This publication reflects only the authors’ views, and the Commission is not responsible for any use that may be made of the information it contains. This article is based upon work from COST Action CA 17140 ‘Cancer Nanomedicine from the Bench to the Bedside’, supported by COST (European Cooperation in Science and Technology). We thank A. Tintaru from Aix-Marseille University in France for NMR recording, G. Bernardini from the University of Rome La Sapienza in Italy for FACS analysis, and E. Sulpice and X. Gidrol from CEA/IRIG in Grenoble France for generously providing mouse *JAK1* siRNA.

### Author contributions

Conceptualization, J.Z., L.P.; writing and editing, J.Z., L.P., J.C., Y.J., J.T., A.E.-M., B.K., C.L., S.G., A.S., A.K.D., F.C., P.N.M.; funding acquisition, L.P., J.J.R., B.K., A.E.-M., C.L., P.N.M.; all authors read and approved the final manuscript.

### Competing interests

The authors declare no competing interests.

### Additional information

**Supplementary information** is available for this paper at <https://doi.org/10.1038/s41596-020-00418-9>.

**Correspondence and requests for materials** should be addressed to J.Z. or L.P.

**Peer review information** *Nature Protocols* thanks Jørn B. Christensen and the other, anonymous, reviewer(s) for their contribution to the peer review of this work.

**Reprints and permissions information** is available at [www.nature.com/reprints](http://www.nature.com/reprints).

**Publisher’s note** Springer Nature remains neutral with regard to jurisdictional claims in published maps and institutional affiliations.

Received: 18 March 2020; Accepted: 22 September 2020;

Published online: 4 December 2020

### Related links

#### Key references using this protocol

- Liu, X. et al. *Angew. Chem. Int. Ed.* **53**, 11822–11827 (2014): <https://doi.org/10.1002/anie.201406764>  
Ellert-Miklaszewska, A. et al. *Nanomedicine (Lond.)* **14**, 2441–2458 (2019): <https://doi.org/10.2217/nmm-2019-0176>  
Garofalo, S. et al. *Nat. Commun.* **11**, 1773 (2020): <https://doi.org/10.1038/s41467-020-15644-8>



**Supplementary information**

---

**Synthesis and use of an amphiphilic dendrimer for siRNA delivery into primary immune cells**

---

In the format provided by the authors and unedited

## Supplementary Information

### Synthesis and use of an amphiphilic dendrimer for siRNA delivery into primary immune cells

Jiaxuan Chen<sup>1,2</sup>, Aleksandra Ellert-Miklaszewska<sup>3</sup>, Stefano Garofalo<sup>4</sup>, Arindam K Dey<sup>5</sup>, Jingjie Tang<sup>1</sup>, Yifan Jiang<sup>1</sup>, Flora Clément<sup>5</sup>, Patrice N Marche<sup>5</sup>, Xiaoxuan Liu<sup>2</sup>, Bozena Kaminska<sup>3</sup>, Angela Santoni<sup>6</sup>, Cristina Limatola<sup>4,6</sup>, John J. Rossi<sup>7</sup>, Jiehua Zhou<sup>7\*</sup>, Ling Peng<sup>1\*</sup>

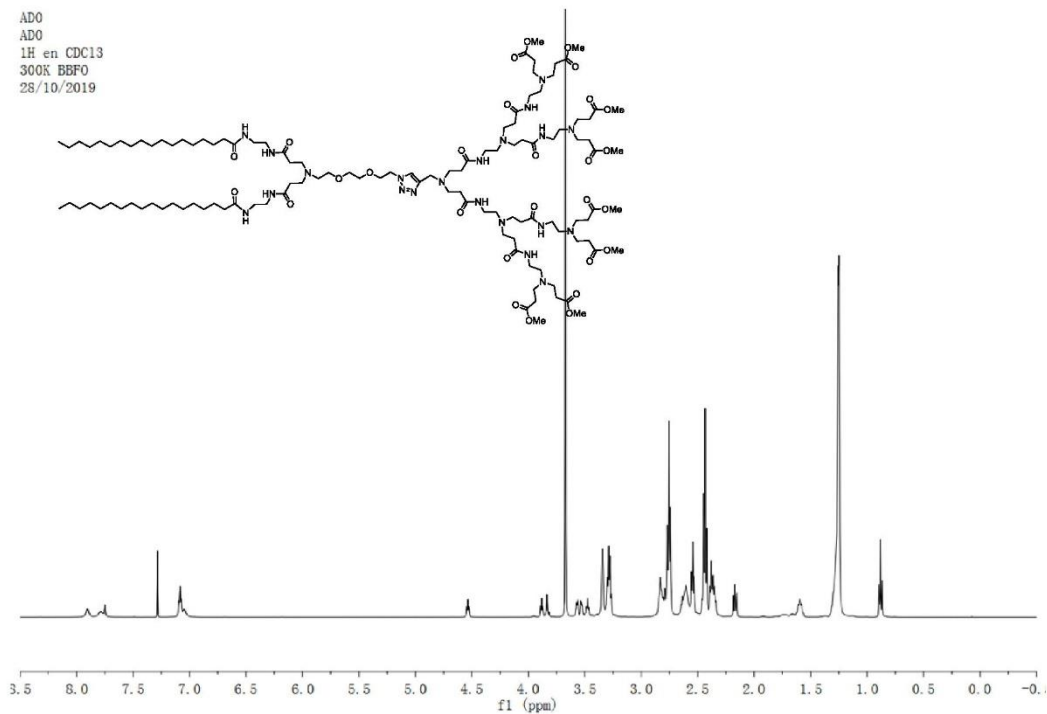
### Table of Content

<b>Supplementary Figure 1.</b> <sup>1</sup> H- and <sup>13</sup> C-NMR spectra of <b>3</b> .....	2
<b>Supplementary Figure 2.</b> High-resolution mass spectra of <b>3</b> .....	3
<b>Supplementary Figure 3.</b> <sup>1</sup> H- and <sup>13</sup> C-NMR spectra of <b>AD</b> . ....	4
<b>Supplementary Figure 4.</b> High-resolution mass spectra of <b>AD</b> . ....	5
<b>Supplementary Figure 5.</b> Cell viability and siRNA delivery in primary T-cells. ....	6
<b>Supplementary Figure 6.</b> Cell viability and siRNA delivery in primary NK-cells. ....	7
<b>Supplementary Figure 7.</b> Cell viability and siRNA delivery in primary macrophages. ....	8
<b>Supplementary Figure 8.</b> Cell viability and siRNA delivery in primary microgli.....	9
<b>Supplementary Results</b> .....	10
Analytical data .....	10
<b>Supplementary Methods</b> .....	11
Isolation of primary CD4 <sup>+</sup> T cells from human donors.....	11
Isolation of PBMCs.....	11
Isolation and activation of CD4 <sup>+</sup> T cells .....	13
HIV-1 challenge of CD4 <sup>+</sup> T cells.....	13
Isolation of murine NK cells .....	14
Isolation of human PBMCs.....	15
Dissociation of mouse spleen tissue.....	15
Magnetic isolation of murine NK cells from spleen or human NK cells from human PBMCs.....	15
Isolation of murine bone marrow derived macrophages (BMDM) .....	16
Preparation of L929 conditioned medium as a source of natural M-CSF for macrophage culture... 17	
Isolation of mice bone marrow cells from tibia and femur .....	17
Isolation and culture of primary microglial cells.....	19
Dissociation of brain tissue and setting the primary glial culture .....	19
Isolation of microglia from the primary mixed glial culture.....	20
<b>References</b> .....	21

**Supplementary Figure 1.** (a)  $^1\text{H}$ - and (b)  $^{13}\text{C}$ -NMR spectra of **3**.

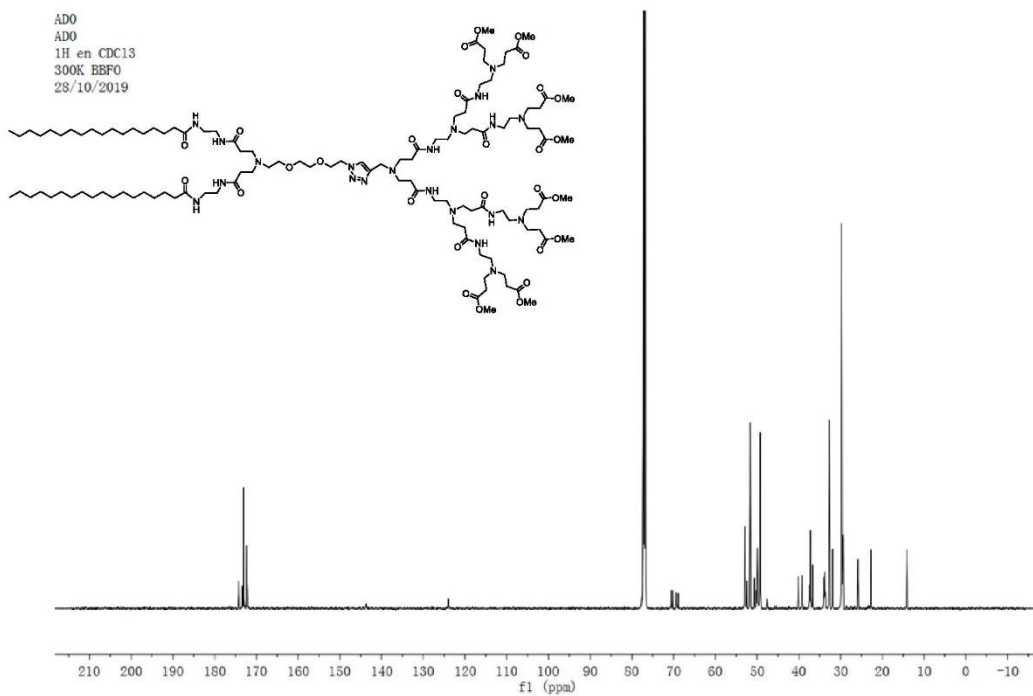
**a**

ADO  
ADO  
1H en CDC13  
300K BBFO  
28/10/2019

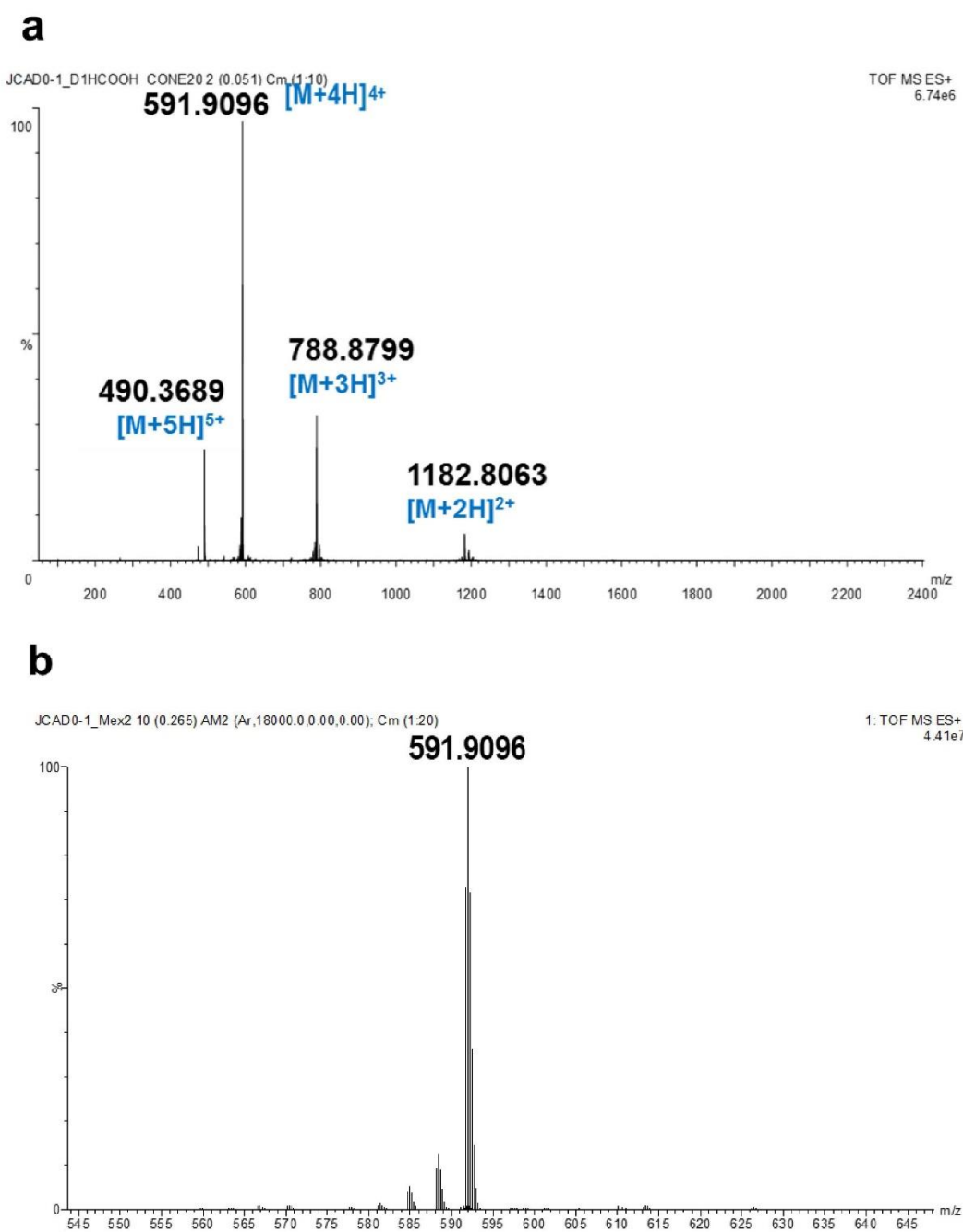


**b**

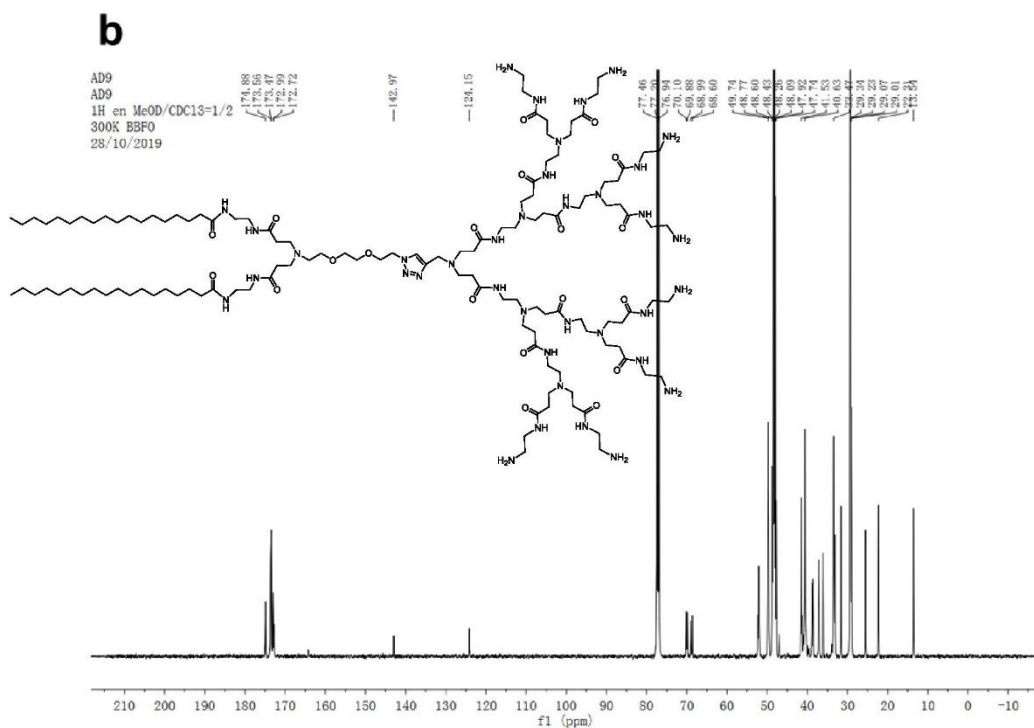
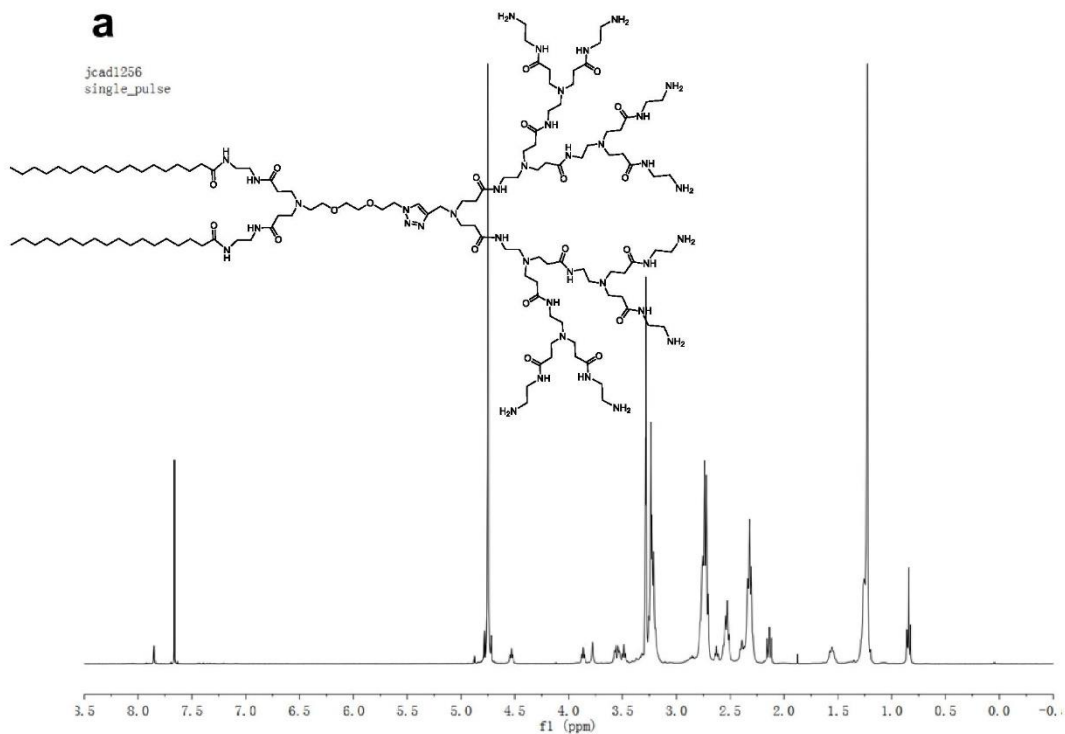
ADO  
ADO  
1H en CDC13  
300K BBFO  
28/10/2019



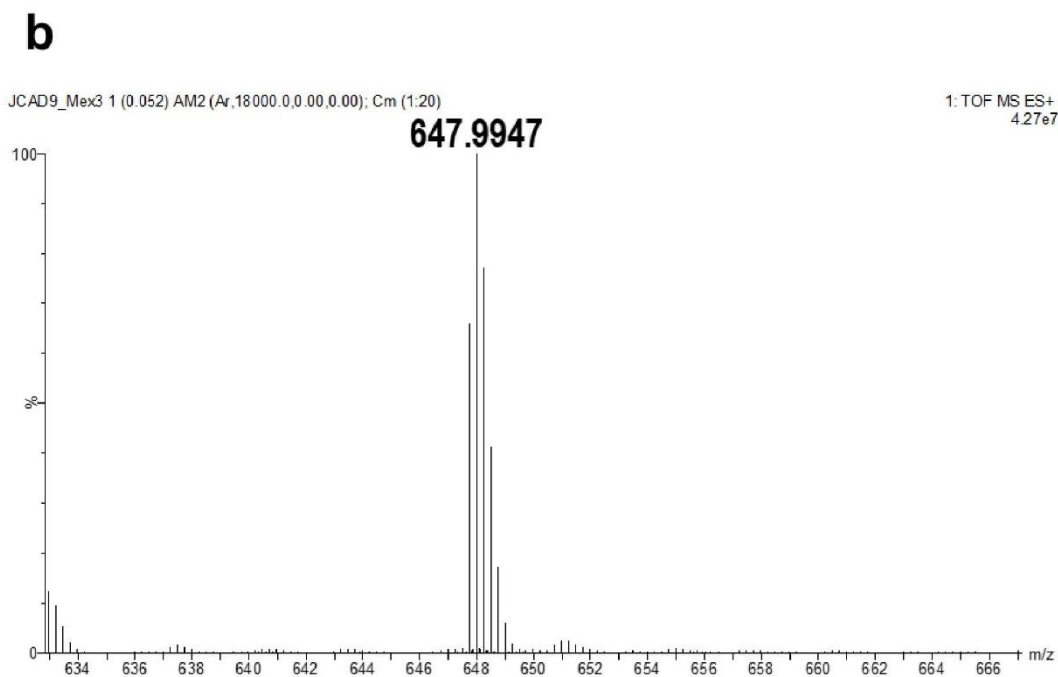
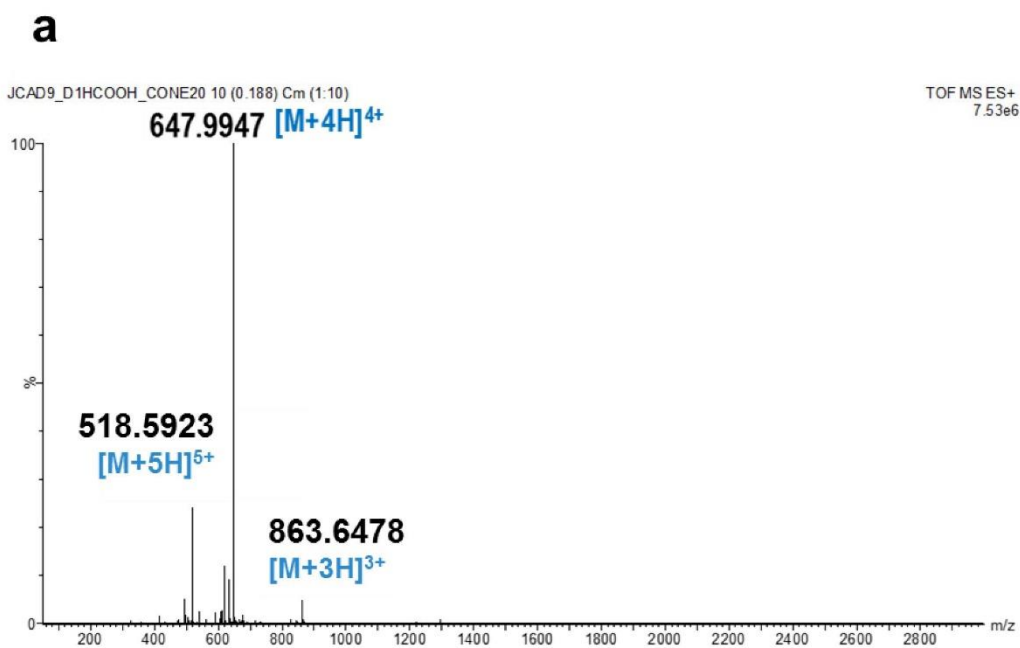
**Supplementary Figure 2.** High-resolution mass spectra of **3**. (a) ESI-HRMS full spectrum; (b) Enlarged spectrum of the expected ionic molecular weight peak with the highest intensity and the corresponding isotopic pattern.



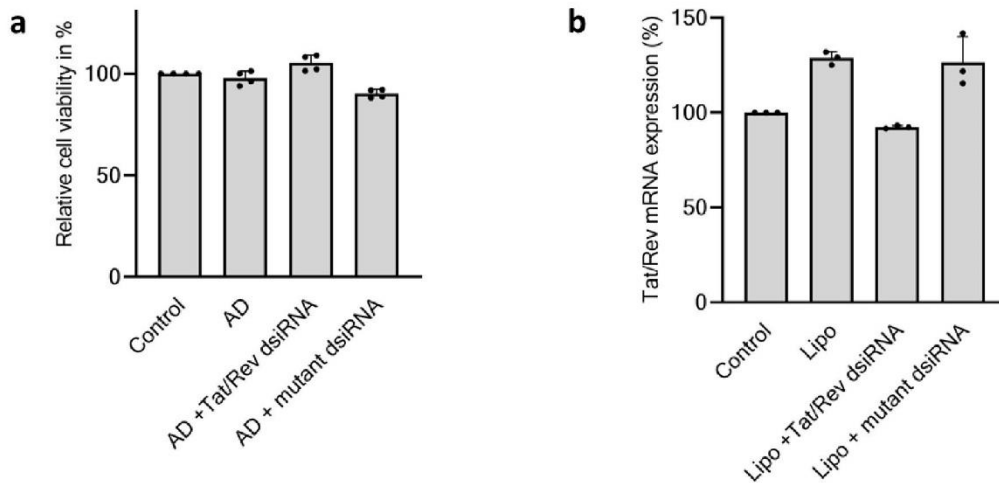
**Supplementary Figure 3.** (a)  $^1\text{H}$ - and (b)  $^{13}\text{C}$ -NMR spectra of AD.



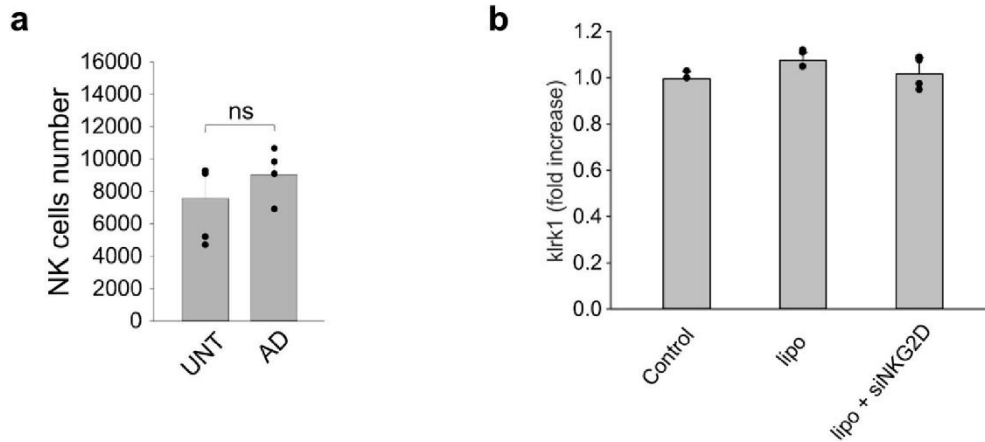
**Supplementary Figure 4.** High-resolution mass spectra of **AD**. (a) ESI-HRMS full spectrum; (b) Enlarged spectrum of the expected ionic molecular weight peak with the highest intensity and the corresponding isotopic pattern.



**Supplementary Figure 5.** Cell viability of primary T-cells after treatment with dendrimer **AD** and siRNA delivery using commercial transfection vector Lipofectamine RNAiMAX (lipo). The MTS assay was performed for cell viability test. (a) No significant toxicity was observed in PBMC CD4+ cells following treatment with **AD** and 50 nM dsRNA at a N/P ratio of 5 (n = 4, data are expressed as mean  $\pm$  SD, one-way ANOVA). (b) No effective gene silencing was achieved using commercial transfection reagent Lipofectamine RNAiMAX (lipo) and dsRNA (50 nM) in primary PBMC CD4+ cells (n = 3, data are expressed as mean  $\pm$  SD, one-way ANOVA). The control is cell alone without any treatment. All measurements were taken from distinct samples. Statistical significance was assessed by one-way ANOVA for parametrical data as indicated by using GraphPad Prism8.0 version. (Reproduced and adapted with permission from ref. 1, John Wiley and Sons.)

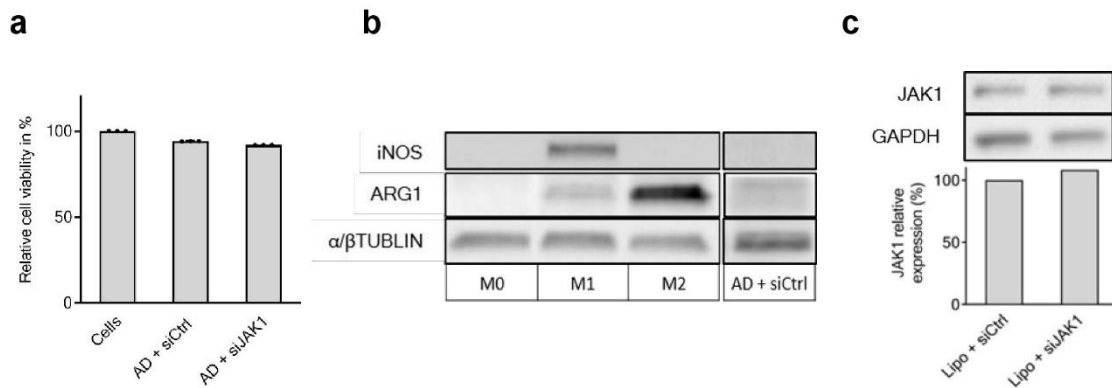


**Supplementary Figure 6.** Cell viability of primary NK-cells after treatment with dendrimer **AD** and *klrk1* gene expression following transfection with commercial transfection vector Lipofectamine RNAiMAX (lipo). (a) Dendrimer **AD** alone does not affect the number of NK cells. Murine NK cells were cultured alone or incubated with **AD** as indicated. The number of NK (NK1.1-/CD3+) cells after 24 h of stimulation was assessed by FACS. (n = 3; data are expressed as mean  $\pm$  S.E.M. ns, not significant, one-way ANOVA). “UNT” represents cells without any treatment. (b) Transfection with commercial vector Lipofectamine RNAiMAX (lipo) did not reduce the expression of *klrk1* in murine NK cells (n = 4; data are expressed as mean  $\pm$  SEM, one-way ANOVA).

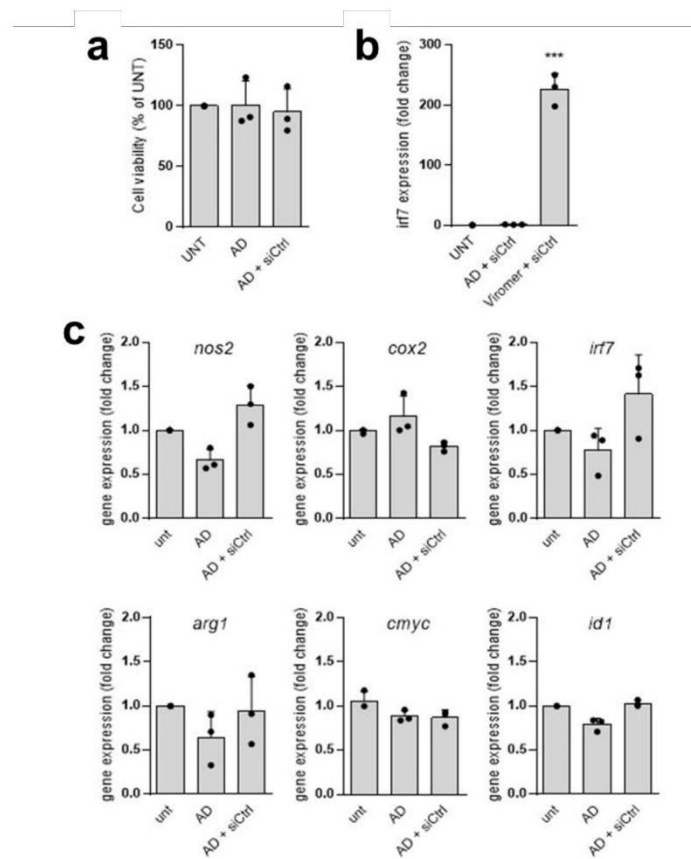




**Supplementary Figure 7.** Assay of cell viability and macrophage polarization upon treatment with siRNA/**AD** complexes as well as siRNA delivery using commercial transfection vector Lipofectamine RNAiMAX (lipo). (a) Cell viability of the primary macrophages was not affected upon treatment with **AD**-mediated delivery of siRNA *JAK1* (siJAK1) and siRNA control (siCtrl). Cell viability was measured using CytoTox-ONE™ Homogeneous Membrane Integrity Assay (n = 3, data are expressed as mean ± SD); (b) The polarization of macrophages was assessed by analyzing the expression of iNOS and Arginase1 (ARG1) using western blotting. M0 stands for unpolarized primary macrophages, M1 for LPS polarized macrophages expressing high level of iNOS and M2 for IL-4 polarized macrophages expressing high level of Arginase1. In the protocol, M0 unpolarized macrophages, which were transfected with siRNA control (siCtrl) complexed with **AD** at N/P ratio of 5, remained unpolarized. The presented blot is representative of three independent experiment. (c) The transfection of siRNA *JAK1* (siJAK1) and siRNA control (siCtrl) in primary macrophages using lipofectamine RNAiMAX (lipo) was not effective. The protein expression was assessed using western blotting (n = 1)



**Supplementary Figure 8.** The effect of **AD** on viability and polarization of primary microglia and siRNA delivery using a commercial transfection reagent Viromer. (a) Viability of rat microglial cells was not affected by **AD** alone or **AD** complexed with non-targeting siRNA (siCtrl) at N/P=10, 12.5 nM siRNA. Number of proliferating cells was evaluated using BrdU incorporation assay at 72 h post-treatment (n = 3, mean ± SD). “UNT” represents cells without any treatment. (b) **AD**-mediated siRNA delivery did not upregulate the inflammatory response in rat microglia in contrast to the commercial vector Viromer. Primary rat microglia cultures were transfected with 25 nM of the control non-targeting siRNA (siCtrl) using **AD** at N/P 10 or commercial vector Viromer. The mRNA level of the inflammatory gene *irf7* was measured using qPCR 24 h post-transfection and presented as a fold change relative to untreated cells (n = 3, mean ± SD). (c) There was no significant change in the expression of genes related to pro-inflammatory (*nos2*, *cox2* and *irf7*) or pro-invasive (*arg1*, *cmyc* and *id1*) phenotype in microglia upon treatment with **AD** alone or **AD** complexed with non-targeting siRNA (siCtrl) at N/P=10, 12.5 nM siRNA. The mRNA levels were measured using qPCR 48 h post-transfection and presented as a fold change relative to untreated cells (n = 3, mean ± SD). All measurements were taken from distinct samples. Groups were compared by one-way ANOVA with a post-hoc Tukey test for multiple comparisons using GraphPad Prism version 6.04. \*\*\* p<0.001. (Reproduced and adapted with permission from ref. 3, Nanomedicine (as agreed by Future Medicine Ltd.))



## Supplementary Results

### Analytical data:

**Dendrimer 3.** Typical isolated yields are 60-70%, from a white to a faint-colored solid;  $^1\text{H}$  NMR (400 MHz,  $\text{CDCl}_3$ )  $\delta$  7.89 (br s, 2H, NH), 7.78 (br s, 2H, NH), 7.73 (s, 1H, CH), 7.08 (br s, 4H, NH), 7.01 (br s, 2H, NH), 4.53 (t, 2H,  $J = 4.8$  Hz,  $\text{CH}_2$ ), 3.87 (t, 2H,  $J = 4.8$  Hz,  $\text{CH}_2$ ), 3.82 (s, 2H,  $\text{CH}_2$ ), 3.66 (s, 24H,  $\text{CH}_3$ ), 3.53-3.56 (br, 4H,  $\text{CH}_2$ ), 3.46 (t, 2H,  $J = 4.5$  Hz,  $\text{CH}_2$ ), 3.34 (br, 8H,  $\text{CH}_2$ ), 3.26-3.29 (m, 12H,  $\text{CH}_2$ ), 2.73-2.81 (m, 32H,  $\text{CH}_2$ ), 2.52-2.62 (m, 14H,  $\text{CH}_2$ ), 2.33-2.44 (m, 32H,  $\text{CH}_2$ ), 2.16 (t, 4H,  $J = 7.8$  Hz,  $\text{CH}_2$ ), 1.58 (br, 4H,  $\text{CH}_2$ ), 1.25 (br, 56H,  $\text{CH}_2$ ), 0.87 (t, 6H,  $J = 7.2$  Hz,  $\text{CH}_3$ );  $^{13}\text{C}$  NMR (126 MHz,  $\text{CDCl}_3$ )  $\delta$  174.21, 173.44, 173.07, 172.31, 124.03, 70.56, 70.21, 69.41, 68.93, 52.94, 52.48, 51.65, 50.66, 50.15, 49.90, 49.26, 40.12, 39.14, 37.44, 37.21, 36.70, 33.99, 33.79, 33.63, 32.71, 31.92, 29.71, 29.59, 29.46, 29.43, 29.35, 25.82, 22.68, 14.11. HRMS  $m/z$  calcd for  $\text{C}_{117}\text{H}_{215}\text{N}_{21}\text{O}_{28}$ ,  $[\text{M}+4\text{H}]^{4+}$  591.9092, found 591.9096.

**Dendrimer AD.** Typical isolated yields are 90%, from a white to a faint-colored foam-like solid after lyophilization;  $^1\text{H}$  NMR (400 MHz,  $\text{CDCl}_3/\text{CD}_3\text{OD}=3/2$ )  $\delta$  7.95 (s, 1H, CH), 4.56 (br, 2H,  $\text{CH}_2$ ), 3.88 (br, 2H,  $\text{CH}_2$ ), 3.82 (s, 2H,  $\text{CH}_2$ ), 3.56-3.58 (m, 6H,  $\text{CH}_2$ ), 3.46-3.48 (m, 16H,  $\text{CH}_2$ ), 3.24-3.29 (m, 20H,  $\text{CH}_2$ ), 3.06-3.08 (m, 16H,  $\text{CH}_2$ ), 2.75-2.88 (m, 34H,  $\text{CH}_2$ ), 2.61 (br, 12H,  $\text{CH}_2$ ), 2.40-2.44 (m, 32H,  $\text{CH}_2$ ), 2.15 (t, 4H,  $J = 7.2$  Hz,  $\text{CH}_2$ ), 1.56 (br, 4H,  $\text{CH}_2$ ), 1.23 (br, 56H,  $\text{CH}_2$ ), 0.85 (t, 6H,  $J = 6.6$  Hz,  $\text{CH}_3$ );  $^{13}\text{C}$  NMR (126 MHz,  $\text{CDCl}_3$ )  $\delta$  174.88, 173.56, 173.47, 172.99, 172.72, 142.97, 124.15, 70.10, 69.88, 68.99, 68.60, 52.30, 52.09, 51.92, 49.84, 49.74, 48.77, 48.60, 48.43, 48.26, 48.09, 47.92, 47.74, 41.53, 41.30, 40.63, 40.40, 38.86, 38.57, 37.15, 36.09, 33.47, 33.32, 33.13, 31.58, 29.34, 29.23, 29.07, 29.01, 25.53, 22.31, 13.54. HRMS  $m/z$  calcd for  $\text{C}_{125}\text{H}_{247}\text{N}_{37}\text{O}_{20}$ ,  $[\text{M}+4\text{H}]^{4+}$  647.9942, found 647.9947.

## **Supplementary Methods:** Isolation of primary immune cells

### **Isolation of primary CD4<sup>+</sup> T cells from human donors.**

We have standardized this technique with frozen PBMCs or fresh blood samples that were recovered using either lithium heparin or EDTA as anticoagulants. However, please be aware that the level of CD4<sup>+</sup> and HIV-1 susceptibility is varying due to different sample resources and donor-to-donor variation. Therefore, experiments conducted with different donors or sample resources (fresh *versus* frozen) should not be compared each other. Generally, we use discarded peripheral blood from anonymous, healthy adult donors for isolation of PBMCs and subsequently primary CD4<sup>+</sup> T cells cultures. Upon personal request, fresh blood samples are obtained from healthy donors at the City of Hope National Medical Center. In 24 hours of blood extraction, PBMCs are isolated from fresh blood by centrifugation through a Ficoll-Hypaque solution. Best results are obtained if the procedure is performed less than 2 hours after blood collection. Typically, the expected PBMCs yield from whole blood of healthy adult human donors are 0.8 – 3.2 million cells per mL blood. PBMCs are usually frozen right away after the Ficoll isolation and used subsequently in functional assay. However, for functional tests on frozen cells, a resting period (typically overnight) is often recommended after cell thawing.

Primary CD4<sup>+</sup> T-cell fractions are purified by negative selection using EasySep™ Human CD4<sup>+</sup> T Cell Isolation Kit (StemCell Technologies). This kit contains a combination of monoclonal antibodies in PBS and a suspension of magnetic particle, in which the untouched CD4<sup>+</sup> T cells are separated from the unwanted cells that are magnetically labeled by using an EasySep™ magnet. The desired CD4<sup>+</sup> T cells are simply poured or pipetted into a new tube and are immediately available for downstream steps. Despite donor-to-donor variations, we typically obtain purities above 95% for CD4<sup>+</sup> T cells and yields of around 25% of the raw PBMCs for CD4<sup>+</sup> T-cells.

### **Isolation of PBMCs • TIMING 1.5 h for Ficoll gradient separation**

1. Store blood tubes at room temperature prior to the isolation of PBMCs. Measure the usable whole blood volume within 0.50 mL.
2. Blood dilution: Transfer fresh blood sample from peripheral vein into a sterile 50 mL conical tube and dilute with an equal volume of PBS. Mix gently the blood and PBS.

▲ **CRITICAL** The amount of blood and number of donors depend on how many cells will be used in the assay and experimental design. It is recommended to start with at least 10 mL of

blood to ensure that enough CD4<sup>+</sup> T cells are recovered (2-3 million CD4<sup>+</sup> T cells from 10 mL of blood).

3. Density gradient cell separation: Gently add Ficoll-PAQUE plus at the bottom of a new tube without touching the side of the tube. Gently overlay the Ficoll with the diluted blood.

▲ **CRITICAL** Use 4 mL Ficoll-PAQUE plus for 6-10 mL diluted blood in a 15 mL conical tube. Use 20 mL Ficoll-PAQUE plus for 20-35 mL diluted blood in a 50 mL conical tube. Please be gentle. Allow the diluted blood to flow down the side of tube and pool on top of the density gradient media surface without breaking surface plane.

4. Gradient centrifugation: Centrifuge at 350 g for 20 min at room temperature (25 °C) with the breaks OFF.

▲ **CRITICAL** Please turn off breaks since the deceleration disrupts the density gradient. Weigh and balance precisely all the tubes.

5. PBMCs collection: Discard as much the top plasma phase (yellow) as possible through gentle aspiration with a 10 mL pipette. Collect the mononuclear cell-containing interface (white, the plasma/Ficoll interface) with a 5 mL pipette and transfer to a new sterile conical 50 mL tube.

6. PBMCs wash: Add PBS to fill up the tube, and centrifuge at 350 g for 10 min at room temperature. Remove carefully the supernatant by tilting the tube and pipetting off the supernatant without touching the pellet. Loosen the cell pellet by gentle pipetting in 1.0 mL PBS and fill the tube with PBS. Repeat PBS wash twice.

▲ **CRITICAL** To ensure the best results, minimize the time that the cells remain in a pellet or in contact with the Ficoll. Because cell pellet is loose due to red blood cells, wash the cells carefully after the Ficoll.

7. PBMCs count and viability: After the last wash, pipet off the supernatant and loosen the pellet by adding 1.0 mL PBS and gently resuspend cells with the 1.0 mL pipette. Mix 10 µL cells with 10 µL Trypan Blue Stain 0.4% and count cells in a hemocytometer. Determine the live cell concentration and the percentage of live cells.

▲ **CRITICAL** Cell viability is calculated as the number of viable cells divided by the total number of cells within the grids on the hemocytometer. If cells take up trypan blue (turn blue), they are considered non-viable. Fresh whole blood should show a fresh PBMCs yield above 0.80 million per mL whole blood and viability above 95%. Long processing time and poor technique may adversely affect the yield and viability.

■ **PAUSE POINT** The isolated PBMCs can be frozen right away after the Ficoll isolation or immediately used for CD4<sup>+</sup> T cells isolation. However, for functional tests on frozen cells, a resting period (typically overnight) is often recommended after PBMCs thawing.

**Isolation and activation of CD4<sup>+</sup> T cells** • **TIMING 0.5 h for CD4<sup>+</sup> T cell isolation, and 2-3 days for the activation of CD4<sup>+</sup> T cells.**

8. Concentrate PBMCs at 400 g for 5 min. Resuspend cells with chilled separation buffer at  $5.0 \times 10^7$  cells per mL within the volume range (0.25- 2.0 mL) in 5 mL polystyrene round-bottom tube.
9. Negative selection of CD4<sup>+</sup> T cells: Gently mix 50  $\mu$ L isolation cocktail per mL cells, and incubate the mixture at room temperature for 5 min. Vortex RapidSpheres™ for 30 seconds to evenly disperse the particles in the solution. Immediately, add RapidSpheres™ to cells (50  $\mu$ L per mL cells). Add separation buffer to top up the sample to the 2.5 mL. Mix by gently pipetting up and down 2-3 times. Place the tube (without lid) into the EasySep™ magnet and incubate at room temperature for 3 min. Finally, pick up the magnet with tube, and carefully transfer the enrich cell suspension in a new tube by simply pouring off or pipetting.
10. Activation of CD4<sup>+</sup> T cells: Remove supernatant and resuspend cell pellet in activation medium to a final concentration of 1 million cells per mL. Place cells into a 6-well plate (2.0 million per 2.0 mL medium in each well) and culture them for 2-3 days at 37 °C, under 5% CO<sub>2</sub> in a humidified atmosphere.

**HIV-1 challenge of CD4<sup>+</sup> T cells** • **TIMING 2 h for HIV-1 infection, 1 h for washing at 24 h post-infection, and totally 5 days for HIV-1 replication.**

11. Transfer the activated CD4<sup>+</sup> T cells (2.0 mL per a well of 6-well plate) from wells to 15 mL conical tubes with 5 mL pipette. Add 5 mL pre-warmed cell culture medium. Centrifuge at 400 g for 5 min at room temperature. Gently aspirate supernatant and resuspend cell pellets in 1.0 mL of IL-2 medium.
12. The activated CD4<sup>+</sup> T cells count and viability: Count cells with a hemocytometer as described. Adjust concentration to 1.0 million per mL with IL-2 medium and place cells into a 6-well plate (2.0 million per 2.0 mL medium in each well).
13. HIV-1 infection of the activated CD4<sup>+</sup> T cells: Dilute viral stocks to the desired concentration and directly add viral suspension to the cells at MOI = 0.001. Incubate plate for 24 h at 37 °C in a humidified incubator under 5% CO<sub>2</sub>.

**!CAUTION** HIV-1 is a class 3 human pathogen and all the HIV-1 related procedures (HIV-1 infection, cell transfection and samples isolation) should be handled in a BSL2/3 level facility. No Sharps and glass are allowed in BSL2/3 level facility. Suction is not allowed for BL2/3 practice. Samples for centrifugation must be prepared in the hood with screw-capped leak-proof tubes and all the tubes should be loaded in the sealed buckets inside of the hood. All liquid waste including culture medium, supernatants and other liquid waste should be collected in a proper container and decontaminated with bleach or wescodyne for 30 min.

▲ **CRITICAL** For HIV-1 challenge, both primary and lab-adapted strains can be used. We routinely assay the HIV-1 infection in parallel against an R5 HIV-1 (Bal) and an X4 HIV-1 (IIIB). The results obtained with both HIV-1 strains are generally comparable. As our previous experience, the use of a multiplicity of infection (MOI) = 0.001 of HIV-1 Bal or IIIB for 5-day infection in primary CD4<sup>+</sup> T cells regularly yields between 10<sup>5</sup>-10<sup>6</sup> pg per mL of HIV-1 p24 antigen at the peak of viral replication. A value below 10<sup>5</sup> pg per mL may not allow a good discrimination between high-efficient and low-efficient siRNA candidates, and infections producing above 10<sup>6</sup> pg per mL of HIV-1 p24 in culture supernatants may be too strong even for most high-efficient siRNA candidates.

14. Washing off free virus: At day 1 after infection, carefully transfer the HIV-1 infected CD4<sup>+</sup> T cells from wells to 15 mL conical tubes with 1.0 mL pipette. Add 5.0 mL pre-warmed cell culture medium. Centrifuge at 400 g for 5 min at room temperature and gently remove supernatant. Repeat washing step twice. After the last wash resuspend cell pellets with an equal volume of IL-2 medium. Place cells into a new 6-well plate and incubate for additional 4 days at 37 °C in a humidified incubator under 5% CO<sub>2</sub>.

▲ **CRITICAL** After centrifugation, the HIV-1-infected cells are concentrated at the bottom of the tube. For aspiration, tilt the tube and place the tips on the wall of the tube, well above the cell pellet, to avoid loss of cells.

15. Washing off free virus: At day 5 after infection, carefully transfer the HIV-1 infected CD4<sup>+</sup> T cells from wells to 15 mL conical tubes with 1.0 mL pipette. Wash cells three time with IL-2 medium.

### **Isolation of murine NK cells**

Two-month-old male C57BL/6 mice were anesthetized and decapitated. Spleen were removed and cut into small pieces and single-cell suspension was achieved in Hank's balanced salt solution (HBSS). The suspension was applied to a 70-µm cell strainer. Cells were processed

immediately for MACS MicroBead separation (Miltenyi Biotec - NK cells isolation kit II cat. No. 130-096-892). This produce has been modified by the users according to the Manufacturer's protocol. Briefly, total cells were magnetically labelled with Biotin-Antibody Cocktail MicroBeads. The cell suspension was loaded onto a MACS Column placed in the magnetic field of a MACS Separator and the negative fraction, corresponding to NK cells, was collected. Live NK cells were assessed by immunofluorescence and flow cytometry (FACS). After sorting, the purity of NK cells is about 95%. NK cells were seeded on culture dishes and used for the experiments after 24 h.

### **Isolation of human NK cells from healthy donors**

Peripheral blood mononuclear cells (PBMCs), freshly isolated by lymphoprep (Nycomed AS, Oslo, Norway) were frozen and stored at -80 °C for up to 2 months. The day before the experiment, cells were thawed and kept in culture o/n for recovering. Then, cells were sorted with NK cell subset specific antibodies (Miltenyi Biotec – human NK cells isolation kit cat. No. 130-092-657) and seeded on culture dishes. Human NK cells were used 24 h after seeding for the experiments.

### **Isolation of human PBMCs • TIMING 1.5 h for Ficoll gradient separation**

Please refer the step 1-7.

### **Dissociation of mouse spleen tissue • TIMING 10 min for tissue dissociation**

16. Collect the isolated spleen from mouse into a sterile culture dish containing ice-cold NK cell Culture medium.

17. Prepare a single-cell suspension applying pressure on the pores of a 70 µm filter (pre-wet with culture medium) with the plunger of a 1.0 mL syringe in a new culture dish.

▲ **CRITICAL** Do not allow the tissue to dry during this step, work fast and keep cells cold.

### **Magnetic isolation of murine NK cells from spleen or human NK cells from human PBMCs • TIMING 45 min for cells magnetic labeling and separation, and 1 day for cell recover.**

18. Count cell number.



▲ **CRITICAL** Generally work with  $10^8$  total cells. When working with higher cell numbers, it could create some non-specific labeling, and it is recommended to scale up all reagent volumes accordingly.

19. Centrifuge single cell suspension at 1000 g for 10 min.

20. Discard the supernatant and resuspend the cell pellet in 200  $\mu$ L of MACS buffer per  $10^8$  total cells.

21. Add 50  $\mu$ L of NK cell Biotin-Antibody Cocktail, mix well with vortex.

22. Incubate for 5 min in the dark in the refrigerator (2-8 °C).

▲ **CRITICAL** Timing and temperature of incubation with the antibody are important to avoid non-specific labeling.

23. Add 2.0 mL of MACS buffer and centrifuge the cells at 1000 g for 10 min.

24. Discard totally the supernatant and resuspend the cell pellet in 400  $\mu$ L of MACS buffer.

25. Add 100  $\mu$ L of Anti-Biotin Microbeads, mix well with vortex.

26. Incubate for an additional 10 min in the dark in the refrigerator (2-8 °C).

27. Place LS large column in the magnetic field of MACS Separator.

28. Rinsing the LS column with 3.0 mL of MACS buffer.

▲ **CRITICAL** For all the step including column, wait until the solution in the column is empty before proceeding. Do not allow the column to dry out.

29. Place a suitable collection tube under the column to collect the flow-through containing the NK cell.

30. Apply the single-cell suspension in the column.

31. Wait until the column reservoir is empty and wash the column with 3.0 mL of MACS buffer. The flow-through represent the unlabeled NK cells.

32. Centrifuge the cells 1000 g for 10 min and resuspended the cell pellet in the culture medium. Seed the cells on culture dishes appropriately.

33. Maintain the culture for 1 day before proceeding with the transfection.

### **Isolation of murine bone marrow derived macrophages (BMDM)**

Primary macrophages can be obtained from various organs of the mouse. Here, we use bone marrow, because it is the initial source of macrophages which yields large quantities of cells in all strains of mice. We recommend using young mice for better yields; with both tibias and femur of a 5-8 week-old C57BL/6 mice, we obtain  $5.0 - 7.0 \times 10^7$  monocytes. In presence of Macrophage Colony Stimulating Factor (M-CSF), monocytes differentiate into macrophages.

The cell line L929 secreted M-CSF, thus we use its culture medium as a source of M-CSF. Usually, with  $4 - 5 \times 10^6$  monocytes seeded in 10 cm Petri dish, we obtain  $8 - 10 \times 10^6$  differentiated macrophages composed of 95 – 98% cells expressing F4/80 and CD11b markers at their surface with 96 – 98% live cells.

**Preparation of L929 conditioned medium as a source of natural M-CSF for macrophage culture** ● **TIMING 21-30 days to obtain one batch of L929 conditioned medium**

34. Plate  $5 \times 10^5$  L929 cells in a T75 flask in 20 mL of BMDM base medium and incubate at 37°C in a humidified incubator under 5% CO<sub>2</sub>.

35. Split the cells every 2 or 3 days.

▲ **CRITICAL** Daily check the cell proliferation under microscope. Once reach 90% confluence, split the cells. The expanded cells can be harvested and frozen for future use.

36. Maintain and expand cells until sixteen T75 flasks. Subsequently, transfer these cells into new sixteen T175 flasks and incubate for additional 3 days in 30 mL of BMDM base medium.

37. Once the cells are confluent, replace with 50 mL of fresh BMDM base medium and incubate for another 7 days.

38. Collect ~50 mL of culture medium from each flask and store in a sterile container for further processing.

39. Meanwhile add 50 mL of fresh BMDM base medium to each flask and incubate cells at 37°C in a humidified incubator under 5% CO<sub>2</sub> for another 7 days. Typically, at least 2 batches of L929 conditioned medium can be collected from the procedures described in Step 37 and 38.

40. Filter the L929 conditioned medium collected in Step 37 and 38 through a 0.45 µM filter.

■ **PAUSE POINT** The filtered L929 conditioned medium is now ready for BMDM culture. The medium can be aliquoted (~40 mL per 50 mL conical tube) and stored at -80°C for up to 1 year.

**Isolation of mice bone marrow cells from tibia and femur** ● **TIMING 1 h**

41. Sacrifice a mouse by cervical dislocation. Harvest long bones (tibia and femur), remove muscle tissue and place the bones immediately in a 35 mm Petri dish containing DPBS-.

▲ **CRITICAL** In order to avoid contamination, from now on all the process is carried out under the tissue culture hood under sterile conditions.

42. Clean each bone using a compress (Non-Woven sterile swabs) and place them on a plate containing sterile DPBS.
43. Cut the head of each bone using a sterile scissor and flush the marrow with DMEM base medium using a 10 mL syringe fitted to a 25 G needle into a 50 mL conical tube.
44. Gently pass the bone marrow cells 3-4 times through a 18 G needle to break the lumps.
45. At the end pass the culture medium containing bone marrow cells through a cell strainer to get rid of any small piece of bone. Wash the strainer with another 5 mL of BMDM base medium.
46. Centrifuge the cells at 400 g for 5 min and discard the supernatant, resuspend the cell pellet in 1 mL of RBC lysis buffer and immediately transfer the conical tube to ice for 4 min.
47. At the end of 4 min, add 10 mL of DMEM base medium to limit the lysis reaction.
48. Meanwhile, prepare BMDM complete medium by supplementing the BMDM base medium with L929 conditioned medium 20% (vol/vol).
49. After centrifugation, discard the supernatant and resuspend the cells in 5 mL BMDM cell culture complete medium; count the cells using a Countess™ II FL Automated Cell Counter using Trypan blue as a viability dye. This cell preparation will serve as source of monocytes.
50. Seed the monocyte cells at a density of  $5.0 \times 10^6$  cells / 10 cm bacteriological plates containing 12 mL of BMDM cell culture complete medium and culture the cells at 37 °C in a humidified incubator under 5% CO<sub>2</sub>.
- ▲**CRITICAL** Use sterile bacteriological plates for culture because if you use tissue culture plates, it is impossible to recover living cells due to their strong attachment to plastic dishes.
51. On day 4, remove half of the culture medium and replace it with fresh BMDM cell culture complete medium.
- ▲**CRITICAL** Do not remove the whole volume because there is autocrine signaling in the culture, thus removal of whole culture medium may lead to poor BMDM differentiation.
52. On day 7 culture, remove medium and wash the plates gently with sterile DPBS<sup>-</sup> to remove all the serum proteins; add 2-3 mL of accutase to each Petri dish and incubate at 37 °C in a humidified incubator under 5 % CO<sub>2</sub> for 5-7 minutes.
53. Once the cells are detached, add 10 mL of DPBS<sup>-</sup> to each Petri dish and wash gently to take out all the macrophages; collect the DPBS<sup>-</sup> in a 50 mL conical tube.
54. At the end, centrifuge cells, discard the supernatant, resuspend the cells in BMDM base medium and count the cells using a Cell Counter using Trypan blue as a viability dye. The cells are now ready for further experiments.

### **Isolation and culture of primary microglial cells**

Microglial primary cultures are prepared from the brains of Wistar rat pups or C57BL/6J mouse pups at postnatal day P0 – P2 as described.<sup>4</sup> The pups are rapidly decapitated and the brain is removed from the cranium. Cells isolated from dissociated cerebral cortices are plated in culture flasks. Culture conditions enable the formation of a mixed primary glial cell culture. After 8 – 10 days, microglial cells, which are loosely adherent on the top of confluent cell culture monolayers are collected by gentle shaking and centrifugation. The cells are checked for viability and seeded on culture dishes appropriately. Typically, more than 96% of the isolated cells are positive for isolectin B4, a specific microglial marker. The average expected yield is 0.30 or 1.0 million cells per one mouse or rat brain, respectively.

#### **Dissociation of brain tissue and setting the primary glial culture • TIMING 3 h for tissue dissociation and starting the culture, and 8-10 days for the maintenance of culture**

55. Collect the isolated brains into a sterile culture dish containing ice-cold Opti-MEM and peel away the meninges. Dissected cerebral cortices, pool all tissue in a new culture dish and chop with a razor blade.

▲ **CRITICAL** Do not allow the tissue to dry during this step.

56. Add 1/10 of the final volume of trypsin solution (0.025% trypsin in HEPES; final volume 10 mL per 1 brain) to the minced tissue and transfer it to a glass bottle. Add the remaining volume of trypsin solution to the bottle and incubate at 37 °C for 20 min with vigorous swirling at 110-150 rpm.

57. Terminate the trypsinization by adding trypsin inhibitor solution (0.20 mL per brain). Swirl gently for 2 min at room temperature. Avoid excessive foaming.

58. Add the MgSO<sub>4</sub> solution (0.20 mL per brain, final concentration of MgSO<sub>4</sub> 3.0 mM) and swirl gently. Next, add the DNase solution (0.10 mL per brain, final concentration of DNase 20 µg/mL) and incubate at room temperature for 5 min with occasional swirling to digest extracellular DNA.

59. Distribute the cell suspension evenly to conical 50 mL tubes and centrifuge.

▲ **CRITICAL** Centrifuge briefly at 750 g and allow the centrifuge to decelerate without breaking. Discard the supernatant gently using the serological pipet.

60. Resuspend the pellet in HEPES (5.0 mL per 50 mL tube) supplemented with DNase solution (final concentration of DNase 20  $\mu\text{g}/\text{mL}$ ) and triturate 15-25 times to create a single cell suspension.
- ▲ **CRITICAL** This step is critical for final yield. Triturate gently using serological pipette, not pipette tips to avoid excessive cell shearing.
61. Allow settling of the non-dissociated tissue chunks for 5 min, then collect the resulting single cell suspension and transfer it to a new conical tube.
- ▲ **CRITICAL** Gently, the pellet is very loose! Remove upper ca. 4.0 mL of suspension. Use separate 50 mL conical tubes.
62. Pool the remaining pellets into one tube and add DNase solution in HEPES up to 5.0 mL of total volume. Triturate the suspension, allow it settle for 5 min as before and collect the cell suspension. Distribute it evenly to previous conical 50 mL tubes already containing 4.0 mL of the cell suspension.
63. Underlay the cell suspension with BSA solution (4.0% BSA in HEPES, 2.0 mL per tube) to form a distinct phase gradient and centrifuge the tubes (8 min, 100 g).
64. Resuspended the cell pellet in culture medium and seed at the density of  $3.0 \times 10^5$  cells/cm<sup>2</sup> on poly-L-lysine coated 75-cm<sup>2</sup> culture flasks.
- ▲ **CRITICAL** Culture flasks should be coated with poly-L-lysine for 1 h at room temperature and just before seeding of the cells, poly-L-lysine should be removed and the flask washed once with 5.0 mL of PBS. Prepare 1 flask per 1.5 mouse brain and 1 rat brain.
65. Maintain the culture for 8-10 days. Culture medium is changed after 3 days and then twice a week.

**Isolation of microglia from the primary mixed glial culture** • **TIMING 1 h for microglia isolation by gentle shaking, 30 min for cell counting and seeding**

66. After 8-10 days, microglial cells are loosely adherent on the top of confluent mixed glial cell culture monolayers. Isolate the cells by gentle shaking (1 h at 100 rpm at 37 °C) and collect by centrifugation (10 min, 90 g).
- ▲ **CRITICAL** Make sure that the centrifuge is at room temperature. Too low temperature during processing may adversely affect the yield and viability.
67. Count the number of viable cells using an automatic cell counter (eg. Nucleocounter) following the manufacturer's protocol or in the hemocytometer after trypan blue staining (follow the protocol described for Isolation of PBMC). Seed the cells on culture dishes appropriately. Microglial cultures are used for experiments 48 h after seeding.

## References

1. Liu, X.X., Zhou, J.H., Yu, T.Z., Chen, C., Cheng, Q., Sengupta, K., Huang, Y.Y., Li, H.T., Liu, C., Wang, Y., Posocco, P., Wang, M.H., Cui, Q., Giorgio, S., Fermeglia, M., Qu, F.Q., Pricl, S., Shi, Y.H., Liang, Z.C., Rocchi, P., Rossi, J.J. & Peng, L. Adaptive Amphiphilic Dendrimer-Based Nanoassemblies as Robust and Versatile siRNA Delivery Systems. *Angewandte Chemie-International Edition* **53**, 11822-11827 (2014). Doi: 10.1002/anie.201406764.
2. Garofalo, S., Coccozza, G., Porzia, A., Inghilleri, M., Raspa, M., Scavizzi, F., Aronica, E., Bernardini, G., Peng, L., Ransohoff, R.M., Santoni, A. & Limatola, C. Natural killer cells modulate motor neuron-immune cell cross talk in models of Amyotrophic Lateral Sclerosis. *Nat Commun* **11**, 1773 (2020). Doi: 10.1038/s41467-020-15644-8.
3. Ellert-Miklaszewska, A., Ochocka, N., Maleszewska, M., Ding, L., Laurini, E., Jiang, Y., Roura, A.J., Giorgio, S., Gielniewski, B., Pricl, S., Peng, L. & Kaminska, B. Efficient and innocuous delivery of small interfering RNA to microglia using an amphiphilic dendrimer nanovector. *Nanomedicine (Lond)* **14**, 2441-2458 (2019). Doi: 10.2217/nnm-2019-0176.
4. Zawadzka, M, and Kaminska, B (2005). A novel mechanism of FK506-mediated neuroprotection: downregulation of cytokine expression in glial cells. *Glia* **49**: 36-51 Doi: 10.1002/glia.20092.

### 9.3.2 Immunotoxicity of Amphiphilic dendrimers

## Amphiphilic dendrimers: A potentially nontoxic siRNA delivery agent

Arindam K Dey<sup>1,2</sup>, Flora Clément<sup>1,2,3</sup>, Ling Peng<sup>4</sup>, and Patrice N Marche<sup>2,3</sup>.

<sup>1</sup> Institute for Advanced Biosciences, Research Center Inserm U 1209 / CNRS 5309, 38700 La Tronche, France

<sup>2</sup> Université Grenoble-Alpes, 38000 Grenoble, France

<sup>3</sup> CEA, INSERM, BIG-BGE

<sup>4</sup> Aix-Marseille Université, CNRS, Center Interdisciplinaire de Nanoscience de Marseille, UMR 7325, « Equipe Labellisée Ligue Contre le Cancer », Marseille, France

This article is still under processing.

### Abstract

Dendrimers are extensively used to deliver genetic material in a wide range of cells, including primary cells. However, the positive charge of the dendrimer might persuade cytotoxicity as well as immunotoxicity by modulating different immune cells function. In this study, we used primary macrophages (M) and dendritic cells (DCs) originating from the bone marrow. We tested the modulation of their functions, including phagocytosis, cell activation, production of cytokines and mediators, and metabolic activity by positively charged amphiphilic dendrimers (ADs). Our study showed that ADs directly do not alter the production of IL-6, TNF- $\alpha$ , NO, and ROS production by M and DCs. However, direct exposure of ADs significantly increased the metabolic activity of M, but no alteration is recorded for DCs.

Interestingly, direct exposure of ADs significantly increased MCP-1 production by both M and DCs. Finally, our data provide new information describing the complex effect of ADs on the immune system. In general, while ADs can be regarded as having no significant direct impact, they may lead to discrete modifications of functions that may vary between immune cells.

**Key words:** Amphiphilic dendrimers, Immunotoxicity, Immunometabolism

## Introduction

Dendrimers are uprising polymeric nanostructured macromolecules with a well-defined structure. First discovered by Fritz Vogtle in 1978 and later by Donald Tomalia in 1980s(1,2), these macromolecules have shown their potential abilities in a lot of applications such as technology field where they can be used as sensors or contrast agents in magnetic resonance imaging. Moreover, dendrimers have shown a significant interest in biomedical field as they can be utilized in cancer treatment through improving pharmacokinetic properties of cancer drugs(3). In addition, their physical properties have shown a remarkable potential as efficient nanovectors for drug and gene delivery(4).

Dendrimers are highly tailored three-dimensional macromolecules with a globular shape. Their structure is comprised of three main parts: the inner core, end-groups also known as dendrons, and branched units linking the core and peripheral groups(4). Actually, the inner core is designated as generation 0 (G0) and the addition of another layer of branches will be G1, G2, G3 etc.(5). As the number of generations increases, the number of peripheral groups will also exponentially increase. These terminal groups can be modified so as to have various functionalities(6). In addition, the newly formed generation of dendrimer will have the double of the molecular weight of the previous generation, this can have an impact on dendrimer pharmacokinetics regarding in vivo application(7).

Amphiphilic dendrimers (ADs) are lipid/dendrimer hybrids that can undergo self-assemble in solution(8). ADs are synthesized using hydrophobic and hydrophilic chemical structures and form self-assembled nanostructures. They present a high loading capacity for large panel of molecules, including proteins nucleic acids and various hydrophobic molecules (Liu, 2015;Torre, 2019). ADs are currently used to deliver a variety of RNA interference (RNAi) molecules to silence specifically gene expression to treat disease models including cancers (9,10) . RNAi is a natural process conserved in eukaryotes that involves in gene expression regulation(11). This mechanism is mediated by small non-coding RNA molecules divided into three classes: microRNA, short interfering RNA and short hairpin RNA. These molecules bind to a specific messenger RNA thereby suppressing its translation(12). Clinical application of RNAi in gene expression related diseases requires an efficient delivery vector(13,14). Other studies on dendrimers, such as polyamidoamine (PAMAM) have also shown an efficient delivery of small interfering RNA (siRNA)(15). Owing to these biocompatible properties, dendrimers have promising therapeutic and biomedical applications including RNAi delivery(16). However, several studies have demonstrated that their use in biological systems could be limited by different challenges such as toxicity issues(17).



It is well known that dendrimer mediated toxicity is closely linked with the structure, surface charge and the generation of a particular dendrimer molecule(18). Nanoparticles (NPs) such as dendrimer have a molecular size similar to that of pathogens, this property allowing them to be uptake by the cell by mimicking the endocytosis of pathogens thus triggering the immune response through antigen presentation specifically by the help of dendritic cells (DCs) and macrophages(19). Therefore, dendrimers efficacy in the delivery of siRNA should be evaluated by understanding on how these nanoparticles target Antigen-presenting cells (APCs) but mostly the impact that it can have on cellular immune responses(20).

Antigen presenting cells (APCs) are immune cells that have the aptitude to express to their cell membrane the peptide antigen through surface markers such as Major Histocompatibility Complex (MHC) I or II(21). The antigen recognition allows then the activation of the immune response by secreting signaling factors such as pro-inflammatory cytokines(22). Hence, while considering the application of dendrimer as carrier vectors it is important to evaluate the effect not only on APCs activation but also on the cell functions involving phagocytic capacity and the ability to secrete messenger factors that play a role in immune response.

Regarding the use of dendrimer as a delivery vector, it is essential to underline that the immunometabolism of macrophages and DCs is one of the mechanisms that controls these cells on how they carry out their functions. This process pathway consists in various metabolic processes including mitochondrial metabolism and glycolysis. Normally, cellular ATP energy is produced in mitochondria, this process entails the breakdown of macromolecules such as glucose and glutamine through a chain reaction. For instance, fatty acid oxidation (FAO) and mitochondrial oxidative phosphorylation (OXPHOS) can be utilized to produce ATP in aerobic conditions whereas in hypoxia conditions ATP can then be produced through glycolysis pathway using glucose as a carbon source(23). Additionally, several studies have shown that stimulating cells by the help of antigens such as lipopolysaccharide (LPS), or interleukin-4 (IL-4) have different metabolic activities compared to unactivated cells(24,25). These observations emphasize on the fact that the use of dendrimers mediated delivery could dysregulate the overall cell metabolism hence impacting on the cellular immune response.

Here we analyzed amphiphilic dendrimer (ADs) toxicity and effect on immunometabolism in vitro in antigen presenting cells (APCs), using a macrophage cell line (J774.1A) or primary cells extracted from bone marrow: macrophages (BMDMs) and dendritic cells (BMDCs). In vivo dendrimer toxicity was also evaluated on embryonic development using White Leghorn eggs. Finally, we analyzed dendrimers as efficient siRNA delivery vectors by silencing JAK1 mRNA using BMDMs and BMDCs primary cells.

## Materials and Methods

### Cell culture

Murine macrophage cell line (J774.1A) was purchased from ATCC, cells were cultured in Dulbecco's modified Eagle's medium (DMEM) supplemented with 10% fetal bovine serum and 1% penicillin-streptomycin.

BMDCs was generated from the bone marrow extracted from C57BL/6 mice (Charles River, l'Arbresle, France). As previously described (26), cells were isolated from bone marrow by flushing from the tibia and femurs. Erythrocytes and GR1 positives cells were removed by magnetic cell sorting using Dynabeads (ThermoFisher, cat.no: 11047) after incubation with Ly-6G/ Ly-6C (BD Pharmingen, cat.no: 553125) and TER-119(BD Pharmingen, cat.no: 553672) antibodies, and the remaining negatively sorted cells were isolated using Dynabeads isolation kit (ThermoFisher, cat.no: 11047) and resuspended at  $5 \times 10^5$  cells/ml in complete Iscove's modified Dulbecco's medium (IMDM) (ThermoFisher, cat.no: 21980065) supplemented with GM-CSF (Peprotech, cat.no: 315-03), FLT-3L (Peprotech, cat.no: 250-31L) and IL-6 (Peprotech, cat.no: 216-16) according to Table 1. The transformation of the progenitors into fully active DC occurred after 10 days of culture.

BMDMs were also generated from bone marrow extracted from C57BL/6 mice. Erythrocytes were removed by RBC lysis buffer, and the remaining cells were cultured in complete DMEM (ThermoFisher, cat.no: 61965026) medium with 20% L929 conditioned medium (source of M-CSF) for 7 days.

Ovalbumin (OVA)-specific CD4<sup>+</sup> T cells were obtained from OT II Mice (Charles River Laboratories). Briefly, mouse spleen was dissociated in RPMI medium, erythrocytes were lysed using Red Blood cell lysis buffer. T cells were isolated by negative selection using Dynabeads® Untouched™ Mouse T Cell Kit (ThermoFisher, cat.no: 11413D) and resuspended in the culture medium of BMDCs.

### ADs

ADs were provided by Aix-Marseille University in the framework of NanoGlio project (Euronanomed II). ADs were synthesized via click chemistry using previously developed protocols developed by Dr. Ling Peng's team(9,27). Mean size of these particles in complete DMEM media (10 % FBS,1 % Pen-strep) is 55.5 to 58.41 nm and a zeta potential of +40 mV.

### Incubation with nanoparticles

The cells were plated either in 12, 24 or 96 wells plates from Falcon® or Seahorse XFe96 cell

culture microplates at a concentration of 106cells/mL with ADs at 1.37, 2.75, 4 µM final concentration according to the different experimental setup and these cells were cultured for 24 h LPS (Sigma, cat.no: L2654) (2 µg/mL) or IL-4 (ThermoFisher, cat.no: 14-8041-80) (20 ng/mL) was used to stimulated the cells for 24 h. The impact of ADs on BMDMs and BMDCs were later measured for various parameters, such as viability, phagocytosis, activation, cytokine secretion, nitric oxide (NO) production, reactive oxygen species (ROS) production, glycolysis or mitochondrial metabolism.

### Toxicity assessment

Different concentrations of ADs were used on cells while culturing in the in a 96 well plate for 24 h at 37°C, with 5% CO<sub>2</sub>. Cell viability was tested by CytoTox-ONE™ Homogeneous Membrane Integrity Assay (Promega, cat.no: G7891) according to the manufacturer's optimized protocol. After 24 h lysis solution (2 µl of Lysis Solution per 100 µl original volume) was used to generate a maximum LDH release as a positive control, later an equal volume of CytoTox-ONE™ Reagent (100 µL) was added to each well, and the plate was placed on a shaker for 30 seconds and then incubated for another 10 min in the dark. After that ½ of the volume of CytoTox-ONE™ Reagent (50 µL) was added to each well and the plate was placed on the shaker for another 10 seconds prior to record fluorescence with an excitation wavelength of 560 nm and an emission wavelength of 590 nm using CLARIOstar® Microplate Reader (BMG LABTECH).

### Phagocytosis assay

ADs exposed J774 cell line was incubated with FluoSpheres® Carboxylate-Modified Microspheres (ThermoFisher, cat.no: F8851), 1.0 µm in diameter, crimson fluorescent at a ratio of 10 microspheres per cell for 6 h at 37°C in 5% CO<sub>2</sub> incubator. Cells were analyzed for their fluorescence using Accuri C6 (Becton-Dickinson) and FCS Express V5 (De Novo Software).

### Cell activation

ADs exposed BMDMs and BMDCs were stimulated with 2 µg/mL Lipopolysaccharide (LPS) from E. Coli for 24 h at 37°C with 5% CO<sub>2</sub>. The supernatant was harvested for cytokine immunoassay, and cells were labelled with antibodies specific for CD11b (Ozyme, cat.no: BLE101226) and CD11c (Ozyme, cat.no: BLE117318) or CD11b (Ozyme, cat.no: BLE101216) and F4/80 (Ozyme, cat.no: BLE123152) cell surface markers of BMDCs and BMDMs respectively after blocking the Fc receptor (BD Pharmingen, cat.no: 553142) to reduce nonspecific binding. To evaluate the cell activation BMDCs and BMDMs were stained

anti-IAb (Ozyme, cat.no: BLE116410) and CD86 (Ozyme, cat.no: BLE105008) antibodies. In both the cases, live cells were selected by 7AAD (7-Aminoactinomycin D) (BD Pharmingen, cat.no: 559925) staining and analyzed by flow cytometry using LSR II (Becton-Dickinson), and the proportion of activated cells was quantified using FCS Express V5 (De Novo Software)

### Cytokine immunoassays

Cytokine production were measured in the supernatant of cell cultures using Cytometric Bead Array (CBA) (BD Pharmingen, cat.no: 552364) mouse inflammation kit against IL-6, IL-12p70, Monocyte chemoattractant protein-1 (MCP-1), Tumor necrosis factor-alpha (TNF- $\alpha$ ), Interleukin 10 (IL-10), and Interferon gamma (IFN $\gamma$ ). Results were acquired by flow cytometry using LSR II and analyzed with FCAP array software v3.0 (BD Pharmingen, cat.no: 652099).

### NO production and ROS Production

Production of NO for BMDMs and BMDCs were determined by measuring nitrite concentration in cell culture media by Griess assay, 50  $\mu$ L of cell supernatant was transferred to a 96-well plate and incubated with equal volume of Sulfanilamide (Sigma, cat.no: S9251) and N-alpha-naphthyl-ethylenediamine (NED) (Sigma, cat.no: 222488) solution respectively and were allowed to sit for 10 min each, in dark. Then the optical density (OD) was measured at 540 nm using CLARIOstar<sup>®</sup> Microplate Reader. A standard curve was used to obtain approximate concentration of nitrite in samples. Production of ROS on BMDMs and BMDCs were determined by ROS-Glo<sup>™</sup> H<sub>2</sub>O<sub>2</sub> Assay kit (Promega, cat.no: G8821). For this assay the cells were cultured at  $5 \times 10^4$  cell/mL concentration in a 96-well plate and later they were exposed to ADs and stimulated with 2  $\mu$ g/mL LPS. 6 h before the experiment, 20  $\mu$ L of H<sub>2</sub>O<sub>2</sub> substrate solution was added to each well. The plate was incubated for 20 min with 100  $\mu$ L of ROS-Glo<sup>™</sup> detection solution at 22°C before reading the luminescence using CLARIOstar<sup>®</sup> Microplate Reader.

### Metabolic flux analysis

Mature BMDCs (on Day 10) were plated ( $1.5 \times 10^5$  cells per well) in 96-well Seahorse culture plate (Agilent, cat.no: 102416-100) precoated with Cell-Tak (Corning, cat.no: 354240) in complete culture media supplemented with GM-CSF (5 ng/mL) and FLT3L (25 ng/mL). Mature BMDMs (on Day 7) were plated ( $0.8 \times 10^5$  cells per well) in 96-well Seahorse culture plate. 1 h after plating, cells were treated with ADs. After 24 h of culture, cells were washed and left unstimulated or stimulated with 1 ng/mL LPS or 20 ng/mL IL-4. After 24 h of stimulation, cells were either washed with glycostress assay medium (XF base medium (Agilent, cat.no: 103575-100) supplemented with 1 mM glutamine (Agilent, cat.no : 103579-100) or

Mitostress assay medium (XF base medium supplemented with 1 mM pyruvate (Agilent, cat.no : 103578-100), 2 mM glutamine, and 10 mM glucose (Agilent, cat.no : 103577-100)) and replenished with the same medium (180  $\mu$ L/well) and the cell culture plate was placed into a 37°C non-CO<sub>2</sub> incubator for 45 min to 1 h before the assay. Seahorse XFe96 takes measurements of the extracellular acidification rate (ECAR) and the oxygen consumption rate (OCR) every 6 to 7 min. Over the course of analysis, inhibitors were introduced to determine which parameters in metabolism were affected because of the ADs treatment by measuring the ECAR and OCR rates. The inhibitors for Mito stress assay, added in the listed order, were oligomycin (Sigma, cat.no: 75351) (1.5  $\mu$ M - inhibits the F<sub>0</sub>/F<sub>1</sub> ATPase), carbonyl cyanide-p-trifluoromethoxyphenylhydrazone (Sigma, cat.no: C2920) (1.5  $\mu$ M - an uncoupling agent), antimycin A (Sigma, cat.no: A8674) and rotenone (Sigma, cat.no: R8875) mixture (1  $\mu$ M - inhibits complex 3 and 1, respectively). In the case of Glycostress assay glucose (10 mM), Oligomycin (1.5  $\mu$ M), and 2-deoxy-D-glucose (30 mM - inhibits glycolysis) were injected sequentially. In the case of both the assay, Hoechst 33342 (ThermoFisher, cat.no: H21492) was injected at the end to normalize the data based on cell count.

#### Antigen presentation assay

ADs exposed BMDCs were stimulated with 2  $\mu$ g/mL LPS for 4 h and incubated with 25  $\mu$ g/mL OVA for additional 4 h at 37°C and 5% CO<sub>2</sub>.  $0.4 \times 10^6$  T cells (extracted from OT-II mice and resuspended in the culture medium of BMDCs) were added to  $0.1 \times 10^6$  BMDCs, at a ratio of 1 BMDCs for 4 T cells. Co-cultures were incubated for 4 days, then supernatants were harvested for cytokine immunoassays to measure IFN- $\gamma$  and IL-17 by using TH1/TH2/TH17 CBA kit (BD Pharmingen, cat.no: 560485) and IL-13 (ThermoFisher, cat.no: 88-7137-77) by ELISA.

#### Western blot Analysis:

BMDCs and BMDMs resulting from primary mouse bone marrow cells were seeded in 12 well plates at a concentration of  $10^6$  cells per well. The cells were transfected using ADs at NP ratio 10 with siJAK1 (Sense Strand sequence: GAAUAAAUGCAGUAUCUAAAU; Anti-sense strand sequence: UUAGAUACUGCAUUUUAUCGG) or siAllStars (Qiagen, cat.no: 1027281) for 48 h. 150  $\mu$ L of RIPA lysis buffer was used per well for cell lysis and further 10  $\mu$ g of protein load was used for western blot. In the western blot primary antibodies revealed the downregulation of JAK1 while  $\beta$ ACTIN was used as housekeeping gene.

### In vivo- CAM assay

Fertilized White Leghorn eggs were incubated at 37.5°C with 50% relative humidity for 9 days. At that moment (E9), the CAM was dropped down by drilling a small hole through the eggshell into the air sac, and a 1 cm<sup>2</sup> window was cut in the eggshell above the CAM. At least 20 eggs (depending on embryo surviving rate after 9 days of development, there could be more than 20 eggs per group) were used for each group. Because some deaths may occur during hours after the CAM dropping down (an invasive surgical act), data may be collected with less than 20 eggs per group (minimum of 15 eggs per group). Before the first treatment, viability of each egg is checked and surviving eggs are randomized in groups. All eggs of a group are treated with a volume of 100 µl of the working solution of compound. Embryonic viability was daily checked. The number of dead embryos was totally counted on E18. Besides, to evaluate treatment-induced embryo toxicity, the gross abnormalities on embryo (head formation, body development, limb evolution, skin aspect) and extra-embryonic structures were also estimated and recorded.

### Statistical analyses

Results are expressed as mean values ± SD. Statistical analysis was performed using Graph Pad Prism version 8.4.2 (679). Statistically significant differences were assessed by ordinary one-way ANOVA or repeated measures ANOVA with Tukey's multiple comparisons test; p-value below 0.05 was considered as statistically significant. Significance of the results is indicated according to p-values \*P ≤ 0.05; \*\*P ≤ 0.01; \*\*\*P ≤ 0.001; \*\*\*\*P ≤ 0.0001). p-values below 0.05 were considered as statistically significant.

## Results

### ADs is not correlated with cell toxicity

We first investigate whether ADs exposure is toxic *in vitro* for phagocytic cells acting as antigen presenting cells (APCs), using a macrophage cell line (J774.1A), a commonly used model to analyse internalization processes and phagocytosis(28), or primary cells derived from bone marrow: macrophages (BMDMs) and dendritic cells (BMDCs). Cells were exposed to various ADs concentrations (0-4 µM) and cell toxicity was measured by the analysis of the cell membrane integrity as a marker of cell death (Figure 1A). For all the tested cells, no increase of cell death was observed after their exposure with in increasing concentrations of ADs up to 4 µM. Three subtoxic doses (1.37,2.75 and 4 µM) were defined where cell viability remains higher than 80% after 24 h incubation for the studies of the effect of ADs on specific cell functions.

### ADs do not interfere with phagocytic capacity of J774 macrophages

J774 is a macrophage cell line commonly used as a model to analyze internalization processes and phagocytosis (28). Phagocytosis capacity of the J774 cells can be evaluated with engulfment of polystyrene microspheres (1  $\mu\text{m}$ ) coupled to a fluorochrome. The engulfment of polystyrene microspheres by the cells can be measured using flow cytometry, where the fluorescence intensity reflects the number of internalized particles (Figure 2A). After exposure to ADs, this analysis was performed and the proportion of cells in each peak of fluorescence was evaluated (Figure 2B). The numbers of the cells which have up taken 2 or 1 or no beads are not modified by the exposure to ADs. Similarly, the numbers of cells which have internalized 3, or more, beads were not altered by the exposure to 1.37  $\mu\text{M}$  of ADs, whereas the exposures to 2.75  $\mu\text{M}$  and 4  $\mu\text{M}$  led to a discrete, but significant increase of fluorescent cells (XX +- YY and XX +- YY) as compared to the unexposed cells (XX +- YY). In conclusion, ADs do not alter the phagocytic capacity macrophage cells which remained able to actively engulf exogenous materials.

### ADs has no impact on antigen presenting cells activation by LPS

The impact of ADs on APCs activation was analysed using primary non-transformed BMDCs and BMDMs that better reproduce immune cell responses *ex vivo* than cell lines. Two scenarios of ADs exposure were investigated: firstly, the direct effects to evaluate putative induction of inflammatory responses; secondly, the indirect effects to evaluate the capacity of the APCs to respond to inflammatory stimulus of LPS. Cells were analysed by flow cytometry for the expression of surface markers differentiation for BMDCs (CD11b and CD11c) and BMDMs (CD11b and F4/80) (Figure 3A). For each cell preparation, double positive cells were gated to analyse the expression of the activation makers (Figure 3B). Activation of BMDCs and BMDMs was analysed by following the expression of CD86 and MHC-II double positive cell population. Exposure to ascending concentrations of ADs increased the double positive cells of BMDCs from 28.85% to 43.74%, but we did not see any alteration in case of BMDMs (Figure 3b). These data highlight the capacity of high concentration of ADs to activate BMDCs but not BMDMs. When cells were exposed to ADs, their capacity to respond to LPS activation was maintained in the same amplitude, *i.e.* between 77.48% and 92.98% of BMDCs and 14.69 % and 10.93% for BMDMs which suggest a saturation in case of both APCs cell activation.

### ADs modify the secretions of signaling factors by APCs

Important features of APCs responses to activation is their capacity to produce different soluble factors, including signalling proteins like cytokines or chemokines and small molecular mediators like NO and ROS. To determine whether the exposure of APCs to ADs could modulate their capacity to secrete cytokines

and chemokines, the supernatants of BMDCs and BMDMs cultures were collected and quantified by ELISA for their content in pro-inflammatory cytokines (IL-6, TNF- $\alpha$ ), immuno-regulatory cytokines (IL-10, IL-12) and chemokine (MCP-1). Interestingly, ADs did not induce cytokine secretion by themselves in both unstimulated BMDCs and BMDMs (Figure 4A-B-C). After LPS stimulation, moderate cumulative effects were observed for the production of IL-6 and TNF- $\alpha$  in both BMDCs and BMDMs depending on the concentration of the ADs (Figure 4A, 4B). On the other hand, the production of IL-10 was slightly decreased in BMDCs whereas not significantly altered in BMDMs (Figure 4C). In case of both BMDCs and BMDMs, production of IL-12 remained undetectable by CBA technique (Data not shown). Altogether, these data support that ADs have low if any effect on the levels of pro inflammatory or immuno-regulatory cytokines produced by APCs.

MCP-1 is one of the essential chemokines that governs the migration and infiltration of monocyte and macrophage. MCP-1 is secreted by a variety of cells such as endothelial, fibroblasts, epithelial, smooth muscle, mesangial, astrocyte, monocytes, and microglial cells(29). Interestingly we noticed direct exposure to ADs resulted increase of MCP-1 production by both unstimulated BMDCs (Figure 4D, left) and BMDMs (Figure 4D, right).

Furthermore, when ADs exposed cells are stimulated by LPS, MCP-1 production is increased 3.46 folds by BMDCs and 8.95-fold by BMDMs at highest concentration of ADs (4 $\mu$ M).

The NO and ROS productions were evaluated in the culture supernatant of APCs cultures respectively with Griess assay or H<sub>2</sub>O<sub>2</sub> quantification. The exposure to ADs of both unstimulated APCs did not provoke the production of either NO nor ROS (figure 5A and 5B respectively). After stimulation by LPS, both APCs produced significant quantities of mediators. ADs significantly decreased NO production by BMDCs while increasing it by BMDMs (Figure 5A). ROS production was significantly increased by LPS stimulated BMDCs whereas ROS production remained unchanged in stimulated BMDMs (Figure 5B). These data indicate that BMDCs and BMDMs are differently affected by ADs in their capacity of NO and ROS productions after their activation by LPS.



### ADs influence the mitochondrial metabolism of BMDMs and not BMDCs

Cell metabolism plays a key role in different function of a particular cell type. Polarized cells display a distinct regulation of cellular metabolism, with LPS-activated proinflammatory cells undergoing a metabolic switch to enhanced glycolysis. Conversely, enhanced fatty acid oxidation (FAO) and mitochondrial oxidative phosphorylation (OXPHOS) provides sustained energy in IL-4-induced anti-inflammatory cells. To analyze the impact of ADs on mitochondrial metabolism, mito-stress testing was performed on both BMDCs and BMDMs.

The exposure to ADs showed no alterations in the basal mitochondrial respiratory capacity of unpolarized or polarized BMDCs (Figure 6A, left panel, black points), although ADs exposure significantly increased basal mitochondrial respiratory capacity of untreated or IL-4 treated BMDMs in a dose dependent effect, without showing substantial change in LPS treated BMDMs (Figure 6A, right panel, black points). We saw no variations in the proton leak in the case of BMDCs (Figure 6B, left), but the exposure of ADs increased significantly the proton leak in untreated or IL-4 treated BMDMs in a dose dependent effect, although no major changes were observed in LPS activated BMDMs (Figure 6B, right). No significant reduction in maximum respiration was observed in the case of unpolarized or polarized BMDCs (Figure 6C, left), whereas an increase in the maximum respiration capacity of untreated or IL-4 treated BMDMs was observed in a concentration-dependent manner, without significant change was observed in the case of LPS activated BMDMs (Figure 6C, right). We found that ADs did not alter ATP production by either polarized or unpolarized BMDCs (Figure 6D, left), whereas ATP production increased significantly in case of untreated or IL-4 treated BMDMs without alteration in the case of LPS treated BMDMs (Figure 6C, right). Non-mitochondrial respiratory ability wasn't altered after ADs exposure in either polarized or unpolarized BMDCs (Figure 6E, let) whereas it significantly increased the respiratory capacity of both the stimulated and unstimulated BMDMs in a concentration dependent manner (Figure 6E, right). Altogether these data revealed that ADs influence the mitochondrial metabolism of untreated or IL4 polarized BMDMs, without impacting BMDCs.

### ADs alter the glycolysis of BMDMs and not of BMDCs

Alteration of the mitochondrial metabolism by ADs leads us to investigate their effects on the glycolytic profile of APCs. In order to evaluate the different glycolytic parameters of BMDCs and BMDMs after ADs exposure, the cells were first pre-treated with different ADs concentrations, then stimulated with LPS or IL-4 or remained unstimulated for 24 hours. After stimulation, the extracellular acidification rate (ECAR) was measured. Both unpolarized or polarized BMDCs exposed to ADs did not show an increase in glycolysis

(Figure 7A, left), whereas glycolysis of BMDMs was increased in unstimulated and IL-4 cells and not in LPS polarized BMDMs (Figure 7A, right). The pre-treatment of ADs did not alter the glycolytic reserve of both polarized and non-polarized BMDCs (Figure 7B, left), but it significantly increased the concentration-dependent glycolytic reserve of all polarized BMDMs (Figure 7B, right). The combination of the results revealed that ADs alter the mitochondrial metabolism of BMDMs and not that of BMDCs.

#### ADs exposure modifies the lymphocyte T polarizing effect of BMDCs

To explore whether alteration of metabolic profile of BMDCs impairs activation of T cell response, we performed an *in vitro* model of antigen presentation. Briefly, ADs-exposed BMDCs were activated with LPS and a model antigen, OVA, were then co-cultured with lymphocytes T (L purified from the spleen of OT-II transgenic mice). OT-II mice exhibit a transgenic T cell receptor (TCR), which recognizes OVA peptide presented by the CPA on MHC-II IAb; all LT from these mice are specific to OVA. After 4 days, the supernatant of the co-cultures was collected and the cell fate of LT was evaluated according to the cytokines they have secreted: gamma interferon (IFN $\gamma$ ) is the major effector of Th1 response, IL-13 and IL-4 are involved in Th2 response and IL-17 is representative of Th17 response. These cytokine secretions were analyzed by CBA. Exposure of ADs and OVA decreased the secretion of both IFN $\gamma$  in a dose-dependent manner, but the alteration was less evident in case of IL-17 and IL-13 production by LT (Figure 8).

#### ADs are a potent siRNA delivery agent

Efficient delivery of an active siRNA to different immune cells remains challenging (30). To demonstrate the validation and application of siRNA delivery into immune cells using the ADs as a transfecting agent, we have used BMDCs and BMDMs as a model system. BMDCs and BMDMs were transfected using ADs using NP ratio 10 with JAK1 targeting siRNA for 48 h. After 48 h western blot was performed to evaluate the knockdown efficiency of ADs-mediated JAK1. Using ADs as the vector for the delivery of anti-JAK1 siRNA into primary BMDCs and BMDMs of mice, the expression of JAK1 protein was decreased to 56% for BMDCs and 80% for BMDMs with an ADs N/P ratio 10/1 (Figure 9A). Neither ADs alone or AllStars negative control siRNA/ADs complex generated any JAK1 gene silencing. The capacity in the modulation of JAK1 activity in primary inflammatory cells such as macrophages opens a new window to intervene in treatment for inflammatory diseases.

## ADs are not toxic during *in vivo* embryonic development

We then analyzed the possibility to use ADs *in vivo* to deliver siRNA. We first analyze the toxicity of the administration of siRNA loaded ADs *in vivo*. Among the *in vivo* model systems, the chorioallantoic membrane (CAM) assay has resurfaced as an adequate model system for the toxicity investigation. The chick embryos, which are in the process of development makes it a suitable model for *in vivo* toxicity assessment. To evaluate whether ADs mediated *in vivo* toxicity, fertilized White Leghorn eggs were used. Embryonic viability was checked daily. The number of dead embryos was counted on E18 and represented in the terms of percentage in figure 10A. Besides, to evaluate treatment-induced embryo toxicity, the gross abnormalities on embryo (head formation, body development, limb evolution, skin aspect) and extra-embryonic structures were also estimated and recorded (Figure 10B). Figure 10C depicts the final death ratio and a Kaplan-Meier curve are provided for all groups.

## Discussion

Dendrimers are a class of well-defined hyper branched polymers that can be used for developing antitumor system(31), biomimetic regeneration(32), drug delivery agents(33,34), contrast agent(35), vaccine development(36), delivery of nucleic acid(37) and other biomedical applications. Despite of having multifunctional potentiality in applicative fields, the use of dendrimers is still limited due to their high cytotoxicity, immunogenicity(38). In order to minimize these issues, a new amphiphilic dendrimer have been devised for different purposes specially for the efficient delivery of siRNA(9). Especially, this ADs is capable of forming small and stable siRNA nanoparticles, thus shielding the siRNA from degradation and facilitating the uptake of siRNA by cells.

APCs function screening should be subject to immunogenicity for nanoparticles as these phagocytic cells are part of the reticuloendothelial network, which is responsible for the elimination of foreign bodies(39). The process for the recognition and clearance of nanoparticles relies on the interaction between opsonins and macrophages.

Although studies record the effect of dendrimer surface chemistry (cationic, neutral and hydrophobic/lipidated) on different cell types(40), a detailed analysis of the effect of dendrimer on phagocytic cells is still lacking. The membrane affinity of the dendrimers was found to depend upon the amount of positive charges on their periphery. Increased membrane affinity was also linked to cytotoxicity as well as hindered different cellular function. The current work provides a study on the influence of ADs in three different subtoxic dosage on two primary phagocytic cells originating from mouse bone marrow, BMDCs and BMDMs on their phagocytic capacity, cytokine, redox and metabolic profiles.

Previous studies have demonstrated that positively charged dendrimer could cause cell death in RAW 264.7 murine macrophage-like cell line which was evident from the increased hypodiploid DNA population and a simultaneous decrease in diploid DNA content, indicating that DNA cleavage occurred after exposure of the cells to cationic dendrimers(41). Here we observed that BMDCs was most susceptible to ADs exposure, but none of the cells exhibited more than 20 percent cytotoxicity within the toxicity test range (0-4  $\mu$ M).

Phagocytosis is one of the key functions of APCs in order to ingest foreign material for clearance, bio-distribution and the tenuous balance between host tolerance and adverse nanotoxicity. Macrophages are demonstrated to be the most important cell type that process nanoparticles(42). It has been shown that different nanocarriers could prejudice the phagocytic capacity of macrophages(42). In the present study, we demonstrated that phagocytosis of polystyrene microspheres by macrophages was increased with increasing concentration of ADs which can be explained by high ADs-cell membrane interaction.

Accumulation of nanoparticles inside the APCs may trigger a major issue of cell activation status. Activation of both APCs can be identified by the expression of CD86 and MHC-II expression in case of BMDCs and CD86 expression in case of BMDMs. We found that high concentration of ADs activates BMDCs but do not alter their activation state upon LPS stimulation probably due to the saturation of cell activation. Interestingly, BMDMs showed a different response when treated with ADs. We found that ADs neither activate BMDMs nor alter their activation state upon LPS stimulation.

Our current study revealed that BMDCs and BMDMs responded differently when treated with ADs. It's reported that PAMAM dendrimers induce IL-6, TNF- $\alpha$  and ROS in J774.1A cell line in time dependent, PAMAM generation and concentration dependent manner(43). In our study we report that although ADs do not induce IL-6, TNF- $\alpha$  and ROS generation by themselves by both APCs but they responded differently when challenged with inflammatory signal by LPS. When ADs treated BMDMs challenged with LPS, IL-6 and TNF- $\alpha$  production increased but ROS production remain unchanged. Interestingly ADs treated BMDCs responded differently upon LPS stimulation. The alteration in IL-6 and TNF- $\alpha$  production by ADs treated LPS stimulated BMDCs was less evident while we observed an increase in ROS production. High ROS production could explain the susceptibility of BMDCs for ADs than BMDMs as reported by LDH mediated toxicity assay. Here we also highlighted that ADs did not induce any NO production by both APCs but ADs treated BMDCs produced less NO upon LPS treatment, while BMDMs showed an elevated level of NO production.

It has been reported that cationic PAMAM dendrimers entered the cell through endocytosis and were transported in endosomes and localized in mitochondria and produced ROS resulting in DNA damage and cell death(44). Accumulation of ADs in mitochondria, classically appreciated for their role as the powerhouse of the cell, introduce the issue of effect of ADs on cell metabolism. To investigate the effect of ADs on the mitochondrial metabolism and glycolysis of BMDMs and BMDCs, we exposed them to different microenvironments to stimulate differently. Such stimulated cells exhibit a distinguishable regulation of their metabolism: LPS-activated proinflammatory cells undergoing a metabolic switch to enhance glycolysis(45,46). Alternatively, IL-4 stimulated cells rely on both FAO and mitochondrial OXPHOS for sustained energy(47). Thus, altered metabolism is not only a key feature of stimulated cell function but also a prerequisite for a proper response to immune stimuli.

To analyse the effect of ADs on mitochondrial metabolism and glycolysis, mitostress and glycostress assays were performed using BMDCs and BMDMs.

We showed that although ADs were found not to alter the basal mitochondrial respiration of BMDCs they increase it for BMDMs. The possible explanation for this phenomenon is the different phagocytic capacity of these cells. Indeed it is established that the phagocytic index of BMDMs is higher than that of BMDC(48), thereby enabling accumulation of a large quantities of ADs in BMDMs, and increasing the basal respiration to meet the endogenous ATP demand of the cell.

Unaltered proton leakage in BMDCs and increased proton leak in BMDMs suggest that ROS generation is not solely governed by mitochondrial proton leak.

Measurement of ATP production showed that pre-treatment with ADs did not alter the ATP production of BMDCs but increased it in BMDMs, which is consistent with basal respiration.

The basal respiration rate does not accurately reflect the ability of cellular respiration to respond to increased energy demand. As such, estimating the maximum capacity of substrate oxidation can be extremely valuable for the discovery of mechanisms by which ADs could affect cell metabolism.

Conversely, spare respiratory capacity indicates the reserve capacity of a cell to respond to an increased ATP demand and withstand periods of stress. Here, we showed that pre-treatment with ADs did not alter the maximal and spare respiratory capacities of unstimulated and IL-4-stimulated BMDCs (cells that largely dependent on mitochondrial metabolism) but increased them significantly in unstimulated and IL-4-stimulated BMDMs. The increase in these two parameters in BMDMs can be explained by the increase in basal respiration as well as ATP production due to the increase in cellular energy demand.

We also analysed the effect of ADs on glycolysis and glycolytic capacity of BMDCs and BMDMs in case of both unstimulated and LPS stimulated cells. Our results revealed that although ADs did not alter the glycolysis and glycolytic capacity in BMDCs, it increased them in BMDMs suggesting that ADs increased the energy demand in BMDMs.

To be activated, T cells have to recognize the antigen presented by MHC-II molecules and to be stimulated by CD86 accessory molecules, which are both expressed at the surface of BMDCs, in the context of inflammatory signal. We investigated the impact of BMDCs on T cell antigen responses by the analysis of the secreted cytokines. A significant decrease of IFN- $\gamma$  was found, reflecting decreased Th1 cell polarisation while little or no alteration in IL-13, and IL-17 production suggested that ADs did not impact Th2 and Th17 cell polarization.

One of the main promising use of ADs is their capacity to deliver siRNA, and their safety profile while being incubated with primary immune cells opens a new avenue in immune-mediated inflammatory diseases (IMID) which include systemic and localized autoimmune diseases that can involve innate immunity or the adaptive immune system(49). As these diseases share similar alteration of cellular signaling, such as JAK/STAT signaling pathway, the same therapies are proposed to treat them(50,51). Conventional therapies, such as 5-aminosalicylates, corticosteroids, immunosuppressants or monoclonal antibodies, have significant side effects and fail to cure patients. In this context, it is crucial to propose new and sustainable therapeutic strategies for long-term patient care(52-55). The recent development of RNAi therapies opens the way of a more specific treatment, that could be also targeting immune cells to benefit to these IMID's patients. However, targeting these cells remains challenging, and the development of better vector is a key issue of this strategy. In this study, we demonstrated the potential of ADs as a very efficient vector of siRNA for primary immune cells targeting.

*In vitro* cytotoxicity assay gives an insight about ADs mediated cellular function modulation that we further investigated using CAM, a widely used preclinical model for toxicity as analysis. Analysis of cytotoxicity in CAM model revealed that ADs did not impose any toxicity in *in vivo* CAM model which widens the preclinical use of ADs for different purposes.

## Legends

Figure 1: Definition of sub-toxic ADs exposure of APCs. [A] Cell mortality (LDH Assay) of BMDCs, BMDMs and J774 was analysed after exposure to different concentration of ADs for 24h. Data is normalized to the untreated cells (No ADs), considering as 100% live. The results are the mean and standard deviation of 3 independent experiments.

Figure 2: Phagocytosis capacity of macrophages. [A] J774 were exposed (gray) or not (black) to 100µg/ml ADs for 24 h then incubated with fluorescent microspheres Fluospheres® for 6h, and analysed by flow cytometry. Overlaid histograms are shown. [B] After exposure to different concentrations of ADs, the proportion of cells in each peak was analysed. The results are the mean +/- SD of 3 independent experiments.

Figure 3: Expression of activation surface marker of APCs. [A] CD11b and CD11c expression of BMDCs and CD11b and F4/80 expression of BMDMs. [B] Expression of activation marker of BMDCs and BMDMs after exposure to ADs for 24 h, followed by LPS stimulation for additional 24h. Percentage of Double positive (CD86 and MHC-II) BMDCs and CD86 positive BMDMs are counted gated on CD11b and Cd11c positive cells for BMDCs and CD11b and F4/80 positive cells for BMDMs and plotted in a bar graph. The results are representative one of the three independent experiment. Results are mean +/- SD from 3 experiments.

Figure 4: Cytokine and chemokine productions by activated APCs. [A, B, C and D] Relative cytokine and chemokine concentration in the supernatant of BMDCs and BMDMs exposed to ADs and activated by LPS. Results are mean +/- SD from 5 experiments. Paired student test was performed ns  $P > 0.05$  \*  $P \leq 0.05$  \*\*  $P \leq 0.01$

Figure 5: NO and ROS productions by activated APCs. [A] Relative NO concentration in the supernatant of BMDCs and BMDMs exposed to ADs and activated by LPS [B] ROS production by BMDCs and BMDMs exposed to ADs and activated by LPS. Paired student test was performed \*  $P \leq 0.05$  \*\*  $P \leq 0.01$ .

Figure 6: Mitochondrial metabolism of activated or un activated APCs. [A] Basal respiration, [B] H+ (Proton) leak, [C] Maximal respiration Production, [D] ATP production, [E] Non-mitochondrial respiration of BMDCs and BMDMs were measured after been exposed to ADs or not for 24h and activated by LPS or IL-4 for another 24 h or not as indicated below the graphs. After measuring Oxygen consumption rate (OCR) by using Seahorse XF analyser, the data were normalized on the basis of cell number by using Hoechst 33342 staining. Results are mean +/- SD from 5 independent experiments. Paired student test was performed \*  $P \leq 0.05$  \*\*  $P \leq 0.01$  \*\*\*  $P \leq 0.001$ .

Figure 7: Glycolysis of activated or unactivated BMDCs and BMDMs. [A] Glycolysis, [B] Glycolytic reserve of BMDCs and BMDMs were evaluated after exposed to ADs or not for 24h and after activation or not by LPS or IL-4 for another 24 h, as indicated below the graphs. After measuring Extracellular acidification rate (ECAR) using Seahorse XF analyser, the data were normalized on the basis of cell number by using Hoechst 33342 staining. Results are mean +/- SD from 5 independent experiments. Paired student test was performed \*P ≤ 0.05 \*\*P ≤ 0.01 \*\*\*P ≤ 0.001.

Figure 8: Antigen specific T-cell responses. [A] OT-II T cells were co-cultured with ADs exposed/OVA loaded/LPS activated BMDCs for 4 days. T-cell cytokine production is shown. Results are mean +/- SD from 3 experiments. Paired student test was performed \*P ≤ 0.05 \*\*P ≤ 0.01 \*\*\*P ≤ 0.001 \*\*\*\*P ≤ 0.0001

Figure 9: Definition of in vivo toxicity imposed by ADs. [A] Fertilized White Leghorn Eggs were exposed to different concentration of ADs and Percentage of Dead and Surviving Embryos per Group (at the End of the Study) was recorded. [B] Representative embryo photos taken in the negative control group and the highest dose (0.25 mg/kg) treated group at the end of study (on day E18). [C] Kaplan-Meier curve showing the survival rate for all group during the study (from graft day to collection day).

Figure 10: JAK1 knockdown in BMDCs and BMDMs. Primary BMDCs and BMDMs were obtained from 5-8 weeks old C57BL/6 mice. After 11 and 7 days of BMDCs and BMDMs culture,  $1 \times 10^6$  cells per condition in 12 well plate were transfected using ADs at NP ratio 10 with siJAK1 or siAS for 48 h. Protein lysis was performed using 150 µL of RIPA lysis buffer. Western blotting was performed using 10 µg of protein load, and primary antibodies revealed the presence of JAK1 and βACTIN as housekeeping gene.

Supplementary Figure 1. ADs exposure alter mitochondrial metabolism of activated or un activated BMDMs and BMDCs. [A, B] Spare respiratory capacity and Coupling Efficiency (%). BMDCs and BMDMs exposed to ADs for 24h and activated by LPS or IL-4 for another 24 h After measuring Oxygen consumption rate (OCR) by using Seahorse XF analyser, data normalized on the basis of cell number by using Hoechst 33342 staining. Results are mean +/- SD from 5 independent experiments. Paired student test was performed \*P ≤ 0.05

## Acknowledgements

We thank Bertin Ndayishimiye for helping to build a library of published studies.



## Funding Statement

This project has received funding from the European Union's Horizon 2020 research and innovation program H2020 "NEWDEAL" (grant agreement No. 720905). AKD and FC were supported by a fellowship from H2020 NEWDEAL project.

## Disclaimer

This publication reflects only the author's view and the Commission is not responsible for any use that may be made of the information it contains.

## References

1. Tomalia, D.A., Baker, H., Dewald, J., Hall, M., Kallos, G., Martin, S., Roeck, J., Ryder, J. and Smith, P. (1985) A New Class of Polymers: Starburst-Dendritic Macromolecules. *Polymer Journal*, **17**, 117-132.
2. Buhleier, E., Wehner, W. and Voegtle, F. (1978) ChemInform Abstract: 'CASCADE'- AND 'NONSKID-CHAIN-LIKE' SYNTHESSES OF MOLECULAR CAVITY TOPOLOGIES. *Chemischer Informationsdienst*, **9**.
3. Baker, J.R., Jr. (2009) Dendrimer-based nanoparticles for cancer therapy. *Hematology Am Soc Hematol Educ Program*, 708-719.
4. Abbasi, E., Aval, S.F., Akbarzadeh, A., Milani, M., Nasrabadi, H.T., Joo, S.W., Hanifehpour, Y., Nejati-Koshki, K. and Pashaei-Asl, R. (2014) Dendrimers: synthesis, applications, and properties. *Nanoscale Res Lett*, **9**, 247-247.
5. Tomalia, D.A. and Fréchet, J.M.J.
6. Castro, R.I., Forero-Doria, O. and GuzmÁN, L. (2018) Perspectives of Dendrimer-based Nanoparticles in Cancer Therapy. *Anais da Academia Brasileira de Ciências*, **90**, 2331-2346.
7. Kaminskis, L.M., Boyd, B.J. and Porter, C.J.H. (2011) Dendrimer pharmacokinetics: the effect of size, structure and surface characteristics on ADME properties. *Nanomedicine*, **6**, 1063-1084.
8. Márquez-Miranda, V., Araya-Durán, I., Camarada, M.B., Comer, J., Valencia-Gallegos, J.A. and González-Nilo, F.D. (2016) Self-Assembly of Amphiphilic Dendrimers: The Role of Generation and Alkyl Chain Length in siRNA Interaction. *Scientific Reports*, **6**, 29436.
9. Liu, X., Zhou, J., Yu, T., Chen, C., Cheng, Q., Sengupta, K., Huang, Y., Li, H., Liu, C., Wang, Y. *et al.* (2014) Adaptive Amphiphilic Dendrimer-Based Nanoassemblies as Robust and Versatile siRNA Delivery Systems. *Angewandte Chemie International Edition*, **53**, 11822-11827.
10. Li, X., Sun, A.n., Liu, Y.-j., Zhang, W.-j., Pang, N., Cheng, S.-x. and Qi, X.-r. (2018) Amphiphilic dendrimer engineered nanocarrier systems for co-delivery of siRNA and paclitaxel to matrix metalloproteinase-rich tumors for synergistic therapy. *NPG Asia Materials*, **10**, 238-254.
11. Carthew, R.W. and Sontheimer, E.J. (2009) Origins and Mechanisms of miRNAs and siRNAs. *Cell*, **136**, 642-655.
12. Almeida, R. and Allshire, R.C. (2005) RNA silencing and genome regulation. *Trends in Cell Biology*, **15**, 251-258.
13. Xin, Y., Huang, M., Guo, W.W., Huang, Q., Zhang, L.z. and Jiang, G. (2017) Nano-based delivery of RNAi in cancer therapy. *Molecular Cancer*, **16**, 134.
14. Mroweh, M., Decaens, T., Marche, P.N., Macek Jilkova, Z. and Clement, F. (2020) Modulating the Crosstalk between the Tumor and Its Microenvironment Using RNA Interference: A Treatment Strategy for Hepatocellular Carcinoma. *Int J Mol Sci*, **21**.

15. Zhou, J., Wu, J., Hafdi, N., Behr, J.P., Erbacher, P. and Peng, L. (2006) PAMAM dendrimers for efficient siRNA delivery and potent gene silencing. *Chem Commun (Camb)*, 2362-2364.
16. Kesharwani, P., Banerjee, S., Gupta, U., Mohd Amin, M.C.I., Padhye, S., Sarkar, F.H. and Iyer, A.K. (2015) PAMAM dendrimers as promising nanocarriers for RNAi therapeutics. *Materials Today*, **18**, 565-572.
17. Duncan, R. and Izzo, L. (2005) Dendrimer biocompatibility and toxicity. *Adv Drug Deliv Rev*, **57**, 2215-2237.
18. Pryor, J.B., Harper, B.J. and Harper, S.L. (2014) Comparative toxicological assessment of PAMAM and thiophosphoryl dendrimers using embryonic zebrafish. *Int J Nanomedicine*, **9**, 1947-1956.
19. Daftarian, P., Kaifer, A.E., Li, W., Blomberg, B.B., Frasca, D., Roth, F., Chowdhury, R., Berg, E.A., Fishman, J.B., Al Sayegh, H.A. et al. (2011) Peptide-Conjugated PAMAM Dendrimer as a Universal DNA Vaccine Platform to Target Antigen-Presenting Cells. *Cancer Research*, **71**, 7452.
20. Posadas, I., Romero-Castillo, L., El Brahmi, N., Manzanares, D., Mignani, S., Majoral, J.P. and Ceña, V. (2017) Neutral high-generation phosphorus dendrimers inhibit macrophage-mediated inflammatory response in vitro and in vivo. *Proceedings of the National Academy of Sciences*, **114**, E7660.
21. Janeway, C.A. (2001) How the immune system works to protect the host from infection: A personal view. *Proceedings of the National Academy of Sciences*, **98**, 7461.
22. Banchereau, J., Briere, F., Caux, C., Davoust, J., Lebecque, S., Liu, Y.J., Pulendran, B. and Palucka, K. (2000) Immunobiology of dendritic cells. *Annu Rev Immunol*, **18**, 767-811.
23. O'Neill, L.A.J. and Pearce, E.J. (2015) Immunometabolism governs dendritic cell and macrophage function. *Journal of Experimental Medicine*, **213**, 15-23.
24. Ying, W., Cheruku, P.S., Bazer, F.W., Safe, S.H. and Zhou, B. (2013) Investigation of macrophage polarization using bone marrow derived macrophages. *Journal of visualized experiments : JoVE*, 50323.
25. Zhang, K., Zheng, J., Bian, G., Liu, L., Xue, Q., Liu, F., Yu, C., Zhang, H., Song, B., Chung, S.K. et al. (2015) Polarized Macrophages Have Distinct Roles in the Differentiation and Migration of Embryonic Spinal-cord-derived Neural Stem Cells After Grafting to Injured Sites of Spinal Cord. *Molecular Therapy*, **23**, 1077-1091.
26. Faure, M., Villiers, C.L. and Marche, P.N. (2004) Normal differentiation and functions of mouse dendritic cells derived from RAG-deficient bone marrow progenitors. *Cellular Immunology*, **228**, 8-14.
27. Cao, Y., Liu, X. and Peng, L. (2017) Molecular engineering of dendrimer nanovectors for siRNA delivery and gene silencing. *Frontiers of Chemical Science and Engineering*, **11**, 663-675.
28. Luo, Y., Cook, E., Fries, B.C. and Casadevall, A. (2006) Phagocytic efficacy of macrophage-like cells as a function of cell cycle and Fcγ receptors (FcγR) and complement receptor (CR)3 expression. *Clin Exp Immunol*, **145**, 380-387.
29. Deshmane, S.L., Kremlev, S., Amini, S. and Sawaya, B.E. (2009) Monocyte chemoattractant protein-1 (MCP-1): an overview. *J Interferon Cytokine Res*, **29**, 313-326.
30. Tatiparti, K., Sau, S., Kashaw, S.K. and Iyer, A.K. (2017) siRNA Delivery Strategies: A Comprehensive Review of Recent Developments. *Nanomaterials (Basel)*, **7**, 77.
31. Kasai, S., Nagasawa, H., Shimamura, M., Uto, Y. and Hori, H. (2002) Design and synthesis of antiangiogenic/heparin-binding arginine dendrimer mimicking the surface of endostatin. *Bioorganic & Medicinal Chemistry Letters*, **12**, 951-954.
32. Wu, D., Yang, J., Li, J., Chen, L., Tang, B., Chen, X., Wu, W. and Li, J. (2013) Hydroxyapatite-anchored dendrimer for in situ remineralization of human tooth enamel. *Biomaterials*, **34**, 5036-5047.

33. El-Sayed, M., Ginski, M., Rhodes, C. and Ghandehari, H. (2002) Transepithelial transport of poly(amidoamine) dendrimers across Caco-2 cell monolayers. *Journal of Controlled Release*, **81**, 355-365.
34. Wilbur, D.S., Pathare, P.M., Hamlin, D.K., Buhler, K.R. and Vessella, R.L. (1998) Biotin Reagents for Antibody Pretargeting. 3. Synthesis, Radioiodination, and Evaluation of Biotinylated Starburst Dendrimers. *Bioconjugate Chemistry*, **9**, 813-825.
35. Kobayashi, H., Kawamoto, S., Jo, S.-K., Bryant, H.L., Brechbiel, M.W. and Star, R.A. (2003) Macromolecular MRI Contrast Agents with Small Dendrimers: Pharmacokinetic Differences between Sizes and Cores. *Bioconjugate Chemistry*, **14**, 388-394.
36. Crespo, L., Sanclimens, G., Pons, M., Giralt, E., Royo, M. and Albericio, F. (2005) Peptide and Amide Bond-Containing Dendrimers. *Chemical Reviews*, **105**, 1663-1682.
37. Kanasty, R., Dorkin, J.R., Vegas, A. and Anderson, D. (2013) Delivery materials for siRNA therapeutics. *Nat Mater*, **12**, 967-977.
38. Madaan, K., Kumar, S., Poonia, N., Lather, V. and Pandita, D. (2014) Dendrimers in drug delivery and targeting: Drug-dendrimer interactions and toxicity issues. *J Pharm Bioallied Sci*, **6**, 139-150.
39. Fröhlich, E. (2015) Value of phagocyte function screening for immunotoxicity of nanoparticles in vivo. *Int J Nanomedicine*, **10**, 3761-3778.
40. Albertazzi, L., Serresi, M., Albanese, A. and Beltram, F. (2010) Dendrimer Internalization and Intracellular Trafficking in Living Cells. *Molecular Pharmaceutics*, **7**, 680-688.
41. Kuo, J.H., Jan, M.S. and Chiu, H.W. (2005) Mechanism of cell death induced by cationic dendrimers in RAW 264.7 murine macrophage-like cells. *J Pharm Pharmacol*, **57**, 489-495.
42. Gustafson, H.H., Holt-Casper, D., Grainger, D.W. and Ghandehari, H. (2015) Nanoparticle Uptake: The Phagocyte Problem. *Nano Today*, **10**, 487-510.
43. Naha, P.C., Davoren, M., Lyng, F.M. and Byrne, H.J. (2010) Reactive oxygen species (ROS) induced cytokine production and cytotoxicity of PAMAM dendrimers in J774A.1 cells. *Toxicology and Applied Pharmacology*, **246**, 91-99.
44. Fox, L.J., Richardson, R.M. and Briscoe, W.H. (2018) PAMAM dendrimer - cell membrane interactions. *Advances in Colloid and Interface Science*, **257**, 1-18.
45. Everts, B., Amiel, E., van der Windt, G.J., Freitas, T.C., Chott, R., Yarasheski, K.E., Pearce, E.L. and Pearce, E.J. (2012) Commitment to glycolysis sustains survival of NO-producing inflammatory dendritic cells. *Blood*, **120**, 1422-1431.
46. Van den Bossche, J., Baardman, J. and de Winther, M.P. (2015) Metabolic Characterization of Polarized M1 and M2 Bone Marrow-derived Macrophages Using Real-time Extracellular Flux Analysis. *J Vis Exp*.
47. O'Neill, L.A., Kishton, R.J. and Rathmell, J. (2016) A guide to immunometabolism for immunologists. *Nat Rev Immunol*, **16**, 553-565.
48. Kiama, S.G., Cochand, L., Karlsson, L., Nicod, L.P. and Gehr, P. (2001) Evaluation of phagocytic activity in human monocyte-derived dendritic cells. *J Aerosol Med*, **14**, 289-299.
49. Sibilia, J. (2007) Comment définir et classer les maladies inflammatoires? *Revue du Rhumatisme*, **74**, 714-725.
50. Kuek, A., Hazleman, B.L. and Ostör, A.J. (2007) Immune-mediated inflammatory diseases (IMIDs) and biologic therapy: a medical revolution. *Postgrad Med J*, **83**, 251-260.
51. David, T., Ling, S.F. and Barton, A. (2018) Genetics of immune-mediated inflammatory diseases. *Clin Exp Immunol*, **193**, 3-12.
52. Baumgart, D.C. and Sandborn, W.J. (2012) Crohn's disease. *The Lancet*, **380**, 1590-1605.
53. Baker, K.F. and Isaacs, J.D. (2018) Novel therapies for immune-mediated inflammatory diseases: What can we learn from their use in rheumatoid arthritis, spondyloarthritis, systemic lupus

- erythematosus, psoriasis, Crohn's disease and ulcerative colitis? *Annals of the Rheumatic Diseases*, **77**, 175.
54. Sandborn, W.J., Feagan, B.G., Rutgeerts, P., Hanauer, S., Colombel, J.F., Sands, B.E., Lukas, M., Fedorak, R.N., Lee, S., Bressler, B. *et al.* (2013) Vedolizumab as induction and maintenance therapy for Crohn's disease. *N Engl J Med*, **369**, 711-721.
55. Gecse, K.B., Végh, Z. and Lakatos, P.L. (2016) Optimizing biological therapy in Crohn's disease. *Expert Review of Gastroenterology & Hepatology*, **10**, 37-45.

# Figures

## Graphical abstract

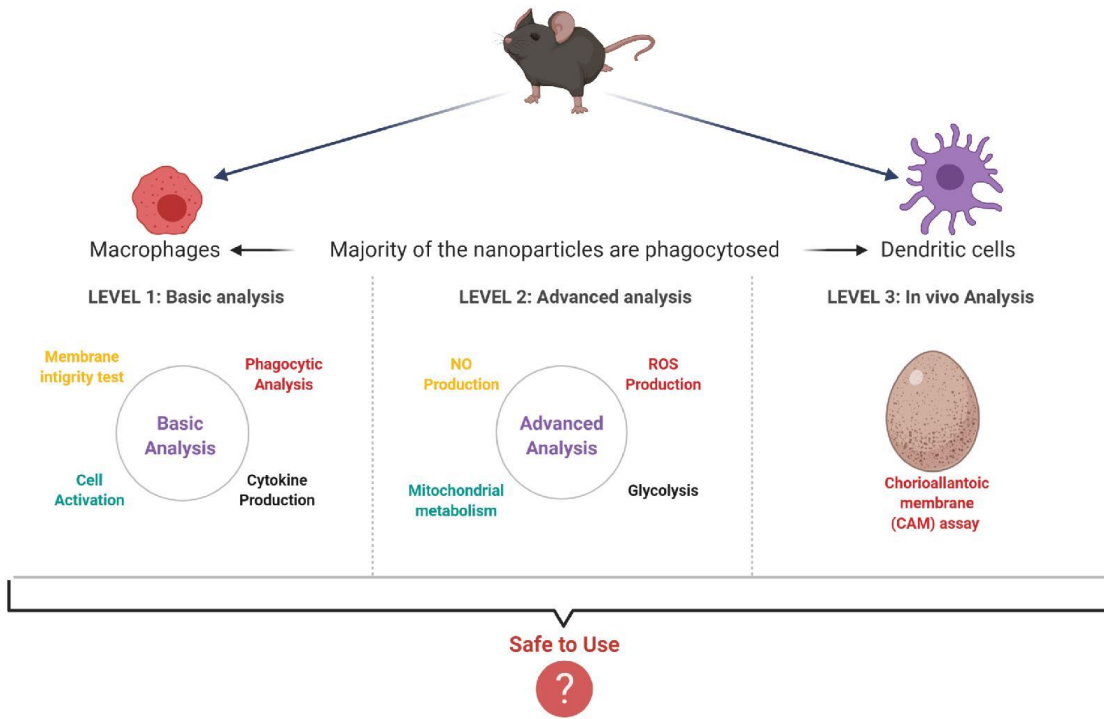


Figure 1

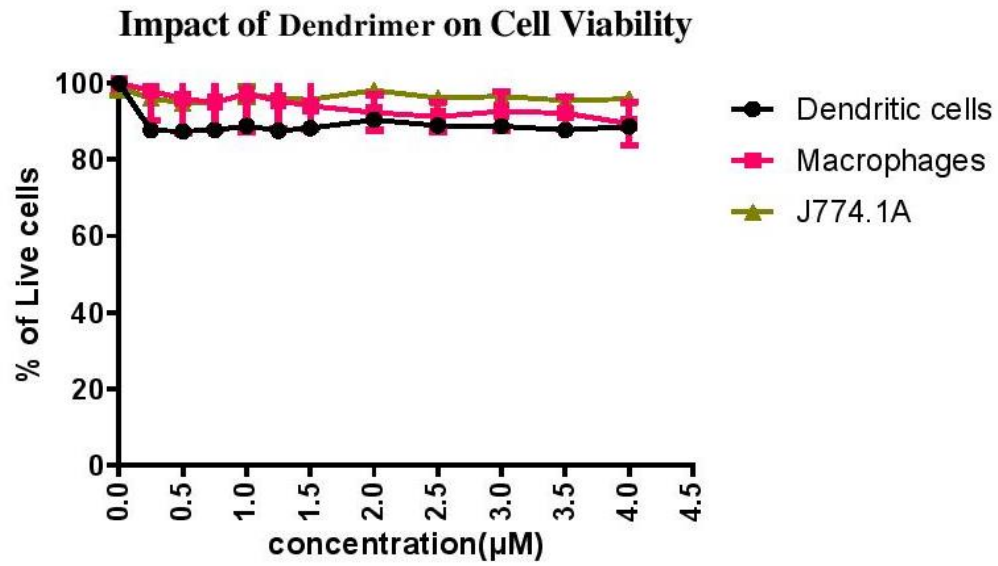


Figure 2

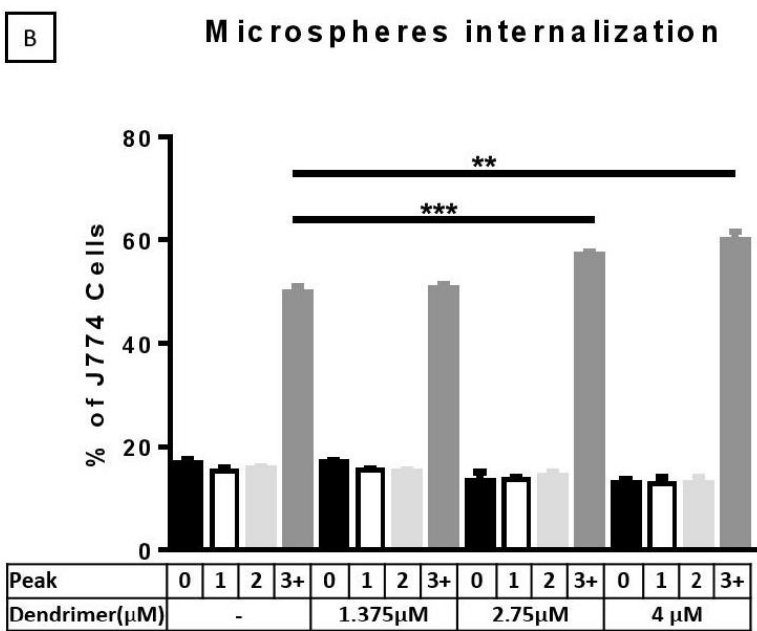
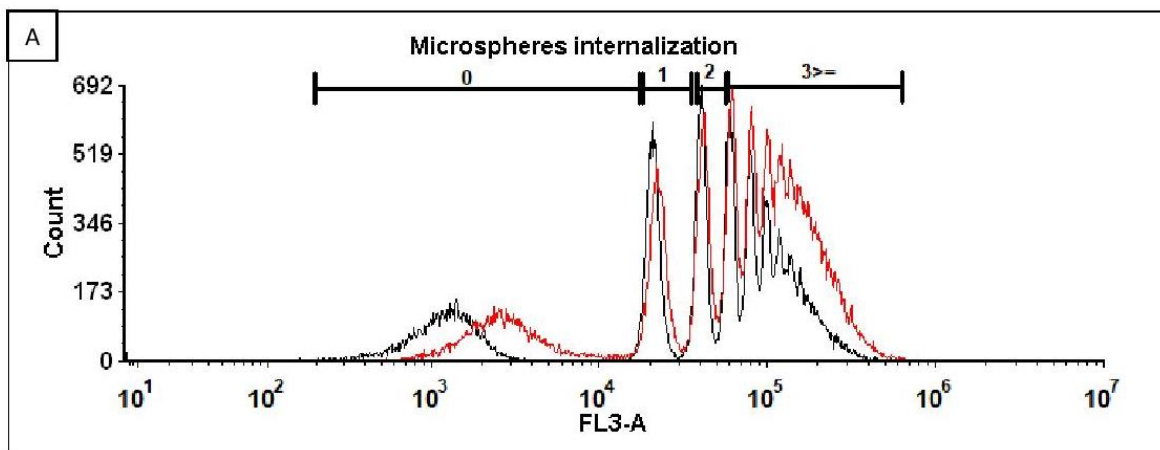


Figure 3

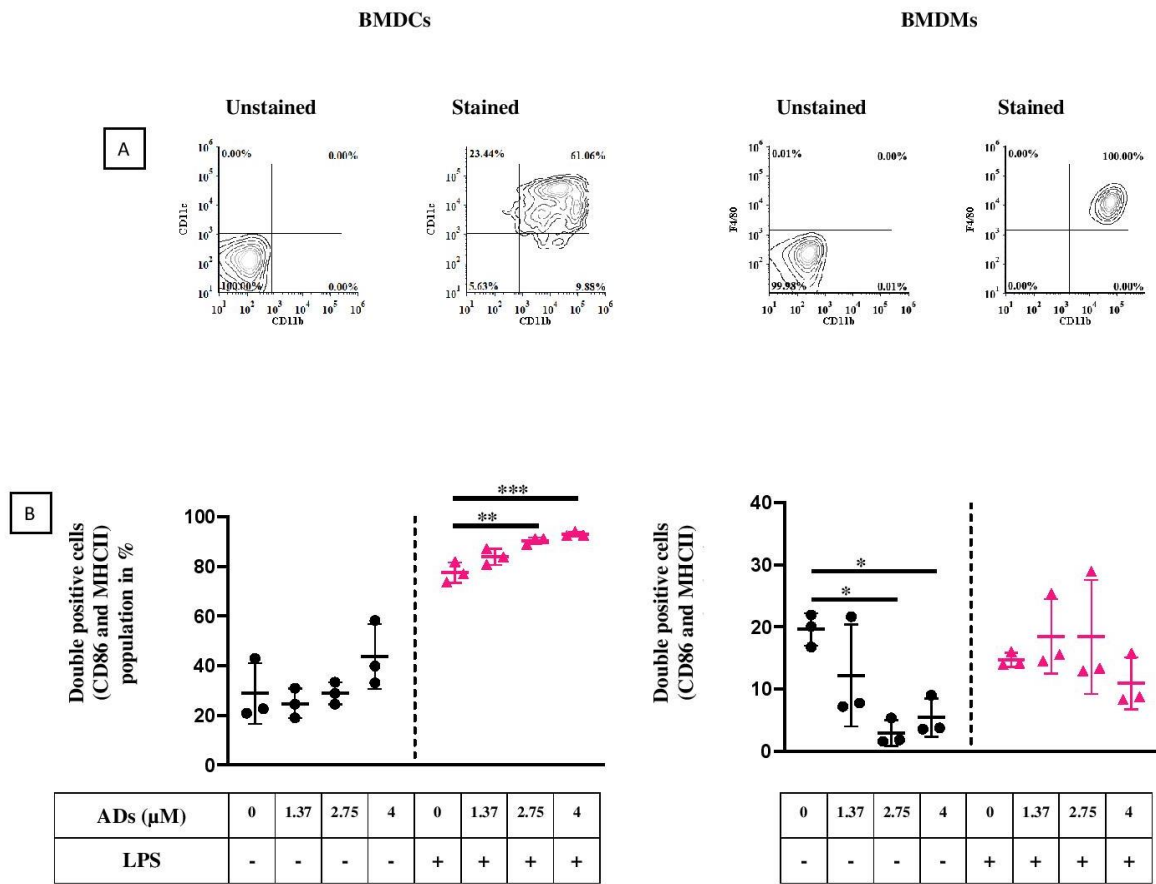




Figure 4

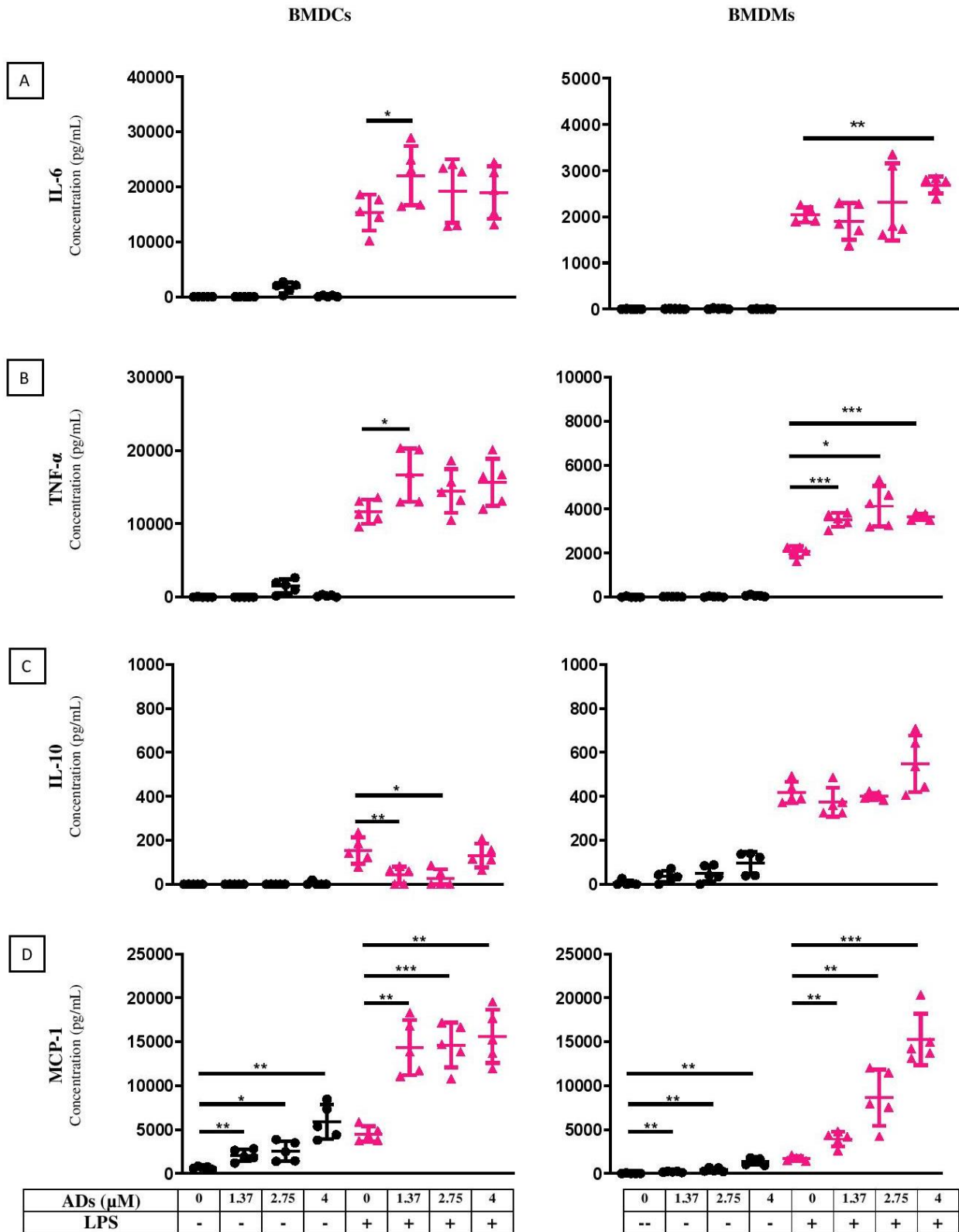


Figure 5

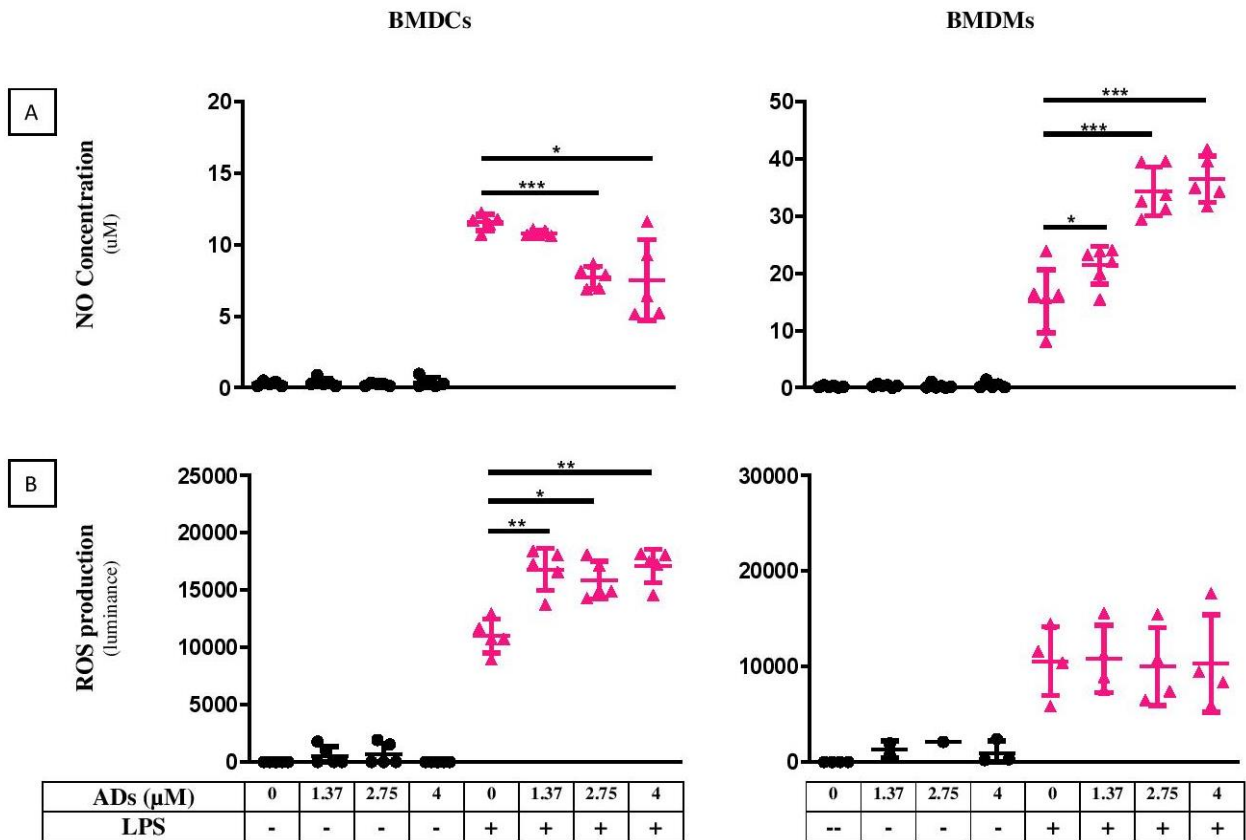


Figure 6

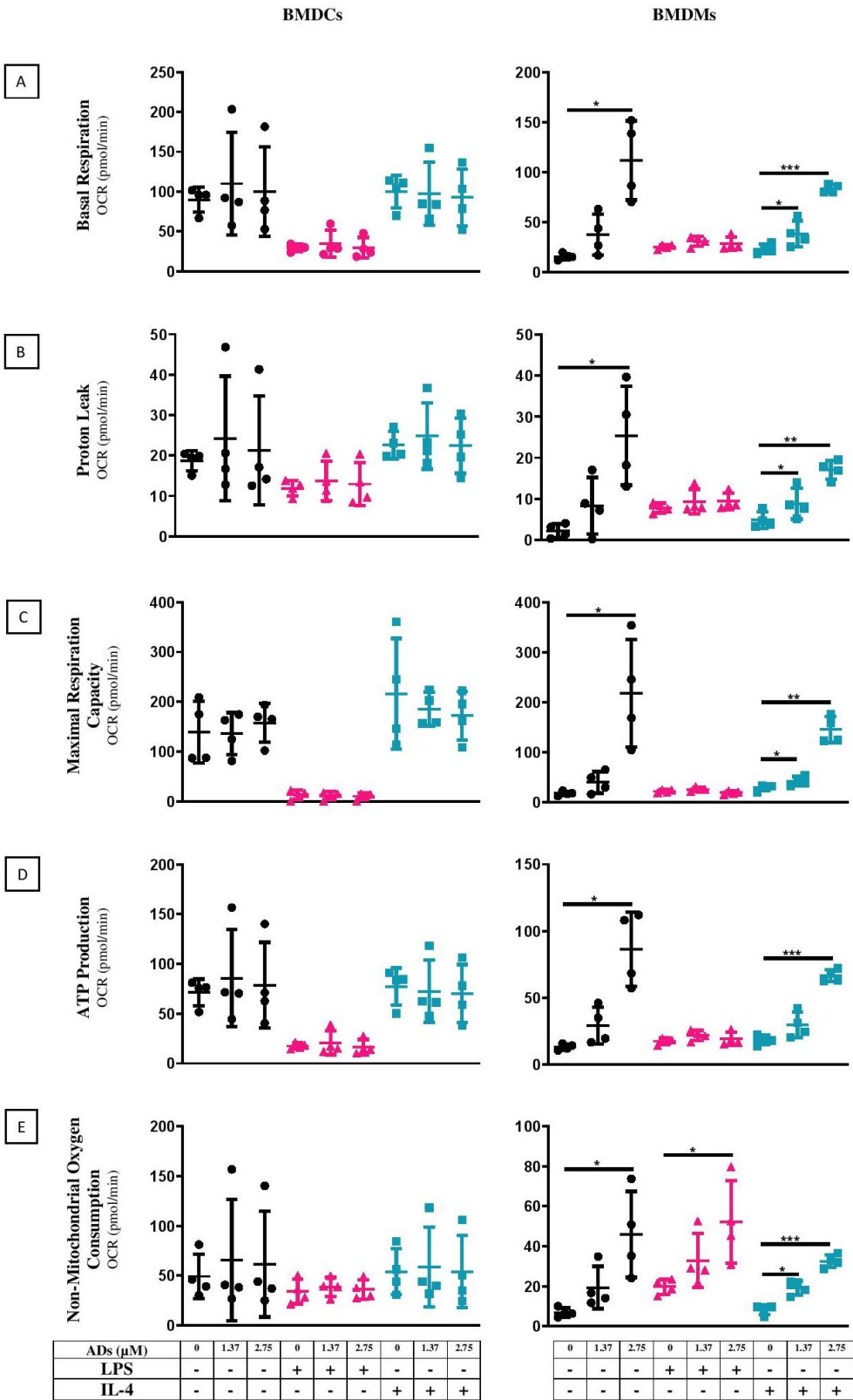


Figure 7

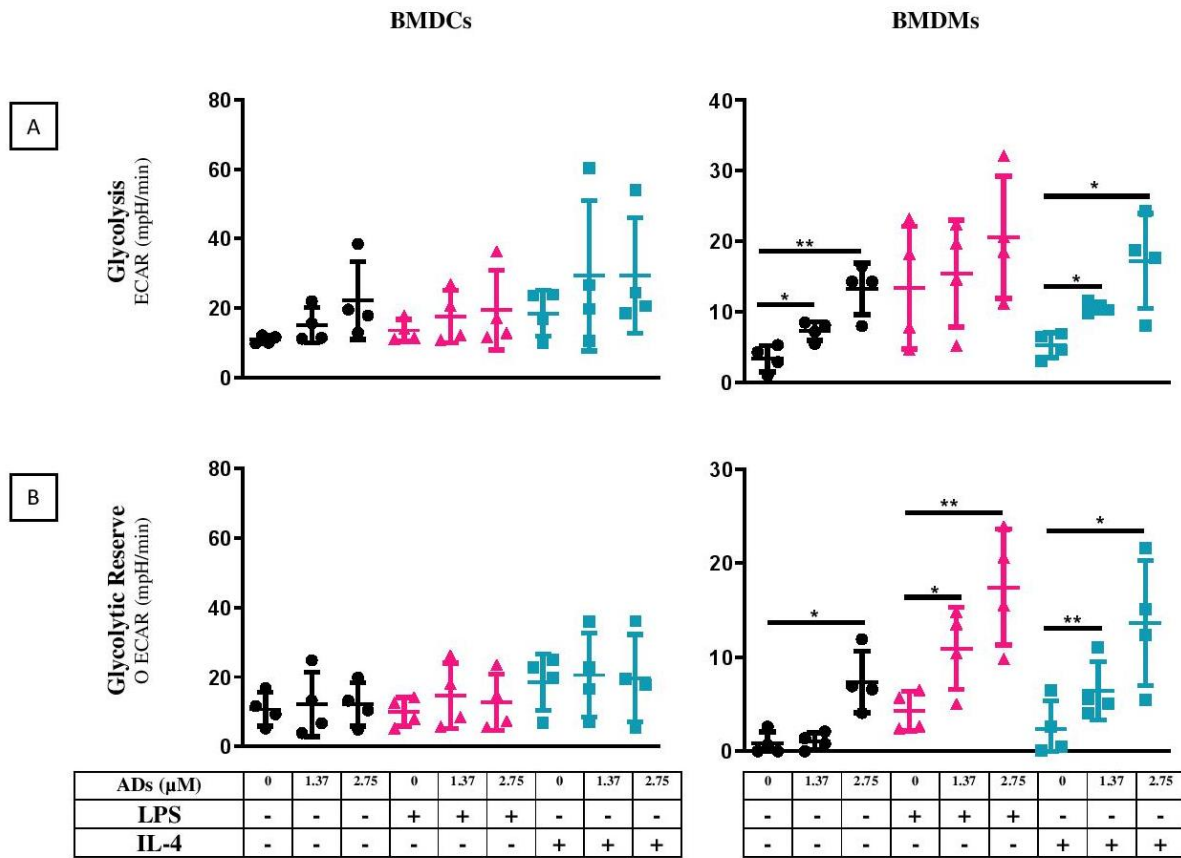


Figure 8

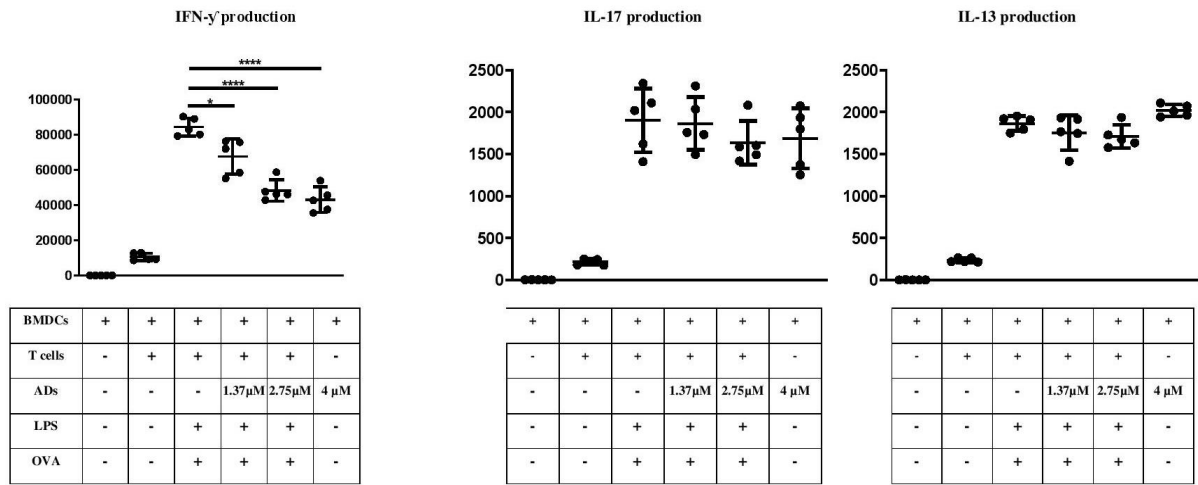


Figure 9

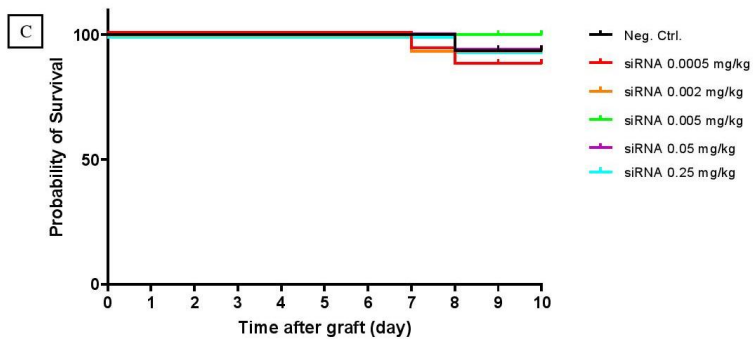
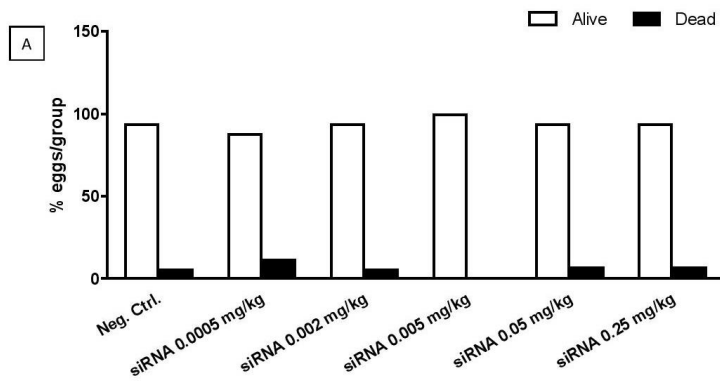
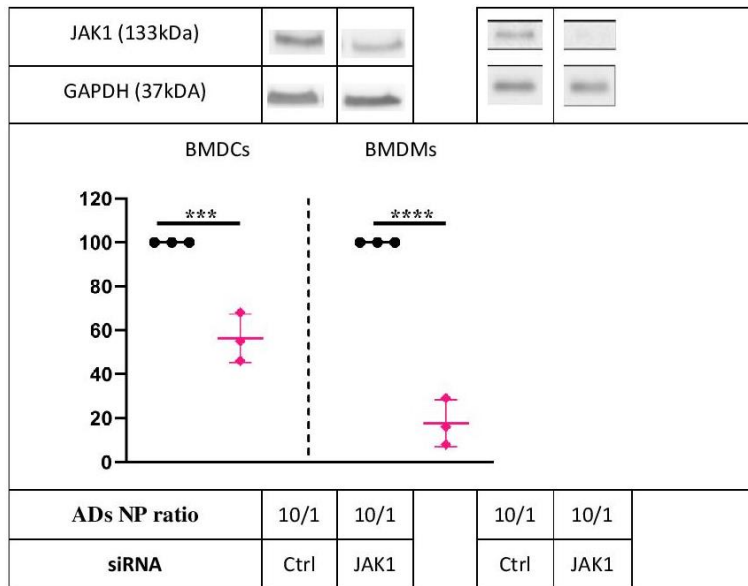
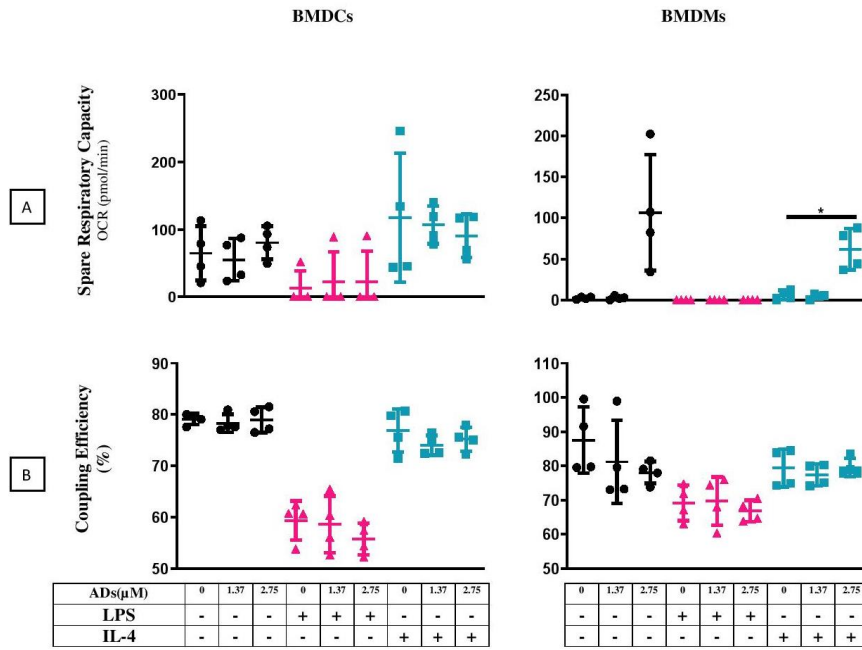


Figure 10



# Supplementary Figure

## Supplementary Figure 1





## Tables

Cells are cultured 100 mm TC-treated Cell Culture Dish with 15 mL culture media						
		Day 0	Day 3	Day 5	Day 7	Day 10
Cell Concentration		0.6 * 10 <sup>6</sup> /mL	0.5 * 10 <sup>6</sup> /mL	0.5 * 10 <sup>6</sup> /mL	0.5 * 10 <sup>6</sup> /mL	According to cell plating
Supplement	IL-6	5 ng /mL	2.5 ng /mL	2.5 ng /mL	-	-
	FLT-3	50 ng /mL	40 ng /mL	30 ng /mL	25 ng /mL	25 ng /mL
	GM-CSF	5 ng /mL				

Table 7: Concentration of GM-CSF, FLT-3L and IL-6 for BMDCs culture.

Double positive (CD86 and MHC-II) cells population in percentage ± SD				
	BMDCs		BMDMs	
	Unstimulated	LPS stimulated	Unstimulated	LPS stimulated
Cells	28.85 ± 10.02	77.48 ± 3.39	19.6 ± 2.13	14.69 ± 0.93
Cells + Den <sub>1.37</sub> uM	24.81 ± 4.87	83.82 ± 2.63	12.2 ± 6.69	18.48 ± 4.9
Cells + Den <sub>2.75</sub> uM	28.95 ± 3.59	90.36 ± 1.051	2.91 ± 1.72	18.4 ± 7.46
Cells + Den <sub>4.00</sub> uM	43.74 ± 10.61	92.98 ± 0.76	5.43 ± 2.52	10.93 ± 3.43

Table 2: Concentration of GM-CSF, FLT-3L and IL-6 for BMDCs culture.

## 10 Discussion

Nanomaterials (NMs), with sizes ranging from 0.1 to 100 nm, are comparable to many biomolecules and organelles, which enable nanomaterials to interact closely with the biological systems and thereby be used in different biomedical applications. NMs can be of different shapes and chemical compositions that significantly defy their properties such as solubility and surface chemistry, which can be engineered to make them suitable for a particular biomedical application. Furthermore, because of their size, NMs have the ability to pass through biological membranes (Clift *et al*, 2008); thus, they may be capable of influencing the physiological and biochemical functions of any cell in the body.

**Immunotoxicity** studies, such as effects on phagocytes, are the most suitable for screening for toxicological studies because these cells are involved in unspecific and specific immune responses. Furthermore, they are present at epithelial barriers, in the blood, and in almost all organs. Since the last decade, several immunotoxicological studies have focused on NMs used for biomedical purposes, such as drug delivery or imaging. However, there is still a need to enrich our knowledge about the effect of these NMs. This is required to understand their toxicological effects and explore their potential beneficial uses that may propose new therapy based on actions on the immune system, such as anti-inflammatory drugs or vaccines.

Gold is one of the first materials developed for medical applications. Indeed, gold-based NPs (AuNPs) are extensively used for several biomedical applications because of their unique optical properties, making them excellent candidates for imaging applications and as a platform for drug delivery.

Two types of organic NMs present great interest in biomedical science: Lipid NMs such as LCs and Dendrimers. On the one hand, LCs are promising multipurpose nano-agents for imaging (Navarro *et al*, 2012b), nucleic acids delivery (Hibbitts *et al*, 2019), siRNA transfection (Tezgel *et al*, 2018), drug delivery (Hinger *et al*, 2016), adjuvant and antigen delivery system (Bayon *et al.*, 2018) and probably many other applications. On the other hand, Dendrimers are broadly used for developing antitumor treatment (Kasai *et al*, 2002), biomimetic regeneration (Wu *et al*, 2013), drug delivery agents (El-Sayed *et al*, 2002; Wilbur *et al*, 1998), contrast agent (Kobayashi *et al*, 2003), vaccine development (Crespo *et al*, 2005), delivery of nucleic acid (Kanasty *et al*, 2013) and other biomedical applications.

Altogether, it is well established that different NMs represents a major stake for the future of the biomedical industry. However, the interaction of NPs with the immune system raises the question of the

biological impact of these NPs on the functions of immune cells and, thus, on possible harmful actions on health.

Cell culture experiments provide a valuable alternative to *in vivo* experiments, allowing for more regulated manipulation of cell functions and processes. Although cell lines played a crucial role in scientific progress for decades, researchers are now increasingly skeptical when interpreting data generated from cell lines only. Factors such as misrepresented and contaminated cell lines have triggered a strong interest in primary cells (ATCC, 2010; Lorsch *et al*, 2014). In our study, to be closer to the physiological conditions, we conducted our experiments on bone marrow-derived primary macrophages (**BMDMs**) and dendritic cells (**BMDCs**). This enabled us to have a closer look in different immune cells function in response to NMs and allowed us to compare between effects of NMs on two important phagocytic cells of the immune system. In this thesis, we summarized the effects of inorganic (**AuNPs**) and organic (**NLCs**, **CLCs**, and **ADs**) NMs on BMDMs and BMDCs.

In contrast to cytotoxicity, the importance of *in vitro* immunotoxicity testing is not well established. The reason is mainly because of the complexity of the immunological system that makes it difficult to extrapolate *in vitro* and animal data to human reactions in establishing NP-specific immunotoxicity. For this purpose, we have designed a panel of *ex vivo* tests to assess the impact of the different NMs on the main functions of primary phagocytic immune cells (Figure 26).

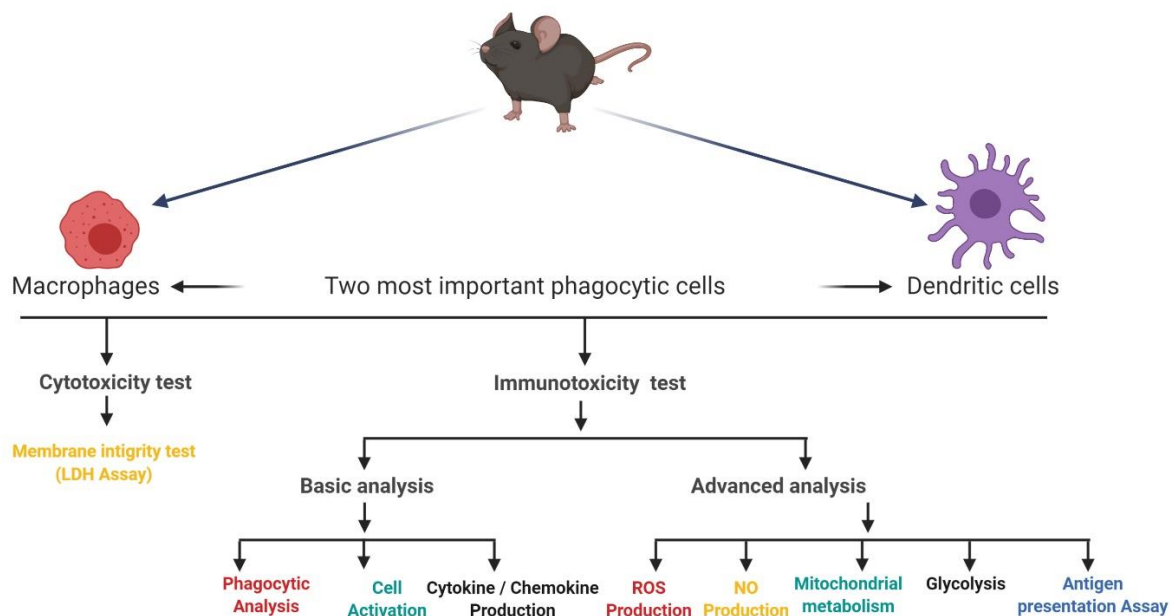


Figure 26: Panel of *ex vivo* tests assesses the impact of different NMs ( Created with BioRender.com).

Several tests are available to identify the effect of a particular molecule, such as acute toxicity, subchronic toxicity, chronic toxicity, carcinogenicity, reproductive toxicity, developmental toxicity, and dermal toxicity, ocular toxicity, neurotoxicity, genotoxicity, immunotoxicity. Before moving to immunotoxicity assays, it is essential to define the subtoxic dose of the NMs. There are several techniques available addressing the cytotoxicity. When treated with a particular molecule, living cells face one of two fates: they could either stop growing and dividing; alternatively, they could die. The most frequently used method to evaluate cell death is based on analyzing the loss of membrane integrity. We selected “**lactate dehydrogenase (LDH) assay**” as a rapid and quantitative cytotoxicity assay, which relies on the release of LDH, a stable intracellular enzyme found inside every living cell, into the surrounding extracellular space when cell membrane is disrupted. Since this is only possible when cell membrane integrity is compromised, the presence of this enzyme in the culture medium acts as an indicator of cell death marker. LDH assay of AuNPs, NLCs, CLCs, and ADs with varying concentrations revealed that BMDCs are more susceptible than BMDMs to all these NMs. Besides, we noted that the different NMs showed various levels of toxicity to macrophages (BMDMs and J774.1A) and dendritic cells (BMDCs). Finally, by this assay, we have defined the subtoxic doses for **AuNPs (10 and 50 µg/mL), NLCs (20 and 100 µg/mL), CLCs (20 and 100 µg/mL), and ADs (1.37, 2.75, and 4 µM)** to be used in further immunotoxicity assays.

After defining the subtoxic doses of each NMs, we analyzed one of the most important function, which is shared by the BMDMs and BMDCs: **phagocytosis**. Phagocytosis is a key mechanism of the immune defense system against an alien agent. It ensures the elimination of pathogens, debris, and apoptotic bodies. Phagocytosis is also necessary to capture antigens in the cellular environment. These antigens are then presented to T cells to induce an adaptive response or to guide tolerance to self (Aderem & Underhill, 1999). Previous studies have demonstrated that phagocytosis can be altered by carbon NPs, metal NPs and metal oxides (Fröhlich, 2015a). J774 is a macrophage cell line commonly used as a model to analyze internalization processes and phagocytosis (Luo et al, 2006). To define whether the NMs lead to the alteration of the phagocytic capacity, we analyzed the phagocytic capacity of J774.1A to engulf **fluorescently labeled polystyrene microspheres** after exposure to NMs. The advantage of using these microspheres is 1) they are inert to phagocytic cells, 2) their phagocytosis by cells can be easily monitored by fluorescence measurement. The data revealed that AuNPs, CLCs, and NLCs did not alter the phagocytic capacity of J774.1A cells, but AD slightly increased the phagocytic capacity only at high concentration. Thus altogether, **phagocytosis capacity of macrophage remains unaffected by the exposure to NMs**.

To investigate the effect of different NMs on the functions of BMDCs and BMDMs, we opted for two approaches. **In the first approach, we investigated the direct effect of exposure to NMs. In the second approach, we studied the indirect effect by activating the NMs exposed cells with different activators (LPS and IL-4).**

To evaluate the **direct effects** (Figure 27), we exposed BMDCs and BMDMs to NMs; then, we evaluate their fate and functions. First, we checked for effect on cell activation; for this, we analyzed the **expression of major histocompatibility class II proteins (MHC-II) and the costimulatory molecule CD86** on cell surface. The function of the MHC II molecules is to present processed antigens, derived essentially from exogenous sources to CD4 T lymphocytes. Thus, MHC-II is critical to antigen-specific immune responses. On the other hand, CD86 provides during antigen presentation costimulatory signals necessary for T cell activation and survival. Our data revealed that exposure to AuNPs, CLCs, NLCs and ADs did not yield to the activation of BMDCs. Interestingly in the case of BMDMs, we observed a drop in the number of activated cells when directly exposed to AuNPs, CLCs, and ADs, whereas NLCs did not alter the number of activated cells. This shows that although NMs did not remarkably influence the number of activated BMDCs but decreased the number of activated BMDMs.

BMDMs and BMDCs produce soluble factors to achieve some of their functions, including **cytokines and chemokines, NO and ROS**. The analysis of the cytokine productions showed that none of the NMs by themselves induced the inflammatory cytokines IL-6 and TNF- $\alpha$  production by either BMDCs or BMDMs. However, the production of MCP-1 by both BMDCs and BMDMs was significantly increased by CLCs and ADs, while AuNPs and NLCs did not. The investigation on NO production revealed that none of the NMs by themselves induced NO production by both BMDCs and BMDMs. The analysis of another important signaling molecule, ROS, showed that only lipid-based NMs, i.e., NLCs and CLCs, induced ROS production in BMDCs, whereas AuNPs and ADs did not. None of the NMs by themselves provoked ROS production by BMDMs. The main effect of NMs exposure on the production of soluble factors resides in the induction of MCP-1 chemokine.

As **immunometabolism** governs immune cell function (Mathis & Shoelson, 2011), we further investigated the effect of the NMs on BMDCs and BMDMs fate by the evaluation of their cellular metabolism based on **mitochondrial metabolism and glycolysis**. It is well known that LPS and IL-4 create different microenvironments for the cells, which affect cellular functions leading to the polarization of the BMDCs and BMDMs. LPS is known to activate classically pro-inflammatory cells that facilitate inflammation and participate in the host defense against various kinds of microbial threats. On the other hand, IL-4

dependent alternatively activated anti-inflammatory cells act as potent suppressors and controllers of ongoing immune responses. Once stimulated, BMDCs and BMDMs, exhibit a distinguishable regulation of their metabolism: LPS-activated pro-inflammatory cells undergoing a metabolic switch to enhance glycolysis (Everts *et al*, 2012a; Van den Bossche *et al*, 2015) while IL-4 stimulated anti-inflammatory cells mainly depends on Krebs' cycle and oxidative phosphorylation (Mills & O'Neill, 2016). In the case of LPS mediated metabolic reprogramming, during the early stage of activation, cells initiate an enhancement of glycolysis mediated by TBK1/IKK $\epsilon$ /Akt signaling, which is independent of mTOR/HIF1 $\alpha$ /iNOS signaling pathway and does not rely on NO (Everts *et al*, 2014a). During the late stage of LPS, mediated cell activation mTOR/HIF1 $\alpha$ /iNOS plays a crucial role in governing glycolysis in a NO-dependent manner (Amiel *et al*, 2014; Everts *et al*, 2012b). NO produced by inflammatory cells break the Krebs' cycle at two stages. The first break inhibits the SDH enzyme, responsible for converting succinate to fumarate (Jha *et al.*, 2015b). This break leads to the accumulation of succinate, which is involved in the biosynthesis of pro-inflammatory molecules such as IL-6 and prostaglandins. The second break occurs because of the transcriptional repression of isocitrate dehydrogenase (Idh), the enzyme responsible for converting isocitrate to alpha-ketoglutarate ( $\alpha$ -KG). This results in the accumulation of citrate, which takes part in fatty biosynthesis and serves as a precursor for NO and ROS (O'Neill, 2011). In turn, NO production ensures the commitment of proinflammatory cells towards glycolysis (Everts *et al.*, 2012b), thus leading to a positive loop maintaining the glycolysis fueling the inflammation. Our data about the effects of NMs exposure revealed that direct exposure to AuNPs, NLCs, CLCs, and ADs did not alter overall mitochondrial metabolism of BMDCs based on Basal respiration, proton leak, ATP production, and non-mitochondrial respiration. However, an in-depth investigation showed an indirect effect of AuNPs on **mitochondrial metabolism** of BMDCs depicted by reduced the Maximal respiration capacity (MRC), Spare respiratory capacity (SRC). The evaluation of MRC and SRC is important because MRC tells us about the maximum respiration rate that the cell can achieve in response to increased energy demand, while SRC gives insight about the ability of a cell to produce energy in stressed conditions. In other words, we can say that SRC allows a cell appropriately responding to an increased ATP demand and withstand periods of stress. Although the precise reason of AuNPs mediated MRC diminution is not known yet, additional investigations are necessary for a better understanding, including analysis of the content of mitochondria and their cristae density, the specificity of permeabilization for substrates and the respiratory chain complex activity (Divakaruni *et al*, 2014).

Further analysis of cellular metabolism showed AuNPs slightly increased the **glycolysis** of BMDCs while other NMs (NLCs, CLCs, and ADs) did not alter the glycolytic profile of these cells. Interestingly, AuNPs,

CLCs, and ADs significantly increased the mitochondrial respiration of BMDMs, whereas NLCs did not. A similar observation was noted in the case of glycolysis. Altogether, these data showed that the NMs, except for NLCs, increased by themselves the cellular energy demand of BMDMs. The possible explanation could be that exposure to NMs initiate several responses such as, MAPK/ERK pathway (Glista-Baker *et al*, 2012) and cellular stress, which require more energy to tackle the situation. This increase of the energy demand in BMDMs leads to rising their mitochondrial respiration and glycolysis.

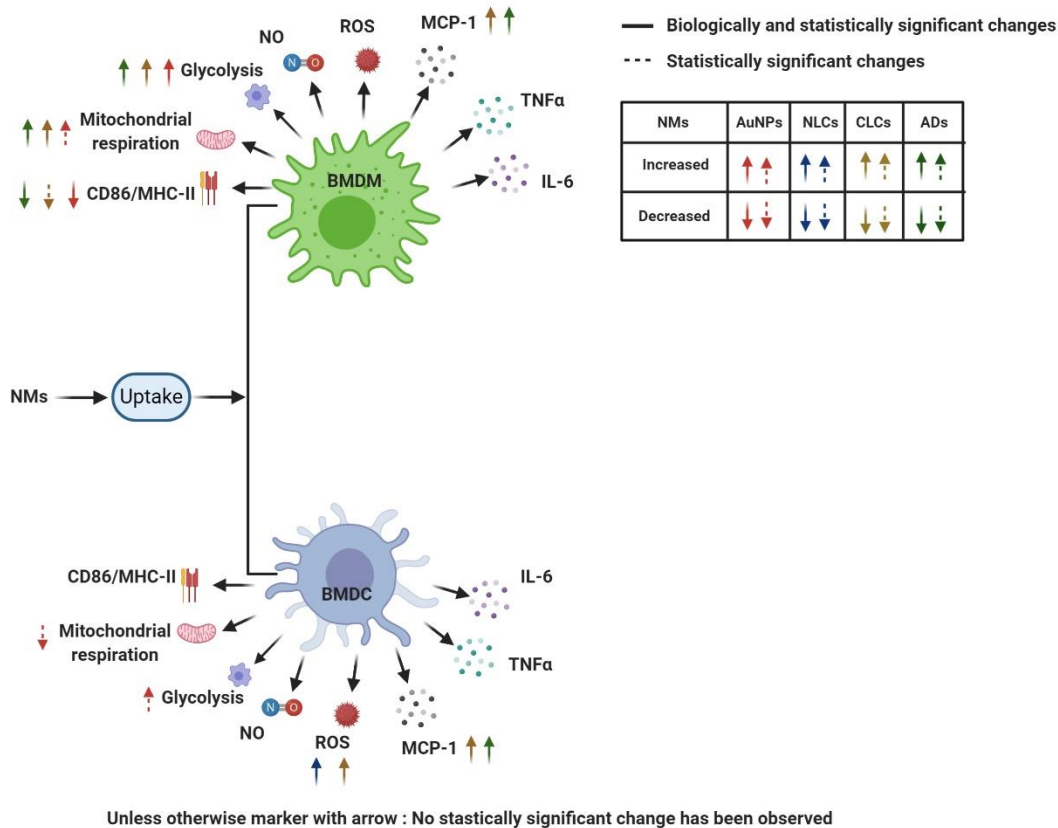


Figure 27: Evaluation of the direct effect of different NMs on APCs. BMDCs and BMDMs were cultured from mouse bone marrow for 11 and 7 days, respectively. After harvesting, the cells were seeded either in 12, 24, or 96 wells plates from Falcon® or Seahorse XFe96 cell culture with different concentrations of AuNPs (10 and or 50 µg/mL), NLCs (20 and or 100 µg/mL), CLCs (20 and or 100 µg/mL), and Ads (1.37, 2.75 and 4 µM). After 24 h of cell culture, cells were washed and remained unstimulated for another 24 h. At the end of 24 h, different downstream experiments were conducted according to the protocol.

To evaluate the **indirect effects** (Figure 28), we studied how BMDMs and BMDCs respond to a particular activation signal after NMs exposure. As phagocytes are primary responders of several immunological challenges, it is essential to understand the possible alteration of BMDCs and BMDMs function after NMs exposure. To investigate that scenario, we exposed BMDMs and BMDCs to different NMs then challenged

with LPS as a model of infection delivering an inflammatory signal. Alternatively, we used IL-4 as an activator, a well-known anti-inflammatory signal influencing the polarization state of the BMDCs and BMDMs. Activation of BMDCs with LPS revealed a significant increase in the double-positive cell population (CD86 and MHC-II positive cells), enhanced IL-6, TNF- $\alpha$ , NO, and ROS production. Activation of BMDMs with LPS showed enhanced IL-6, TNF- $\alpha$ , NO, and ROS production, except LPS, did not significantly increase the number of activated cells in BMDMs.

Investigation of LPS activation BMDCs after NMs exposure revealed that except AuNPs and ADs, none of the NMs (NLCs, CLCs, ADs) altered their activation. Although we observed a statistically significant increase in the number of activated cells in the case of AuNPs and ADs exposed BMDCs, this elevation is relatively minor, only from 74.97% to 83.37% for AuNPs and 77.48% to 92.98% for ADs. In the case of BMDMs, we observed AuNPs, NLCs, and ADs did not affect the LPS activation of the cells, but CLCs significantly increased the number of activated BMDMs. These data demonstrate that the BMDCs and BMDMs when exposed to different NMs, respond with different amplitudes to the activation by LPS. Investigation on the effect of NMs on different cytokine productions upon activation to danger signal is also necessary because of the activated cells secrete numerous signaling molecules, which directly or indirectly control cell functions. For example, IL-6 is rapidly and transiently secreted in response to infections and tissue injuries; it significantly participates in the host defense system by inducing acute inflammatory reactions, hematopoiesis, and immune responses. Another important cytokine produced in response to an inflammatory immune response is TNF- $\alpha$ , which participates in the activation of the cellular and humoral responses. An important chemokine secreted by macrophage and DCs is MCP-1, which regulates migration and infiltration of monocytes/macrophages.

Our study of LPS activated BMDCs demonstrated that ADs slightly increased the IL-6 production while other NMs (AuNPs, NLCs, and CLCs) did not. The TNF- $\alpha$  production was differently affected by NM exposures: no effect with AuNPs, a slight increase with ADs, and a significant decrease with CLCs and NLCs. On the other side, the MCP-1 production was not affected by AuNPs and NLCs but significantly increased with CLCs and ADs. These data indicate that activation of BMDCs is not correlated for all NMs with the production of cytokines such as MCP-1, IL-6, and TNF- $\alpha$ .

Interestingly, in case of LPS activated BMDMs, we noticed CLCs and ADs significantly increased the IL-6 production while AuNPs and NLCs did not. The production of TNF- $\alpha$  and MCP-1 was differently affected by NMs exposures: no effect with NLCs and a significant increase with AuNPs, CLCs, and ADs. Just like



observed for BMDCs, we found that activation of NMs exposed BMDMs is not associated with the production of different cytokines and chemokines such as IL-6, TNF- $\alpha$  and MCP-1.

Overall observation on **cytokine and chemokine** productions by NMs exposed cells revealed that MCP-1 is the most sensitive indicator of NMs exposure. Upregulation of MCP-1 production is not only related to NMs exposed BMDMs and BMDCs, since even mesothelial 2 (NRM2) cells have been shown upregulating MCP-1 production upon exposure of nickel NPs (Glista-Baker *et al.*, 2012), thus further supporting MCP-1 as an important responder to NMs exposure.

In addition to cytokines and chemokines, **NO** is an essential secretory molecule when cells are activated by LPS, a TLR4 agonist. NO also plays direct or indirect role in the production of other pro-inflammatory secretory molecules as well as cellular metabolism. TLR-mediated NO production occurs in two distinct phases. In the early phase of TLR driven activation relies on urea cycle as a major source of NO, generated from extracellular arginine, which is imported following activation (Qualls *et al.*, 2012). When extracellular arginine levels are depleted, citrulline is imported and converted to arginine to support NO production later in the late phase of activation (Qualls *et al.*, 2012). Investigation on NO production revealed that, except AuNPs, all the NMs (NLCs, CLCs, ADs) significantly downregulated NO production by LPS activated BMDCs. Notably, CLCs and ADs increased NO production in LPS activated BMDMs while AuNPs and NLCs did not.

One of the important factors closely related to NO production is the expression level of iNOS. It is well known that the ability to express iNOS greatly varies between different subsets of splenic DCs (Everts *et al.*, 2012b). Here, we hypothesize that iNOS expression level also differs between BMDCs vs. BMDMs. Different levels of iNOS expression lead to different behaviors of NMs exposed BMDCs and BMDMs in NO production.

In response to LPS, **ROS** is secreted to influence the production of pro-inflammatory cytokines such as IL-6 and TNF- $\alpha$  (Bulua *et al.*, 2011). TLR mediated cell activation leads to the initiation of PPP (Tannahill *et al.*, 2013). One of the important outcomes of PPP is NADPH. NADPH is used by NADPH oxidase to generate ROS as well as a counterbalance of ROS, which is glutathione and other antioxidants. During infection, proinflammatory cells go for rapid ROS production to clear the infectious agent, followed by the induction of antioxidants to prevent excessive tissue damage. Study of ROS production by LPS activated BMDCs depicted AuNPs significantly reduced while ADs significantly increased, and the other two NMs (CLCs and NLCs) did not alter ROS production. Investigation on BMDMs revealed all four NMs (AuNPs, NLCs, CLCs,

and ADs) did not alter the ROS production by these cells. All together, we can conclude that **NMs do not interface with the ROS production of LPS activated BMDMs.**

Experiments on **metabolic profile** showed that only exposure to AuNPs indirectly affected mitochondrial respiration of activated BMDCs by reducing MRC and SRC. The exposure to the other three NMs (NLCs, CLCs, and ADs) did not alter the mitochondrial metabolic profile of BMDCs upon activation by either LPS or IL-4. Strikingly, we noticed in case of BMDMs, all three NMs (AuNPs, CLCs, ADs) significantly enhanced mitochondria respiration of activated cells, but NLCs did not. Data on glycolytic profile of BMDCs showed only AuNPs slightly increased glycolysis in IL-4 activated BMDCs while the other three NMs (NLCs, CLCs, and ADs) did not. In the case of BMDMs, we observed all three NMs (AuNPs, CLCs, ADs) significantly increased glycolysis in activated BMDMs except NLCs. All together, we can conclude that exposure of **NMs remarkably increased energy flux in activated BMDMs.**

One of the most important functions of BMDCs is to activate the naïve **T Cell**. To be activated, T cells have to recognize the antigen under the form of a peptide presented by MHC molecules and be stimulated by CD86 accessory molecules, which are both expressed at the surface of DCs in the context of the inflammatory signal. We studied the cytokine production by T cells when activated by NMs exposed BMDCs. Different NMs showed a different effect on T cell response when NMs exposed BMDCs presented an antigen to T cells. In the case of AuNPs, we observed a significant increase of IFN- $\gamma$ , IL-13, and IL-17 productions, reflecting Th1, Th2, and Th17 cell responses, which could be correlated with the activation of the BMDCs seen by high CD86 and MHC-II expression levels. In the case of CLCs, we observed a significant decrease of IFN- $\gamma$ , IL-13, and IL-17 productions. For ADs, only IFN- $\gamma$  production is dropped, but IL-13 and IL-17 production is not or discreetly altered. **Therefore, we can conclude that the effect of all the NMs on T cell response is not universal.**

To further understand the mechanism of action of NMs on T cell responses, we need to consider several issues: 1) the direct effect of NMs on T cell response; 2) the effect of NMs on the peptide processing and antigen presentation by BMDCs. The direct effect of NMs on T cell response could be evaluated by exposing the T cells to different NMs, followed by activation with anti CD3/CD28. The effect of NMs on the antigen processing by BMDCs could be addressed in comparing T cell responses obtained with whole OVA protein with those obtained with already processed OVA antigenic peptides.

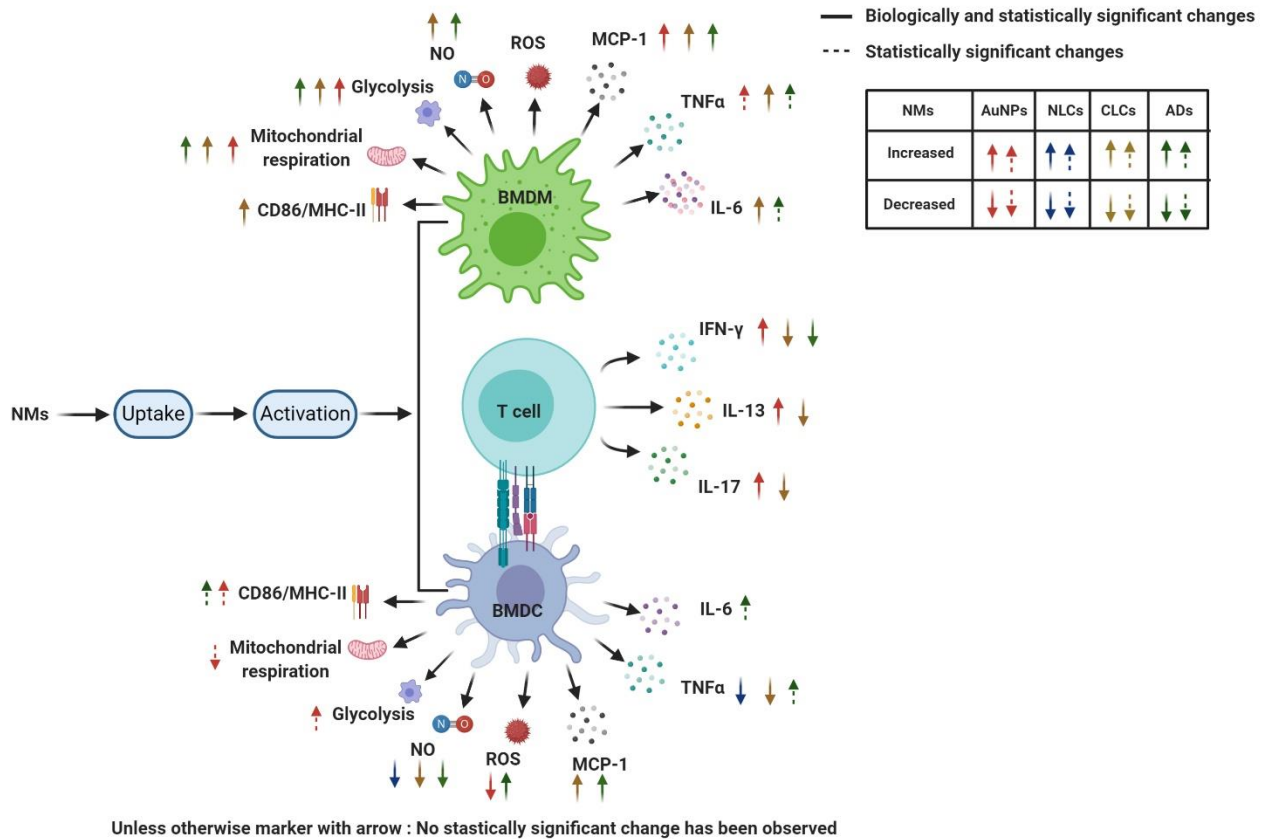


Figure 28: Evaluation of the indirect effect of different NMs on APCs. BMDCs and BMDMs were cultured from mouse bone marrow for 11 and 7 days, respectively. After harvesting, the cells were seeded either in 12, 24, or 96 wells plates from Falcon® or Seahorse XFe96 cell culture with different concentrations of AuNPs (10 and or 50 µg/mL), NLCs (20 and or 100 µg/mL), CLCs (20 and or 100 µg/mL), and Ads (1.37, 2.75 and 4 µM). After 24 h of cell culture, cells were washed and stimulated with LPS or IL-4 for another 24 h. At the end of 24 h, different downstream experiments were conducted according to the protocol.

Indirect effect of NMs on the production of secretory molecules by BMDCs				
	AuNPs	NLCs	CLCs	ADs
IL-6	0	0	0	+1
TNF- $\alpha$	0	-1	-2	+1
MCP-1	0	0	+2	+2
NO	0	-2	-2	-2
ROS	-2	0	0	+2
Total Score	-2	-3	+2	+4

Table 8: Changes in different secretory molecule production by NMs exposed BMDCs after 24 h of LPS stimulation. IL-6, TNF- $\alpha$ , MCP-1, NO and ROS are key proinflammatory molecules produced after TLR mediated cell activation. In the table. Alteration in different proinflammatory molecule production is recorded accordingly: minor increase ( $p > 0.05$ ) = +1, major increase ( $p \leq 0.05$ ) = +2, minor decrease ( $p > 0.05$ ) = -1, major decrease ( $p \leq 0.05$ ) = -2

Indirect effect of NMs on the production of secretory molecules by BMDMs				
	AuNPs	NLCs	CLCs	ADs
IL-6	0	0	+2	+1
TNF- $\alpha$	+1	0	-2	+2
MCP-1	+2	0	+2	+2
NO	0	0	+2	+2
ROS	0	0	0	0
Total Score	+3	0	+4	+7

Table 9 : Changes in different secretory molecule production by NMs exposed BMDMs after 24 h of LPS stimulation. IL-6, TNF- $\alpha$ , MCP-1, NO and ROS are key proinflammatory molecules produced after TLR mediated cell activation. Alteration in different proinflammatory molecule production is recorded accordingly: minor increase ( $p > 0.05$ ) = +1, major increase ( $p \leq 0.05$ ) = +2, minor decrease ( $p > 0.05$ ) = -1, major decrease ( $p \leq 0.05$ ) = -2.

The effects of NMs exposure on cell response to LPS are summarized in Table 8 for BMDCs and in Table 9 for BMDMs. During the analysis, we noticed, in many cases, NMs mediated alteration is statistically significant, but the amplitude of alteration is low. In other cases, we observed a major alteration of

different secretory molecule production. To better understand the indirect effect of NMs on BMDCs and BMDMs, alteration in the production of secretory molecules by these cells is scored in the form of numerical values. Scoring is mainly based on the p-value. A minor increase ( $p > 0.05$ ) is scored as +1, major increase ( $p \leq 0.05$ ) is scored as +2, minor decrease ( $p > 0.05$ ) is scored as -1, major decrease ( $p \leq 0.05$ ) is scored as -2. In the end, an overall score is calculated; a positive score indicates an overall increase of pro-inflammatory molecule production, while a negative score indicates a reduction of pro-inflammatory molecule production. This score helps us to understand the pro-inflammatory or anti-inflammatory effects of NMs.

From Table 8, Table 9, we noticed that positively charged CLCs (+45.8 mV) and ADs (+35.9mV) exposed BMDCs and BMDMs remarkably show an increased overall score of pro-inflammatory molecule production than AuNPs (+19.573mV) and NLCs (-16.7mV). This score suggests that positively charged NMs promote proinflammatory behavior of BMDCs and BMDMs upon infection. Altogether, the data of secretory molecule production and cell metabolism showed BMDMs upon activation (LPS or IL4) remarkably enhanced IL-6, TNF- $\alpha$ , MCP-1, NO, Glycolysis, and Mitochondrial activity by positively charged CLCs and ADs. This observation leads us to hypothesize that the positive charge of CLCs and ADs is responsible for enhancing different functions in BMDMs. To establish our hypothesis, we used CLCs as a representative of positively charged NMs and reversed the charge of CLCs by combining with negatively charged siRNA. Our experiments showed that by reversing the charge, we could reverse the effect of positively charged CLCs on IL-6, TNF- $\alpha$ , MCP-1, and NO production as well as cellular metabolism (glycolysis and mitochondrial activity) (Table 10) of BMDMs. Thus, the output of this experiment supports that the **positive charge of an NM can be reversed by using negatively charged siRNA.**

	CLC	N/P 8	N/P 4	N/P 2	N/P 1	NLC
Zeta potential (mV)	45.8	29.3	20.1	4.95	-9.97	-16.5
<b>Reversal of charge by combining CLC with siRNA at different N/P ratio</b>						
IL-6 (ng/mL)	8.08	7.70	6.60	4.40	3.92	3.45
TNF- $\alpha$ (ng/mL)	7.9	7.54	6.52	4.96	5.10	3.56
MCP-1(ng/mL)	22.00	20.81	18.51	16.86	18.74	4.88
NO ( $\mu$ M)	60.65	61.60	59.10	57.73	49.38	31.23
Glycolysis (ECAR)	52.72	50.05	49.72	49.62	46.27	29.62
Basal Respiration (OCR)	133.65	124.9	119.1	111.47	94.57	76.85
ATP Production (OCR)	95.2	88.67	84.95	79.77	68.92	50.77
<b>Effect of charge reversal on the different cellular function of BMDMs</b>						

Table 10: Zeta potential measurement of CLC with siRNA at different N/P ratios was performed on a zeta sizer. IL-6, TNF $\alpha$ , MCP-1, NO production was quantified from the supernatant of BMDMs exposed to 100  $\mu$ g/mL of CLC or CLC +siRNA complexes at different N/P ratios and activated by LPS. Glycolysis in BMDMs exposed to 100  $\mu$ g/mL of CLC or CLC +siRNA complexes at different N/P ratios and activated by LPS was determined by ECAR. Basal respiration, ATP production in BMDMs exposed to 100  $\mu$ g/mL of CLC or CLC +siRNA complexes at different N/P ratios and activated or not by IL-4 was determined by OCR.

Several studies reported some effect of the charge of nanoparticles on cell behavior. For instance, N-Arginine-N-octyl chitosan (AOCS) is used to synthesize pH-sensitive charge-reversal lysosomolytic nanocarriers (ANLC), which could reduce the potential toxicity of the nanocarrier as well as the increase drug delivery efficiency (Sun *et al*, 2017). In addition, Chen and coworkers showed that charge-reversal nanocarriers enhanced gene delivery to the tumor site (Chen *et al*, 2016). Furthermore, Han and colleagues demonstrated that the use of chitosan and the pH-responsive charge-reversible polymer enhanced the siRNA delivery (Han *et al*, 2012). Here, we provide evidence that the level of the charge proportionally modifies several functions and metabolism activity of BMDMs. **Therefore, we can conclude that the reversal of the effects of a charged NMs helps to design efficient NMs to treat a particular disease condition, especially for the delivery of siRNA.**

Finally, we conclude that different NMs differently effect functions of a particular immune cell type; thus, an NMs specific detailed immunotoxicity assay is much required, not only to prevent the unexpected toxic

effect but also to improve the knowledge about the usage of a particular NMs to modulate the immune system in a specific disease condition such as different pro/anti- inflammatory diseases.

## 11 References

- Aderem A, Underhill DM (1999) MECHANISMS OF PHAGOCYTOSIS IN MACROPHAGES. *Annual Review of Immunology* 17: 593-623
- Alvarez D, Vollmann EH, von Andrian UH (2008) Mechanisms and consequences of dendritic cell migration. *Immunity* 29: 325-342
- Amiel E, Everts B, Fritz D, Beauchamp S, Ge B, Pearce EL, Pearce EJ (2014) Mechanistic Target of Rapamycin Inhibition Extends Cellular Lifespan in Dendritic Cells by Preserving Mitochondrial Function. *The Journal of Immunology* 193: 2821
- Anderson RL, Lefever FR, Maurer JK (1988) The effect of various saccharin forms on gastrointestinal tract, urine and bladder of male rats. *Food Chem Toxicol* 26: 665-669
- ATCC (2010) Cell line misidentification: the beginning of the end. *Nat Rev Cancer* 10: 441-448
- Battah SH, Chee C-E, Nakanishi H, Gerscher S, MacRobert AJ, Edwards C (2001) Synthesis and Biological Studies of 5-Aminolevulinic Acid-Containing Dendrimers for Photodynamic Therapy. *Bioconjugate Chemistry* 12: 980-988
- Bayon E, Morlieras J, Dereuddre-Bosquet N, Gonon A, Gosse L, Courant T, Le Grand R, Marche PN, Navarro FP (2018) Overcoming immunogenicity issues of HIV p24 antigen by the use of innovative nanostructured lipid carriers as delivery systems: evidences in mice and non-human primates. *npj Vaccines* 3: 46
- Benoit M, Desnues B, Mege JL (2008) Macrophage polarization in bacterial infections. *J Immunol* 181: 3733-3739
- Bhaskar K, Anbu J, Ravichandiran V, Venkateswarlu V, Rao YM (2009) Lipid nanoparticles for transdermal delivery of flurbiprofen: formulation, in vitro, ex vivo and in vivo studies. *Lipids Health Dis* 8: 6
- Bianchi ME (2007) DAMPs, PAMPs and alarmins: all we need to know about danger. *J Leukoc Biol* 81: 1-5
- Blanco P, Palucka AK, Pascual V, Banchereau J (2008) Dendritic cells and cytokines in human inflammatory and autoimmune diseases. *Cytokine Growth Factor Rev* 19: 41-52
- Buchmann K (2014) Evolution of Innate Immunity: Clues from Invertebrates via Fish to Mammals. *Frontiers in Immunology* 5: 459
- Bulua AC, Simon A, Maddipati R, Pelletier M, Park H, Kim KY, Sack MN, Kastner DL, Siegel RM (2011) Mitochondrial reactive oxygen species promote production of proinflammatory cytokines and are elevated in TNFR1-associated periodic syndrome (TRAPS). *J Exp Med* 208: 519-533
- Cabon Q, Sayag D, Texier I, Navarro F, Boisgard R, Virieux-Watrelet D, Ponce F, Carozzo C (2016) Evaluation of intraoperative fluorescence imaging-guided surgery in cancer-bearing dogs: a prospective proof-of-concept phase II study in 9 cases. *Transl Res* 170: 73-88
- Castell-Rodríguez A, Piñón-Zárate G, Herrera-Enríquez M, Jarquín-Yáñez K, Medina-Solares I (2017) Dendritic Cells: Location, Function, and Clinical Implications. In: *Biology of Myelomonocytic Cells*,
- Cella M, Facchetti F, Lanzavecchia A, Colonna M (2000) Plasmacytoid dendritic cells activated by influenza virus and CD40L drive a potent TH1 polarization. *Nat Immunol* 1: 305-310
- Chan WCW, Nie S (1998) Quantum Dot Bioconjugates for Ultrasensitive Nonisotopic Detection. *Science* 281: 2016
- Chaplin DD (2010a) Overview of the immune response. *The Journal of allergy and clinical immunology* 125: S3-S23
- Chaplin DD (2010b) Overview of the immune response. *J Allergy Clin Immunol* 125: S3-23
- Chen CZ, Beck-Tan NC, Dhurjati P, van Dyk TK, LaRossa RA, Cooper SL (2000) Quaternary Ammonium Functionalized Poly(propylene imine) Dendrimers as Effective Antimicrobials: Structure-Activity Studies. *Biomacromolecules* 1: 473-480



- Chen X, Liu L, Jiang C (2016) Charge-reversal nanoparticles: novel targeted drug delivery carriers. *Acta Pharm Sin B* 6: 261-267
- Chistiakov DA, Sobenin IA, Orekhov AN, Bobryshev YV (2015) Myeloid dendritic cells: Development, functions, and role in atherosclerotic inflammation. *Immunobiology* 220: 833-844
- Clementi E, Brown GC, Feelisch M, Moncada S (1998) Persistent inhibition of cell respiration by nitric oxide: crucial role of S-nitrosylation of mitochondrial complex I and protective action of glutathione. *Proc Natl Acad Sci U S A* 95: 7631-7636
- Clift MJ, Rothen-Rutishauser B, Brown DM, Duffin R, Donaldson K, Proudfoot L, Guy K, Stone V (2008) The impact of different nanoparticle surface chemistry and size on uptake and toxicity in a murine macrophage cell line. *Toxicol Appl Pharmacol* 232: 418-427
- Courant T, Bayon E, Reynaud-Dougier HL, Villiers C, Menneteau M, Marche PN, Navarro FP (2017) Tailoring nanostructured lipid carriers for the delivery of protein antigens: Physicochemical properties versus immunogenicity studies. *Biomaterials* 136: 29-42
- Crespo L, Sanclimens G, Pons M, Giralt E, Royo M, Albericio F (2005) Peptide and Amide Bond-Containing Dendrimers. *Chemical Reviews* 105: 1663-1682
- Dal Porto JM, Gauld SB, Merrell KT, Mills D, Pugh-Bernard AE, Cambier J (2004) B cell antigen receptor signaling 101. *Mol Immunol* 41: 599-613
- de la Isla A, Brostow W, Bujard B, Estevez M, Rodriguez JR, Vargas S, Castaño VM (2003) Nanohybrid scratch resistant coatings for teeth and bone viscoelasticity manifested in tribology. *Materials Research Innovations* 7: 110-114
- Delmas T, Couffin A-C, Bayle PA, de Crécy F, Neumann E, Vinet F, Bardet M, Bibette J, Texier I (2011) Preparation and characterization of highly stable lipid nanoparticles with amorphous core of tuneable viscosity. *J Colloid Interface Sci* 360: 471-481
- Divakaruni AS, Paradyse A, Ferrick DA, Murphy AN, Jastroch M (2014) Analysis and interpretation of microplate-based oxygen consumption and pH data. *Methods Enzymol* 547: 309-354
- Doktorovová S, Araújo J, Garcia ML, Rakovský E, Souto EB (2010) Formulating fluticasone propionate in novel PEG-containing nanostructured lipid carriers (PEG-NLC). *Colloids Surf B Biointerfaces* 75: 538-542
- Domínguez-Amorocho O, Takiishi T, da Cunha FF, Camara NOS (2019) Immunometabolism: A target for the comprehension of immune response toward transplantation. *World J Transplant* 9: 27-34
- Dong Y, Yu T, Ding L, Laurini E, Huang Y, Zhang M, Weng Y, Lin S, Chen P, Marson D *et al* (2018) A Dual Targeting Dendrimer-Mediated siRNA Delivery System for Effective Gene Silencing in Cancer Therapy. *Journal of the American Chemical Society* 140: 16264-16274
- Donnelly RP, Finlay DK (2015) Glucose, glycolysis and lymphocyte responses. *Molecular Immunology* 68: 513-519
- Donnelly RP, Loftus RM, Keating SE, Liou KT, Biron CA, Gardiner CM, Finlay DK (2014) mTORC1-dependent metabolic reprogramming is a prerequisite for NK cell effector function. *J Immunol* 193: 4477-4484
- Doughty CA, Bleiman BF, Wagner DJ, Dufort FJ, Mataraza JM, Roberts MF, Chiles TC (2006) Antigen receptor-mediated changes in glucose metabolism in B lymphocytes: role of phosphatidylinositol 3-kinase signaling in the glycolytic control of growth. *Blood* 107: 4458-4465
- Dranoff G (2004) Cytokines in cancer pathogenesis and cancer therapy. *Nature Reviews Cancer* 4: 11-22
- Duncan B, Kim C, Rotello VM (2010) Gold nanoparticle platforms as drug and biomacromolecule delivery systems. *J Control Release* 148: 122-127

- Dzionek A, Fuchs A, Schmidt P, Cremer S, Zysk M, Miltenyi S, Buck DW, Schmitz J (2000) BDCA-2, BDCA-3, and BDCA-4: three markers for distinct subsets of dendritic cells in human peripheral blood. *J Immunol* 165: 6037-6046
- Dzionek A, Sohma Y, Nagafune J, Cella M, Colonna M, Facchetti F, Günther G, Johnston I, Lanzavecchia A, Nagasaka T *et al* (2001) BDCA-2, a novel plasmacytoid dendritic cell-specific type II C-type lectin, mediates antigen capture and is a potent inhibitor of interferon alpha/beta induction. *J Exp Med* 194: 1823-1834
- El-Sayed M, Ginski M, Rhodes C, Ghandehari H (2002) Transepithelial transport of poly(amidoamine) dendrimers across Caco-2 cell monolayers. *Journal of Controlled Release* 81: 355-365
- Elsabahy M, Wooley KL (2013) Cytokines as biomarkers of nanoparticle immunotoxicity. *Chemical Society reviews* 42: 5552-5576
- Everts B, Amiel E, Huang SC-C, Smith AM, Chang C-H, Lam WY, Redmann V, Freitas TC, Blagih J, van der Windt GJW *et al* (2014a) TLR-driven early glycolytic reprogramming via the kinases TBK1-IKKe supports the anabolic demands of dendritic cell activation. *Nature Immunology* 15: 323-332
- Everts B, Amiel E, Huang SC, Smith AM, Chang CH, Lam WY, Redmann V, Freitas TC, Blagih J, van der Windt GJ *et al* (2014b) TLR-driven early glycolytic reprogramming via the kinases TBK1-IKKe supports the anabolic demands of dendritic cell activation. *Nat Immunol* 15: 323-332
- Everts B, Amiel E, van der Windt GJ, Freitas TC, Chott R, Yarasheski KE, Pearce EL, Pearce EJ (2012a) Commitment to glycolysis sustains survival of NO-producing inflammatory dendritic cells. *Blood* 120: 1422-1431
- Everts B, Amiel E, van der Windt GJW, Freitas TC, Chott R, Yarasheski KE, Pearce EL, Pearce EJ (2012b) Commitment to glycolysis sustains survival of NO-producing inflammatory dendritic cells. *Blood* 120: 1422-1431
- Flajnik MF, Kasahara M (2010a) Origin and evolution of the adaptive immune system: genetic events and selective pressures. *Nat Rev Genet* 11: 47-59
- Flajnik MF, Kasahara M (2010b) Origin and evolution of the adaptive immune system: genetic events and selective pressures. *Nature Reviews Genetics* 11: 47-59
- Fontana G, Maniscalco L, Schillaci D, Cavallaro G, Giammona G (2005) Solid lipid nanoparticles containing tamoxifen characterization and in vitro antitumoral activity. *Drug Deliv* 12: 385-392
- Franco R, Martínez-Pinilla E, Lanciego JL, Navarro G (2016) Basic Pharmacological and Structural Evidence for Class A G-Protein-Coupled Receptor Heteromerization. *Frontiers in Pharmacology* 7: 76
- Friess MD, Pluhackova K, Böckmann RA (2018) Structural Model of the mIgM B-Cell Receptor Transmembrane Domain From Self-Association Molecular Dynamics Simulations. *Frontiers in Immunology* 9: 2947
- Fröhlich E (2015a) Value of phagocyte function screening for immunotoxicity of nanoparticles in vivo. *International journal of nanomedicine* 10: 3761-3778
- Fröhlich E (2015b) Value of phagocyte function screening for immunotoxicity of nanoparticles in vivo. *Int J Nanomedicine* 10: 3761-3778
- Glista-Baker EE, Taylor AJ, Sayers BC, Thompson EA, Bonner JC (2012) Nickel nanoparticles enhance platelet-derived growth factor-induced chemokine expression by mesothelial cells via prolonged mitogen-activated protein kinase activation. *Am J Respir Cell Mol Biol* 47: 552-561
- Gordon S (2003) Alternative activation of macrophages. *Nat Rev Immunol* 3: 23-35
- Goutayer M, Dufort S, Josserand V, Royère A, Heinrich E, Vinet F, Bibette J, Coll JL, Texier I (2010) Tumor targeting of functionalized lipid nanoparticles: assessment by in vivo fluorescence imaging. *Eur J Pharm Biopharm* 75: 137-147

- Gravier J, Navarro FP, Delmas T, Mittler F, Couffin AC, Vinet F, Texier I (2011) Lipidots: competitive organic alternative to quantum dots for in vivo fluorescence imaging. *J Biomed Opt* 16: 096013
- Grouard G, Clark EA (1997) Role of dendritic and follicular dendritic cells in HIV infection and pathogenesis. *Curr Opin Immunol* 9: 563-567
- Guilliams M, Ginhoux F, Jakubzick C, Naik SH, Onai N, Schraml BU, Segura E, Tussiwand R, Yona S (2014) Dendritic cells, monocytes and macrophages: a unified nomenclature based on ontogeny. *Nat Rev Immunol* 14: 571-578
- Halkes SBA, Vrasidas I, Rooijer GR, van den Berg AJJ, Liskamp RMJ, Pieters RJ (2002) Synthesis and biological activity of polygalloyl-dendrimers as stable tannic acid mimics. *Bioorganic & Medicinal Chemistry Letters* 12: 1567-1570
- Han L, Zhao J, Zhang X, Cao W, Hu X, Zou G, Duan X, Liang XJ (2012) Enhanced siRNA delivery and silencing gold-chitosan nanosystem with surface charge-reversal polymer assembly and good biocompatibility. *ACS Nano* 6: 7340-7351
- Hayder M, Varilh M, Turrin C-O, Saoudi A, Caminade A-M, Poupot R, Liblau RS (2015) Phosphorus-Based Dendrimer ABP Treats Neuroinflammation by Promoting IL-10-Producing CD4+ T Cells. *Biomacromolecules* 16: 3425-3433
- Hedrick SM, Nielsen EA, Kavalier J, Cohen DI, Davis MM (1984) Sequence relationships between putative T-cell receptor polypeptides and immunoglobulins. *Nature* 308: 153-158
- Hentschel A, Gramdorf S, Müller RH, Kurz T (2008) Beta-carotene-loaded nanostructured lipid carriers. *J Food Sci* 73: N1-6
- Hibbitts A, Lucía A, Serrano-Sevilla I, De Matteis L, McArthur M, de la Fuente JM, Aínsa JA, Navarro F (2019) Co-delivery of free vancomycin and transcription factor decoy-nanostructured lipid carriers can enhance inhibition of methicillin resistant *Staphylococcus aureus* (MRSA). *PLOS ONE* 14: e0220684
- Hinger D, Navarro F, Käch A, Thomann JS, Mittler F, Couffin AC, Maake C (2016) Photoinduced effects of m-tetrahydroxyphenylchlorin loaded lipid nanoemulsions on multicellular tumor spheroids. *J Nanobiotechnology* 14: 68
- Hodge P (1993) Polymer science branches out. *Nature* 362: 18-19
- Hu FQ, Jiang SP, Du YZ, Yuan H, Ye YQ, Zeng S (2006) Preparation and characteristics of monostearin nanostructured lipid carriers. *Int J Pharm* 314: 83-89
- Huynh A, Du M, Priyadharshini B, Sage PT, Quiros J, Borges CM, Townamchai N, Gerriets VA, Rathmell JC, Sharpe AH *et al* (2015) Control of PI(3) kinase in Treg cells maintains homeostasis and lineage stability. *Nat Immunol* 16: 188-196
- Infantino V, Convertini P, Cucci L, Panaro MA, Di Noia MA, Calvello R, Palmieri F, Iacobazzi V (2011) The mitochondrial citrate carrier: a new player in inflammation. *Biochem J* 438: 433-436
- Jain D, Banerjee R (2008) Comparison of ciprofloxacin hydrochloride-loaded protein, lipid, and chitosan nanoparticles for drug delivery. *J Biomed Mater Res B Appl Biomater* 86: 105-112
- Janeway CA, Jr. (1989) Approaching the asymptote? Evolution and revolution in immunology. *Cold Spring Harb Symp Quant Biol* 54 Pt 1: 1-13
- Jang JH, Shin HW, Lee JM, Lee HW, Kim EC, Park SH (2015) An Overview of Pathogen Recognition Receptors for Innate Immunity in Dental Pulp. *Mediators Inflamm* 2015: 794143
- Jarrossay D, Napolitani G, Colonna M, Sallusto F, Lanzavecchia A (2001) Specialization and complementarity in microbial molecule recognition by human myeloid and plasmacytoid dendritic cells. *Eur J Immunol* 31: 3388-3393
- Jenkins SJ, Ruckerl D, Cook PC, Jones LH, Finkelman FD, van Rooijen N, MacDonald AS, Allen JE (2011) Local macrophage proliferation, rather than recruitment from the blood, is a signature of TH2 inflammation. *Science* 332: 1284-1288

- Jha Abhishek K, Huang Stanley C-C, Sergushichev A, Lampropoulou V, Ivanova Y, Loginicheva E, Chmielewski K, Stewart Kelly M, Ashall J, Everts B *et al* (2015a) Network Integration of Parallel Metabolic and Transcriptional Data Reveals Metabolic Modules that Regulate Macrophage Polarization. *Immunity* 42: 419-430
- Jha AK, Huang SC, Sergushichev A, Lampropoulou V, Ivanova Y, Loginicheva E, Chmielewski K, Stewart KM, Ashall J, Everts B *et al* (2015b) Network integration of parallel metabolic and transcriptional data reveals metabolic modules that regulate macrophage polarization. *Immunity* 42: 419-430
- Joncker NT, Raulet DH (2008) Regulation of NK cell responsiveness to achieve self-tolerance and maximal responses to diseased target cells. *Immunol Rev* 224: 85-97
- Kadowaki N, Antonenko S, Lau JY, Liu YJ (2000) Natural interferon alpha/beta-producing cells link innate and adaptive immunity. *J Exp Med* 192: 219-226
- Kanasty R, Dorkin JR, Vegas A, Anderson D (2013) Delivery materials for siRNA therapeutics. *Nat Mater* 12: 967-977
- Kasai S, Nagasawa H, Shimamura M, Uto Y, Hori H (2002) Design and synthesis of antiangiogenic/heparin-binding arginine dendrimer mimicking the surface of endostatin. *Bioorganic & Medicinal Chemistry Letters* 12: 951-954
- Khan I, Saeed K, Khan I (2019) Nanoparticles: Properties, applications and toxicities. *Arabian Journal of Chemistry* 12: 908-931
- Kim H, Beack S, Han S, Shin M, Lee T, Park Y, Kim KS, Yetisen AK, Yun SH, Kwon W *et al* (2018) Multifunctional Photonic Nanomaterials for Diagnostic, Therapeutic, and Theranostic Applications. *Adv Mater* 30
- Klopffleisch R (2016) Macrophage reaction against biomaterials in the mouse model - Phenotypes, functions and markers. *Acta Biomater* 43: 3-13
- Kobayashi H, Kawamoto S, Jo S-K, Bryant HL, Brechbiel MW, Star RA (2003) Macromolecular MRI Contrast Agents with Small Dendrimers: Pharmacokinetic Differences between Sizes and Cores. *Bioconjugate Chemistry* 14: 388-394
- Kobayashi KS, van den Elsen PJ (2012) NLRC5: a key regulator of MHC class I-dependent immune responses. *Nature Reviews Immunology* 12: 813-820
- Kolahalam LA, Kasi Viswanath IV, Diwakar BS, Govindh B, Reddy V, Murthy YLN (2019) Review on nanomaterials: Synthesis and applications. *Materials Today: Proceedings* 18: 2182-2190
- Lawless SJ, Kedia-Mehta N, Walls JF, McGarrigle R, Convery O, Sinclair LV, Navarro MN, Murray J, Finlay DK (2017) Glucose represses dendritic cell-induced T cell responses. *Nat Commun* doi: 10.1038/ncomms15620 [PREPRINT]
- Levet S, Ciais D, Merdzhanova G, Mallet C, Zimmers TA, Lee S-J, Navarro FP, Texier I, Feige J-J, Bailly S *et al* (2013) Bone morphogenetic protein 9 (BMP9) controls lymphatic vessel maturation and valve formation. *Blood* 122: 598-607
- Ley K (2017) M1 Means Kill; M2 Means Heal. *The Journal of Immunology* 199: 2191
- Li J, Yin W, Jing Y, Kang D, Yang L, Cheng J, Yu Z, Peng Z, Li X, Wen Y *et al* (2019) The Coordination Between B Cell Receptor Signaling and the Actin Cytoskeleton During B Cell Activation. *Frontiers in Immunology* 9: 3096
- Liu J, Detrembleur C, De Pauw-Gillet M-C, Mornet S, Jérôme C, Duguet E (2015) Gold Nanorods Coated with Mesoporous Silica Shell as Drug Delivery System for Remote Near Infrared Light-Activated Release and Potential Phototherapy. *Small* 11: 2323-2332
- Liu X, Zhou J, Yu T, Chen C, Cheng Q, Sengupta K, Huang Y, Li H, Liu C, Wang Y *et al* (2014) Adaptive Amphiphilic Dendrimer-Based Nanoassemblies as Robust and Versatile siRNA Delivery Systems. *Angewandte Chemie International Edition* 53: 11822-11827

- Liu Y, Chen C (2016) Role of nanotechnology in HIV/AIDS vaccine development. *Advanced Drug Delivery Reviews* 103: 76-89
- Lorsch JR, Collins FS, Lippincott-Schwartz J (2014) Cell Biology. Fixing problems with cell lines. *Science (New York, NY)* 346: 1452-1453
- Love A, Makarov V, Sinitsyna O, Shaw J, Yaminsky I, Kalinina N, Taliansky M (2015) A genetically modified tobacco mosaic virus that can produce gold nanoparticles from a metal salt precursor. *Frontiers in Plant Science* 6
- Lu X, Dong X, Zhang K, Han X, Fang X, Zhang Y (2013) A gold nanorods-based fluorescent biosensor for the detection of hepatitis B virus DNA based on fluorescence resonance energy transfer. *Analyst* 138: 642-650
- Luo W, Hu H, Chang R, Zhong J, Knabel M, O'Meally R, Cole RN, Pandey A, Semenza GL (2011) Pyruvate kinase M2 is a PHD3-stimulated coactivator for hypoxia-inducible factor 1. *Cell* 145: 732-744
- Luo Y, Cook E, Fries BC, Casadevall A (2006) Phagocytic efficacy of macrophage-like cells as a function of cell cycle and Fcγ receptors (FcγR) and complement receptor (CR)3 expression. *Clin Exp Immunol* 145: 380-387
- MacDonald KP, Munster DJ, Clark GJ, Dzionek A, Schmitz J, Hart DN (2002) Characterization of human blood dendritic cell subsets. *Blood* 100: 4512-4520
- Mahtab R, Rogers JP, Murphy CJ (1995) Protein-Sized Quantum Dot Luminescence Can Distinguish between "Straight", "Bent", and "Kinked" Oligonucleotides. *Journal of the American Chemical Society* 117: 9099-9100
- Maki R, Kearney J, Paige C, Tonegawa S (1980) Immunoglobulin gene rearrangement in immature B cells. *Science* 209: 1366
- Manjunath HM, Joshi CG, Raju NG (2017) Biofabrication of gold nanoparticles using marine endophytic fungus – *Penicillium citrinum*. *IET Nanobiotechnology* doi: [PREPRINT]
- Marshall JS, Warrington R, Watson W, Kim HL (2018) An introduction to immunology and immunopathology. *Allergy Asthma Clin Immunol* 14: 49-49
- Mathis D, Shoelson SE (2011) Immunometabolism: an emerging frontier. *Nature reviews Immunology* 11: 81-81
- Matzinger P (1994) Tolerance, Danger, and the Extended Family. *Annual Review of Immunology* 12: 991-1045
- McNamara K, Tofail SAM (2017) Nanoparticles in biomedical applications. *Advances in Physics: X* 2: 54-88
- Meyers SR, Juhn FS, Griset AP, Luman NR, Grinstaff MW (2008) Anionic Amphiphilic Dendrimers as Antibacterial Agents. *Journal of the American Chemical Society* 130: 14444-14445
- Michelucci A, Cordes T, Ghelfi J, Pailot A, Reiling N, Goldmann O, Binz T, Wegner A, Tallam A, Rausell A *et al* (2013) Immune-responsive gene 1 protein links metabolism to immunity by catalyzing itaconic acid production. *Proceedings of the National Academy of Sciences* 110: 7820
- Mills EL, O'Neill LA (2016) Reprogramming mitochondrial metabolism in macrophages as an anti-inflammatory signal. *European Journal of Immunology* 46: 13-21
- Mintzer MA, Grinstaff MW (2011) Biomedical applications of dendrimers: a tutorial. *Chemical Society Reviews* 40: 173-190
- Molday RS, Mackenzie D (1982) Immunospesific ferromagnetic iron-dextran reagents for the labeling and magnetic separation of cells. *Journal of Immunological Methods* 52: 353-367
- Moon JS, Hisata S, Park MA, DeNicola GM, Ryter SW, Nakahira K, Choi AMK (2015) mTORC1-Induced HK1-Dependent Glycolysis Regulates NLRP3 Inflammasome Activation. *Cell Rep* 12: 102-115

- Mudshinge SR, Deore AB, Patil S, Bhargat CM (2011) Nanoparticles: Emerging carriers for drug delivery. *Saudi Pharm J* 19: 129-141
- Nakagawa Y, Chiba K (2014) Role of microglial m1/m2 polarization in relapse and remission of psychiatric disorders and diseases. *Pharmaceuticals (Basel)* 7: 1028-1048
- Narang J, Malhotra N, Singh G, Pundir CS (2015) Electrochemical impedimetric detection of anti-HIV drug taking gold nanorods as a sensing interface. *Biosensors and Bioelectronics* 66: 332-337
- Nathan C, Ding A (2010) Nonresolving inflammation. *Cell* 140: 871-882
- Navarro FP, Berger M, Guillermet S, Josserand V, Guyon L, Neumann E, Vinet F, Texier I (2012a) Lipid nanoparticle vectorization of indocyanine green improves fluorescence imaging for tumor diagnosis and lymph node resection. *J Biomed Nanotechnol* 8: 730-741
- Navarro FP, Mittler F, Berger M, Josserand V, Gravier J, Vinet F, Texier I (2012b) Cell tolerability and biodistribution in mice of indocyanine green-loaded lipid nanoparticles. *J Biomed Nanotechnol* 8: 594-604
- Niemann CU, Wiestner A (2013) B-cell receptor signaling as a driver of lymphoma development and evolution. *Semin Cancer Biol* 23: 410-421
- Nish S, Medzhitov R (2011) Host defense pathways: role of redundancy and compensation in infectious disease phenotypes. *Immunity* 34: 629-636
- O'Neill LA (2011) A critical role for citrate metabolism in LPS signalling. *Biochem J* 438: e5-6
- O'Neill LAJ, Kishton RJ, Rathmell J (2016) A guide to immunometabolism for immunologists. *Nature Reviews Immunology* 16: 553-565
- Paliwal R, Paliwal SR, Kenwat R, Kurmi BD, Sahu MK (2020) Solid lipid nanoparticles: a review on recent perspectives and patents. *Expert Opinion on Therapeutic Patents* 30: 179-194
- Palsson-McDermott EM, Curtis AM, Goel G, Lauterbach MA, Sheedy FJ, Gleeson LE, van den Bosch MW, Quinn SR, Domingo-Fernandez R, Johnston DG *et al* (2015) Pyruvate kinase M2 regulates Hif-1 $\alpha$  activity and IL-1 $\beta$  induction and is a critical determinant of the warburg effect in LPS-activated macrophages. *Cell Metab* 21: 65-80
- Pandey R, Khuller GK (2005) Solid lipid particle-based inhalable sustained drug delivery system against experimental tuberculosis. *Tuberculosis (Edinb)* 85: 227-234
- Pantarotto D, Partidos CD, Hoebeke J, Brown F, Kramer E, Briand J-P, Muller S, Prato M, Bianco A (2003) Immunization with Peptide-Functionalized Carbon Nanotubes Enhances Virus-Specific Neutralizing Antibody Responses. *Chemistry & Biology* 10: 961-966
- Parak WJ, Boudreau R, Le Gros M, Gerion D, Zanchet D, Micheel CM, Williams SC, Alivisatos AP, Larabell C (2002) Cell Motility and Metastatic Potential Studies Based on Quantum Dot Imaging of Phagokinetic Tracks. *Advanced Materials* 14: 882-885
- Pilling AM, Harman RM, Jones SA, McCormack NAM, Lavender D, Haworth R (2002) The Assessment of Local Tolerance, Acute Toxicity, and DNA Biodistribution Following Particle-Mediated Delivery of a DNA Vaccine to Minipigs. *Toxicologic Pathology* 30: 298-305
- Piqueras B, Connolly J, Freitas H, Palucka AK, Banchereau J (2006) Upon viral exposure, myeloid and plasmacytoid dendritic cells produce 3 waves of distinct chemokines to recruit immune effectors. *Blood* 107: 2613-2618
- Pissuwan D, Niidome T, Cortie MB (2011) The forthcoming applications of gold nanoparticles in drug and gene delivery systems. *J Control Release* 149: 65-71
- Qualls JE, Subramanian C, Rafi W, Smith AM, Balouzian L, DeFreitas AA, Shirey KA, Reutterer B, Kernbauer E, Stockinger S *et al* (2012) Sustained generation of nitric oxide and control of mycobacterial infection requires argininosuccinate synthase 1. *Cell Host Microbe* 12: 313-323
- Rahmati M, Mozafari M (2019) Biological Response to Carbon-Family Nanomaterials: Interactions at the Nano-Bio Interface. *Frontiers in Bioengineering and Biotechnology* 7: 4

- Rawlings DJ, Metzler G, Wray-Dutra M, Jackson SW (2017) Altered B cell signalling in autoimmunity. *Nature reviews Immunology* 17: 421-436
- Rehman A, Hemmert KC, Ochi A, Jamal M, Henning JR, Barilla R, Quesada JP, Zambirinis CP, Tang K, Ego-Osuala M *et al* (2013) Role of fatty-acid synthesis in dendritic cell generation and function. *J Immunol* 190: 4640-4649
- Robbins SH, Walzer T, Dembélé D, Thibault C, Defays A, Bessou G, Xu H, Vivier E, Sellars M, Pierre P *et al* (2008) Novel insights into the relationships between dendritic cell subsets in human and mouse revealed by genome-wide expression profiling. *Genome Biology* 9: R17
- Rodríguez-Prados JC, Través PG, Cuenca J, Rico D, Aragonés J, Martín-Sanz P, Cascante M, Boscá L (2010) Substrate fate in activated macrophages: a comparison between innate, classic, and alternative activation. *J Immunol* 185: 605-614
- Ruckmani K, Sivakumar M, Ganeshkumar PA (2006) Methotrexate loaded solid lipid nanoparticles (SLN) for effective treatment of carcinoma. *J Nanosci Nanotechnol* 6: 2991-2995
- Sakaguchi S, Ono M, Setoguchi R, Yagi H, Hori S, Fehervari Z, Shimizu J, Takahashi T, Nomura T (2006) Foxp3+ CD25+ CD4+ natural regulatory T cells in dominant self-tolerance and autoimmune disease. *Immunol Rev* 212: 8-27
- Salazar-González JA, González-Ortega O, Rosales-Mendoza S (2015) Gold nanoparticles and vaccine development. *Expert Review of Vaccines* 14: 1197-1211
- Sanchez-Villamil JI, Tapia D, Torres AG (2019) Development of a Gold Nanoparticle Vaccine against Enterohemorrhagic Escherichia coli O157:H7. *mBio* 10: e01869-01819
- Schatz DG, Oettinger MA, Baltimore D (2008) Pillars Article: The V(D)J Recombination Activating Gene, RAG-1. *Cell*; 1989. 59: 1035–1048. *The Journal of Immunology* 180: 5
- Segura E, Amigorena S (2013) Inflammatory dendritic cells in mice and humans. *Trends Immunol* 34: 440-445
- Segura E, Touzot M, Bohineust A, Cappuccio A, Chiochia G, Hosmalin A, Dalod M, Soumelis V, Amigorena S (2013) Human inflammatory dendritic cells induce Th17 cell differentiation. *Immunity* 38: 336-348
- Setyawati MI, Xie J, Leong DT (2014) Phage Based Green Chemistry for Gold Ion Reduction and Gold Retrieval. *ACS Applied Materials & Interfaces* 6: 910-917
- Shah DK, Zúñiga-Pflücker JC (2014) An Overview of the Intrathymic Intricacies of T Cell Development. *The Journal of Immunology* 192: 4017
- Shapiro H, Lutaty A, Ariel A (2011) Macrophages, meta-inflammation, and immuno-metabolism. *ScientificWorldJournal* 11: 2509-2529
- Shinkai M, Yanase M, Suzuki M, Hiroyuki H, Wakabayashi T, Yoshida J, Kobayashi T (1999) Intracellular hyperthermia for cancer using magnetite cationic liposomes. *Journal of Magnetism and Magnetic Materials* 194: 176-184
- Silva AC, Santos D, Ferreira DC, Souto EB (2009) Minoxidil-loaded nanostructured lipid carriers (NLC): characterization and rheological behaviour of topical formulations. *Pharmazie* 64: 177-182
- Simons K (2016) Cell membranes: A subjective perspective. *Biochimica et Biophysica Acta (BBA) - Biomembranes* 1858: 2569-2572
- Smith NC, Rise ML, Christian SL (2019) A Comparison of the Innate and Adaptive Immune Systems in Cartilaginous Fish, Ray-Finned Fish, and Lobe-Finned Fish. *Frontiers in immunology* 10: 2292-2292
- Sun M, Li J, Zhang C, Xie Y, Qiao H, Su Z, Oupický D, Ping Q (2017) Arginine-Modified Nanostructured Lipid Carriers with Charge-Reversal and pH-Sensitive Membranolytic Properties for Anticancer Drug Delivery. *Adv Healthc Mater* 6
- Supattapone S, Nishina K, Rees JR (2002) Pharmacological approaches to prion research. *Biochemical Pharmacology* 63: 1383-1388

- Tannahill GM, Curtis AM, Adamik J, Palsson-McDermott EM, McGettrick AF, Goel G, Frezza C, Bernard NJ, Kelly B, Foley NH *et al* (2013) Succinate is an inflammatory signal that induces IL-1 $\beta$  through HIF-1 $\alpha$ . *Nature* 496: 238-242
- Texier I, Goutayer M, Da Silva A, Guyon L, Djaker N, Josserand V, Neumann E, Bibette J, Vinet F (2009) Cyanine-loaded lipid nanoparticles for improved in vivo fluorescence imaging. *J Biomed Opt* 14: 054005
- Tezgel Ö, Szarpak-Jankowska A, Arnould A, Auzély-Velty R, Texier I (2018) Chitosan-lipid nanoparticles (CS-LNPs): Application to siRNA delivery. *Journal of Colloid and Interface Science* 510: 45-56
- Thomas LR, Cobb RM, Oltz EM (2009) Dynamic regulation of antigen receptor gene assembly. *Adv Exp Med Biol* 650: 103-115
- Thwe PM, Pelgrom LR, Cooper R, Beauchamp S, Reisz JA, D'Alessandro A, Everts B, Amiel E (2017) Cell-Intrinsic Glycogen Metabolism Supports Early Glycolytic Reprogramming Required for Dendritic Cell Immune Responses. *Cell Metab* 26: 558-567.e555
- Tomalia DA, Reyna LA, Svenson S (2007) Dendrimers as multi-purpose nanodevices for oncology drug delivery and diagnostic imaging. *Biochemical Society Transactions* 35: 61-67
- Tonegawa S (1983) Somatic generation of antibody diversity. *Nature* 302: 575-581
- Tripathy S, Das M, 2013. Dendrimers and their Applications as Novel Drug Delivery Carriers.
- Turvey SE, Broide DH (2010) Innate immunity. *J Allergy Clin Immunol* 125: S24-32
- Van den Bossche J, Baardman J, de Winther MP (2015) Metabolic Characterization of Polarized M1 and M2 Bone Marrow-derived Macrophages Using Real-time Extracellular Flux Analysis. *J Vis Exp*
- van der Windt GJ, Everts B, Chang CH, Curtis JD, Freitas TC, Amiel E, Pearce EJ, Pearce EL (2012) Mitochondrial respiratory capacity is a critical regulator of CD8+ T cell memory development. *Immunity* 36: 68-78
- van Panhuys N, Prout M, Forbes E, Min B, Paul WE, Le Gros G (2011) Basophils Are the Major Producers of IL-4 during Primary Helminth Infection. *The Journal of Immunology* 186: 2719
- Venkateswarlu V, Manjunath K (2004) Preparation, characterization and in vitro release kinetics of clozapine solid lipid nanoparticles. *J Control Release* 95: 627-638
- Villanueva S, Puente J, Sapag-Hagar M (1987) The action of hormones on the rat uterus and mammary gland gamma-glutamyltranspeptidase activity. *Res Commun Chem Pathol Pharmacol* 57: 99-105
- Villiers C, Freitas H, Couderc R, Villiers MB, Marche P (2010) Analysis of the toxicity of gold nano particles on the immune system: effect on dendritic cell functions. *J Nanopart Res* 12: 55-60
- von Boehmer H, Kisielow P, Kishi H, Scott B, Borgulya P, Teh HS (1989) The expression of CD4 and CD8 accessory molecules on mature T cells is not random but correlates with the specificity of the alpha beta receptor for antigen. *Immunol Rev* 109: 143-151
- Vu Manh T-P, Bertho N, Hosmalin A, Schwartz-Cornil I, Dalod M (2015) Investigating Evolutionary Conservation of Dendritic Cell Subset Identity and Functions. *Frontiers in Immunology* 6: 260
- Wang R, Dillon Christopher P, Shi Lewis Z, Milasta S, Carter R, Finkelstein D, McCormick Laura L, Fitzgerald P, Chi H, Munger J *et al* (2011) The Transcription Factor Myc Controls Metabolic Reprogramming upon T Lymphocyte Activation. *Immunity* 35: 871-882
- Warburg O, Wind F, Negelein E (1927) THE METABOLISM OF TUMORS IN THE BODY. *Journal of General Physiology* 8: 519-530
- Weissleder R, Elizondo G, Wittenberg J, Rabito CA, Bengel HH, Josephson L (1990) Ultrasmall superparamagnetic iron oxide: characterization of a new class of contrast agents for MR imaging. *Radiology* 175: 489-493



- Wilbur DS, Pathare PM, Hamlin DK, Buhler KR, Vessella RL (1998) Biotin Reagents for Antibody Pretargeting. 3. Synthesis, Radioiodination, and Evaluation of Biotinylated Starburst Dendrimers. *Bioconjugate Chemistry* 9: 813-825
- Wilson R (2008) The use of gold nanoparticles in diagnostics and detection. *Chem Soc Rev* 37: 2028-2045
- Wong HL, Rauth AM, Bendayan R, Manias JL, Ramaswamy M, Liu Z, Erhan SZ, Wu XY (2006) A new polymer-lipid hybrid nanoparticle system increases cytotoxicity of doxorubicin against multidrug-resistant human breast cancer cells. *Pharm Res* 23: 1574-1585
- Wu D, Molofsky AB, Liang HE, Ricardo-Gonzalez RR, Jouihan HA, Bando JK, Chawla A, Locksley RM (2011) Eosinophils sustain adipose alternatively activated macrophages associated with glucose homeostasis. *Science* 332: 243-247
- Wu D, Yang J, Li J, Chen L, Tang B, Chen X, Wu W, Li J (2013) Hydroxyapatite-anchored dendrimer for in situ remineralization of human tooth enamel. *Biomaterials* 34: 5036-5047
- Wynn TA (2008) Cellular and molecular mechanisms of fibrosis. *J Pathol* 214: 199-210
- Zhang X-D, Luo Z, Chen J, Wang H, Song S-S, Shen X, Long W, Sun Y-M, Fan S, Zheng K *et al* (2015) Storage of Gold Nanoclusters in Muscle Leads to their Biphasic in Vivo Clearance. *Small* 11: 1683-1690
- Zhao Z, Wakita T, Yasui K (2003) Inoculation of plasmids encoding Japanese encephalitis virus PrM-E proteins with colloidal gold elicits a protective immune response in BALB/c mice. *J Virol* 77: 4248-4260
- Zhou Z, Song X, Li B, Greene MI (2008) FOXP3 and its partners: structural and biochemical insights into the regulation of FOXP3 activity. *Immunol Res* 42: 19-28
- Zinkernagel RM, Doherty PC (1997) The discovery of MHC restriction. *Immunol Today* 18: 14-17